
Supersymmetry with non-universal high-scale parameters and the Large Hadron Collider

By

Subhaditya Bhattacharya

Harish-Chandra Research Institute, Allahabad

A Thesis submitted to the
Board of Studies in Physical Science Discipline
In partial fulfilment of requirements
For the degree of
DOCTOR OF PHILOSOPHY
of
Homi Bhabha National Institute



May, 2010

Certificate

This is to certify that the Ph. D. thesis titled "Supersymmetry with non-universal high-scale parameters and the Large Hadron Collider" submitted by Subhadya Bhattacharya is a record of bonafide research work done under my supervision. It is further certified that the thesis represents independent work by the candidate and collaboration was necessitated by the nature and scope of the problems dealt with.

Date:

Biswarup Mukhopadhyaya

Thesis Adviser

Declaration

This thesis is a presentation of my original research work. Whenever contributions of others are involved, every effort is made to indicate this clearly, with due reference to the literature and acknowledgment of collaborative research and discussions.

The work is original and has not been submitted earlier as a whole or in part for a degree or diploma at this or any other Institution or University.

This work was done under guidance of Biswarup Mukhopadhyaya, at Harish-Chandra Research Institute, Allahabad.

Date:

Subhaditya Bhattacharya
Ph. D. Candidate

To the memory of my Father

Acknowledgments

First and foremost I would like to take this opportunity to thank my Adviser Professor Biswarup Mukhopadhyaya for his sincere and affectionate guidance during the four years of my Ph.D work. His methods of identifying and working through research problems and excellent collaborative skills have been exemplary to me for going ahead in the world of research.

I would like to thank my collaborator Dr. Aresh Krishna Datta, from whom I learned various technical aspects of collider physics. His emphasis on rigor and perfection has been a very good lesson for me. I enjoyed working with Professor Debajyoti Choudhuri and would like to thank him for his critical suggestions at all stages of work. I am also thankful to my collaborators Dr. Utpal Chattopadhyay and Dr. Debottam Das. I learned various aspects of dark matter search and related physics issues from them. I thank Dr. Paramita Dey; She has been a friend, philosopher and guide during the last couple of years of my work. I learned some techniques and skills for model building from her. I perhaps enjoyed the most, working with Joydeep Chakraborty. I have learnt many issues of the Grand Unified Theory from him. I am also thankful to Sanjoy Biswas and Nishita Desai, two of my younger colleagues, with whom I am collaborating right now. It has really been an wonderful experience to work with them and I am benefited to learn different technical issues of collider physics from them. My sincere thanks are due to my friend Priyotosh Bandyopadhyay, with whom I started learning collider physics. Our discussions have been very helpful to me. I would also like to thank Satyanarayan Mukhopadhyay. I enjoyed discussing different physics issues with him.

Apart from my research collaborators, I thank the members of the particle physics phenomenology group at the Harish-Chandra Research Institute (HRI), Amitava Raychaudhuri, V. Ravindran, Raj Gandhi, Andreas Nyffeler, Srubabati Goswami, Anindya Datta, Sandhya Choubey and Manimala Mitra, from whom I had the opportunity to learn different aspects of the subject either by doing a project or by discussion. I am thankful to Sudhir Kumar Gupta for his help on numerous occasions, especially on technical physics issues.

I thank the Regional Centre for Accelerator-based Particle Physics (RECAPP), at HRI for providing monetary support for visits at different institutes in India and abroad for academic collaboration. I am grateful to RECAPP for organising different schools and conferences on topical issues which have benefitted for me immensely. I enjoyed the exciting physics discussions at the 'Pheno Lunch' organised on regular basis. This has helped me keep myself up-to-date on the recent developments of the subject.

I am thankful to the faculty members of HRI for the course work that we were given. To name a few of them from which I benefitted: Quantum Field Theory by Ashoke Sen and Debashis Ghoshal, Particle Physics by Rajesh Gopakumar, General Theory of Relativity by Biswarup Mukhopadhyaya, Statistical Mechanics by Pinaki Majumdar, Classical Electrodynamics by Jasjeet Singh Bagla.

I was fortunate to have excellent batch mates at HRI. I thank my friends Arjun Bagchi, Nabamita Banerjee, Shamik Banerjee, Turbasu Biswas, Soumya Das, Sudipta Das, Dhiraj Hazra, Girish Kulkarni and Archana Morye for whom my stay at HRI became meaningful. Exciting discussions on various issues over a midnight cup of tea were the most refreshing parts of my stay at HRI. In addition, I acknowledge and thank to Google, Spires, Wikipedia and the ArXiv to whom I have turned many times during these days of research.

During my thesis work, I have visited the Indian Association for the Cultivation of Science (IACS) many times. I would like to thank the Department of Theoretical Physics for their hospitality and support. I also thank the group members of IACS for exciting physics discussions during these days. I am also grateful to Professor Satya Nandi and Professor Howard Baer for their support and intense physics discussions during my visits to USA.

Apart from a very congenial academic environment, I thank HRI for giving me the opportunity to work for Spic-Macay, a society for promoting Indian Classical Music. This gave me an opportunity to deepen my connection with Indian Classical Music and an introduction to its rich art-forms. I am thankful to Dr. Rukmini Dey for organising 'Music-Poetry' session at HRI, which I enjoyed greatly.

HRI is a wonderful place for students. I thank all the members and supporting staff at HRI, particularly Seema Agarwal and Archana Tandon, for all their support during my stay. I have also received excellent cooperation from the HRI

library and computer division. The cluster computing facility of this institute has been of great help in my computational work (<http://cluster.mri.ernet.in>).

I was motivated to pursue research in Physics by a few excellent teachers at the Jadavpur University during my bachelor and masters degree. I am grateful to Professors Narayan Banerjee, Ranjan Bhattacharya, Amitava Datta, Dhiranjan Roy, Soumen Kumar Roy and Soumitra Sengupta.

My thanks are due to Arjun Bagchi, Biswarup Mukhopadhyaya, Satyanarayan Mukhopadhyay and Nishita Desai for carefully reading the thesis and providing useful suggestions. I am also thankful to Sudhir Kumar Gupta and Nabamita Banerjee for their technical help in preparing the manuscript.

However, none of this would have been meaningful without the support from my mother. She has supported me all these days with love and affection. Her stay at HRI for a few months motivated me to work harder and better. I would like to express my sincere regards and love to her. I would like to end by thanking my younger brother who is extremely dear to me. We have shared all our successes and failures together and he has been my inspiration in many ways. My love and best wishes to him.

List of Publications

(The thesis is based on those marked with asteriks)

*1) S. Bhattacharya, A. Datta and B. Mukhopadhyaya, "Non-universal gaugino masses: A Signal-based analysis for the Large Hadron Collider," JHEP **0710**, 080 (2007) [arXiv:0708.2427 [hep-ph]].

*2) S. Bhattacharya, A. Datta and B. Mukhopadhyaya, "Non-universal scalar masses: A Signal-based analysis for the Large Hadron Collider," Phys. Rev. D **78**, 035011 (2008) [arXiv:0804.4051 [hep-ph]].

*3) S. Bhattacharya, A. Datta and B. Mukhopadhyaya, "Non-universal gaugino and scalar masses, hadronically quiet tripletons and the Large Hadron Collider," Phys. Rev. D **78**, 115018 (2008) [arXiv:0809.2012 [hep-ph]].

*4) S. Bhattacharya and J. Chakraborty, "Gaugino mass non-universality in an SO(10) supersymmetric Grand Unified Theory: low-energy spectra and collider signals," Phys. Rev. D **81**, 015007 (2010) [arXiv:0903.4196 [hep-ph]].

5) S. Bhattacharya, P. Dey and B. Mukhopadhyaya, "Unitarity violation in sequential neutrino mixing in a model of extra dimensions," Phys. Rev. D **80**, 075013 (2009) [arXiv:0907.0099 [hep-ph]].

*6) S. Bhattacharya, U. Chattopadhyay, D. Choudhury, D. Das and B. Mukhopadhyaya, "Non-universal scalar mass scenario with Higgs funnel region of SUSY dark matter: a signal-based analysis for the Large Hadron Collider," Phys. Rev. D **81**, 075009 (2010) [arXiv:0907.3428 [hep-ph]].

Synopsis

-
- **Name:** Subhaditya Bhattacharya
 - **Thesis Title:** Supersymmetry with non-universal high-scale parameters and the Large Hadron Collider
 - **Supervisor:** Prof. Biswarup Mukhopadhyaya
 - **Submitted to** Homi Bhaba National Institute (HBNI)
-

Low energy (TeV scale) supersymmetry (SUSY) has persistently remained one of the leading candidates among scenarios beyond the SM, not only because of its attractive theoretical framework, but also for the variety of phenomenological implications it offers. The stabilization of the electroweak symmetry breaking (EWSB) scale by a systematic cancellation between different contribution to the δm_H^2 and the possibility of having a cold dark-matter (CDM) candidate with conserved R -parity ($R = (-1)^{(3B+L+2S)}$) in form of the lightest neutralino are a few elegant phenomenological features of SUSY. Side by side, the possibility of paving the path towards a Grand Unified Theory (GUT) is one of its most exciting theoretical prospects, where one can relate the $SU(3)$, $SU(2)$ and $U(1)$ gauge couplings and the corresponding gaugino masses at a high scale.

Gravity mediated SUSY-breaking, or in other words a scenario based on Supergravity (SUGRA) has been one of the most popular SUSY-breaking schemes. Within the ambit of SUGRA, the most simple-minded phenomenological framework is the so called minimal supergravity (mSUGRA) scheme where one can parametrise all the SUSY breaking terms by four and a half parameters, namely, a high-scale universal gaugino mass ($M_{1/2}$), a high-scale universal scalar mass (m_0), a high-scale universal trilinear coupling parameter A_0 , the ratio of the vacuum expectation values (v_{ev}) of the two Higgses ($\tan \beta$) (traded from the bilinear $B\mu$ term) and the sign of the SUSY-conserving Higgs mass parameter, ($\text{sgn}(\mu)$). The high-scale is usually taken to be the GUT scale ($\simeq 2 \times 10^{16} \text{GeV}$). The key behind the popularity of this framework is mostly because of its simplicity, reasonable consistency with different low-energy constraints (in spite of some tension with flavour changing neutral current (FCNC)) and economy of parameters and hence of its predictive nature.

However, within a SUGRA-inspired GUT scenario itself, one might find

some deviations from the simplified and idealized situations mentioned above. For instance, the unified gaugino mass parameter ($M_{1/2}$) or the common scalar mass parameter (m_0) can become *non-universal* at the GUT scale. It is also sometimes favourable from different low energy constraints coming from FCNC, CP violation and cold dark matter. On the other hand, a high-scale non-universality can also lead to a region of low-scale MSSM¹ parameter space, which is unattainable from mSUGRA, which has strikingly different collider implications. Thus, it is indeed necessary to study such models with high-scale non-universality in gaugino or scalar mass parameters particularly in context of the upcoming experiment at the Large Hadron Collider (LHC).

With this motivation, the following studies have been undertaken in this thesis:

Gaugino masses, arising after GUT-breaking and SUSY-breaking at a high scale, crucially depend on the gauge kinetic function. One achieves universal gaugino masses if the Higgses, involved in GUT-breaking, are singlets under the underlying GUT group. However, if one includes higher dimensional terms (dimension five, in particular) in the non-trivial expansion of the gauge-kinetic function, the Higgses now belong to the symmetric product of the adjoint representation of the underlying GUT group and can be non-singlets. If these non-singlet Higgses are responsible for GUT breaking, the gaugino masses M_1 , M_2 and M_3 can become non-universal at the high scale itself. It is also possible to have more than one non-singlet representations involved in GUT breaking, in which case the non-universality arises from a linear combination of the effects mentioned above. This is possible in SUSY-GUTs involving $SU(5)$ or $SO(10)$ gauge groups. The possible non-singlet Higgses can belong to representations **24**, **75** or **200** in case of $SU(5)$ and **54**, **210** and **770** in case of $SO(10)$ or any linear combinations of the above with themselves or with the singlet one. All these different representations predict gaugino mass non-universality with different ratios of $M_1 : M_2 : M_3$ at the GUT scale. The non-universal ratios are identified with the non-universal group theoretic coefficients that arise due to the GUT breaking through different non-singlet Higgs representations. For example, in case of **24** of $SU(5)$ or **54** of $SO(10)$ breaking through the Pati-Salam gauge group $SU(4)_C \otimes SU(2)_L \otimes SU(2)_R$ (G_{224}), the ratio at high scale is: $M_3 : M_2 : M_1 = 2:-3:-1$, while the other representations predict a non-universal ratio with $M_2, M_1 > M_3$ at the GUT scale [1,2]. It is

¹minimal supersymmetric extension of the Standard Model

worthy of mentioning here that the gauge coupling unification is also affected by the inclusion of this dimension-five terms in the gauge kinetic function. But, the common practice is to neglect these contributions as they are rather small. All these different high-scale non-universal gaugino mass ratios affect the low-lying chargino-neutralino mass composition and more importantly their mass difference with the gluino which often has a large production at LHC. These affect the final state event rates to a large extent by changing the cascade decay branching fractions through the charginos or neutralinos in a decay chain. This in turn, indicate a departure from the scenario with high-scale gaugino mass universality as far as the various event rates at the colliders are concerned. On considering a comprehensive set of SUSY signals, such as *jets + \cancel{E}_T , same-sign* as well as *opposite-sign dileptons, one isolated lepton* and *trileptons* along with *jets + \cancel{E}_T* , in context of LHC, some remarkable features emerged which may point a distinguishability of these various non-universal schemes from the mSUGRA in a large region of parameter space [1, 2]. It is also important to point out that the uncertainty due to the choice of parton distribution functions (PDF) and renormalisation and factorisation scales get reduced when one takes the ratio of two different final state event rates and they serve as good discriminator as well. It has been observed that the scenarios with non-universal ratios where $M_2, M_1 > M_3$ (for eg, **75** or **200** in case of $SU(5)$, and **770** of $SO(10)$ breaking though G_{224}) at the GUT scale is well distinguished from the mSUGRA, both in signal and in ratio space when all these frameworks are compared by tuning to same gluino masses at the low scale with the mSUGRA. This is because, such cases yield low-lying charginos and neutralinos heavier and more often with a larger higgsino component. While at one hand, it reduces the decay branching fraction of the gluino through the second neutralino $\tilde{\chi}_2^0$ or first chargino $\tilde{\chi}_1^\pm$, their subsequent decays to leptons also get suppressed additionally due to the their larger higgsino component. It is then reflected as a overall suppression in the leptonic final states for these non-universal gaugino mass scenarios when compared to mSUGRA. Similar is the observation when the case of **770** is compared with mSUGRA at dark matter compatible points [2]. However, the case with $M_1 < M_3, M_2 > M_1$ as predicted from **24** of $SU(5)$, is not clearly distinguishable from mSUGRA in most regions of the parameter space, excepting for a relative increase in opposite sign dilepton events through larger mass difference in $\tilde{\chi}_2^0$ with $\tilde{\chi}_1^0$ (artifact of $M_2 > M_1$) which in turn increase the possibility of $\tilde{\chi}_2^0$ decaying through

slepton-lepton [1].

A situation where the strongly interacting superparticles are all heavy (i.e. the gluino mass $m_{\tilde{g}}$ as well as the squark masses $m_{\tilde{q}}$ are close to 5 TeV), while the sleptons and electroweak gauginos are light, can be achieved from a high-scale gaugino mass non-universality with hierarchy $M_3 \gg M_1, M_2$. Such a hierarchy can also be obtained in a SUSY-GUT set up with the inclusion of dimension five operator in the non-trivial gauge kinetic function and taking a suitable combination of the singlet and non-singlet representation **24** in case of $SU(5)$, employing a fine cancellation in M_1, M_2 . Such a case is worth studying since the coloured sparticles being rather heavy and effectively decoupled, the strong processes can not contribute substantially to SUSY signals. In such cases, one may wish to make the best of electroweak processes at the LHC. Thus, it can be viewed as a *new benchmark among non-universal scenarios*. Hadronically quiet trileptons with electrons and muons could be useful in such a situation, not only in terms of rates, which renders it as most viable channel to probe such a spectrum but also through the cleanliness of the signal. Hadronically quiet trileptons occur mostly from the production $pp \rightarrow \tilde{\chi}_2^0 \tilde{\chi}_1^\pm$. The hadronically quiet trilepton events have the best chance when the squarks are very heavy compared to the sleptons and decays of charginos and neutralinos to on-shell sleptons and leptons are allowed. From this point of view, the decoupled nature of squarks favours the trilepton final states. On the other hand, they have less of a chance when the decay modes $\tilde{\chi}_2^0 \rightarrow \tilde{\chi}_1^0 h$ and $\tilde{\chi}_2^0 \rightarrow \tilde{\chi}_1^0 Z$ have substantial branching ratios. It has been shown that there is a large region of parameter space which shows a significance more than 5σ for hadronically quiet trileptons for 100 fb^{-1} luminosity at the LHC when a systematic scan is performed in $M_1 - M_2$ plane [3]. The region of the parameter space in this scenario, which are consistent with WMAP data have also been identified.

It is also interesting to look for the distinction in different high-scale non-universal scalar mass scenarios compared to mSUGRA in the signature space of LHC. Specifically, three different types of non-universal scenarios has been studied [4]. These are (a) non-universality of the squark and slepton masses, (b) non-universality of the third family sfermions with respect to the first two, and (c) non-universality due to high-scale D -terms, pertinent to an $SO(10)$ model. While the first scenario is purely phenomenological, it embodies a complete independence of the coloured and uncoloured sector of the scalar masses at the high-scale. The second one is motivated by the so-called ‘inverted hierarchy’

which is advocated as a solution to the flavour problem and CP violation. Although the parameter points in this case were chosen phenomenologically, such a case may arise from string motivated set-up with flavour dependent couplings to the modular fields. The third case on the other hand concerns a particular theoretical picture where physics between the Planck and GUT scales affects the masses of sfermions in different sub-representations of $SO(10)$, leading to different low-energy mass patterns. The case with squark-slepton non-universality has been studied with a minimal extension to the mSUGRA scalar mass set-up assuming two different high-scale mass generators for squarks and sleptons as $m_{0\bar{q}}$ and $m_{0\bar{l}}$ respectively. A wide region of the parameter space was scanned in such a framework. Among them, most interesting was the case, where gluino is light ($\simeq 500$ GeV), 1,2 generation squarks are as heavy as 1000 GeV, but sleptons are light ($\simeq 250$ GeV). Such a scenario is definitely unattainable from a universal scalar mass set-up. Lighter sleptons in such a case, yields a larger leptonic final state when compared to mSUGRA in a similar $(m_{\tilde{g}}, m_{\bar{q}^{1,2}})$ values. In this case, the Higgs mass parameters $m_{H_u}^2$ & $m_{H_d}^2$ were taken to evolve from the high-scale slepton masses for the sake of REWSB. A scalar mass non-universality in family, on the other hand, yields the most interesting phenomenological framework where the first two generation squarks can be made much heavier than the third generation ones. Similar to the squark-slepton non-universal framework, this case was studied assuming two different mass generating parameters for third family and first two family scalars as m_0^3 , and $m_0^{(1,2)}$ respectively. The advantage of such a scenario is that the gluino dominantly decays to stop-top or sbottom-bottom channel, thus boosting the leptonic final states which are outcomes of the decay of heavy quarks when compared to mSUGRA set up tuned at similar $(m_{\tilde{g}}, m_{\tilde{t}_1})$ values. The distinction in this case was spectacular in both signal and ratio spaces and has little dependence on other parameters like μ and $\tan\beta$. In an $SO(10)$ framework, the matter fields belong to the representation **16**, and can be further classified into sub-multiplets, depending on the representations of $SU(5)$ to which they belong. In this classification, expressing the (s)fermions generically to include all families, the superfields D^c and L belong to $\bar{\mathbf{5}}$, while Q , U^c and E^c belong to $\mathbf{10}$, where Q and L denote $SU(2)$ doublets and the others, singlets. The breakdown of $SO(10)$ (without any intermediate scale) to the SM gauge group, which amounts to a reduction of rank, will therefore endow the scalars in these different $SU(5)$ representations with different D -

terms. Consequently, the high-scale scalar mass parameters will be different for the two multiplets $\mathbf{5}$ and $\mathbf{10}$ respectively as: $m_{\mathbf{5}}^2 = m_0^2 - 1.5Dm_0^2$ (for D^c & L) and $m_{\mathbf{10}}^2 = m_0^2 + 0.5Dm_0^2$ (for E^c, U^c & Q), thus leading to a predestined non-universality in the GUT scale itself. Here D is a dimensionless parameter quantifying the added contribution to the SUSY breaking masses in terms of the ‘universal’ high-scale mass parameter m_0 . The value of D were chosen in order to avoid tachyonic modes at high scale. Thus $D = 0.5, -0.5$ and -1.25 have been considered. However, the way such a non-universality affects the low-energy scalar mass hierarchy, it is difficult to distinguish these different non-universal models among themselves as well as from mSUGRA.

Another framework where scalar mass non-universality arises in family was considered in [5]. Here, the third generation squark masses and the Higgs scalar mass parameters were kept at small values for the sake of compatibility with REWSB and naturalness in a larger region of parameter space. This very smallness also serves to keep the degree of fine-tuning within control while the model addresses the FCNC issue by invoking very large masses for the first two generations of squarks and sleptons. As far as the third generation sleptons are concerned, a very small SUSY-breaking mass at the GUT scale is not phenomenologically viable since the larger Yukawa coupling serves to drive down the mass of the lighter stau, thereby rendering it the lightest of the supersymmetric partners (LSP) at the electroweak scale. Consequently, the SUSY-breaking mass in this sector has to be sizable. Rather than introducing a new parameter, it was assumed to be same as that of first two generations of squarks or sleptons. To summarize, at the GUT scale all sfermion masses are diagonal; and, apart from the those pertaining to the stop and the sbottom, they are universal. The last-mentioned, along with the Higgs scalars, have a vanishing mass at this scale. While this construction might seem artificial, it is noted that this accords a special status only to those fields that are expected to play a direct role in EWSB. Interestingly, the model satisfies WMAP constraint on neutralino relic density for a large region of the parameter space without requiring any delicate mixing of Binos and Higgsinos. This was due to small m_A in a large region of parameter space such that $2m_{\tilde{\chi}_1^0} \simeq m_A$ is responsible for right degree of pair-annihilation via s -channel Higgs-exchanges, so as to satisfy the WMAP limits on the neutralino relic density. This is the so-called Higgs funnel region, which appears only for very high $\tan\beta$ values in a mSUGRA set up. For simplicity, a universal gaugino mass and

a vanishing trilinear soft-breaking parameter (A_0) at M_G was assumed. This also yields the similar boost in the leptonic final states due to the reasons already mentioned for an inverted scalar mass hierarchy significant and a significant distinction from mSUGRA in multilepton channels at a few benchmark points satisfying WMAP data is observed when tuned at similar gluino masses. Also studied in this context was the 4ℓ inclusive signature which is an outcome of gluino decaying through stop-top in such a scenario. Apart from being a good discriminator, it can also register a discovery at $30 fb^{-1}$ luminosity.

Bibliography

- [1] S. Bhattacharya, A. Datta and B. Mukhopadhyaya, “Non-universal gaugino masses: A Signal-based analysis for the Large Hadron Collider,” JHEP **0710**, 080 (2007) [arXiv:0708.2427 [hep-ph]].
- [2] S. Bhattacharya and J. Chakraborty, “Gaugino mass non-universality in an SO(10) supersymmetric Grand Unified Theory: low-energy spectra and collider signals,” Phys. Rev. D **81**, 015007 (2010) [arXiv:0903.4196 [hep-ph]].
- [3] S. Bhattacharya, A. Datta and B. Mukhopadhyaya, “Non-universal gaugino and scalar masses, hadronically quiet trileptons and the Large Hadron Collider,” Phys. Rev. D **78**, 115018 (2008) [arXiv:0809.2012 [hep-ph]].
- [4] S. Bhattacharya, A. Datta and B. Mukhopadhyaya, “Non-universal scalar masses: A Signal-based analysis for the Large Hadron Collider,” Phys. Rev. D **78**, 035011 (2008) [arXiv:0804.4051 [hep-ph]].
- [5] S. Bhattacharya, U. Chattopadhyay, D. Choudhury, D. Das and B. Mukhopadhyaya, “Non-universal scalar mass scenario with Higgs funnel region of SUSY dark matter: a signal-based analysis for the Large Hadron Collider,” Phys. Rev. D **81**, 075009 (2010) [arXiv:0907.3428 [hep-ph]].

Contents

I	Introduction	1
<hr/>		
1	The Standard Model and beyond	3
1.1	The Standard Model of Particle Physics	3
1.2	Going beyond the Standard Model:	6
1.3	What kind of new physics can we look for at the TeV Scale?	8
2	The Large Hadron Collider	15
2.1	Basic Notions	15
2.2	The ATLAS detector	19
2.3	The CMS detector	20
2.4	Physics at the LHC	21
2.5	Some technical details	22
3	Supersymmetry and its signals: basic features	29
3.1	Motivation	29
3.2	SUSY Algebra	34
3.3	SUSY Lagrangians	35
3.4	Supersymmetry Breaking	41
3.5	The minimal supersymmetric standard model (MSSM)	43
3.5.1	Ingredients of the MSSM Lagrangian	43
3.5.2	Masses and Mixing	45
3.5.3	The R-parity	47
3.6	High-scale SUSY breaking: some illustrations	48
3.7	Supersymmetry search at Colliders	55

4 Non-universal gaugino masses in $SU(5)$: a signal-based analysis for the Large Hadron Collider	65
4.1 Introduction	65
4.2 Non-universal SUSY GUT and gaugino mass ratios in $SU(5)$	68
4.3 SUSY signals and backgrounds: strategy for analysis	71
4.3.1 Choice of SUSY parameters	72
4.3.2 Collider simulation	74
4.3.3 Backgrounds	76
4.4 Prediction for different GUT representations in $SU(5)$	76
4.5 Summary and conclusions	87
5 Non-universal gaugino masses in $SO(10)$: a signal-based analysis for the Large hadron Collider	103
5.1 Introduction	103
5.2 Non-universal Gaugino mass ratios for $SO(10)$	105
5.2.1 Implication of the Intermediate Scale	106
5.3 Low energy spectra, Consistency and Benchmark Points	107
5.4 Collider Simulation and Numerical Results	114
5.4.1 Strategy for Simulation	115
5.4.2 Numerical Results	119
5.5 Summary and Conclusions	125
6 Non-universal masses, hadronically quiet trileptons and the Large Hadron Collider	133
6.1 Introduction	133
6.2 Non-universality and hadronically quiet signals	135
6.3 Signal and backgrounds: hadronically quiet trileptons	139
6.4 Other signals	146
6.5 Conclusions	148
7 Non-universal scalar masses: a signal-based analysis for the Large Hadron Collider	

Collider	153
7.1 Introduction	153
7.2 Strategy for simulation	155
7.3 Squark-slepton Non-universality	157
7.3.1 Choice of SUSY parameters	158
7.3.2 Numerical results	160
7.4 Non-universality in the third family	161
7.4.1 Choice of parameters	162
7.4.2 Numerical results	163
7.5 Non-universality due to $SO(10)$ D -terms	166
7.5.1 Choice of parameters	166
7.5.2 Numerical results	167
7.6 Summary and conclusions	170
8 Non-universal scalar mass scenario with Higgs funnel region of SUSY	
dark matter: a signal-based analysis for the Large Hadron Collider	185
8.1 Introduction	185
8.2 The Non-Universal Scalar Mass model (NUSM) and benchmark points	188
8.2.1 The NUSM parameter space	188
8.2.2 Cosmological and low energy constraints in NUSM	189
8.2.3 Benchmark points	192
8.3 Collider Signatures	197
8.3.1 The general strategy	197
8.3.2 Detection and Kinematical Requirements	201
8.3.3 Results	204
8.4 Summary and Conclusions	211
9 Conclusions	221

Part I

Introduction

Chapter 1

The Standard Model and beyond

1.1 The Standard Model of Particle Physics

The quest for the laws of nature governing elementary particles and their interactions has led to the subject of particle physics. In its present form, the Standard Model (SM) of particle physics has been a successful description of sub-nuclear particles to a large extent at least up to a few hundred GeVs [1]. In this section, we briefly discuss the basic construct of the SM and various important features it incorporates. Later in this chapter we outline the issues which have led us to believe that we need to go beyond the SM and some new physics scenarios we are interested to look at.

We know of four fundamental forces in nature till date. These are: i) Gravitational force, ii) Weak force, iii) Electromagnetic force and iv) Strong force. While the SM successfully describes the weak, electromagnetic and strong forces, it keeps out gravitation. The basic construct of SM is based on relativistic quantum field theory (QFT), a framework that merges the principles of quantum mechanics, and the special theory of relativity. It is consistent with Lorentz invariance, which is in essence the requirement of independence of the choice of one among many inertial frames. On the other hand, the interaction between two fundamental particles in the SM is successfully described by a continuous symmetry of the

fields in the Lagrangian, known as the local gauge invariance. For example, we associate a continuous $U(1)$ symmetry to the electromagnetic Lagrangian and demand it to be intact at the local space-time level (naively, this is what is known as gauge invariance). As a result, we obtain a spin-one ‘gauge boson’ which is the mediator of the particular type of interaction described by the specific symmetry group chosen.

As a whole, SM is well established as a quantum gauge field theory described by $SU(3)_C \otimes SU(2)_L \otimes U(1)_Y$, which describes the strong and electroweak interactions respectively [2–4]. The gauge boson corresponding to the strong interaction is gluon (g), those mediating weak interaction are W^\pm and Z while the ubiquitous photon conducts electromagnetic interaction. The gauge bosons belong to the adjoint representation of the corresponding gauge groups. The subscripts corresponding to $SU(3)$ and $U(1)$ gauge groups above denote the conserved charges: C is the colour charge associated to the strong interaction, and Y is the weak-hypercharge corresponding to $U(1)$ symmetry. L indicates an additional interesting feature of weak interaction, namely, parity violation. It has been observed that $SU(2)$ interaction involves only the left-chiral fermions while the right-chiral components are singlets under this gauge interaction. Hence L stands for ‘left’ in this context. Weak isospin is the conserved charge associated with $SU(2)$ gauge symmetry.

The ‘matter particles’ of SM are spin-1/2 fermions which belong to the fundamental representation of whichever among the aforementioned gauge groups they are non-singlets under. They are categorised as leptons and quarks. Leptons do not have strong interaction while the quarks have strong, electromagnetic and weak interactions. All of these fermions have left and right chiral components as mentioned above, an exception being the neutrinos, which are only left-chiral in the SM. Hence, the left-handed components are represented by $SU(2)$ doublets, while the right-handed components are singlets under $SU(2)$. Another interesting point is that the leptons and quarks have three family each. The SM fermion content and their charges are shown in Table 1.1.

However, the SM spectrum is not complete yet. Invariance under $SU(2)_L \otimes U(1)_Y$ requires that all fermions have to be massless to start with. In addition, gauge invariance also demands that the gauge bosons be massless. In order to generate the masses for the weak gauge bosons as well as for the fermions, one requires a spontaneous breakdown of the $SU(2)_L \otimes U(1)_Y$ into $U(1)_{em}$. Such a

Fermion	Hypercharge, Y	Isospin	T_3	EM Charge, Q
d_R	$-\frac{2}{3}$	0	0	$-\frac{1}{3}$
u_R	$+\frac{4}{3}$	0	0	$\frac{2}{3}$
$\begin{pmatrix} u \\ d \end{pmatrix}_L$	$+\frac{1}{3}$	$\frac{1}{2}$	$+\frac{1}{2}$ $-\frac{1}{2}$	$+\frac{2}{3}$ $-\frac{1}{3}$
e_R^-	-2	0	0	-1
$\begin{pmatrix} \nu_e \\ e^- \end{pmatrix}_L$	-1	$\frac{1}{2}$	$+\frac{1}{2}$ $-\frac{1}{2}$	0 -1

Table 1.1: *Standard model fermions and their gauge quantum numbers.*

symmetry breaking can be implemented with the introduction of a complex scalar $SU(2)$ doublet in the minimal form, known as Higgs doublet [5], whose neutral component acquires a non-zero vacuum expectation value (vev). This vev in the gauge invariant scalar kinetic energy yields masses for the weak gauge bosons (W^\pm and Z bosons). As it leaves $SU(3)_C$ and $U(1)_{em}$ intact, the corresponding gauge bosons, gluon and photon remain massless. A set of interaction terms with this Higgs doublet to the fermions, known as Yukawa interaction, can now be written in a gauge invariant way. The Higgs vev make fermions massive from such terms, breaking the gauge symmetry only at the ground state of the Higgs potential, keeping the Lagrangian gauge invariant otherwise. Hence, it is called spontaneous breakdown of the electroweak symmetry. Three components of the complex scalar doublet are absorbed as longitudinal components of the W^\pm and the Z . The physical neutral scalar field which is retained in the SM is called the Higgs boson. The whole process preserves the renormalisability as well as unitarity of the theory.

SM also obeys two accidental symmetries related to gauge invariance and the Lorentz structure as well as the requirement that the SM should be renormalisable. The theory thus conserves lepton (L) and baryon (B) number in its minimal

form.

The success of the SM is that, all the predictions from such an abstract quantum field theoretical framework have been precisely measured in experiments which have established SM as a benchmark as far as building fundamental theories is concerned. Higher order predictions of non-abelian gauge interactions have been quite accurately established at the LEP and the Tevatron experiments. Tevatron has also discovered top quark, the heaviest elementary particle known so far.

The only missing object in this set-up is the Higgs boson, which is yet to be discovered. A lower bound on the Higgs mass of 114.4 GeV has been established by the LEP Higgs search group [6]. Also as of January 2010, combined data from CDF and DO experiments at the Tevatron excluded the Higgs boson in the range between 162 GeV to 166 GeV at the 95% confidence level [7]. Although different indirect evidences (the relation between Z and W) point towards the usual belief of electroweak symmetry breaking (EWSB), it is really imperative to discover Higgs at the LHC to really establish the phenomenon that will truly complete the standard electroweak model.

1.2 Going beyond the Standard Model:

In spite of the huge success of the SM of particle physics, it is unlikely to be a complete description of nature at the fundamental level. We therefore need to go beyond this. We discuss below various issues that have led us to believe that a theory beyond the SM is quite imperative. We categorise them as: i) Phenomenological dissatisfactions, ii) Theoretical issues, and iii) Concrete and persistent problems.

Phenomenological dissatisfactions:

- The SM suffers from a huge number of parameters ($\simeq 20$). All the masses and couplings are free parameters of this theory.
- Another issue is the replication of fermion families. Within the SM framework there is no hint why this is so with a remarkable repetition of quantum numbers.
- A big question remains in the huge spread in the fermion masses across

families. Electron mass is 0.5 MeV while the top mass is about 172 GeV. Neutrinos are massless compared to this. While all the fermions (excepting the neutrinos) acquire mass from the Yukawa interaction with the Higgs boson, we assign this huge hierarchy to the Yukawa couplings of the fermions. However, that keeps the problem essentially unsolved.

- Also, SM predicts maximal violation of Parity while a small degree of CP violation is observed (Measured in $K_0 - \bar{K}_0$ mixing [8] or in B systems [9]). There is no clue why this is so.

Theoretical issues:

- Perhaps the most important issue that SM keeps out is gravity. There is no consistent and testable theory of quantum gravity. So, it is usually assumed that SM is an effective theory up to the Planck scale (M_{Pl}) where the effects of gravity become dominant. String theory [10] is perhaps the most popular alternative which predicts a finite, quantised description of gravity.
- Unification of the electroweak and strong couplings (Grand unification) [11] is not achieved within the SM framework.
- One of the most compelling reasons to look for physics beyond the SM is perhaps the issue of stabilization of Higgs mass. The Higgs mass is unstable against quantum corrections. Unlike the chiral symmetry of fermions and gauge symmetry of vector bosons, there is no symmetry principle which could protect it from diverging quadratically when radiative corrections to its mass are calculated. For example, if the Higgs field couples to some fermion f with a term in the Lagrangian $\lambda_f H \bar{f} f$, then the one loop correction from the fermionic loop yields a correction

$$\Delta m_H^2 = -\frac{|\lambda_f|^2}{8\pi^2} \Lambda_{UV}^2 \quad (1.1)$$

Here Λ_{UV} is an ultraviolet momentum cutoff used to regulate the loop integral; it should be interpreted as the energy scale at which new physics intervenes to alter the high-energy behavior. Each of the leptons and quarks of the Standard Model can play the role of f ; for quarks, this should be multiplied by 3 to account for color. The largest correction comes when f is the top quark with $\lambda_f \approx 1$. Adding further the contributions from the gauge boson and scalar self interaction loops, the correction becomes

$$\Delta m_H^2 = \left(\frac{3}{2}g_1^2 + \frac{9}{2}g_2^2 + 6\lambda^2 - 12|\lambda_t|^2 \right) \frac{\Lambda_{UV}^2}{16\pi^2}, \quad (1.2)$$

where g_1, g_2 are the $U(1)$ and $SU(2)$ gauge couplings and λ is the Higgs self coupling. The problem is that if Λ_{UV} is of order M_{Pl} , say, then this quantum correction to m_H^2 is about 30 orders of magnitude larger than the required value of $m_H^2 \sim -(100 \text{ GeV})^2$. In order to achieve a Higgs mass around 100 GeV, we need a tremendous fine tuning. This is known as the hierarchy or naturalness problem [12].

Concrete and persistent problems:

- It has been almost conclusively proved by now that neutrinos are massive. Data on the solar and atmospheric neutrino deficits point rather strongly towards neutrino mass and mixing [13–15]. For this, physics beyond the SM needs to be involved at some level.
- The rotation curve of spiral galaxies and recent experiments have indicated that there should be some non-luminous matter constituted of weakly interacting massive particles (WIMP) amounting to about 24 percent of the energy of universe [16]. This is known as dark matter (DM). Within the SM framework, there is no such particle which can contribute to this. This is an issue which indicates the need for a theory beyond the SM.
- SM is also silent about the matter-antimatter asymmetry in the universe which has inputs of B/L violation and adequate CP-violation. Neither of these is attainable within the SM framework.
- A tiny positive cosmological constant commensurate with recent observables is also unattainable within the SM framework [16].

1.3 What kind of new physics can we look for at the TeV Scale?

After the points discussed in the previous section, it is obvious now that SM itself can not be a complete theory of nature. The search for theories beyond the SM has been carried out in many directions for various issues. For example, the search for a theory which consistently quantises gravity has yielded a field like string theory.

Different kinds of see-saw models and related scenarios to take care of neutrino mass and mixing have been proposed and studied [17–19]. Search for a Grand Unified Theory (GUT) in form of an extended gauge group like $SU(5)$ or $SO(10)$ [11] has always been an issue with compelling motivation. However, to take care of the hierarchy problem, new physics precisely at the TeV scale is expected, which cancels quadratic divergences that arise in the quantum correction to the SM Higgs. If one does not have $\lambda_{UV} \simeq \text{TeV}$, the Higgs boson mass becomes very large, raising the Higgs self coupling strength at the same time. As a result, the longitudinal components of the W/Z bosons have strong couplings at the TeV scale, which should also register as new physics signals at that scale.

With the Large Hadron Collider (LHC) already in operation, it is of interest to search for models whose features are observable within the reach of the LHC. LHC is operating now with 7 TeV centre-of-mass energy and is expected to run with 14 TeV around 2012 and shortly afterwards.

Some candidate theories beyond the SM, which take care of the hierarchy problems and have a possibility of discovery at the LHC, are:

- Supersymmetry (SUSY), in the simplest form, as a minimal supersymmetric extension to the SM (MSSM) and variations therein [20, 21].
- Theories with extra space like dimensions which can be large or warped or universal (ADD, RS and Universal respectively) very broadly are also of considerable interest [22–24].
- Little Higgs models which postulate the Higgs to be pseudo-goldstone boson of a broken symmetry [25, 26].

All the above models address the hierarchy problem while some of them provide a cold dark matter candidate, especially with some Z_2 symmetry imposed.

In this thesis we discuss some features of supersymmetry, particularly from the collider search point of view. Supersymmetry which has been one of the most popular frameworks beyond the SM since almost half a decade, has a very good chance of getting unravelled at the LHC, as the proposed centre-of-mass energy is as large as 14 TeV while the integrated luminosity per year can rise up to 100 fb^{-1} and higher. Hence, it is indeed an exciting as well as challenging task to look into the different aspects of SUSY in context of the LHC.

This thesis is organised as follows. We review various aspects of the LHC

experiment in the next chapter, while the important features of a SUSY scenario and its signals at the LHC are discussed in Chapter 3. In the subsequent chapters, we discuss different aspects of collider search for models with non-universal high-scale inputs. We conclude in Chapter 9.

Bibliography

- [1] For introduction, see, for example, F. Hebbeker and A.D. Martin, *Quarks and Leptons: An introductory course in modern particle physics*, (Ed. John Wiley, 1984); C. Quigg, *Gauge Theories of the Strong, Weak and Electromagnetic Interactions*, (Westview Press 1997); T.P. Cheng and L.F. Li, *Gauge theory of elementary particle physics*, (Oxford Univ. Press, 1991).
- [2] M. Gell-Mann, *Phys. Lett.* **8**, 214 (1964); O. W. Greenberg, *Phys. Rev. Lett.* **13**, 598 (1964); D. J. Gross and F. Wilczek, *Phys. Rev. Lett.* **30**, 1343 (1973); H. D. Politzer, *Phys. Rev. Lett.* **30**, 1346 (1973).
- [3] S. L. Glashow, *Nucl. Phys.* **22**, 579 (1961); S. Weinberg, *Phys. Rev. Lett.* **19**, 1264 (1967); A. Salam, *Proceedings of 8th Nobel Symposium*, Ed. N. Svartholm (1968).
- [4] G. 't Hooft, *Nucl. Phys. B* **35**, 167 (1971); G. 't Hooft and M. J. G. Veltman, *Nucl. Phys. B* **44**, 189 (1972).
- [5] F. Englert and R. Brout, *Phys. Rev. Lett.* **13**, 321 (1964); P. W. Higgs, *Phys. Rev. Lett.* **13**, 508 (1964); G. S. Guralnik, C. R. Hagen and T. W. B. Kibble, *Phys. Rev. Lett.* **13**, 585 (1964); P. W. Higgs, *Phys. Rev.* **145**, 1156 (1966); T. W. B. Kibble, *Phys. Rev.* **155**, 1554 (1967).
- [6] LEP Higgs Working Group, arXiv:hep-ex/0107030; R. Barate *et al.* [LEP Working Group for Higgs boson searches], *Phys. Lett. B* **565**, 61 (2003) [arXiv:hep-ex/0306033].
- [7] T. Aaltonen *et al.* [CDF and D0 Collaborations], *Phys. Rev. Lett.* **104**, 061802 (2010) [arXiv:1001.4162].
- [8] J. H. Christenson, J. W. Cronin, V. L. Fitch and R. Turlay, *Phys. Rev. Lett.* **13**, 138 (1964).
- [9] B. Aubert *et al.* [BABAR Collaboration], *Phys. Rev. Lett.* **87**, 091801 (2001)

- [arXiv:hep-ex/0107013]; K. Abe *et al.* [Belle Collaboration], Phys. Rev. Lett. **87**, 091802 (2001) [arXiv:hep-ex/0107061].
- [10] See for example, *Superstring theory* by M. Green, J. H. Schwarz and E. Witten (1987), Cambridge University Press; *String Theory* by J. Polchinski (1998), Cambridge University Press; *A First Course in String Theory* by B. Zwiebach (2004), Cambridge University Press.
- [11] See for example, *Grand Unified Theories* by G. Ross(1984), Westview Press; H. Georgi and S. L. Glashow, Phys. Rev. Lett. **32**, 438 (1974); J. C. Pati and A. Salam, Phys. Rev. D **10**, 275 (1974) [Erratum-ibid. D **11**, 703 (1975)]; P. Langacker, "Grand Unified Theories And Proton Decay," Phys. Rept. **72** (1981) 185.
- [12] S. Weinberg, Phys. Rev. D **13**, 974 (1976), Phys. Rev. D **19**, 1277 (1979); E. Gildener, Phys. Rev. D **14**, 1667 (1976); L. Susskind, Theory," Phys. Rev. D **20**, 2619 (1979); G. 't Hooft, in *Recent developments in gauge theories*, Proceedings of the NATO Advanced Summer Institute, Cargese 1979, (Plenum, 1980).
- [13] R. N. Mohapatra *et al.*, Rept. Prog. Phys. **70**, 1757 (2007) [arXiv:hep-ph/0510213]; A. Y. Smirnov, J. Phys. Conf. Ser. **136**, 012002 (2008) [arXiv:0810.2668 [hep-ph]]; A. Y. Smirnov, arXiv:0910.1778.
- [14] B. Kayser, Phys. Rev. D **24**, 110 (1981); F. Boehm and P. Vogel, Physics of Massive Neutrinos (Cambridge University Press, Cambridge, 1987) p. 87; C. Giunti, C. Kim, and U. Lee, Phys. Rev. D **44**, 3635 (1991); J. Rich, Phys. Rev. D **48**, 4318 (1993); H. Lipkin, Phys. Lett. B **348**, 604 (1995); A. Bandyopadhyay, S. Choubey, S. Goswami and D. P. Roy, Phys. Lett. B **540**, 14 (2002) [arXiv:hep-ph/0204286].
- [15] S. Fukuda *et al.* [Super-Kamiokande Collaboration], Phys. Lett. B **539**, 179 (2002) [arXiv:hep-ex/0205075]; S. N. Ahmed *et al.* [SNO Collaboration], Phys. Rev. Lett. **92**, 181301 (2004) [arXiv:nucl-ex/0309004]; T. Araki *et al.* [KamLAND Collaboration], Phys. Rev. Lett. **94**, 081801 (2005) [arXiv:hep-ex/0406035]; E. Aliu *et al.* [K2K Collaboration], Phys. Rev. Lett. **94**, 081802 (2005) [arXiv:hep-ex/0411038]; Y. Ashie *et al.* [Super-Kamiokande Collaboration], Phys. Rev. D **71**, 112005 (2005) [arXiv:hep-ex/0501064].
- [16] E. Komatsu *et al.* [WMAP Collaboration], Astrophys. J. Suppl. **180**, 330 (2009) [arXiv:0803.0547 [astro-ph]].

- [17] See, for example, P. Minkowski, Phys. Lett. **B67**, 421 (1977); T. Yanagida, in *Proceedings of the Workshop on the Unified Theory and the Baryon Number in the Universe*, O. Sawada and A. Sugamoto (eds.), KEK, Tsukuba, Japan, 1979, p. 95; M. Gell-Mann, P. Ramond and R. Slansky, *Supergravity*, P. van Nieuwenhuizen *et al.* (eds.), North Holland, Amsterdam, 1980, p. 315; R.N. Mohapatra and G. Senjanovic, Phys. Rev. Lett. **44**, 912 (1980).
- [18] See, for example, R.N. Mohapatra, A. Perez-Lorenzana and C.A. de Sousa Pires, Phys. Lett. **B474**, 355 (2000) [hep-ph/9911395]; G. Altarelli and F. Feruglio, Springer Tracts Mod. Phys. **190**, 169 (2003) [hep-ph/0206077]; G. Altarelli and F. Feruglio, New J. Phys. **6**, 106 (2004) [hep-ph/0405048]; S. Bertolini, M. Frigerio and M. Malinsky, Phys. Rev. **D70**, 095002 (2004) [hep-ph/0406117]; S.F. King, Rept. Prog. Phys. **67**, 107 (2004) [hep-ph/0310204].
- [19] J. Schechter and J.W.F. Valle, Phys. Rev. **D22**, 2227 (1980); J. Schechter and J.W.F. Valle, Phys. Rev. **D25**, 774 (1982); A. Mendez and F.I. Olness, Int. J. Mod. Phys. **A2**, 1085 (1987); J.F. Gunion, J. Grifols, A. Mendez, B. Kayser and F.I. Olness, Phys. Rev. **D40**, 1546 (1989); N.G. Deshpande, J.F. Gunion, B. Kayser and F.I. Olness, Phys. Rev. **D44**, 837 (1991); E. Ma, Phys. Rev. Lett. **81**, 1171 (1998); P.Q. Hung, Phys. Lett. **B649**, 275 (2007) [arXiv:0612004 [hep-ph]]; A. Hektor, M. Kadastik, M. Muntel, M. Raidal and L. Rebane, Nucl. Phys. **B787**, 198 (2007) [arXiv:0705.1495 [hep-ph]]; T. Han, B. Mukhopadhyaya, Z. Si and K. Wang, Phys. Rev. **D76**, 075013 (2007) [arXiv:0706.0441 [hep-ph]].
- [20] For introductory reviews see, for example, H. P. Nilles, Phys. Rept. **110**, 1 (1984); J. Wess and J. Bagger, *Supersymmetry and Supergravity*, (Princeton Univ. Press, 1992). P.C. West, *Introduction to Supersymmetry and Supergravity*, (World Scientific, 1990); D. Bailin and A. Love, *Supersymmetric Gauge Field Theory and String Theory*, (Institute of Physics Publishing, 1994); M. Drees, R. Godbole and P. Roy, *Theory and Phenomenology of Sparticles*, (World Scientific, 2004); H. Baer and X. Tata *Weak Scale Supersymmetry From Superfields to Scattering Events*, (Cambridge University Press, 2006).
- [21] For reviews see, for example, H. E. Haber and G. L. Kane, Phys. Rept. **117**, 75 (1985); *Perspectives on Supersymmetry* by G. Kane(ed), (World Scientific, 1998) and articles therein; M. Drees and S.P. Martin, [hep-ph/9504324]; M. Drees, arXiv:hep-ph/9611409; J.D. Lykken, TASI-96 lectures, [hep-

- th/9612114]; S. P. Martin, arXiv:hep-ph/9709356, and references therein; J.F. Gunion, [hep-ph/9704349], M. E. Peskin, arXiv:0801.1928 [hep-ph].
- [22] I. Antoniadis, Phys. Lett. B **246**, 377 (1990); I. Antoniadis, N. Arkani-Hamed, S. Dimopoulos and G. R. Dvali, Phys. Lett. B **436**, 257 (1998) [arXiv:hep-ph/9804398]; N. Arkani-Hamed, S. Dimopoulos and G. R. Dvali, Phys. Lett. B **429**, 263 (1998) [arXiv:hep-ph/9803315]; T. Han, J. D. Lykken and R. J. Zhang, Phys. Rev. D **59**, 105006 (1999) [arXiv:hep-ph/9811350].
- [23] L. Randall and R. Sundrum, Phys. Rev. Lett. **83**, 4690 (1999) [arXiv:hep-th/9906064].
- [24] T. Appelquist, H. C. Cheng and B. A. Dobrescu, Phys. Rev. D **64**, 035002 (2001) [arXiv:hep-ph/0012100].
- [25] N. Arkani-Hamed, A. G. Cohen and H. Georgi, Phys. Lett. B **513**, 232 (2001) [arXiv:hep-ph/0105239]; N. Arkani-Hamed, A. G. Cohen, T. Gregoire and J. G. Wacker, JHEP **0208**, 020 (2002) [arXiv:hep-ph/0202089]; T. Han, H. E. Logan, B. McElrath and L. T. Wang, Phys. Rev. D **67**, 095004 (2003) [arXiv:hep-ph/0301040].
- [26] For reviews, see M. Schmaltz and D. Tucker-Smith, Ann. Rev. Nucl. Part. Sci. **55**, 229 (2005); M. Perelstein, Prog. Part. Nucl. Phys. **58**, 247 (2007); M. C. Chen, Mod. Phys. Lett. A **21**, 621 (2006); E. Accomando *et al.*, hep-ph/0608079, Chapter 7.

Chapter 2

The Large Hadron Collider

2.1 Basic Notions

The search for the laws of nature at high energy means the search for physics at very small distance scales. Hence, high energy accelerators and colliders are indispensable in testing a theory of particle physics. For the past several decades, high energy accelerators and colliders have been our primary tool for unravelling physics at the sub-nuclear level. In this chapter, we discuss the basic notions of the on-going LHC experiment, its running schedule as of now, important aspects of its different detectors and the physics goal.

The basic principle of particle accelerators is to use electric fields to propel electrically-charged particles to high speeds and to collide them. There are two basic types of accelerators: fixed target and colliding beam. The centre-of-mass energy achieved in a fixed target experiment ($\simeq \sqrt{2E_1m_2}$ where E_1 is the beam energy, m_2 is the target mass, assuming $m_1 \ll E_1, m_2$) is much less than the one in a colliding beam ($\simeq \sqrt{4E_1E_2}$ where E_1 and E_2 are the beam energies and $E \gg m$) with similar beam energy. This is the reason why colliding beam experiments are much more popular. The disadvantage of the colliding beam experiments over the fixed target ones is in achieving high luminosity, or event rate. The colliders can also be of two types: linear accelerator and storage ring. A

linear accelerator (often described as 'linac') is the one that considerably increases the velocity of charged particles by subjecting them to a series of oscillating electric potentials along a linear beamline. A storage ring, on the other hand, is a type of circular accelerator in which a continuous or pulsed particle beam may be kept circulating for a long period of time. An Electric field is used to accelerate them while a magnetic field is used to rotate them in a synchronised way. The main disadvantages of a linear collider is the device length, which limits the locations. Also a large number of driver devices and their associated power supplies are required, increasing the construction and maintenance expense. On the other hand, synchrotron radiation loss is the main obstacle for the circular accelerators, especially when the energy is high and one has a light particle like electron to accelerate. Examples of linear accelerators are the Stanford Linear Collider (SLC) or the proposed International Linear collider (ILC). Examples of circular accelerators are, Large Electron Positron collider (LEP) at CERN, the Fermilab Tevatron and the Large Hadron Collider (LHC) [1].

Stable particles are good candidates for serving as the colliding beams. Thus one uses electrons, positrons, protons and also anti protons. They are electrically charged so that they can be accelerated by electric field, and are stable so that they can be put in a storage ring for reuse to increase luminosity. But, they have their own advantage and disadvantages. The advantages and disadvantages of e^+e^- colliders are as follows:

- The environment is clean as the hard scattering takes place via electroweak interaction. The SM processes are predictable without large uncertainties of strong interaction.
- With symmetric beams between the electrons and positrons, the laboratory frame is the same as the centre of mass frame, so that the total centre-of-mass energy is fully exploited to reach the highest possible physics threshold.
- With well-understood beam properties, the scattering kinematics can be studied in both longitudinal and transverse directions.
- It is possible to achieve high degrees of beam polarizations, so that chiral couplings and other asymmetries can be effectively explored.
- One major disadvantage is the very high synchrotron radiation ($1/m^4$ per cycle in a storage ring) as the electron mass is small.

- It is difficult to achieve high centre-of-mass energy with light electron mass.
- When performing realistic simulations for high energy e^+e^- reactions at high luminosities, the beamstrahlung effects on the luminosity and the centre-of-mass energy become substantial.

On the other hand, hadron colliders have the following broad features:

- Due to the larger mass of the proton, hadron colliders can provide much higher centre of mass energies in head-on collisions.
- Protons participate in strong interactions and thus hadronic reactions yield larger cross sections. Also with many quarks (valence as well as sea) and gluons participating in hard scattering, diverse types of events are possible. At higher energies, many possible channels open up for resonant productions with different charge and spin as induced by different initial parton combinations (such as $q\bar{q}$, qg , and gg).
- One of the major disadvantages of hadron colliders is the absence of the knowledge of sub-process or partonic centre of mass energy.
- The environment is less clean. Backgrounds, particularly those from strong interaction, are a serious problem.
- A large number of underlying and pile-up events are expected.
- Strong dependence on the parton distribution functions and renormalisation and factorisation scale for processes calculated at the leading order makes it difficult to predict the cross-sections for different processes unambiguously.

In a nutshell, hadron collider is important as a discovery machine for its higher energy reach while the electron-positron collider is more favourable for precision measurements. The Large Hadron Collider is proton-proton collider operating at CERN in Geneva, Switzerland. The LHC is a circular tunnel with a circumference almost of 27 kilometers, at a depth ranging from 50 to 175 meters underground. The tunnel has been used for the LEP, an electron-positron collider. The collider tunnel contains two pipes, each one containing a proton beam enclosed within superconducting magnets cooled by liquid helium. Additional magnets are used to direct the beams towards four intersection points where the interactions take place.

The present LHC schedule is as follows: It is now running with a centre-of-

mass energy $E_{cm} = 7$ TeV and the integrated luminosity at this energy is expected to pile up to several hundreds of pb^{-1} , or close to $1 fb^{-1}$. A long shutdown at the end of 2011 is scheduled for up gradation of the centre-of-mass energy and luminosity. It is expected that, when it reopens, it will directly start running at the $E_{cm} = 14$ TeV.

The LHC can also be used to collide heavy ions such as lead (Pb) with a centre-of-mass energy of 2.76 TeV. The ions will be first accelerated by the linear accelerator Linac 3, and the Low-Energy Injector Ring (LEIR) will be used as an ion storage and cooler unit. The ions are then further accelerated by the Proton Synchrotron (PS) and Super Proton Synchrotron (SPS).

Six detectors are being constructed at the LHC. ATLAS and CMS are large, "general purpose" particle detectors. The other detectors, namely, ALICE, LHCb, TOTEM AND LHCf are smaller in size and more specialized in purpose.

ATLAS (A Toroidal LHC Apparatus)

ATLAS [2] is the bigger one of the two 'general-purpose' detectors at the LHC. It is designed to investigate a wide range of physics, including the search for the Higgs boson, extra dimensions, and particles that could make up dark matter.

CMS (Compact Muon Solenoid)

The CMS detector [3] has a similar 'general purpose' goal as the ATLAS experiment. However, it uses different technical solutions and design of its detector magnet system to achieve these.

ALICE (A Large Ion Collision Experiment)

In ALICE experiment [4], lead ions are collided to study a state of matter known as quark gluon plasma (QGP), which is believed to have existed soon after the Big Bang.

LHCb (Large Hadron Collider beauty)

The LHCb experiment [5] will help to understand the properties of heavy flavours and gain further insight into the phenomenon of CP- violation, by studying the 'bottom (beauty) quark' or 'b-quark'.

TOTEM (TOTAl Elastic and diffractive cross section Measurement)

The TOTEM experiment [6] studies forward particles to focus on physics that is not accessible to the general-purpose experiments. Among a range of stud-

ies, it will measure, in effect, the size of the proton and also monitor accurately the LHC's luminosity.

LHCf (Large Hadron Collider forward)

The forward particles created inside the LHC are used as a source to simulate cosmic rays in laboratory conditions in LHCf experiment [7]. It allows one to study how collisions inside the LHC cause cascades of particles similar to what we observe, due to collision of cosmic rays with nuclei in the atmosphere. This in turn, enables one to interpret and calibrate large-scale cosmic-ray experiments that can cover thousands of kilometers.

Next, we discuss some features of the ATLAS and CMS detectors as these are likely to address broad issues on the SM and also look for various signals of new physics.

2.2 The ATLAS detector

The basic design criterion of the ATLAS detector is as follows [8]:

- Very good electromagnetic (EM) calorimetry for e^\pm and γ identification and mass measurements, complemented by full coverage of hadronic calorimetry for accurate jets and missing transverse energy \cancel{E}_T measurements.
- High-precision muon momentum measurements, with the capability to guarantee accurate measurements at the highest luminosity using the external muon spectrometer alone.
- Efficient tracking at high luminosity for high- p_T lepton momentum measurements. electron and photon identification, τ -lepton and heavy flavor identification, and full event reconstruction capability at lower luminosity.
- Large acceptance of pseudo-rapidity (η) with almost full azimuthal angle (ϕ) coverage.
- Triggering and measurements of particles at low- p_T thresholds, providing high efficiencies for most physics processes.

Broadly, various layers of the detectors contain the following components:

1. Superconducting magnet system

It is an arrangement of a central solenoid (CS) providing the inner detector with magnetic field, surrounded by a system of three large air-core toroids

generating the magnetic field for the muon spectrometer. The CS provides a central field of 2 Tesla with a peak magnetic field of 2.6 Tesla at the superconductor itself. The magnets are kept cooled at the liquid helium temperature. The CS and EM calorimeter are kept in such a way that they later achieve a desired performance.

2. Inner detector

This combines several high energy detectors and is contained in the CS. These detectors provide very high precision momentum and vertex resolution using the silicon micro-strip and pixel technologies. A large number of tracking points (about 36 per track) are provided by the straw tube trackers.

3. Calorimeters

An EM calorimeter with $|\eta| < 3.2$, a hadronic barrel calorimeter with $|\eta| < 1.7$, hadronic end cap calorimeters with $1.5 < |\eta| < 3.2$ and forward calorimeters with $3.1 < |\eta| < 4.9$ are employed. ATLAS uses an iron/scintillator system to provide the hadronic calorimetry in the central part of the detector.

4. Muon Spectrometer

This surrounds the calorimeters. Its large superconducting air-core toroid system with a long barrel and two inserted end-cap magnets, generate a large magnetic field with a strong bending power which deflects the muon tracks.

2.3 The CMS detector

As the name suggests, it is compact compared to the ATLAS detector and its central focus is on observing muons more precisely. The main distinctive features of the CMS detector are as follows [9]:

- The central solenoid provides two times larger (4 Tesla) magnetic field compared to the ATLAS central solenoid.
- The inner detector uses only silicon-based (pixels and strip) inner tracking system i.e. it does not use the straw trackers.
- CMS uses a scintillating crystal EM calorimeter and a compact scintillator/brass hadron calorimeter and in contrast with ATLAS which has liquid-

argon technology for the EM measurements. The hadron calorimeters of both experiments are similar in constitution.

- An iron-core muon spectrometer is used in CMS whereas in ATLAS, it is gas filled.

2.4 Physics at the LHC

As discussed in detail in the introduction, the search for the Higgs boson is one of the primary goals of LHC. Without this the SM is really incomplete. It is expected that if there is a Higgs boson within the perturbative regime, it will be discovered at the LHC. Electroweak precision data, including recent results from the Tevatron, indicate that the Higgs boson (if it has properties predicted in the SM) should lie in the mass range 115 GeV to 148 GeV with 90% confidence level. This range, especially at the lower end, poses strong challenge in Higgs detection. This is because the Higgs then may have to be looked for in the diphoton channel. Including other motivations, the physics goals of LHC are as follows:

- To discover the Higgs boson and complete the SM.
- To know more about the top quark.
- To understand strong interaction better.
- To study B-hadrons better.
- To look for quark-gluon-plasma.
- To look for physics beyond the SM.

Among different proposals beyond the SM, following are the most important ones which have a possibility of getting discovered at the LHC [9, 10].

- Supersymmetry (SUSY) with different kinds of particle spectra and phenomenology, depending on the SUSY breaking schemes and also on additional symmetry principles underlying the scenario [10, 11].
- Little Higgs models, which proposes that the Higgs is a pseudo Goldstone boson of a broken global symmetry [10, 12, 13].
- Extra dimensional scenarios such as, flat extra dimensions, warped extra-dimension and Universal extra-dimension [14–16].
- Composite models and additional resonances.

As mentioned in the introduction, many of these models with discrete Z_2 symmetry predicts the existence of a stable particle, which can serve as a weakly interacting massive particle and contribute to cold dark matter relic density. Search for dark matter is thus an important aspect of the LHC experiment.

2.5 Some technical details

In this section, we discuss the main physics issues related to a hadron collider machine, namely the general expression for the cross-section related to a parton level process, the relation between the laboratory frame and the partonic reference frame, variables that are longitudinal boost invariant and hence relevant in a hadron collider machine. We also discuss very briefly the issues regarding the formation of jets, effects of initial state radiation and final state radiation (ISR and FSR), multiple interactions and underlying events [1].

As we know, protons are composite particles constituted of quarks and gluons ('parton's in general), the most important issue regarding the computation of a process in a proton proton collision is to relate the parton level cross-section to the hadron level process. The parton-level hard scattering cross section can easily be calculated perturbatively in QCD. Thanks to the assumptions on factorization, the high energy hadronic reactions with a large momentum transfer can be factorised into a parton-level "hard scattering" process convoluted with the parton "distribution functions". For example, the cross-section related to the scattering of two hadrons A and B to produce a final state F of our interest, can be written as a sum over the sub-process cross sections from the contributing partons

$$\sigma(AB \rightarrow F X) = \sum_{a,b} \int dx_1 dx_2 P_{a/A}(x_1, Q^2) P_{b/B}(x_2, Q^2) \hat{\sigma}(ab \rightarrow F), \quad (2.1)$$

where X is the inclusive scattering remnant, and Q^2 is the factorization scale (the typical momentum transfer) in the parton-level hard scattering process $\hat{\sigma}(ab \rightarrow F)$. Equation (2.1) is valid when Q^2 is much larger than $\Lambda_{QCD}^2 (\simeq (200 \text{ MeV})^2)$. Parton distribution functions $P(x, Q^2)$ parametrise the non-perturbative aspect and can be only obtained by some ansatz and by fitting the data. The variable $x_{1/2}$ denotes the energy fraction with which the partons collide and it is integrated over all possible values. Parton distribution functions are used in various

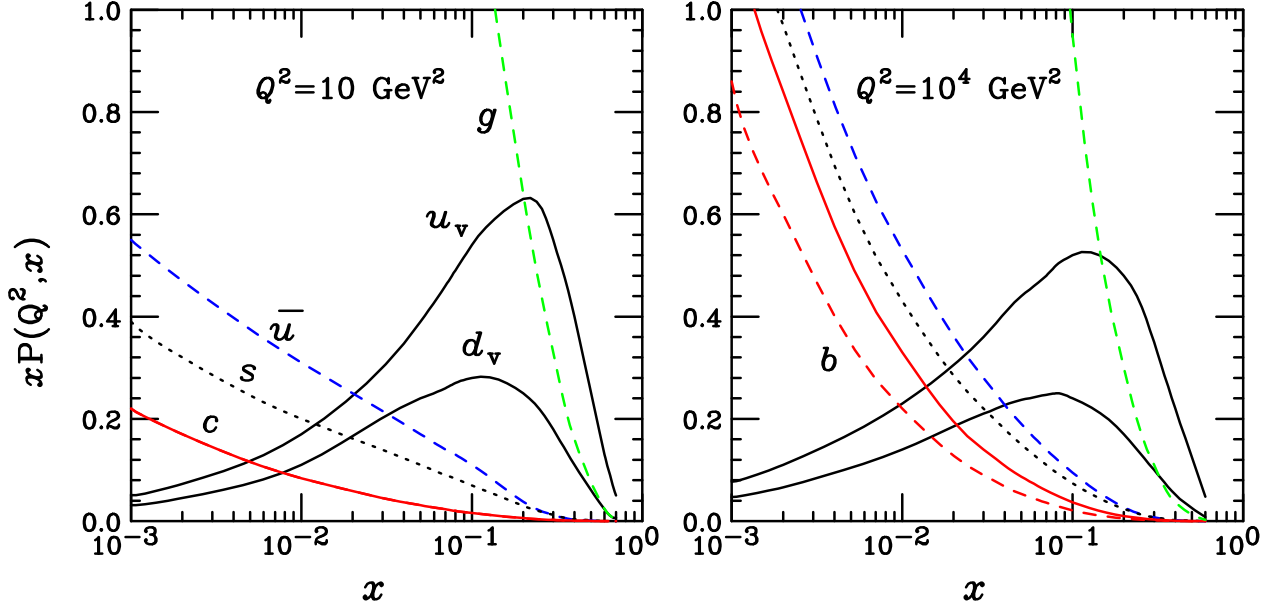


Figure 2.1: Parton momentum distributions versus their energy fraction x at two different factorization scales, from CTEQ-5. Taken from T.Han in [1]

parametrisations [17] and are available at the leading or next to leading order. Figure 2.1 shows the parton momentum distributions versus the energy fraction x for two different Q^2 . The valence quarks u_v, d_v , as well as the gluons carry a large proportion of proton momentum. The 'sea quarks' ($\bar{u} = u_{sea}, \bar{d} = d_{sea}, s, c, b$) have small x , and are significantly enhanced at higher Q^2 [18].

In the parton-level hard scattering process $\hat{\sigma}(ab \rightarrow F)$ for hadronic collisions like in Equation (2.1), the partonic centre-of-mass frame is not the same as the hadronic centre-of-mass frame, the laboratory frame for the collider. Consider a collision between two hadrons A and B with four-momenta $P_A = (E_A, 0, 0, p_A)$ and $P_B = (E_A, 0, 0, -p_A)$ in the laboratory frame. The two partons participating the subprocess have momenta $p_1 = x_1 P_A$ and $p_2 = x_2 P_B$.

The parton system thus moves in the laboratory frame with a four-momentum

$$P_{cm} = [(x_1 + x_2)E_A, 0, 0, (x_1 - x_2)p_A] \quad (E_A \approx p_A), \quad (2.2)$$

or with a speed $\beta_{cm} = (x_1 - x_2)/(x_1 + x_2)$, or with a rapidity

$$y_{cm} = \frac{1}{2} \ln \frac{x_1}{x_2}. \quad (2.3)$$

The total hadronic centre-of-mass energy is $S = 4E_A^2$. If the partonic centre-

of-mass energy is denoted by s , we can write

$$s \equiv \tau S, \quad \tau = x_1 x_2 = \frac{s}{S}. \quad (2.4)$$

The partonic energy fractions are then given by

$$x_{1,2} = \sqrt{\tau} e^{\pm y_{cm}}. \quad (2.5)$$

One always encounters the integration over the energy fractions as in Equation (2.1).

With this variable change, one has

$$\int_{\tau_0}^1 dx_1 \int_{\tau_0/x_1}^1 dx_2 = \int_{\tau_0}^1 d\tau \int_{\frac{1}{2} \ln \tau}^{-\frac{1}{2} \ln \tau} dy_{cm}. \quad (2.6)$$

The variable τ characterizes the (invariant) mass of the reaction, with $\tau_0 = m_{res}^2/S$ and m_{res} is the threshold for the parton level final state (sum over the masses in the final state); while y_{cm} specifies the longitudinal boost of the partonic centre-of-mass frame with respect to the laboratory frame. $\tau - y_{cm}$ variables are better for numerical evaluations as they are invariant under unknown longitudinal boosts. Since the relative motion between the parton centre-of-mass frame and the laboratory frame is along the beam direction (\vec{z}), variables involving only the transverse components are invariant under longitudinal boosts. It is thus convenient to write the phase space element in the cylindrical coordinate as

$$\frac{d^3 \vec{p}}{E} = dp_x dp_y \frac{dp_z}{E} = p_T dp_T d\phi \frac{dp_z}{E}, \quad (2.7)$$

where ϕ is the azimuthal angle about the \vec{z} axis, and

$$p_T = \sqrt{p_x^2 + p_y^2} = p \sin \theta \quad (2.8)$$

is the transverse momentum. Both p_T and ϕ are boost-invariant, so is dp_z/E .

The rapidity of a particle of momentum $p^\mu = (E, \vec{p})$ is defined to be

$$y = \frac{1}{2} \ln \frac{E + p_z}{E - p_z}. \quad (2.9)$$

One can also show that a particle four-momentum can be rewritten as

$$p^\mu = (E_T \cosh y, p_T \sin \phi, p_T \cos \phi, E_T \sinh y), \quad E_T = \sqrt{p_T^2 + m^2}. \quad (2.10)$$

The phase space element then can be expressed as

$$\frac{d^3 \vec{p}}{E} = p_T dp_T d\phi dy = E_T dE_T d\phi dy. \quad (2.11)$$

Consider the rapidity in a boosted frame (say the parton centre-of-mass frame), and perform the Lorentz transformation,

$$y' = \frac{1}{2} \ln \frac{E' + p'_z}{E' - p'_z} = \frac{1}{2} \ln \frac{(1 - \beta_0)(E + p_z)}{(1 + \beta_0)(E - p_z)} = y - y_0. \quad (2.12)$$

In the massless limit, $E \approx |\vec{p}|$, so that

$$y \rightarrow \frac{1}{2} \ln \frac{1 + \cos \theta}{1 - \cos \theta} = \ln \cot \frac{\theta}{2} \equiv \eta, \quad (2.13)$$

where η is the pseudo-rapidity, which has one-to-one correspondence with the scattering polar angle $\pi \geq \theta \geq 0$ for $-\infty < \eta < \infty$.

Since y as well as η is additive under longitudinal boosts as seen in Eq. (2.12), the rapidity difference $\Delta y = y_2 - y_1 = y'_2 - y'_1$ is invariant in the two frames. Thus the shape of rapidity distributions $d\sigma/dy$ in the two frames would remain the same if the boost is by a constant velocity. Another important variable in the azimuthal-pseudorapidity plane is the separation defined as

$$\Delta R = \sqrt{\Delta\eta^2 + \Delta\phi^2}. \quad (2.14)$$

As a quantitative illustration, for two objects back-to-back in the central region, typically $\Delta\eta < \Delta\phi$ and $\Delta R \approx \Delta\phi \sim \pi$.

Due to $SU(3)$ interaction of the partons, the quarks and gluons that are produced in a partonic subprocess can not exist in isolation due to colour confinement, and are showered using fragmentation functions to form the bound states like baryons and mesons. This has no unambiguous prescription. The most popular model used in this connection is the Lund string model. This process is also called hadronisation. The Parton Shower (PS) Monte Carlo programs such as Pythia [19] and Herwig [20] describe parton radiation as successive parton emissions using Markov chain techniques based on Sudakov form factors. This description is formally correct only in the limit of soft and collinear emissions, but has been shown to give a good description elsewhere. However, for the production of hard and widely separated QCD radiation jets, this description breaks down. For that case, it is necessary to use the full tree-level amplitudes for the heavy particle production plus additional hard partons. Additional contribution from initial state radiation (ISR) and final state radiation (FSR) emitting extra gluon or photon is also important in context of the Large Hadron Collider. Figure (2.2) shows the outcome of a typical collision, with all complicated particle emissions, that it may entail.

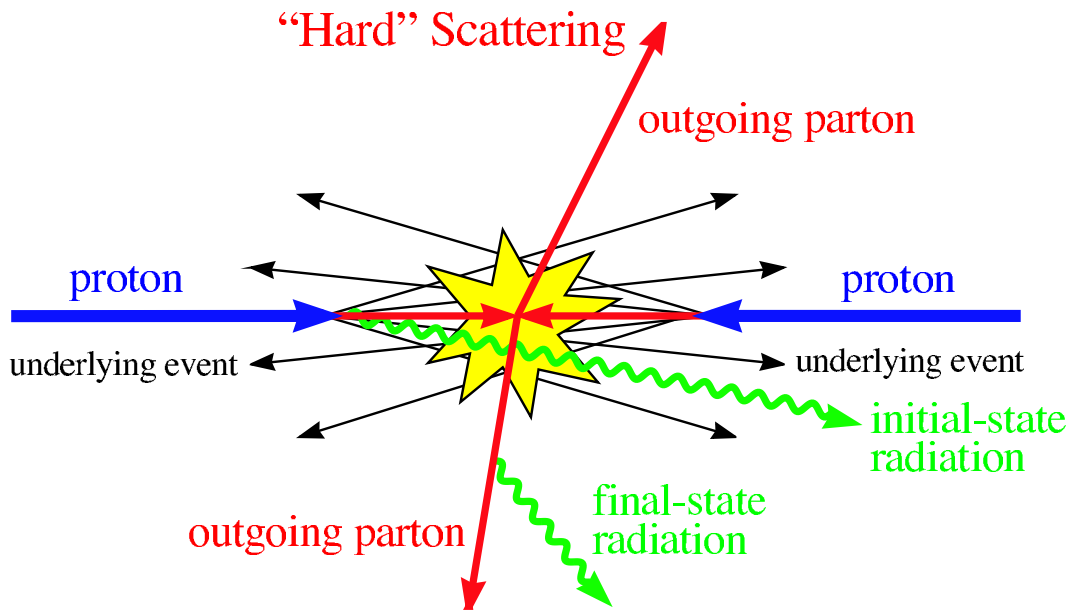


Figure 2.2: An illustrative event in hadronic collisions. Taken from T.Han in reference [1]

Once the partons are hadronised, they are clustered together to form jets. This is specifically parametrised for the detector used to identify them. Jets are usually identified at the Hadron Calorimeter (HCAL) as mentioned earlier. Cone-jet algorithm is one of the most popular models used in this purpose, while the k_T or anti- k_T formalisms are being used very recently. The basic principle however, remains the same. A hadron with p_T greater than some threshold value (specific to the detector, > 5 GeV for ATLAS) is identified as a jet initiator. Within a cone of certain ΔR (< 0.4) around this, all the hadrons are clubbed to form a jet and the accumulated transverse momentum should be more than a $(p_T)_{thresh}$ ($\simeq 20$ GeV for ATLAS) to register as a jet in HCAL. Instead of a threshold value of p_T or ΔR in a cone-jet algorithm, a k_T value is used for k_T or anti- k_T jet algorithm. Validity of these different jet formation and showering prescriptions have been tested and is under further scrutiny from the Tevatron data. It is expected to work well for LHC as well. However, to what extent this suffices to describe the real physics at LHC, can only be known after studying the available data carefully.

Bibliography

- [1] See for review, the book by V. Berger and J. N. Phillips, '*Collider Physics*', Addison-Wesley Pub. Co.(1987); T. Han, arXiv:hep-ph/0508097.
- [2] ATLAS Technical proposal, CERN/LHCC/94-43.
- [3] CMS Technical proposal, CERN/LHCC/94-38.
- [4] ALICE Technical Proposal, CERN/LHCC/95-71.
- [5] LHCb Technical Proposal, CERN-LHCC-98-04.
- [6] TOTEM Technical Proposal, CERN/LHCC/99-07.
- [7] LHCf Technical Proposal, CERN-LHCC-05-32.
- [8] ATLAS: Detector and physics performance technical design report, Volume 1.
- [9] G. L. Bayatian *et al.* [CMS Collaboration], CMS physics: Technical design report.
- [10] ATLAS: Detector and physics performance technical design report, Volume 2.
- [11] I. Hinchliffe *et al.*, Phys. Rev. D **55** (1997) 5520; S. Abdullin *et al.*, J. Phys. G **28** (2002) 469; D. Denegri, Nuovo Cim. B **120** (2005) 687; A. V. Gladyshev, D. I. Kazakov, hep-ph/0606288 (2006); M. Della Negra *et al.*, CERN-LHCC-2006-021 (2006); R. Kitano, Y. Nomura, Phys. Rev. D **73** (2006) 095004.
- [12] N. Arkani-Hamed, A. G. Cohen and H. Georgi, Phys. Lett. B **513**, 232 (2001) [arXiv:hep-ph/0105239]; N. Arkani-Hamed, A. G. Cohen, T. Gregoire and J. G. Wacker, JHEP **0208**, 020 (2002) [arXiv:hep-ph/0202089]; T. Han, H. E. Logan, B. McElrath and L. T. Wang, Phys. Rev. D **67**, 095004 (2003) [arXiv:hep-ph/0301040].

- [13] For reviews, see M. Schmaltz and D. Tucker-Smith, *Ann. Rev. Nucl. Part. Sci.* **55**, 229 (2005); M. Perelstein, *Prog. Part. Nucl. Phys.* **58**, 247 (2007); M. C. Chen, *Mod. Phys. Lett. A* **21**, 621 (2006); E. Accomando *et al.*, hep-ph/0608079, Chapter 7.
- [14] I. Antoniadis, *Phys. Lett. B* **246**, 377 (1990); I. Antoniadis, N. Arkani-Hamed, S. Dimopoulos and G. R. Dvali, *Phys. Lett. B* **436**, 257 (1998) [arXiv:hep-ph/9804398]; N. Arkani-Hamed, S. Dimopoulos and G. R. Dvali, *Phys. Lett. B* **429**, 263 (1998) [arXiv:hep-ph/9803315]; T. Han, J. D. Lykken and R. J. Zhang, *Phys. Rev. D* **59**, 105006 (1999) [arXiv:hep-ph/9811350].
- [15] L. Randall and R. Sundrum, *Phys. Rev. Lett.* **83**, 4690 (1999) [arXiv:hep-th/9906064].
- [16] T. Appelquist, H. C. Cheng and B. A. Dobrescu, *Phys. Rev. D* **64**, 035002 (2001) [arXiv:hep-ph/0012100].
- [17] H. L. Lai *et al.* [CTEQ Collaboration], *Eur. Phys. J. C* **12**, 375 (2000) [arXiv:hep-ph/9903282].
- [18] See for example, R.K. Ellis, W.J. Stirling, and B.R. Webber, *QCD and Collider Physics*, Cambridge University Press (1996).
- [19] T. Sjostrand, S. Mrenna and P. Skands, *JHEP* **0605**, 026 (2006) [arXiv:hep-ph/0603175].
- [20] G. Corcella *et al.*, *JHEP* **0101**, 010 (2001) [arXiv:hep-ph/0011363].

Chapter 3

Supersymmetry and its signals: basic features

3.1 Motivation

Clearly, the issues mentioned in Chapter 1 point towards the existence of some new (TeV scale) physics beyond the standard model (BSM). A lot of alternatives have been suggested over the past several decades among which supersymmetry (SUSY) [1,2] stands out as one of the most popular ones.

The primary motivation of a SUSY theory is to address the hierarchy problem connected with the stability of SM Higgs mass. SUSY introduces a boson corresponding to every known fermion and vice versa. These bring in additional loop diagrams contributing to the Higgs mass correction and controls the otherwise unwieldy divergences. For example, in Figure 3.1a we have a correction to m_H^2 from a loop containing a Dirac fermion f with mass m_f .

The correction yields a quadratic divergence which needs unnatural fine tuning [3] to yield a Higgs mass around $\simeq 100$ GeV as also mentioned in Chapter 1.

$$\Delta m_H^2 = -\frac{|\lambda_f|^2}{8\pi^2} \Lambda_{UV}^2 + \dots \quad (3.1)$$

If there is a complex scalar field S that couples to the Higgs as $-\lambda_S |H|^2 |S|^2$

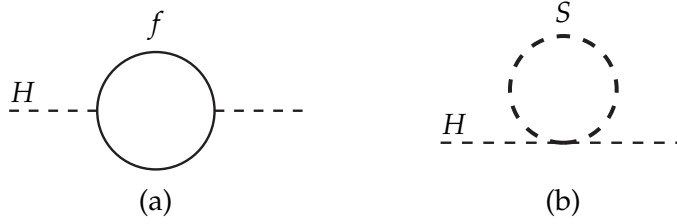


Figure 3.1: One-loop quantum corrections to the Higgs squared mass parameter m_H^2 , due to (a) a Dirac fermion f , and (b) a scalar S . . Taken from S.P. Martin in [2].

(Figure 3.1b), one-loop contribution (with mass m_S) also yields a quadratic divergence, but with a relative negative sign compared to the fermionic contribution.

$$\Delta m_H^2 = \frac{\lambda_S}{16\pi^2} [\Lambda_{UV}^2 - 2m_S^2 \ln(\Lambda_{UV}/m_S) + \dots]. \quad (3.2)$$

Equations (3.1) and (3.2) strongly suggest that a symmetry relating the fermions and bosons, cancels the quadratic divergence in the calculation of Δm_H^2 (Note that λ_S must be positive if the scalar potential has to be bounded from below.). If each of the quarks and leptons of the Standard Model is accompanied by two complex scalars with $\lambda_S = |\lambda_f|^2$, then the Λ_{UV}^2 contributions of Figures 3.1a and 3.1b cancel. This is what is achieved with supersymmetry [4].

Another strong theoretical issue is to look for models where all the fundamental forces (i.e the gauge couplings) unify. This is referred to as Grand Unified Theory (GUT) [5]. According to the hypothesis of GUT, the strong, weak and electromagnetic interactions are unified to a single interaction associated with a simple gauge group at high energy, which includes $SU(3)_c \otimes SU(2)_L \otimes U(1)_Y$ as subgroups. $SU(5)$ or $SO(10)$ stands as the most popular unifying groups. However, this is difficult to achieve within the SM framework. The renormalisation group equations (RGE) at one-loop, describing the evolution of the gauge coupling parameters with energy, fail to unify them at a high energy with β functions (b_i s) calculated in SM.

$$\frac{1}{\alpha_i(Q^2)} = \frac{1}{\alpha_i(\mu^2)} - b_i \log\left(\frac{Q^2}{\mu^2}\right), \quad (3.3)$$

where Q is any scale where we evaluate the values of α_i and μ is the reference scale, usually taken at electroweak scale. Index i refers to the gauge groups $U(1)_Y$, $SU(2)_L$ and $SU(3)_C$ respectively, and for the SM one has $b_i = (41/10, -19/6, -7)$. This is shown in the left part of Figure 3.3 [6], where the evolution of

Unification of the Coupling Constants in the SM and the MSSM

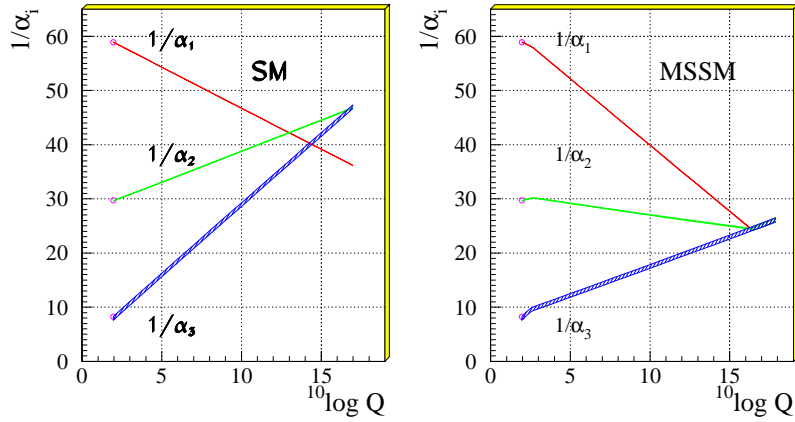


Figure 3.2: Evolution of the inverse gauge couplings in the SM (left) and in the MSSM (right). Taken from [6].

the inverse couplings is shown as functions of energy. The slopes of RG curves change with the introduction of SUSY which provide new thresholds at the TeV scale. For the minimal supersymmetric extension of the SM (MSSM) one has, $b_i = (33/5, 1, -3)$ and one achieves unification at a scale $\simeq 10^{16}$ GeV as shown in the right part of Figure 3.3 [7]. Fitting the curves one can also get the scale of SUSY breaking parameters $M_{SUSY} \sim 1$ TeV. This is another motivation for SUSY to become a popular model beyond the SM.

The understanding of existence of dark (non-luminous) matter in the universe and the failure to have a suitable candidate for the same within the SM is another important issue which prompts one to look for theories beyond SM. As has already been mentioned, visible matter constitutes only a small part of the energy density of the universe; and there has to be a significant amount of non-baryonic or *dark matter* (DM) contributing to the energy density. A direct indication on the existence of dark matter comes from rotation curves of spiral galaxies [8]. The rotational velocity v of an object on a stable Keplerian orbit with radius r around a galaxy scales like $v(r) \propto \sqrt{M(r)/r}$ where $M(r)$ is the mass inside the orbit. If r lies outside the visible part of the galaxy, then one would expect $v(r) \propto \sqrt{1/r}$. Instead, in most galaxies one finds that v is constant out to the largest values of

r , where the rotation curve can be measured. To explain these curves one usually assumes the existence of a galactic halo consisting of non-luminous matter which takes part in gravitational interaction.

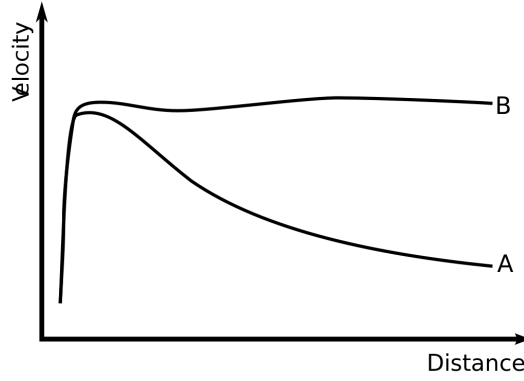


Figure 3.3: *Rotation curve of a typical spiral galaxy: predicted (A) and observed (B). The discrepancy between the curves is attributed to dark matter. Taken from <http://www.wikipedia.org>.*

According to recent data, for example, using measurements of the anisotropy of the cosmic microwave background radiation (CMBR) [9], the energy content of the Universe is the following:

$$\Omega_{total}h^2 = 1.02 \pm 0.02$$

$$\Omega_{vacuum}h^2 = 0.73 \pm 0.04, \quad \Omega_{dark-matter}h^2 = 0.23 \pm 0.04, \quad \Omega_{baryon}h^2 = 0.044 \pm 0.004\%$$

where Ω is the cosmological density parameter defined as the energy density relative to the critical density and h is the Hubble constant in units of 100 km/(s.Mpc). Hence, dark matter makes up a considerable part exceeding the visible baryonic matter by almost an order of magnitude. There are two possible kinds of non-baryonic Dark matter: hot DM, consisting of light relativistic particles, and cold DM, consisting of weakly interacting massive particles (WIMPs). Existence of warm dark matter (WDM) has also been postulated having properties intermediate between cold and hot dark matter. Sterile neutrinos and gravitinos are the most common WDM candidates. In general, candidates for non-baryonic DM must satisfy several conditions: they must be stable on cosmological time scale (otherwise they would have decayed by now), they must interact very weakly with electromagnetic radiation (otherwise they do not qualify as dark matter) and

they must have the right relic density [10]. Hot DM might consist of neutrinos; however, this is problematic from the point of view of large structure formation in the Universe as well as the anisotropy in CMBR.

Very recent studies of the Bullet cluster (1E 0657-56), announced in August 2006, provide a strong evidence to date for the existence of dark matter. At a statistical significance of 8σ , it was found that the spatial offset of the center of the total mass from the center of the baryonic mass peaks can not be explained with an alteration of the gravitational force law [11]. The major components of the cluster pair viz., stars, gas and the putative dark matter, behave differently during collision, allowing them to be studied separately. The stars of the galaxies, observable in visible light, were not greatly affected by the collision, gravitationally slowed but not otherwise altered. The hot gas of the two colliding components, seen in X-rays, represents most of the mass of the ordinary (baryonic) matter in the cluster pair. The gases interact electromagnetically, causing the gases of both clusters to slow much more than the stars. The third component, the dark matter, was detected indirectly by the gravitational lensing of background objects. In theories without dark matter, such as Modified Newtonian Dynamics (MOND), the lensing would be expected to follow the baryonic matter; i.e. the X-ray gas. However, the lensing is strongest in two separated regions near the visible galaxies. This provides support for the idea that most of the mass in the cluster pair is in the form of collisionless dark matter. Also, the wide spread in dark matter distribution, as visible from lensing effects, disfavours its baryonic character.

As for the cold DM, WIMPs need to have mass roughly between 10 GeV and a few TeV and in the SM there is no appropriate particle. Supersymmetry provides a candidate for the cold dark matter, namely the lightest supersymmetric particle (LSP) [12], which remains stable due to a Z_2 symmetry, called R -parity. In principle, a gravitino can also be a dark matter candidate (with mass $\simeq 10$ GeV) even when the R -parity is broken. It also turns out that the region of SUSY parameter space, where LSP mass fits the data on dark matter also addresses the problems on the Higgs mass and Grand Unification.

3.2 SUSY Algebra

SUSY in its essence relates bosons and fermions. It is based on the Coleman-Mandula Theorem, according to which the Poincaré symmetry can not be extended with additional symmetry generators following definite commutation relations. Following this, Haag, Lopuszanski and Sohnius proved that SUSY as a graded Lie algebra (consisting of additional anticommuting generators) is the only symmetry of the S-matrix consistent with the Poincaré invariance [13].

A supersymmetry transformation turns a bosonic state into a fermionic state and vice versa. Schematically,

$$Q^i_\alpha |Boson \rangle = |Fermion \rangle \quad Q^i_\alpha |Fermion \rangle = |Boson \rangle \quad (3.4)$$

The operators $Q^i_\alpha [i = 1, \dots, \mathcal{N}]$ are fermionic, with spinor indices α , and are called SUSY generators and the transformations are known as SUSY transformations. \mathcal{N} is the number of SUSY generators. Using the four dimensional flat Minkowski space-time metric

$$g_{\mu\nu} = g^{\mu\nu} = (1, -1, -1, -1) \quad (3.5)$$

the Poincaré algebra involving four-momenta P_μ and the Lorentz generators $M_{\mu\nu}$ reads:

$$[P^\mu, P^\nu] = 0, \quad (3.6a)$$

$$[M^{\mu\nu}, P^\rho] = i(g^{v\rho} P^\mu - g^{\mu\rho} P^\nu), \quad (3.6b)$$

$$[M^{\mu\nu}, M^{\rho\lambda}] = i(g^{v\rho} M^{\mu\lambda} + g^{\mu\lambda} M^{v\rho} - g^{\mu\rho} M^{v\lambda} - g^{v\lambda} M^{\mu\rho}), \quad (3.6c)$$

Now, in order that the Coleman-Mandula Theorem is bypassed, Q^i_α and its complex conjugate $Q^{i\dagger}_{\dot{\alpha}}$ must satisfy the graded Lie algebra which consists of the following commutation and anti-commutation relations with the four-momenta P_μ and the Lorentz generators $M_{\mu\nu}$:

$$[Q_\alpha, P_\mu] = [\bar{Q}_{\dot{\alpha}}, P_\mu] = 0, \quad (3.7a)$$

$$\{Q_\alpha, Q_\beta\} = \{\bar{Q}_{\dot{\alpha}}, \bar{Q}_{\dot{\beta}}\} = 0, \quad (3.7b)$$

$$[M^{\mu\nu}, Q_\alpha] = -i(\sigma^{\mu\nu})_\alpha{}^\beta Q_\beta, \quad (3.7c)$$

$$[M^{\mu\nu}, \bar{Q}_{\dot{\alpha}}] = -i(\bar{\sigma}^{\mu\nu})^{\dot{\alpha}}{}_{\dot{\beta}} \bar{Q}_{\dot{\beta}}, \quad (3.7d)$$

$$\{Q_\alpha, \bar{Q}_{\dot{\beta}}\} = 2\sigma^\mu_{\alpha\dot{\beta}} P_\mu. \quad (3.7e)$$

where the indices α, β of Q and $\dot{\alpha}, \dot{\beta}$ of \bar{Q} take values 1 or 2 and indicate two-component Weyl spinors; $\sigma^\mu = (1, \sigma_i)$ with σ_i being the Pauli matrices and $\sigma^{\mu\nu} = i/4(\sigma^\mu \bar{\sigma}^\nu - \sigma^\nu \bar{\sigma}^\mu)$.

Using the anti-commutation relation one can also show that the number of fermionic degrees of freedom is equal to the number of bosonic degree of freedom in a supermultiplet¹. In addition, masses of superpartners of the SM constituents belonging to the same supermultiplet will be same in exact SUSY limit. Moreover, all quantum numbers except spin are same for bosons and fermions related by SUSY as the gauge transformation generators commute with the SUSY generators.

Here we focus only on the simplest phenomenologically viable supersymmetric theory i.e. $\mathcal{N} = 1$ SUSY. SUSY with $\mathcal{N} > 1$ is called extended SUSY and is widely used in string theories.

3.3 SUSY Lagrangians

For supersymmetric theories it is easier to construct the supersymmetrically invariant Lagrangian using the superfield formalism rather than the basic bosonic and fermionic fields.

The momentum operator P^μ and the generators, Q and \bar{Q} , of the SUSY transformations form a subgroup of the extended Poincaré group. This allows us to construct a function $S(x^\mu, \theta, \bar{\theta})$, the superfield, which is a linear representation of this subgroup. The change in this function induced by the action of a member of the subgroup,

¹The single-particle states of a supersymmetric theory fall into irreducible representations of the supersymmetry algebra, called supermultiplets.

$$G(a^\mu, \zeta, \bar{\zeta}) = \exp i(\zeta Q + \bar{\zeta} \bar{Q} - a^\mu P_\mu), \quad (3.8)$$

is generated by

$$P_\mu = i\partial_\mu, \quad (3.9a)$$

$$Q_\alpha = -i\frac{\partial}{\partial\theta^\alpha} - \sigma_{\alpha\dot{\alpha}}^\mu \bar{\theta}^{\dot{\alpha}} \partial_\mu, \quad (3.9b)$$

$$\bar{Q}_{\dot{\alpha}} = i\frac{\partial}{\partial\bar{\theta}^{\dot{\alpha}}} + \theta^\alpha \sigma_{\alpha\dot{\alpha}}^\mu \partial_\mu, \quad (3.9c)$$

where ζ , $\bar{\zeta}$, θ and $\bar{\theta}$ are anti-commuting Grassmann variables which transform as Weyl spinors. Essentially, the Grassmanian, or fermionic, character of the superspace variables stems from the fact that they are instrumental in mixing bosons and fermions which have disparate angular momenta. It is only through fermionic mixing parameters that angular momentum is retained as a conserved quantum number for all states.

Fermionic derivatives which anti-commute with the generators of SUSY algebra and transform covariantly can be defined as

$$D_\alpha = \frac{\partial}{\partial\theta^\alpha} + i\sigma_{\alpha\dot{\alpha}}^\mu \bar{\theta}^{\dot{\alpha}} \partial_\mu, \quad (3.10a)$$

$$\bar{D}_{\dot{\alpha}} = -\frac{\partial}{\partial\bar{\theta}^{\dot{\alpha}}} - i\theta^\alpha \sigma_{\alpha\dot{\alpha}}^\mu \partial_\mu. \quad (3.10b)$$

The general superfield, $S(x^\mu, \theta, \bar{\theta})$, belongs to a reducible representation of the supersymmetric algebra. However, we can obtain irreducible representations by imposing further conditions:

$$\bar{D}_{\dot{\alpha}} S = 0 \quad \text{left chiral superfield;} \quad (3.11a)$$

$$D_\alpha S^\dagger = 0 \quad \text{right chiral superfield;} \quad (3.11b)$$

$$S^\dagger = S \quad \text{vector superfield.} \quad (3.11c)$$

Since θ and $\bar{\theta}$ are two-component Grassmann variables the expansion of the superfield as a power series in θ and $\bar{\theta}$ can not involve terms with more than two powers of θ or $\bar{\theta}$. The chiral superfield $\Phi(x^\mu, \theta, \bar{\theta})$, can be written as an expansion in terms of the Grassmann variables θ and $\bar{\theta}$ giving

$$\begin{aligned} \Phi(x^\mu, \theta, \bar{\theta}) = & \phi(x) + \sqrt{2}\theta\psi(x) + \theta\theta F(x) + i\partial_\mu\phi(x)\theta\sigma^\mu\bar{\theta} \\ & - \frac{i}{\sqrt{2}}\theta\theta\partial_\mu\psi(x)\sigma^\mu\bar{\theta} - \frac{1}{4}\partial^\mu\partial_\mu\phi(x)\theta\theta\bar{\theta}\bar{\theta} \end{aligned} \quad (3.12)$$

This superfield includes a Weyl spinor ψ , and a complex scalar field ϕ . The field F is an auxiliary field which is introduced to ensure the closure of SUSY algebra even under off-shell condition. It can be eliminated using the equations of motion. The component fields of a left chiral superfield transform in the following way under the SUSY transformation:

$$\delta\phi = \sqrt{2}\xi\psi; \quad (3.13a)$$

$$\delta\psi = \sqrt{2}\xi F - i\sqrt{2}\bar{\partial}_\mu\phi\sigma^\mu\bar{\xi}; \quad (3.13b)$$

$$\delta F = i\sqrt{2}\bar{\partial}_\mu\psi\sigma^\mu\bar{\xi}. \quad (3.13c)$$

A right chiral superfield can be obtained by taking Hermitian conjugate. We refer to the coefficient of the $\theta\theta$ term as the F -term. Equation(3.13c) shows that the change, under the SUSY transformations, of the F -term is a total derivative. Hence the F -term is suitable for use as a supersymmetrically-invariant Lagrangian.

Similarly, the vector superfield can be expanded in powers of θ and $\bar{\theta}$,

$$\begin{aligned} S(x^\mu, \theta, \bar{\theta}) = & C(x) + i\theta\chi(x) - i\bar{\theta}\bar{\chi}(x) + \frac{i}{2}\theta\theta [M(x) + iN(x)] \\ & - \frac{i}{2}\bar{\theta}\bar{\theta} [M(x) - iN(x)] + \theta\sigma^\mu\bar{\theta}V_\mu(x) \\ & + i\theta\bar{\theta}\bar{\theta} \left[\bar{\lambda}(x) + \frac{i}{2}\bar{\sigma}^\mu\partial_\mu\chi(x) \right] - i\bar{\theta}\bar{\theta}\theta \left[\lambda(x) + \frac{i}{2}\sigma^\mu\partial_\mu\bar{\chi}(x) \right] \\ & + \frac{1}{2}\theta\theta\bar{\theta}\bar{\theta} \left[D(x) - \frac{1}{2}\partial_\mu\partial^\mu C(x) \right], \end{aligned} \quad (3.14)$$

where the real scalar fields C , M , N and the Weyl fermion χ can be eliminated by a SUSY gauge transformation leaving the physical degrees of freedom, *i.e.* the gauge field V_μ and its superpartner gaugino field λ , and the auxiliary field D . This is done by the choice of the Wess-Zumino gauge which is in some sense analogous to the unitary gauge in the SM, since it removes unphysical degrees of freedom. The component fields transform in the following way under the SUSY transformations:

$$\delta C = i(\xi\chi - \bar{\xi}\bar{\chi}); \quad (3.15a)$$

$$\delta\lambda_\alpha = -iD\xi_\alpha - \frac{1}{2}(\sigma^\mu\bar{\sigma}^\nu)_\alpha{}^\beta\xi_\beta(\partial_\mu V_\nu - \partial_\nu V_\mu); \quad (3.15b)$$

$$\delta V^\mu = i(\xi\sigma^\mu\bar{\lambda} - \lambda\sigma^\mu\bar{\xi}) - \partial^\mu(\xi\chi + \bar{\xi}\bar{\chi}); \quad (3.15c)$$

$$\delta D = \partial_\mu(-\xi\sigma^\mu\bar{\lambda} + \lambda\sigma^\mu\bar{\xi}). \quad (3.15d)$$

Here the variation of the coefficient of the $\theta\theta\bar{\theta}\bar{\theta}$ term, the D -term, is a total derivative and hence this can also be used as a supersymmetrically-invariant Lagrangian.

Using these superfields we can construct supersymmetric Lagrangians. In the supersymmetric extension of the SM, we will use left handed chiral superfields to represent the left-handed components of the SM fermions (or anti-fermions), together with their superpartners and right chiral (Hermitian conjugate of the left chiral) superfields to represent the right-handed components, and their superpartners. The gauge bosons are represented by vector superfields.

Let us consider how to construct the Lagrangian for the chiral superfields. This can be done by taking products of chiral superfields. In particular, the product of two left chiral superfields is also a left chiral superfield. Hence the F -term of a product of left chiral superfields can be used to give a suitable term in the Lagrangian. The product of a left and a right chiral superfield gives a vector superfield. The D -term of the product of a left and a right chiral superfield can therefore also be used to give a term in the Lagrangian. The simplest example of this is a single left chiral superfield. We can form the product of this field with its hermitian conjugate and take the D -term. This gives

$$[\Phi\Phi^\dagger]_{\theta\theta\bar{\theta}\bar{\theta}} = FF^\dagger + \partial_\mu\phi^*\partial^\mu\phi + i\bar{\psi}\bar{\sigma}^\mu\partial_\mu\psi, \quad (3.16)$$

which, after eliminating the auxiliary field F using the equations of motion, gives the final Lagrangian. Therefore using the D -term of the product of the superfield and its hermitian conjugate we can form the kinetic term for the fermionic field and its superpartner. It is important to note that a proper gauge choice allows us to retain only the auxiliary field D^a .

We can add interaction and mass terms to this theory by taking products of the left chiral superfields. This can be done by forming the superpotential for the theory. For example, in a theory with only one chiral superfield,

$$\mathbf{W}(\Phi) = \frac{m}{2}\Phi\Phi + \frac{l}{3}\Phi\Phi\Phi. \quad (3.17)$$

In general we can only include terms which are at most cubic in the superfields in order for the theory to be renormalisable. This gives the interaction Lagrangian

$$\mathcal{L} = [W(\Phi)]_{\theta\theta} + \text{h.c.}, \quad (3.18)$$

$$= m(\phi F - \frac{1}{2}\psi\psi) + \lambda(\phi^2 F - \phi\psi\psi) + \text{h.c.}. \quad (3.19)$$

Another important property of the superpotential is that SUSY invariance requires it to be analytic (holomorphic) in terms of complex scalar fields ϕ , so that W can not contain terms with ϕ and ϕ^* at the same time. This is the main reason for requiring two Higgs doublets in SUSY theories (with appropriate gauge charges) to provide masses to the up-and down-type quarks.

We can then write the full Lagrangian for this theory and use the equations of motion to eliminate the auxiliary field F ,

$$F^\dagger = -m\phi - \lambda\phi^2, \quad (3.20)$$

giving the result

$$\begin{aligned} \mathcal{L}_{chiral} &= [\Phi\Phi^\dagger]_{\theta\theta\bar{\theta}\bar{\theta}} + ([W(\Phi)]_{\theta\theta} + \text{h.c.}), \\ &= \partial_\mu\phi^*\partial^\mu\phi + i\bar{\psi}\bar{\sigma}^\mu\partial_\mu\psi - |\lambda\phi^2 + m\phi|^2 - \left(\frac{m}{2}\psi\psi + \lambda\psi\psi\phi + \text{h.c.}\right) \end{aligned} \quad (3.21)$$

By taking the relevant combinations of the chiral superfields, the kinetic terms and the interactions of the chiral fields with each other can be constructed. In general the superpotential gives the Yukawa-type interactions and part of the scalar potential of the theory.

The Lagrangian density for a gauge supermultiplet can be written as

$$\mathcal{L}_{\text{gauge}} = -\frac{1}{4}F_{\mu\nu}^a F^{\mu\nu a} + i\lambda^{\dagger a}\bar{\sigma}^\mu D_\mu\lambda^a + \frac{1}{2}D^a D^a \quad (3.23)$$

where

$$F_{\mu\nu}^a = \partial_\mu A_\nu^a - \partial_\nu A_\mu^a + gf^{abc}A_\mu^b A_\nu^c \quad (3.24)$$

is the usual Yang-Mills field strength, and

$$D_\mu\lambda^a = \partial_\mu\lambda^a + gf^{abc}A_\mu^b\lambda^c \quad (3.25)$$

is the covariant derivative of the gaugino field. The index a here runs over the adjoint representation of the gauge group ($a = 1, \dots, 8$ for $SU(3)_C$ color gluons and gluinos; $a = 1, 2, 3$ for $SU(2)_L$ weak isospin; $a = 1$ for $U(1)_Y$ weak hypercharge). f^{abc} are the totally antisymmetric structure constants that define the gauge group. Like the chiral auxiliary fields F_i , the gauge auxiliary field D^a has dimensions of $[\text{mass}]^2$ and no kinetic term, so it can be eliminated on-shell using its algebraic equation of motion.

We also have to consider whether there are any other interactions allowed by gauge invariance and involving the gaugino and D^a fields, which might have to be included to make a supersymmetric Lagrangian. Since A_μ^a couples to ϕ_i and ψ_i , it makes sense that λ^a and D^a should couple as well.

In fact, there are three such possible interaction terms that are renormalisable (of field mass dimension ≤ 4), namely

$$(\phi^* T^a \psi) \lambda^a, \quad \lambda^{\dagger a} (\psi^\dagger T^a \phi), \quad \text{and} \quad (\phi^* T^a \phi) D^a. \quad (3.26)$$

After some algebra one can now fix the coefficients for the terms in Equation (3.26), with the result that the full Lagrangian density for a renormalisable supersymmetric theory is

$$\mathcal{L} = \mathcal{L}_{\text{chiral}} + \mathcal{L}_{\text{gauge}} - \sqrt{2}g(\phi^* T^a \psi) \lambda^a - \sqrt{2}g\lambda^{\dagger a} (\psi^\dagger T^a \phi) + g(\phi^* T^a \phi) D^a \quad (3.27)$$

where $\mathcal{L}_{\text{chiral}}$ means the chiral supermultiplet Lagrangian and $\mathcal{L}_{\text{gauge}}$ is the one related to the gauge supermultiplet as mentioned above. The first two interaction terms represent direct coupling of gauginos to matter fields; this can be thought of as the ‘‘supersymmetrisation’’ of the usual gauge boson couplings to matter fields. It is also to be noted that SUSY invariance of the gauge (gaugino) interaction requires the superpotential to be gauge invariant. The last term combines with the term $D^a D^a / 2$ in $\mathcal{L}_{\text{gauge}}$ to provide an equation of motion

$$D^a = -g(\phi^* T^a \phi). \quad (3.28)$$

Thus, like the auxiliary fields F_i and F^{*i} , the D^a are expressible purely algebraically in terms of the scalar fields. Replacing the auxiliary fields in eq. (3.27) using eq. (3.28), one finds that the complete scalar potential is (recall that \mathcal{L} contains $-V$):

$$V(\phi, \phi^*) = F^{*i} F_i + \frac{1}{2} \sum_a D^a D^a = W_i^* W^i + \frac{1}{2} \sum_a g_a^2 (\phi^* T^a \phi)^2. \quad (3.29)$$

The two types of terms in this expression are called ‘‘ F -term’’ and ‘‘ D -term’’ contributions, respectively. In the second term in Equation (3.29), we have now written an explicit sum \sum_a to cover the cases where the gauge group has several distinct factors with different gauge couplings g_a . [For instance, in the MSSM the three factors $SU(3)_C$, $SU(2)_L$ and $U(1)_Y$ have different gauge couplings g_3 , g and g' .] Since $V(\phi, \phi^*)$ is a sum of squares, it is always greater than or equal to

zero for every field configuration. It is an interesting and unique feature of supersymmetric theories that the scalar potential is completely determined by the *other* interactions in the theory. The F -terms are fixed by Yukawa couplings and fermion mass terms, and the D -terms are fixed by the gauge interactions.

In the following section we will construct a supersymmetric extension of the Standard Model using these superfield techniques. However, before one does that, phenomenological considerations necessitate the introduction of terms that break SUSY without destroying its desirable features.

3.4 Supersymmetry Breaking

In the exact SUSY limit, masses of superpartners should be exactly same as those of the SM counterparts. In that case they would have been seen in experiments, which is certainly not the case. Hence, SUSY if exists, must be broken [14].

SUSY breaking in masses [15] is safe from the viewpoint of naturalness problem. In a broken SUSY the (quadratic) ultraviolet sensitivity in Higgs boson mass up to all orders in perturbation theory can be removed if the SUSY breaking could be incorporated through the masses, not the couplings.

The spontaneous breakdown of SUSY can be introduced through the following scalar potential, consisting of the F -term and D -term contributions,

$$V(\phi) = F^i F^{i*} + \frac{1}{2} D^a D^a \quad (3.30)$$

keeping either $\langle F^i \rangle = 0$ or $\langle D^a \rangle = 0$, where, $F^i = \frac{\delta W}{\delta \phi_i}$, and, $D^a = g_a \Sigma_{i,j} |\phi_i^* T^a_{ij} \phi_j|$. However, this alone as the SUSY breaking mechanism does not lead to acceptable results because of the super-trace theorem. According to this:

$$S\text{Tr}(m^2) = \Sigma_j (-)^{2j} (2j + 1) \text{Tr}(m^2_j) = 0 \quad (3.31)$$

where j is the spin angular momentum of a particle with mass m_j . This means in a supermultiplet, $\Sigma_b m^2_b = \Sigma_f m^2_f$, with m_b and m_f are masses of bosons and fermions respectively. This theorem, valid for cases when SUSY is broken spontaneously via renormalisable terms, leads to some phenomenologically unacceptable consequences. For example, there are two spin- zero partners for the electron corresponding to the states e_L and e_R . The super-trace theorem implies that one

of these spin zero states has to be lighter than the electron itself, something that is inadmissible.

This difficulty can be bypassed by introducing soft SUSY breaking mass terms which arises either through loop-induced terms or through non-renormalisable interactions in a different sector of the theory. Therefore, the complete Lagrangian will consist of

$$\mathcal{L} = \mathcal{L}_{SUSY} + \mathcal{L}_{soft} \quad (3.32)$$

where, \mathcal{L}_{SUSY} is SUSY conserving Lagrangian which include gauge and Yukawa interactions of SM particles and their superpartners, and, \mathcal{L}_{soft} (with mass dimension $D < 4$ which does not contribute to quadratic divergence) contains (SUSY violating) soft mass terms for all the superparticles.

Let us now turn to the soft supersymmetry breaking terms that can be written in a gauge invariant and lepton number and baryon number invariant way. We write down the most general set of such terms in the minimal SUSY extension of the SM (MSSM), whose detailed account is given in the next section:

$$\begin{aligned} \mathcal{L}_{soft} = & -\frac{1}{2} (M_1 \tilde{B}\tilde{B} + M_2 \tilde{W}_a \tilde{W}^a + M_3 \tilde{g}_\alpha \tilde{g}^\alpha + \text{c.c.}) \\ & - \left(A_{ij}^L \tilde{L}_i^a H_d^b \tilde{E}_j^* + A_{ij}^D \tilde{Q}_i^a H_d^b \tilde{D}_j^* + A_{ij}^U \tilde{Q}_i^b H_u^a \tilde{U}_j^* + \text{c.c.} \right) \\ & - M_{\tilde{L},ij}^2 \tilde{L}_{ia}^* \tilde{L}_j^a - M_{\tilde{E},ij}^2 \tilde{E}_i^* \tilde{E}_j \\ & - M_{\tilde{Q},ij}^2 \tilde{Q}_{ia}^* \tilde{Q}_j^a - M_{\tilde{U},ij}^2 \tilde{U}_i^* \tilde{U}_j - M_{\tilde{D},ij}^2 \tilde{D}_i^* \tilde{D}_j \\ & - M_{H_d}^2 H_{da}^* H_d^a - M_{H_u}^2 H_{ua}^* H_u^a - \left(B\mu H_d^a H_u^b + \text{c.c.} \right). \end{aligned} \quad (3.33)$$

In eq. (3.33), M_3 , M_2 , and M_1 are the gluino, wino, and bino mass terms ($a = 1, 2, 3; \alpha = 1, 2, \dots, 8$). The next set of terms in Equation (3.33) contains the (scalar)³ couplings. Each of A_{ij}^L , A_{ij}^D , A_{ij}^U is a complex 3×3 matrix in family space, with dimensions of [mass]. They are in one-to-one correspondence with the Yukawa couplings of the superpotential. Q, L, U, D, E are all three-component column vectors containing all the fermion families. Q, L are quark and lepton doublet superfields respectively while U, D, E are singlets. Terms in the next two lines of Equation (3.33) consist of squark and slepton mass terms of the $(m^2)_i^j \phi^{*i} \phi_j$ type. Each of $M_{\tilde{L},ij}^2$, $M_{\tilde{E},ij}^2$, $M_{\tilde{Q},ij}^2$, $M_{\tilde{U},ij}^2$, $M_{\tilde{D},ij}^2$ is a 3×3 matrix in family space, having in general complex entries, but they must be hermitian so that the Lagrangian is real. Finally, in the last line of Equation (3.33) we have supersymmetry-breaking contributions to the Higgs potential; $M_{H_d}^2$ and $M_{H_u}^2$ are squared-mass terms of

the $(m^2)_i^j$ type, while $B\mu$ is the only bilinear squared-mass term that can occur in MSSM with terms of $(m^2)^{ij}\phi_i\phi_j$ type. We expect

$$M_1, M_2, M_3, A_{ij}^L, A_{ij}^D, A_{ij}^D \sim m_{\text{soft}}, \quad (3.34)$$

$$M_{L,ij}^2, M_{E,ij}^2, M_{Q,ij}^2, M_{U,ij}^2, M_{D,ij}^2, m_{H_u}^2, m_{H_d}^2, B\mu \sim m_{\text{soft}}^2, \quad (3.35)$$

with a characteristic mass scale m_{soft} that is not much larger than 1000 GeV.

3.5 The minimal supersymmetric standard model (MSSM)

Besides having the SM fields, the MSSM [2, 16] has left and right chiral sleptons $\tilde{L}_{L,R}$, squarks $\tilde{q}_{L,R}$, gluinos \tilde{g}^α ($\alpha = 1, \dots, 8$), Winos \tilde{W}^a [$a = 1, 2, 3$], Bino \tilde{B} , and Higgsinos $\tilde{H}_d^0, \tilde{H}_u^0, \tilde{H}_d^\pm$ and \tilde{H}_u^\pm . Detail of all these are given in Table 3.1.

An important feature of the SUSY is that the superpartners listed in Table 3.1 are not necessarily the mass eigen-states of the theory as after the electroweak symmetry breaking (EWSB) and SUSY breaking take place, there can be mixing among various sets of squarks and sleptons as well as between gauginos and Higgsinos. Thus, finally, the physical spectrum consists of the following:

- Mass eigen-states of left and right chiral sleptons, $\tilde{l}_{1,2}$
- Mass eigen-states of left and right chiral squarks, $\tilde{q}_{1,2}$
- Neutralinos $\tilde{\chi}_i^0$ [$i = 1 \dots 4$] as mass eigen-states of bino \tilde{B} , neutral-wino \tilde{W}^3 , and neutral Higgsinos, \tilde{H}_d^0 , and \tilde{H}_u^0 ,
- Charginos $\tilde{\chi}_i^\pm$ [$i = 1, 2$] as mass eigen-states of Winos $\tilde{W}^{1,2}$ and charged Higgsinos \tilde{H}_d^\pm and \tilde{H}_u^\pm .

In addition to these, the scalar sector will have two CP-even and one CP-odd neutral Higgs, h , H and A respectively and, also, a charged Higgs pair H^\pm . Superpartners of the SM contents are called with a suffix '-ino' added in it in case of gauge bosons and Higgses and with a prefix 's' added in case of fermions.

3.5.1 Ingredients of the MSSM Lagrangian

The supersymmetric part of the Lagrangian, in addition to kinetic terms and gauge interactions is specified by Superpotential \mathcal{W} giving the Yukawa interactions

Superfields		Bosonic Fields	Fermionic Fields	$SU(3)_c$	$SU(2)_L$	Y
Field	Type					
Gauge Multiplets						
G^a	Vector	Gluons	Gluginos	Octet	Singlet	0
W^a	Vector	W	Winos	Singlet	Triplet	0
B^a	Vector	B	Bino	Singlet	Singlet	0
Matter Multiplets						
L_i	Left Chiral	$(\tilde{\nu}_L, \tilde{\ell}_L^-)$	(ν_L, ℓ_L)	Singlet	Doublet	-1
E_i	Right Chiral	$\tilde{\ell}_R^-$	ℓ_R	Singlet	Singlet	-2
Q_i	Left Chiral	$(\tilde{u}_L, \tilde{d}_L)$	(u_L, d_L)	Triplet	Doublet	1/3
U_i	Right Chiral	\tilde{u}_R	u_R	Triplet	Singlet	4/3
D_i	Right Chiral	\tilde{d}_R	d_R	Triplet	Singlet	-2/3
Higgs Multiplets						
H_d	Left Chiral	(H_d^0, H_d^-)	$(\tilde{H}_d^0, \tilde{H}_d^-)_L$	Singlet	Doublet	-1
H_u	Left Chiral	(H_u^+, H_u^0)	$(\tilde{H}_u^+, \tilde{H}_u^0)_L$	Singlet	Doublet	1

Table 3.1: *MSSM particle contents and corresponding superfields. The subscript $i = 1, 2, 3$ gives the generation of the matter fields. Taken from the thesis by Dr. Sudhir Kumar Gupta.*

$$\mathcal{W} = \left(Y_{ij}^L \hat{L}_i^a \hat{H}_d^b \hat{E}_j^c + Y_{ij}^D \hat{Q}_i^a \hat{H}_d^b \hat{D}_j^c + Y_{ij}^U \hat{Q}_i^b \hat{H}_u^a \hat{U}_j^c - \mu \hat{H}_d^a \hat{H}_u^b \right) \quad (3.36)$$

where \hat{L} , \hat{E} , \hat{Q} , \hat{D} , and \hat{U} denote the matter superfields. The $SU(2)_L$ representation indices are denoted by $a, b = 1, 2$ and the generation indices by $i, j = 1, 2, 3$.

The next ingredient is the soft SUSY breaking Lagrangian, which includes mass terms as already mentioned in Section 3.4, for the gauginos

$$\mathcal{L}_{\text{soft},1}^{\text{MSSM}} = \frac{1}{2} (M_1 \tilde{B} \tilde{B} + M_2 \tilde{W}_a \tilde{W}^a + M_3 \tilde{g}_\alpha \tilde{g}^\alpha) + h.c. , \quad (3.37)$$

mass terms for scalar matter fields and Higgs fields

$$\begin{aligned} \mathcal{L}_{\text{soft},2}^{\text{MSSM}} = & -M_{H_d}^2 H_{da}^* H_d^a - M_{H_u}^2 H_{ua}^* H_u^a - M_{\tilde{L},ij}^2 \tilde{L}_{ia}^* \tilde{L}_j^a - M_{\tilde{E},ij}^2 \tilde{E}_i^* \tilde{E}_j \\ & - M_{\tilde{Q},ij}^2 \tilde{Q}_{ia}^* \tilde{Q}_j^a - M_{\tilde{U},ij}^2 \tilde{U}_i^* \tilde{U}_j - M_{\tilde{D},ij}^2 \tilde{D}_i^* \tilde{D}_j \end{aligned} \quad (3.38)$$

and trilinear and bilinear couplings of scalar matter fields and Higgs fields

$$\begin{aligned} \mathcal{L}_{\text{soft},3}^{\text{MSSM}} = & - \left(A_{ij}^L \tilde{L}_i^a H_d^b \tilde{E}_j^* + A_{ij}^D \tilde{Q}_i^a H_d^b \tilde{D}_j^* + A_{ij}^U \tilde{Q}_i^b H_u^a \tilde{U}_j^* - B \mu H_d^a H_u^b \right) \\ & + h.c. \end{aligned} \quad (3.39)$$

3.5.2 Masses and Mixing

The various SUSY-breaking mass terms are induced by the soft SUSY breaking parameters and the vevs v_i [$i = d, u$] of the neutral Higgs fields $v_i = \langle H_i^0 \rangle$. The ratio of the two vevs is denoted by $\tan \beta = v_u / v_d$. The sum of the vevs squared is fixed by the gauge boson masses

$$m_W^2 = \frac{1}{4} g^2 (v_d^2 + v_u^2), \quad m_Z^2 = \frac{1}{4} (g^2 + g'^2) (v_d^2 + v_u^2). \quad (3.40)$$

Ignoring the inter-generational mixing, masses of the SM fermion are given by

$$m_{u_i} = \frac{1}{\sqrt{2}} Y_{ii}^U v_u, \quad m_{d_i} = \frac{1}{\sqrt{2}} Y_{ii}^D v_d, \quad m_{l_i} = \frac{1}{\sqrt{2}} Y_{ii}^L v_d \quad (3.41)$$

for up-type quarks, down-type quarks and leptons, respectively.

The gluino acquire a mass $m_{\tilde{g}} = |M_3|$, where M_3 denotes the soft mass in the $SU(3)_c$ sector. The chargino mass terms take the form

$-(\tilde{\psi}^-)^T X \tilde{\psi}^+$ where $\psi^- = (-i\tilde{W}^-, \tilde{h}_d^-)^T$, $\psi^+ = (-i\tilde{W}^+, \tilde{h}_u^+)^T$ and

$$X = \begin{pmatrix} M_2 & \frac{g}{\sqrt{2}}v_u \\ \frac{g}{\sqrt{2}}v_d & \mu \end{pmatrix}. \quad (3.42)$$

The matrix is diagonalized by two unitary matrices U and V :

$$M_{D,\tilde{\chi}^\pm} = U^* X V^{-1}. \quad (3.43)$$

The neutral gauginos \tilde{B}, \tilde{W}^3 as well as the neutral Higgsinos $\tilde{H}_d^0, \tilde{H}_u^0$ form the neutralinos.

In the basis $\tilde{\psi}^0 = (\tilde{B}, \tilde{W}^3, \tilde{H}_d^0, \tilde{H}_u^0)^T$ one finds the mass term $-\frac{1}{2}[(\tilde{\psi}^0)^T Y \tilde{\psi}^0 + h.c.]$ with

$$Y = \begin{pmatrix} M_1 & 0 & -\frac{g'}{2}v_d & \frac{g'}{2}v_u \\ 0 & M_2 & \frac{g}{2}v_d & -\frac{g}{2}v_u \\ -\frac{g'}{2}v_d & \frac{g}{2}v_d & 0 & -\mu \\ \frac{g'}{2}v_u & -\frac{g}{2}v_u & -\mu & 0 \end{pmatrix} \quad (3.44)$$

This matrix is diagonalized by an unitary matrix N :

$$M_{D,\tilde{\chi}^0} = N^* Y N^\dagger. \quad (3.45)$$

The CP-even EW eigen-states (H_d^0, H_u^0) are rotated by the angle α into the Higgs mass eigen-states (h^0, H^0) as follows

$$\begin{pmatrix} h^0 \\ H^0 \end{pmatrix} = \begin{pmatrix} -\sin \alpha & \cos \alpha \\ \cos \alpha & \sin \alpha \end{pmatrix} \begin{pmatrix} H_d^0 \\ H_u^0 \end{pmatrix} \quad (3.46)$$

with $m_{h^0} < m_{H^0}$. Masses of the Higgs scalars of the MSSM are given by,

$$M_{h^0, H^0}^2 = .5(M_{A^0}^2 + M_Z^2 \mp \sqrt{(M_{A^0}^2 + M_Z^2)^2 - 4M_{A^0}^2 M_Z^2 \cos^2 2\beta}) \quad (3.47)$$

$$M_{A^0}^2 = M_{H_u}^2 + M_{H_d}^2 + 2\mu^2, \quad M_{H^\pm}^2 = M_{A^0}^2 + M_W^2 \quad (3.48)$$

at tree level.

The general form of sfermion mass matrix, in the absence of inter-generational mixing can be written as

$$M_{\tilde{f}} = \begin{pmatrix} m_{\tilde{f}LL}^2 & m_{\tilde{f}LR}^2 \\ m_{\tilde{f}LR}^2 & m_{\tilde{f}RR}^2 \end{pmatrix} \quad (3.49)$$

where,

$$m_{\tilde{f}_{LL}}^2 = m_{\tilde{f}_L}^2 + m_Z^2 (T_{3L}^{\tilde{f}} - Q_f \sin^2 \theta_W) \cos 2\beta + m_f^2 \quad (3.50)$$

$$m_{\tilde{f}_{RR}}^2 = m_{\tilde{f}_R}^2 + Q_f m_Z^2 \sin^2 \theta_W \cos 2\beta + m_f^2 \quad (3.51)$$

$$m_{\tilde{f}_{LR}}^2 = -m_f (A^f + \mu \cot \beta) \quad (\text{For up - type}) \quad (3.52)$$

$$m_{\tilde{f}_{LR}}^2 = -m_f (A^f + \mu \tan \beta) \quad (\text{For down - type}) \quad (3.53)$$

Clearly, the diagonal entries consist of a soft-mass term for sfermion and the additional D-term contribution where the later is proportional to the hypercharge (Recall the equation, $D^a = g_a \sum_{i,j} |\phi_i^* T^a_{ij} \phi_j|$).

3.5.3 The R-parity

A SUSY scenario can also have an artificially imposed symmetry called R-parity [2, 17]. This is defined as

$$R = (-1)^{3B+L+2S} \quad (3.54)$$

with B, L and S as baryon number, lepton number and spin respectively. All the SM particles are R-even, but, since all the superpartners differ by a factor 1/2 in their spins from the corresponding SM contents, they will be odd under R-parity. Due to R-parity, only those interaction vertices are allowed where even number of superpartners are present. An important consequence of R-parity is that in experiments superparticles will be produced in pairs. Also, the lightest superparticle (LSP) will be stable. Thus cascade decays of superparticles terminate at the LSP, if R-parity is conserved. The LSP in such a case is stable, and is a viable candidate for the cold dark matter in the universe [18]. This further requires LSP to be electrically neutral and weakly interacting. The lightest neutralino is the LSP in most SUSY scenarios.

Note, however, there is nothing sacred about the R-parity conservation, although its conservation enhances the credibility of SUSY as an explanation of cold dark matter. However, R-parity violating scenarios [19] normally postulate the non-conservation of either L or B , as the non-conservation of both of them will result in fast proton decay. When R-parity is violated the following can happen:

- single sparticles can be produced,
- the LSP can decay into SM particles,

- the LSP can be any SUSY particle and need not be neutral,

These lead to different search strategies for SUSY compared to scenarios conserving R-parity.

3.6 High-scale SUSY breaking: some illustrations

The $\mathcal{L}_{\text{soft}}^{\text{MSSM}}$ introduces many new parameters that were not present in the ordinary Standard Model. A careful count reveals that there are 105 masses, phases and mixing angles in the MSSM Lagrangian that can not be rotated away by re-defining the phases and flavor basis for the quark and lepton supermultiplets, and that have no counterpart in the ordinary Standard Model. Thus, in principle, supersymmetry *breaking* (as opposed to supersymmetry itself) appears to introduce a tremendous arbitrariness in the Lagrangian, which can lead to dangerous FCNC and CP violating contributions. Hence, an organising principle is badly needed to evade such constraints.

On the other hand, the super-trace theorem prohibits us from breaking SUSY in the visible sector by renormalisable interactions. Hence, the origin of such soft mass terms can be explained on the basis of supersymmetry breaking in some postulated 'hidden' sector which can be communicated to the 'visible' sector. Two illustrative schemes of 'hidden' sector SUSY breaking are gravity mediated SUSY breaking (SUGRA) [20] and the other is known as gauge-mediated SUSY breaking (GMSB) [21, 22].

The supergravity effective Lagrangian contains non-renormalisable terms that communicate between the two sectors and are suppressed by powers of the Planck mass M_{Planck} . Thus, taking a toy model of such kind,

$$\mathcal{L}_{\text{NR}} = -\frac{1}{M_{\text{Planck}}} F \left(\frac{1}{2} f_a \lambda^a \lambda^a + \frac{1}{6} y^{ijk} \phi_i \phi_j \phi_k + \frac{1}{2} \mu^{ij} \phi_i \phi_j \right) + \text{c.c.} \\ - \frac{1}{M_{\text{Planck}}^2} F F^* k_j^i \phi_i \phi^{*j} \quad (3.55)$$

where F is the auxiliary field for a chiral supermultiplet in the hidden sector, and ϕ_i and λ^a are the scalar and gaugino fields in the MSSM, and f^a , y^{ijk} , and k_j^i are dimensionless constants. Now if one assumes that $\sqrt{\langle F \rangle} \sim 10^{10}$ or 10^{11} GeV, then \mathcal{L}_{NR} will give us nothing other than a Lagrangian of the form $\mathcal{L}_{\text{soft}}$ with MSSM soft terms of order $m_{\text{soft}} \sim \langle F \rangle / M_{\text{Planck}} = \text{a few hundred GeV}$.

The parameters f_a, k_j^i, y^{ijk} and μ^{ij} in \mathcal{L}_{NR} are to be determined by the underlying theory. This is a difficult enterprise in general, but a dramatic simplification occurs if one assumes a “minimal” form for the normalization of kinetic terms and gauge interactions in the full, non-renormalisable supergravity Lagrangian. In that case, there is a common $f_a = f$ for the three gauginos; $k_j^i = k\delta_j^i$ is the same for all scalars; and the other couplings are proportional to the corresponding superpotential parameters, so that $y^{ijk} = \alpha y^{ijk}$ and $\mu^{ij} = \beta\mu^{ij}$ with universal dimensionless constants α and β . Then the soft terms in $\mathcal{L}_{\text{soft}}^{\text{MSSM}}$ are all determined by just four parameters:

$$m_{1/2} = f \frac{\langle F \rangle}{M_{\text{Planck}}}, \quad m_0^2 = k \frac{|\langle F \rangle|^2}{M_{\text{Planck}}^2}, \quad A_0 = \alpha \frac{\langle F \rangle}{M_{\text{Planck}}}, \quad B_0 = \beta \frac{\langle F \rangle}{M_{\text{Planck}}} \quad (3.56)$$

This is usually known as mSUGRA where the B term is traded for $\tan\beta$ and one needs only the $\text{sgn}(\mu)$ as a high-scale parameter to determine μ , the Higgsino mass parameter, thanks to radiative electroweak symmetry breaking (REWSB). We will specify the conditions of REWSB later. It is a matter of some controversy whether the assumptions going into this parametrisation are well-motivated on purely theoretical grounds, but from a phenomenological perspective they make the scenario economical and predictive.

In general, a supersymmetric theory containing gauge and chiral supermultiplets whose Lagrangian may contain terms that are non-renormalisable, is determined by specifying three functions of the complex scalar fields (or more formally, of the chiral superfields). They are:

- The superpotential $W(\phi_i)$, which we have already talked about in the case of renormalisable supersymmetric Lagrangians. It must be an analytic function of the superfields treated as complex variables and must be invariant under the gauge symmetries of the theory, and has dimensions of $[\text{mass}]^3$.
- The *Kähler potential* $K(\phi_i, \phi^{*i})$. Unlike the superpotential, the Kähler potential is a function of both ϕ_i and ϕ^{*i} . It is gauge-invariant, real, and has dimensions of $[\text{mass}]^2$.
- The *gauge kinetic function* $f_{ab}(\phi_i)$ is also an analytic function of the left-chiral superfields ϕ_i . It is dimensionless and symmetric under interchange of its two indices a, b , which run over members of the adjoint representations of the gauge groups of the model. In the special case of renormalisable supersymmetric Lagrangians, it is just a constant (independent of the ϕ_i),

and is equal to the identity matrix : $f_{ab} = \delta_{ab}$. However, in models under SUSY-GUT, one can have non-trivial extensions of the gauge kinetic functions including terms of dimension five, which crucially determines gaugino masses. We will discuss some such cases in details in following chapters.

The whole Lagrangian with up to two derivatives can now be written down in terms of these. This is a non-trivial consequence of supersymmetry, because many different individual couplings in the Lagrangian are determined by these three functions. In addition, in supergravity models, the part of the scalar potential that does not depend on the gauge kinetic function can be written in terms of real, dimensionless *Kähler function*:

$$G = K/M_{Planck}^2 + \ln(W/M_{Planck}^3) + \ln(W^*/M_{Planck}^3). \quad (3.57)$$

In scenarios with GMSB [21], soft masses arise due to loop corrections mediated by some flavour-blind messenger particles which have gauge coupling and inherit SUSY breaking at a relatively lower energy scale than in the gravity-mediated case. Such loop induced masses have the form: $m_{soft} \sim \frac{\alpha_a \langle F \rangle}{4\pi M_{mes}}$, where $\alpha_a/4\pi$ is a loop factor for Feynman diagrams involving gauge interactions, and M_{mes} is a characteristic mass scale of the messenger fields.

Besides the aforesaid SUSY breaking schemes, there are other proposed scenarios. Some of these are based on braneworld pictures [23, 24]. Scenarios with braneworld picture assume the existence of additional spatial dimensions of Klauza-Klein or warped type, so that a physical distance separates the observable and hidden sectors. Examples of such scenarios are string theories which employ six additional dimensions, and the extra-dimensional mediated supersymmetry breaking (XMSB) which make use of one additional dimension. Now, if the gauge supermultiplet of the MSSM are confined in the physical brane and the SUSY breaking is purely due to high-scale effects, so that the soft masses induced by gravity are suppressed. Then SUSY breaking at the TeV scale may be triggered by terms answering to superconformal anomaly and such a scenario is called anomaly-mediated SUSY breaking. Here the resulting soft mass terms can be understood in terms of the anomalous violation of a local superconformal invariance which is an extension of scale invariance. Recently another model became very popular which has been motivated from string inspired modelling and is called mixed moduli mediated SUSY breaking [25], where one mimics a mirage unification of the gauge couplings. Phenomenologically, this is an admixture of

SUGRA and anomaly mediation.

In any of such models, once the SUSY-breaking parameters arise at the high-scale, they run down to the electroweak symmetry breaking scale by the renormalisation group equations (RGE). Here we discuss the RGEs connected to a model like mSUGRA and various features that it embodies in this regard [26].

$$16\pi^2 \frac{d}{dt} g_i = -b_i g_i^3 \quad i = 1, 2, 3; \quad (3.58)$$

$$16\pi^2 \frac{d}{dt} M_i = -2b_i M_i g_i^2 \quad i = 1, 2, 3; \quad (3.59)$$

for the three gauge couplings and three gaugino masses, respectively, and above the superpartner mass thresholds,

$$\begin{aligned} b_i &= -\frac{3}{5} - 2n_f \quad (i = 1) \\ &= 5 - 2n_f \quad (i = 2) \\ &= 9 - 2n_f \quad (i = 3) \end{aligned} \quad (3.60)$$

with $i = 1$ for weak hypercharge in a GUT normalization, $i = 2$ for $SU(2)_L$ and $i = 3$ for $SU(3)_c$. Together, they imply that the three quantities M_i/α_i do not run with scale:

$$\frac{M_i(t)}{\alpha_i(t)} = \frac{M_i(t_0)}{\alpha_i(t_0)}. \quad (3.61)$$

Since the gauge couplings are observed to unify at $Q = M_U \simeq 2 \times 10^{16}$ GeV, the gaugino masses also unify to a value called $m_{1/2}$ at that scale in the minimal version of SUGRA and one can recast above relation in the following way:

$$\frac{M_1}{g_1^2} = \frac{M_2}{g_2^2} = \frac{M_3}{g_3^2} = \frac{m_{1/2}}{g_U^2} \quad (3.62)$$

This is valid at any RG scale up to one-loop level. Here g_U is the unified gauge coupling at $Q = M_U$. Later we will show this relation doesn't hold in some models with SUSY-GUT.

The light squark and slepton masses obey the RG equations

$$\begin{aligned}
16\pi^2 \frac{d}{dt} m_{\tilde{Q}_L}^2 &= -\frac{2}{15} g_1^2 M_1^2 - 6g_2^2 M_2^2 - \frac{32}{3} g_3^2 M_3^2 + \frac{1}{5} g_1^2 \text{Tr}(Y m^2), \\
16\pi^2 \frac{d}{dt} m_{\tilde{u}_R}^2 &= -\frac{32}{15} g_1^2 M_1^2 - \frac{32}{3} g_3^2 M_3^2 - \frac{4}{5} g_1^2 \text{Tr}(Y m^2), \\
16\pi^2 \frac{d}{dt} m_{\tilde{d}_R}^2 &= -\frac{8}{15} g_1^2 M_1^2 - \frac{32}{3} g_3^2 M_3^2 + \frac{2}{5} g_1^2 \text{Tr}(Y m^2), \\
16\pi^2 \frac{d}{dt} m_{\tilde{L}_L}^2 &= -\frac{6}{5} g_1^2 M_1^2 - 6g_2^2 M_2^2 - \frac{3}{5} g_1^2 \text{Tr}(Y m^2), \\
16\pi^2 \frac{d}{dt} m_{\tilde{e}_R}^2 &= -\frac{24}{5} g_1^2 M_1^2 + \frac{6}{5} g_1^2 \text{Tr}(Y m^2)
\end{aligned} \tag{3.63}$$

where

$$\text{Tr}(Y m^2) = m_{H_u}^2 - m_{H_d}^2 + \sum_1^{n_f} \left(m_{\tilde{Q}_L}^2 - 2m_{\tilde{u}_R}^2 + m_{\tilde{d}_R}^2 - m_{\tilde{L}_L}^2 + m_{\tilde{e}_R}^2 \right). \tag{3.64}$$

The renormalization group equations for the sparticles of the third family are different because they involve the Yukawa couplings; for the squarks they read

$$\begin{aligned}
16\pi^2 \frac{d}{dt} m_{\tilde{t}_L, \tilde{b}_L}^2 &= 2y_t^2 \Sigma_t^2 + 2y_b^2 \Sigma_b^2 - \frac{2}{15} g_1^2 M_1^2 - 6g_2^2 M_2^2 - \frac{32}{3} g_3^2 M_3^2 + \frac{1}{5} g_1^2 \text{Tr}(Y m^2), \\
16\pi^2 \frac{d}{dt} m_{\tilde{t}_R}^2 &= 4y_t^2 \Sigma_t^2 - \frac{32}{15} g_1^2 M_1^2 - \frac{32}{3} g_3^2 M_3^2 - \frac{4}{5} g_1^2 \text{Tr}(Y m^2), \\
16\pi^2 \frac{d}{dt} m_{\tilde{b}_R}^2 &= 4y_b^2 \Sigma_b^2 - \frac{8}{15} g_1^2 M_1^2 - \frac{32}{3} g_3^2 M_3^2 + \frac{2}{5} g_1^2 \text{Tr}(Y m^2),
\end{aligned} \tag{3.65}$$

and for the sleptons,

$$\begin{aligned}
16\pi^2 \frac{d}{dt} m_{\tilde{\tau}_L, \tilde{\nu}_\tau}^2 &= 2y_\tau^2 \Sigma_\tau^2 - \frac{6}{5} g_1^2 M_1^2 - 6g_2^2 M_2^2 - \frac{3}{5} g_1^2 \text{Tr}(Y m^2), \\
16\pi^2 \frac{d}{dt} m_{\tilde{\tau}_R}^2 &= 4y_\tau^2 \Sigma_\tau^2 - \frac{24}{5} g_1^2 M_1^2 + \frac{6}{5} g_1^2 \text{Tr}(Y m^2),
\end{aligned} \tag{3.66}$$

where

$$\begin{aligned}
\Sigma_t^2 &= (m_{H_u}^2 + m_{\tilde{t}_L}^2 + m_{\tilde{t}_R}^2 + A_t^2), \\
\Sigma_b^2 &= (m_{H_d}^2 + m_{\tilde{b}_L}^2 + m_{\tilde{b}_R}^2 + A_b^2), \\
\Sigma_\tau^2 &= (m_{H_d}^2 + m_{\tilde{\tau}_L}^2 + m_{\tilde{\tau}_R}^2 + A_\tau^2).
\end{aligned} \tag{3.67}$$

When all of the squark, slepton and Higgs masses are the same at the GUT scale, we have

$$\text{Tr}(Y m^2) = m_0^2 \text{Tr}(Y) = 0, \tag{3.68}$$

as required by the absence of the gravitational mixed anomaly. Furthermore the condition is maintained by the RG evolution, and so holds at all scales. Hence one can neglect it in the analysis, which greatly simplifies these equations.

Next we consider the 1-loop RG equations for soft parameters A . In models obeying unification, these matrices start off proportional to the corresponding Yukawa couplings at the input scale. The RG evolution respects this property, in the approximation

$$A^U \approx a_t, \quad A^D \approx a_b, \quad A^L \approx a_\tau, \quad (3.69)$$

as single diagonal entries, which define² the running parameters a_t , a_b , and a_τ . In this approximation, the RG equations for these parameters are:

$$16\pi^2 \frac{d}{dt} a_t = a_t \left[18y_t^* y_t + y_b^* y_b - \frac{16}{3}g_3^2 - 3g_2^2 - \frac{13}{15}g_1^2 \right] + 2a_b y_b^* y_t + y_t \left[\frac{32}{3}g_3^2 M_3 + 6g_2^2 M_2 + \frac{26}{15}g_1^2 M_1 \right], \quad (3.70)$$

$$16\pi^2 \frac{d}{dt} a_b = a_b \left[18y_b^* y_b + y_t^* y_t + y_\tau^* y_\tau - \frac{16}{3}g_3^2 - 3g_2^2 - \frac{7}{15}g_1^2 \right] + 2a_t y_t^* y_b + 2a_\tau y_\tau^* y_b + y_b \left[\frac{32}{3}g_3^2 M_3 + 6g_2^2 M_2 + \frac{14}{15}g_1^2 M_1 \right], \quad (3.71)$$

$$16\pi^2 \frac{d}{dt} a_\tau = a_\tau \left[12y_\tau^* y_\tau + 3y_b^* y_b - 3g_2^2 - \frac{9}{5}g_1^2 \right] + 6a_b y_b^* y_\tau + y_\tau \left[6g_2^2 M_2 + \frac{18}{5}g_1^2 M_1 \right] \quad (3.72)$$

The β -function for each of these soft parameters is *not* proportional to the parameter itself, because couplings that violate supersymmetry are not protected by the supersymmetric non-renormalization theorem. So, even if a_t , a_b , a_τ vanish at the input scale, the RG corrections proportional to gaugino masses ensure that they will not vanish at the electroweak scale.

Another important aspect of such models in SUGRA is the achievement of EWSB radiatively. It turns out that the Yukawa coupling of the top quark drives the mass-squared parameter $m_{H_u}^2$ from positive to negative value around the electroweak scale, thus, 'naturally' creating the condition for spontaneous symmetry breaking. With all relevant quantities derived from their high-scale values, the conditions for minimization of the scalar potential relate them. One can thus express μ^2 and $B\mu$ in terms of the other parameters at the electroweak scale as follows:

²Rescaled soft parameters $A_t = a_t/y_t$, $A_b = a_b/y_b$, and $A_\tau = a_\tau/y_\tau$ are commonly used in the literature

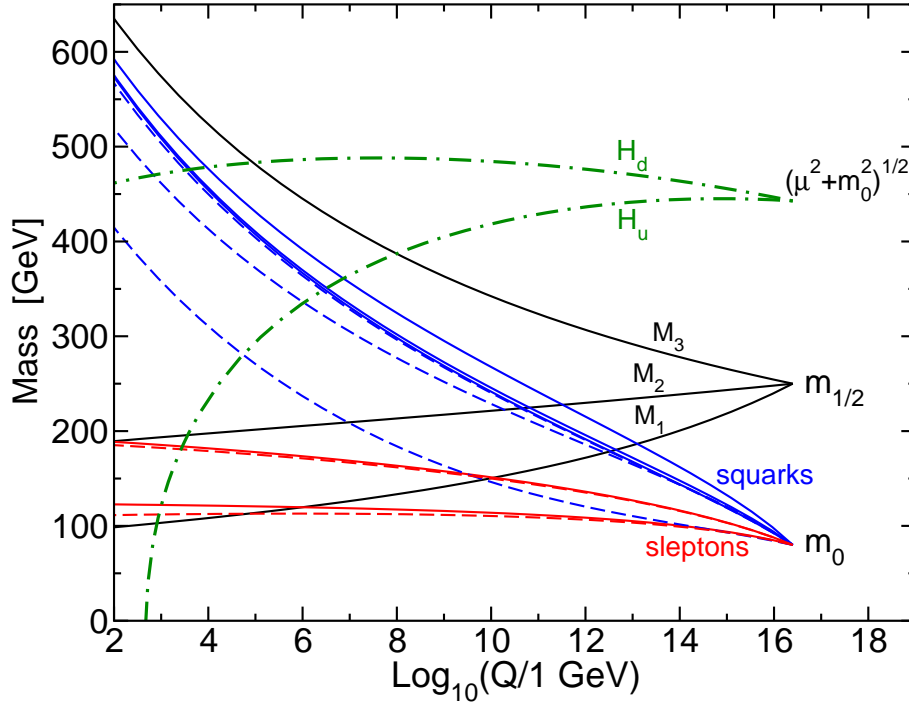


Figure 3.4: RG evolution of scalar and gaugino mass parameters in the MSSM with typical minimal supergravity-inspired boundary conditions imposed at $Q_0 = 2.5 \times 10^{16}$ GeV. The parameter $\mu^2 + m_{H_u}^2$ runs negative, provoking electroweak symmetry breaking. Taken from S. P. Martin in [2].

$$|\mu|^2 = -\frac{1}{2}M_Z^2 + \left(\frac{m_{H_d}^2 - m_{H_u}^2 \tan^2 \beta}{\tan^2 \beta - 1} \right), \quad (3.73)$$

$$2B\mu = (m_{H_d}^2 - m_{H_u}^2) \tan 2\beta + M_Z^2 \sin 2\beta. \quad (3.74)$$

Figure 3.4 shows the RG running of scalar and gaugino masses in a typical model based on the minimal supergravity boundary conditions imposed at $Q_0 = 2.5 \times 10^{16}$ GeV.

One has to mention that the low-scale values of all the parameters depend crucially on the boundary condition at the high scale. With high-scale non-universal gaugino or scalar mass scenarios which have imprints of different SUSY breaking schemes, the low scale sparticle hierarchy as well as the composition of charginos and neutralinos get altered to a large extent as compared to the mSUGRA. This has non-trivial consequences in collider search as well as in the dark matter search experiments. These issues have been discussed in detail in the

following chapters in different contexts.

3.7 Supersymmetry search at Colliders

As has already been mentioned, the production of sparticles takes places in pairs in a R-conserving SUSY. This means that the allowed SUSY production channels in experiments are: $\tilde{g}\tilde{g}$, $\tilde{q}_{L,R}\tilde{q}_{L,R}$, $\tilde{q}_{L,R}\tilde{g}$, $\tilde{l}_{L,R}\tilde{l}_{L,R}$, $\tilde{\chi}_i^0\tilde{\chi}_i^0$, $\tilde{\chi}_i^\pm\tilde{\chi}_i^\pm$, $\tilde{\chi}_i^0\tilde{\chi}_i^\pm$, $\tilde{q}_{L,R}\tilde{\chi}_i^0$, $\tilde{q}_{L,R}\tilde{\chi}_i^\pm$, $\tilde{l}_{L,R}\tilde{l}_{L,R}$ and $\tilde{l}_{L,R}\tilde{\nu}_L$. Direct search limits from the LEP experiment has been imposed on the superparticle masses from non-observation of the relevant final states. Such limits has been upgraded at the on going Tevatron experiment. This limit is best given for the gluinos and squarks as they have larger production rates in hadron collider. The limits are as follows:

- $m_{\tilde{g}} > 390$ GeV at 95 % confidence level (CL) assuming $m_{\tilde{q}} = m_{\tilde{g}}$. The limit is 308 GeV for any values of squark masses. These limits in addition, assume GUT unification of gaugino masses and gauge couplings and weakly depends on $\tan\beta$.
- $m_{\tilde{q}} > 379$ GeV with 95% CL. Although this is specifically for $\mu < 0$ and $\tan\beta = 2$, this limit is weakly sensitive to these parameters. Limits on third generation squarks are lower.
- Limits on sleptons are also around 100 GeV. Same is the case for lightest chargino. For lightest neutralino the limit is around 50 GeV assuming it to be the LSP.

The limits on the coloured superparticles can be raised to $\gtrsim 2$ TeV at the LHC [27]. However, the exact limits in all cases depend on the spectrum and is thus model-dependent. As a rule, all superpartners are short-lived and decay into the ordinary particles and the lightest superparticle. The main available decay modes for the particles produced as mentioned above are shown in the Table 3.2.

As a consequence of R-parity conservation, all SUSY cascades terminate at the LSP. In most SUSY models, lightest neutralino is the LSP. Since the $\tilde{\chi}_1^0$ LSP interacts only weakly, the signals of SUSY with conserved R-parity are marked by large missing energy and transverse momentum. This enables one to separate the signals from the background processes of the Standard Model. The missing energy is carried away by the heavy particle with the mass of the order of 100 GeV that is essentially different from the processes with neutrinos in the final state.

Creation	The main decay modes	Signature
• $\tilde{g}\tilde{g}, \tilde{q}\tilde{q}, \tilde{g}\tilde{q}$	$\left. \begin{array}{l} \tilde{g} \rightarrow q\bar{q}\tilde{\chi}_1^0 \\ q\bar{q}'\tilde{\chi}_1^\pm \\ g\tilde{\chi}_1^0 \end{array} \right\} m_{\tilde{q}} > m_{\tilde{g}}$ $\left. \begin{array}{l} \tilde{q} \rightarrow q\tilde{\chi}_i^0 \\ \tilde{q} \rightarrow q'\tilde{\chi}_i^\pm \end{array} \right\} m_{\tilde{g}} > m_{\tilde{q}}$	$\cancel{E}_T + \text{multijets (+leptons)}$
• $\tilde{\chi}_1^\pm \tilde{\chi}_2^0$	$\tilde{\chi}_1^\pm \rightarrow \tilde{\chi}_1^0 \ell^\pm \nu, \tilde{\chi}_2^0 \rightarrow \tilde{\chi}_1^0 \ell \ell$ $\tilde{\chi}_1^\pm \rightarrow \tilde{\chi}_1^0 q \bar{q}', \tilde{\chi}_2^0 \rightarrow \tilde{\chi}_1^0 \ell \ell,$	trilepton + \cancel{E}_T dileptons + jet + \cancel{E}_T
• $\tilde{\chi}_1^+ \tilde{\chi}_1^-$	$\tilde{\chi}_1^+ \rightarrow \ell \tilde{\chi}_1^0 \ell^\pm \nu$	dilepton + \cancel{E}_T
• $\tilde{\chi}_i^0 \tilde{\chi}_i^0$	$\tilde{\chi}_i^0 \rightarrow \tilde{\chi}_1^0 X, \tilde{\chi}_i^0 \rightarrow \tilde{\chi}_1^0 X'$	dilepton+jet + \cancel{E}_T
• $\tilde{t}_1 \tilde{t}_1$	$\tilde{t}_1 \rightarrow c \tilde{\chi}_1^0$ $\tilde{t}_1 \rightarrow b \tilde{\chi}_1^\pm, \tilde{\chi}_1^\pm \rightarrow \tilde{\chi}_1^0 q \bar{q}'$ $\tilde{t}_1 \rightarrow b \tilde{\chi}_1^\pm, \tilde{\chi}_1^\pm \rightarrow \tilde{\chi}_1^0 \ell^\pm \nu,$	2 noncollinear jets + \cancel{E}_T single lepton + $\cancel{E}_T + b$'s dilepton + $\cancel{E}_T + b$'s
• $\tilde{l}, \tilde{l}\tilde{\nu}, \tilde{\nu}\tilde{\nu}$	$\tilde{\ell}^\pm \rightarrow \ell^\pm \tilde{\chi}_i^0, \tilde{\ell}^\pm \rightarrow \nu_\ell \tilde{\chi}_i^\pm$ $\tilde{\nu} \rightarrow \nu \tilde{\chi}_1^0$	dilepton + \cancel{E}_T single lepton + \cancel{E}_T

Table 3.2: Creation of superpartners and the main decay modes. Taken from [6]

A typical SUSY signature at colliders is seen in the form of

$$n \text{ leptons} + m \text{ jets} + \cancel{E}_T$$

where the leptons are hard missing transverse energy (\cancel{E}_T) is very high due to a pair of lightest neutralinos. We tabulate some such final states that is obtained by the cascade decays of a gluino pair production. In scenarios other than these based on SUGRA, for example, in gauge mediated SUSY breaking, one can also have typical signals characterized by hard photons. In practice, \cancel{E}_T is obtained from data by measuring the vector sum of the transverse momenta of all the visible final state particles, namely $\Sigma \vec{p}_T$.

The other useful selection criterion applied on a general basis are hardness and centrality of jets and leptons, as decay products of heavy particles usually carry a large transverse momenta (p_T). There exist direct limits on sparticle masses based on direct searches at high energy colliders (LEP II, SLC, Tevatron).

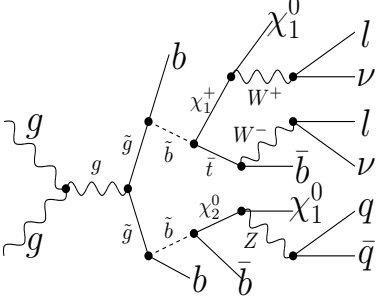
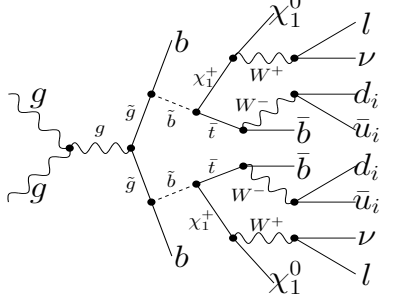
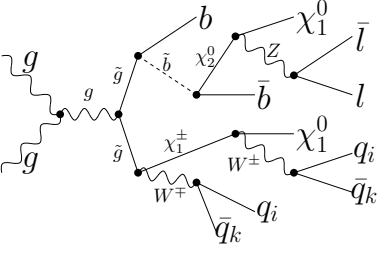
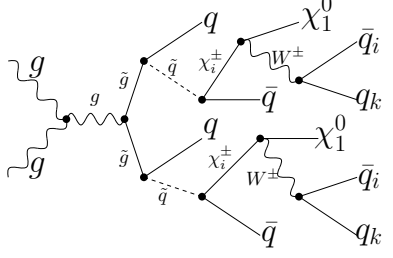
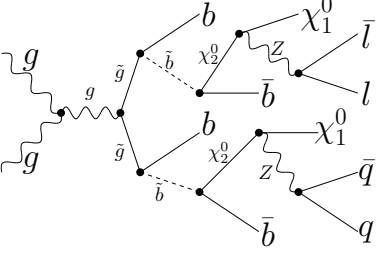
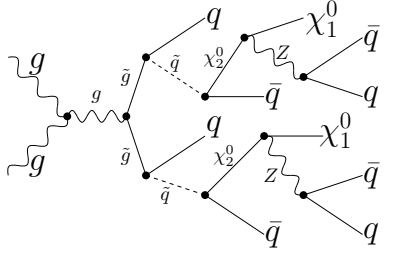
Process	final states	Process	final states
	$2l$ 2ν $6j$ $\cancel{\not{E}_T}$		$2l$ 2ν $8j$ $\cancel{\not{E}_T}$
	$2l$ $6j$ $\cancel{\not{E}_T}$		$8j$ $\cancel{\not{E}_T}$
	$2l$ $6j$ $\cancel{\not{E}_T}$		$8j$ $\cancel{\not{E}_T}$

Table 3.3: Creation of a pair of gluinos, followed by their cascade decays. Taken from [6]

Although hadron colliders can achieve larger center-of-mass energies than e^+e^- ones, and also lead to wider varieties of events, their event samples contain larger backgrounds that make the analysis more difficult. This drawback can be avoided if the signal-to-background ratio is improved. Therefore, finding proper event selection criteria is one of the prime concerns of LHC-based research on SUSY.

Bibliography

- [1] For introductory reviews see, for example, H. P. Nilles, Phys. Rept. **110**, 1 (1984); J. Wess and J. Bagger, *Supersymmetry and Supergravity*, (Princeton Univ. Press, 1992). P.C. West, *Introduction to Supersymmetry and Supergravity*, (World Scientific, 1990); D. Bailin and A. Love, *Supersymmetric Gauge Field Theory and String Theory*, (Institute of Physics Publishing, 1994); M. Drees, R. Godbole and P. Roy, *Theory and Phenomenology of Sparticles*, (World Scientific, 2004); H. Baer and X. Tata *Weak Scale Supersymmetry From Superfields to Scattering Events*, (Cambridge University Press, 2006).
- [2] For reviews see, for example, H. E. Haber and G. L. Kane, Phys. Rept. **117**, 75 (1985); *Perspectives on Supersymmetry* by G. Kane(ed), (World Scientific, 1998) and articles therein; M. Drees and S.P. Martin, [hep-ph/9504324]; M. Drees, arXiv:hep-ph/9611409; J.D. Lykken, TASI-96 lectures, [hep-th/9612114]; S. P. Martin, arXiv:hep-ph/9709356, and references therein; J.F. Gunion, [hep-ph/9704349], M. E. Peskin, arXiv:0801.1928 [hep-ph].
- [3] S. Weinberg, Phys. Rev. D **13**, 974 (1976), Phys. Rev. D **19**, 1277 (1979); E. Gildener, Phys. Rev. D **14**, 1667 (1976); L. Susskind, Theory," Phys. Rev. D **20**, 2619 (1979); G. 't Hooft, in *Recent developments in gauge theories*, Proceedings of the NATO Advanced Summer Institute, Cargese 1979, (Plenum, 1980).
- [4] S. Dimopoulos and S. Raby, Nucl. Phys. B **192**, 353 (1981); E. Witten, Nucl. Phys. B **188**, 513 (1981); M. Dine, W. Fischler and M. Srednicki, Nucl. Phys. B **189**, 575 (1981); S. Dimopoulos and H. Georgi, Nucl. Phys. B **193**, 150 (1981); N. Sakai, Z. Phys. C **11**, 153 (1981); R.K. Kaul and P. Majumdar, Nucl. Phys. B **199**, 36 (1982).
- [5] See for example, the book *Grand Unified Theories* by G. Ross(1984), Westview Press; H. Georgi and S. L. Glashow, Phys. Rev. Lett. **32**, 438 (1974); J. C. Pati

- and A. Salam, Phys. Rev. D **10**, 275 (1974) [Erratum-ibid. D **11**, 703 (1975)]; P. Langacker, "Grand Unified Theories And Proton Decay," Phys. Rept. **72** (1981) 185.
- [6] A. V. Gladyshev and D. I. Kazakov, Phys. Atom. Nucl. **70**, 1553 (2007) [arXiv:hep-ph/0606288].
- [7] P. Langacker, *Precision Tests Of The Standard Model*, in Proceedings of the PASCOS90 Symposium, (World Scientific, 1990); J. Ellis, S. Kelley, and D. Nanopoulos, Phys. Lett. B **260**, 131 (1991); U. Amaldi, W. de Boer, and H. Furstenau, Phys. Lett. B **260**, 447 (1991); P. Langacker and M. Luo, Phys. Rev. D **44**, 817 (1991); C. Giunti, C.W. Kim and U.W. Lee, Mod. Phys. Lett. A **6**, 1745 (1991);
- [8] For a brief history of DM, see V. Trimble, in *Proceedings of the First International Symposium on Sources of Dark Matter in the Universe*, by D.B. Cline (ed.), World Scientific, Singapore, Bel Air, California (1994) ; See also the recent review by G. Bertone, D. Hooper, and J. Silk, Phys. Rep. **405**, 279 (2005).
- [9] E. Komatsu *et al.* [WMAP Collaboration], Astrophys. J. Suppl. **180**, 330 (2009) [arXiv:0803.0547 [astro-ph]].
- [10] See for example, E.W. Kolb and M.E. Turner, *The Early Universe*, Addison-Wesley (1990).
- [11] D. Clowe, M. Bradac, A. H. Gonzalez, M. Markevitch, S. W. Randall, C. Jones and D. Zaritsky, Astrophys. J. **648**, L109 (2006) [arXiv:astro-ph/0608407].
- [12] For a review, see G. Jungman, M. Kamionkowski, and K. Griest, Phys. Reports **267**, 195 (1996); A. B. Lahanas, N. E. Mavromatos and D. V. Nanopoulos, Int. J. Mod. Phys. D **12**, 1529 (2003); C. Munoz, Int. J. Mod. Phys. A **19**, 3093 (2004); M. Drees, Plenary talk at 11th International Symposium on Particles, Strings and Cosmology (PASCOS 2005), Gyeongju, Korea, 30 May - 4 Jun 2005 (published in AIP Conf.Proc., **805**, 48-54, (2006).
- [13] S. R. Coleman and J. Mandula, Phys. Rev. **159**, 1251 (1967); R. Haag, J. Lopuszanski, and M. Sohnius, Nucl. Phys. B **88**, 257 (1975).
- [14] M. E. Peskin, Prog. Theor. Phys. Suppl. **123**, 507 (1996) [arXiv:hep-ph/9604339].

- [15] L. Girardello and M.T. Grisaru Nucl. Phys. B **194**, 65 (1982); D.J.H. Chung et al., Phys. Rept. **407**, 1 (2005) [hep-ph/0312378]; M.A. Luty, [hep-th/0509029].
- [16] X. Tata, [hep-ph/9706307]; I. Aitchison, [hep-ph/0505105].
- [17] G.R. Farrar and P. Fayet, Phys. Lett. B **76**, 575 (1978).
- [18] H. Goldberg, Phys. Rev. Lett. **50**, 1419 (1983); J. Ellis, J. Hagelin, D.V. Nanopoulos, K. Olive, and M. Srednicki, Nucl. Phys. B **238**, 453 (1984).
- [19] For reviews, see G. Bhattacharyya, Nucl. Phys. Proc. Suppl. **52A**, 83 (1997) [hep-ph/9608415]; H.K. Dreiner, [hep-ph/9707435]; R. Barbier *et al.*, [hep-ph/9810232]; B. Allanach *et al.*, [hep-ph/9906224]; B. Allanach, A. Dedes and H.K. Dreiner, Phys. Rev. D **69**, 115002 (2004) [hep-ph/0309196]; M. Chemtob, Prog. Part. Nucl. Phys. **54**, 71 (2005) [hep-ph/0406029].
- [20] P. Nath and R. Arnowitt, Phys. Lett. B **56**, 177 (1975); R. Arnowitt, P. Nath and B. Zumino, Phys. Lett. B **56**, 81 (1975); S. Ferrara, D.Z. Freedman and P. van Nieuwenhuizen, Phys. Rev. D **13**, 3214 (1976); S. Deser and B. Zumino, Phys. Lett. B **62**, 335 (1976); D.Z. Freedman and P. van Nieuwenhuizen, Phys. Rev. D **14**, 912 (1976); E. Cremmer et al., Nucl. Phys. B **147**, 105 (1979); J. Bagger, Nucl. Phys. B **211**, 302 (1983); A. Chamseddin, R. Arnowitt and P. Nath, 'Applied $N=1$ Supergravity', World Scientific, Singapore (1984).
- [21] M. Dine, A. E. Nelson, Phys. Rev. D **48**, 1277 (1993) [hep-ph/9303230]; M. Dine, A.E. Nelson, Y. Shirman, Phys. Rev. D **51**, 1362 (1995) [hep-ph/9408384]; M. Dine, A.E. Nelson, Y. Nir, Y. Shirman, Phys. Rev. D **53**, 2658 (1996) [hep-ph/9507378].
- [22] D.E. Kaplan, G.D. Kribs and M. Schmaltz, Phys. Rev. D **62**, 035010 (2000) [hep-ph/9911293]; Z. Chacko, M.A. Luty, A.E. Nelson and E. Ponton, JHEP **0001**, 003 (2000) [hep-ph/9911323].
- [23] L. Randall and R. Sundrum, Nucl. Phys. B **557**, 79 (1999) [hep-th/9810155]; G.F. Giudice, M.A. Luty, H. Murayama and R. Rattazzi, JHEP **9812**, 027 (1998) [hep-ph/9810442].
- [24] J. Scherk and J.H. Schwarz, Phys. Lett. B **82**, 60 (1979); Nucl. Phys. B **153**, 61 (1979).
- [25] S. Kachru, R. Kallosh, A. D. Linde and S. P. Trivedi, Phys. Rev. D **68**, 046005 (2003) [arXiv:hep-th/0301240]; K. Choi, A. Falkowski, H. P. Nilles

- and M. Olechowski, Nucl. Phys. B **718**, 113 (2005) [arXiv:hep-th/0503216];
A. Falkowski, O. Lebedev and Y. Mambrini, JHEP **0511**, 034 (2005)
[arXiv:hep-ph/0507110]; H. Baer, E. K. Park, X. Tata and T. T. Wang, JHEP
0706, 033 (2007) [arXiv:hep-ph/0703024].
- [26] S. P. Martin and P. Ramond, Phys. Rev. D **48**, 5365 (1993) [arXiv:hep-ph/9306314].
- [27] See for example, books in reference 1, specifically the ones by H. Baer and X. Tata or the one by M. Drees, R. Godbole and P. Roy; article by A. Datta, M. Guchait and S. Roy in *Physics at the Large Hadron Collider* by A. Datta, B. Mukhopadhyaya and A. Raychaudhuri (ed.), Springer India (2009); J. L. Feng, J. F. Grivaz and J. Nachtman, arXiv:0903.0046 [hep-ex].

Part II

Investigations on high-scale non-universality in supersymmetry and collider signals

Chapter 4

Non-universal gaugino masses in $SU(5)$: a signal-based analysis for the Large Hadron Collider

4.1 Introduction

In the simplest SUGRA models and their phenomenological studies, all low-scale parameters are derived from a universal gaugino mass ($M_{1/2}$), a universal scalar mass (m_0), the trilinear soft SUSY-breaking parameter (A_0) and the sign of the Higgsino mass parameter ($\text{sgn}(\mu)$) for each value of $\tan\beta$, the ratio of the two Higgs vacuum expectation values [1, 2]. A universal gaugino mass occurs in the simplest form of a SUSY GUT. Its immediate consequence is that the three low-energy gaugino masses corresponding to $SU(3)$, $SU(2)$ and $U(1)$ are in the ratio of the corresponding fine-structure constants: $\frac{M_3}{\alpha_3} = \frac{M_2}{\alpha_2} = \frac{M_1}{\alpha_1}$ [1]. This relation governs the low-energy chargino and neutralino masses vis-a-vis the gluino mass. It has profound implications on the strengths of different types of signals, since gluinos are liable to be copiously produced at the LHC, and the cascades initiated by them involve the charginos and neutralinos at various stages [3]. Therefore, if gaugino mass universality at high scale does not hold, it means that both

the spectrum and the compositions of the charginos and neutralinos are subject to marked variations, so that the final states have different rates compared to the universal case both through kinematics and dynamics.

While departure from universality may well indicate that one is not facing a SUSY GUT scenario, it may, interestingly, still be the consequence of a GUT framework. The gaugino masses arise from the gauge kinetic function whose trivial nature, as we shall see in the next section, implies a universal gaugino mass when SUSY is broken at high scale. This is possible if the combination of hidden sector fields involved in the function is a singlet under the GUT group. However, it is always possible to generate mass terms via higher GUT representations, which in turn create inequality among M_1 , M_2 and M_3 at the high scale itself [4–7]. It is also possible to have more than one GUT representations involved in SUSY breaking, in which case the non-universality arises from a linear combination of the effects mentioned above.

Identifying departure from universality in SUSY signals is important at more than one levels [8–12]. First, one would like to know whether or not the gaugino mass relation corresponding to a particular GUT representation is involved. The absence of any such obvious relation, however, still keeps SUSY GUT's alive, if the analysis of signals reveals that a linear combination of GUT multiplets is involved. It is only the decisive failure of such a finer analysis that can rule out a framework based on GUT. Therefore, if SUSY signals in some channel(s) are indeed seen at the LHC, the exercise of tracing them back to some underlying GUT framework, be it with gaugino mass universality or not, is of utmost importance.

Testing gaugino non-universality at the LHC, however, is not easy, especially if the ambitious task of looking for higher GUT representations has to be undertaken. There has been some detailed analysis of events and kinematics for non-universal gaugino masses in the context of the Tevatron [13, 14], with reference to $SU(5)$. Some phenomenological studies have been performed on different types of signals at the LHC, too [15–18], but the systematic investigation that is required to link the departure from universality to GUT representations has not so far been carried out in detail.

In this chapter [19], different representations of SUSY $SU(5)$ are considered; some aspects of $SO(10)$ is taken in the next chapter. No specific SUGRA origin of scalar masses is assumed in the general analyses, and we deliberately adhere

to degenerate squark and slepton masses at low energy in each case. However, we also present side by side the consequences of a SUGRA scenario with universal scalar masses at high scale. In each case, we consider a comprehensive set of SUSY signals, such as *jets + \cancel{E}_T* , *same-sign* as well as *opposite-sign dileptons*, *one isolated lepton* and *trileptons* along with *jets + \cancel{E}_T* (so called multichannel analysis [20, 21]). After subjecting the calculated event rates for these different final states and for different parameter values to such cuts as to suppress the standard model (SM) backgrounds, we look at their various ratios. This reduces uncertainties due to jet energy resolution, jet energy scale, parton distribution functions and so on. It also ensures that the departure from gaugino universality, rather than the overall scale of superparticle masses, is the decisive factor. Thereafter, we compare these ratios with the corresponding cases with a universal gaugino mass. The squark and gluino masses are kept at the same values during this comparison, since the most important cascades are dictated by them, and their masses can be approximately found out from the LHC data from \cancel{E}_T and effective mass distributions. Although we confine ourselves to a relatively rudimentary analysis, it is expected that more elaborate ones can be built on it following the same strategy. It is our belief that such an approach will mean full utilization of the LHC data in following up on any signature of SUSY, an exercise that is eminently appropriate at the present juncture [22].

In Section 4.2, we briefly review the process by which non-universality may arise at the GUT scale, and summarise the high-scale mass relations of gauginos in different GUT representations under $SU(5)$ responsible for the non-universality. The strategy adopted in selecting the relevant SUSY parameters, and the event selection criteria for LHC, are outlined in Section 4.3. The analysis of predicted signals for different representations of $SU(5)$ are presented in Section 4.4. We summarise and conclude in Section 4.5. Appendix A contains the various chargino and neutralino masses for different scenarios, while the absolute values of event rates in different channels (which has been found to be necessary supplements to the various ratios presented in the main text) are listed in Appendix B provided at the end of this chapter.

4.2 Non-universal SUSY GUT and gaugino mass ratios in $SU(5)$

In this section we review the issues that govern non-universality of supersymmetry breaking gaugino masses, arising under the influence of various GUT representations responsible for the SUSY breaking terms.

We adhere to a scenario where all soft SUSY breaking effects arise via hidden sector interactions in an underlying supergravity (SUGRA) framework. Specifically, we are considering supersymmetric $SU(5)$ gauge theories with an arbitrary chiral matter superfield content coupled to N=1 supergravity. The essential theoretical principles governing high-scale non-universality in gaugino masses as well as in gauge couplings have been discussed in a number of earlier works in the context of both $SU(5)$ [4,5] and $SO(10)$ [6] gauge groups respectively. Later works that addressed the related phenomenology (mostly in the context of $SU(5)$) are by and large based on these principles [7, 13, 14].

All gauge and matter terms including gaugino masses in the N=1 supergravity Lagrangian depend crucially on two fundamental functions of chiral superfields [23]. One of them is the gauge kinetic function $f_{\alpha\beta}(\Phi)$ which is an analytic function of the left-chiral superfields Φ_i . It transforms as a symmetric product of the adjoint representation as gauge superfields belong to the adjoint representation of the underlying gauge group (α, β being the gauge generator indices). The other is the real function $G(\Phi_i, \Phi_i^*)$ with $G = K + \ln|W|$ where K is the Kähler potential and W is the superpotential. G is a real function of the chiral superfields Φ_i and is a gauge singlet. However, $f_{\alpha\beta}$ in general has a non-trivial gauge transformation property. Based on whether its functional dependence on the chiral superfields involves singlet or non-singlet irreducible representations of the underlying gauge group, one has universal or non-universal gaugino masses at the GUT scale, when SUSY is broken.

In the component field notation, the part of the N=1 supergravity Lagrangian containing kinetic energy and mass terms for gauginos and gauge bosons (including only terms containing the real part of $f(\Phi)$) reads [5, 23]

$$e^{-1}\mathcal{L} = -\frac{1}{4}Re f_{\alpha\beta}(\phi)(-1/2\bar{\lambda}^\alpha \not{D}\lambda^\beta) - \frac{1}{4}Re f_{\alpha\beta}(\phi)F_{\mu\nu}^\alpha F^{\beta\mu\nu} + \frac{1}{4}e^{-G/2}G^i((G^{-1})_i^j)[\partial f_{\alpha\beta}^*(\phi^*)/\partial\phi^{*j}]\lambda^\alpha\lambda^\beta + h.c \quad (4.1)$$

where $G^i = \partial G / \partial \phi_i$ and $(G^{-1})^i_j$ is the inverse matrix of $G^j_i \equiv \partial G / \partial \phi^{*i} \partial \phi_j$, λ^α is the gaugino field, and ϕ is the scalar component of the chiral superfield Φ . The F -component of Φ enters the last term to generate gaugino masses. Thus, following Equation 4.1, the Lagrangian can be expressed as [14]

$$e^{-1} \mathcal{L} = -\frac{1}{4} \text{Re} f_{\alpha\beta}(\phi) (-1/2 \bar{\lambda}^\alpha \not{D} \lambda^\beta) - \frac{1}{4} \text{Re} f_{\alpha\beta}(\phi) F_{\mu\nu}^\alpha F^{\beta\mu\nu} + \frac{F^j_{\dot{\alpha}\dot{\beta}}}{2} [\partial f_{\alpha\beta}^*(\phi^{*j}) / \partial \phi^{*j}_{\dot{\alpha}\dot{\beta}}] \lambda^\alpha \lambda^\beta + h.c \quad (4.2)$$

where

$$F^j_{\dot{\alpha}\dot{\beta}} = \frac{1}{2} e^{-G/2} [G^i ((G^{-1})^j_i)]_{\dot{\alpha}\dot{\beta}} \quad (4.3)$$

The Φ^j s can be classified into two categories: a set of GUT singlet supermultiplets Φ^S , and a set of non-singlet ones Φ^N . The non-trivial gauge kinetic function $f_{\alpha\beta}(\Phi^j)$ can be expanded in terms of the non-singlet components in the following way [4,5,14]:

$$f_{\alpha\beta}(\Phi^j) = f_0(\Phi^S) \delta_{\alpha\beta} + \sum_N \zeta_N(\Phi^S) \frac{\Phi^N_{\alpha\beta}}{M} + \mathcal{O}(\frac{\Phi^N}{M})^2 \quad (4.4)$$

where f_0 and ζ^N are functions of chiral singlet superfields, and M is the reduced Planck mass = $M_{Pl} / \sqrt{8\pi}$.

In principle, the gauge kinetic function $f_{\alpha\beta}$ is a function of all chiral superfields Φ^j . However, those which contribute significantly at the minimum of the potential by acquiring large vacuum expectation values (vev) are (i) gauge singlet fields which are part of the hidden sector (i.e. the fields Φ^S), and (ii) fields associated with the spontaneous breakdown of the GUT group to $SU(3) \otimes SU(2) \otimes U(1)$ (i.e. the fields Φ^N) [4,5]. In Equation 4.4, the contribution to the gauge kinetic function from Φ^N has to come through symmetric products of the adjoint representation of associated GUT group, since $f_{\alpha\beta}$ on the left side of 4.4 has such transformation property. Thus $f_{\alpha\beta}$ can have the 'non-trivial' contribution of the second type of terms only if one has chiral superfields belonging to representations which can arise from the symmetric products of two adjoint representations [4–7]. For $SU(5)$, for example, one can have contributions to $f_{\alpha\beta}$ from all possible non-singlet irreducible representations to which Φ^N can belong :

$$(24 \otimes 24)_{symm} = 1 \oplus 24 \oplus 75 \oplus 200$$

The contribution to $f_{\alpha\beta}$ can also come from any linear combination of the singlet and possible non-singlet representations (as shown above). It is now almost clear from Equations 4.1 and 4.2 that these non-singlet representations can be responsible for non-universal gaugino mass terms at the GUT scale.

In order to obtain the low energy effective theory, we replace the fields Φ^S and Φ^N in the gauge kinetic term (Equation 4.4) by their vev's and get $\langle f_{\alpha\beta} \rangle$. The value of $\langle f_{\alpha\beta} \rangle$ which determines the gaugino mass matrix crucially depends on the specific representation (or their linear combinations) responsible for the process [4, 5]. The breakdown of the symmetry from $SU(5)$ to the SM gauge group has been assumed to take place at the GUT scale (M_X).

Next, the kinetic energy terms are restored to the canonical form by rescaling the gauge superfields, by defining

$$F^\alpha_{\mu\nu} \rightarrow \hat{F}^\alpha_{\mu\nu} = \langle \text{Re} f_{\alpha\beta} \rangle^{\frac{1}{2}} F^\beta_{\mu\nu} \quad (4.5)$$

and

$$\lambda^\alpha \rightarrow \hat{\lambda}^\alpha = \langle \text{Re} f_{\alpha\beta} \rangle^{\frac{1}{2}} \lambda^\beta \quad (4.6)$$

Simultaneously, the gauge couplings are also rescaled (as a result of Equation 4.4):

$$g_\alpha(M_X) \langle \text{Re} f_{\alpha\beta} \rangle^{\frac{1}{2}} \delta_{\alpha\beta} = g_c(M_X) \quad (4.7)$$

where g_c is the universal coupling constant at the GUT scale. This shows clearly that the first consequence of a non-trivial gauge kinetic function is non-universality of the gauge couplings g_α at the GUT scale, if $\langle f_{\alpha\beta} \rangle$ carries a gauge index [4, 5, 24].

Once SUSY is broken by non-zero vev's of the F components of hidden sector chiral superfields, the coefficient of the last term in Equation 4.2 is replaced by [4, 5, 14]

$$\langle F_{\alpha\beta}{}^i \rangle = \mathcal{O}(m_{\frac{3}{2}} M) \quad (4.8)$$

where $m_{\frac{3}{2}} = \exp(-\frac{G}{2})$ is the gravitino mass. Taking into account the rescaling of the gaugino fields (as stated earlier in Equation 4.5 and 4.6) in Equation 4.1 and 4.2, the gaugino mass matrix can be written down as in [14] or [4, 7]

$$M_\alpha(M_X) \delta_{\alpha\beta} = \sum_i \frac{\langle F_{\hat{\alpha}\hat{\beta}}^i \rangle}{2} \frac{\langle \partial f_{\alpha\beta}(\phi^{*i}) / \partial \phi^{*i}{}_{\hat{\alpha}\hat{\beta}} \rangle}{\langle \text{Re} f_{\alpha\beta} \rangle} \quad (4.9)$$

or

$$M_\alpha(M_X) \delta_{\alpha\beta} = \frac{1}{4} e^{-G/2} G^i ((G^{-1})^j{}_i) \frac{\langle \partial f_{\alpha\beta}^*(\phi^*) / \partial \phi^{*j} \rangle}{\langle \text{Re} f_{\alpha\beta} \rangle} \quad (4.10)$$

which demonstrates that the gaugino masses are non-universal at the GUT scale. The underlying reason for this is the fact that $\langle f_{\alpha\beta} \rangle$ can be shown to acquire the form $f_\alpha \delta_{\alpha\beta}$ [4, 5], where the f_α 's are purely group theoretic factors, thanks to the symmetric character of the representations. Consequently, the derivatives on the right-hand side of the above equations acquire such forms as to render M_α non-universal in the gauge indices. On the contrary, if symmetry breaking occurs via gauge singlet fields only, one has $f_{\alpha\beta} = f_0 \delta_{\alpha\beta}$ from Equation 4.4 and as a result, $\langle f_{\alpha\beta} \rangle = f_0$. Thus both gaugino masses and the gauge couplings are unified at the GUT scale, as can be seen from Equations 4.9 and 4.10.

Following the approach in [4, 5, 7, 14], we make a further simplification by neglecting the non-universal contributions to the gauge couplings at the GUT scale. The gaugino mass ratios at high scale thus obtained [4, 6] are shown in Table 4.1. We also present the approximate values of the ratios at the Electroweak Symmetry Breaking scale (EWSB) after running by one-loop RGE in this table.

Representation	$M_3 : M_2 : M_1$ at M_{GUT}	$M_3 : M_2 : M_1$ at M_{EWSB} (One loop RGE)
1	1:1:1	6:2:1
24	2:(-3):(-1)	12:(-6):(-1)
75	1:3:(-5)	6:6:(-5)
200	1:2:10	6:4:10

Table 4.1: *High-scale and approximate low-scale gaugino mass ratios for different representations in $SU(5)$*

4.3 SUSY signals and backgrounds: strategy for analysis

In this section we discuss and analyse the difference in the collider signature due to non-universal gaugino masses at the GUT scale for various non-singlet representations of $SU(5)$ GUT group in the context of the LHC.

4.3.1 Choice of SUSY parameters

In our analysis we have confined ourselves to R -parity conserving supersymmetry where the lightest neutralino is the LSP. Thus all SUSY signals at the LHC are characterized by a large amount of missing E_T carried by the LSP, together with jets and/or leptons of various multiplicity.

A large part of our analysis is done for a scenario where the gaugino masses are obtained through one-loop running from the non-universal mass parameters at the high scale, whereas the low-energy scalar masses are all treated as phenomenological inputs. Furthermore, since we wish to examine the effects of gaugino non-universality in isolation, we have taken all the squark and slepton masses to be degenerate. This not only avoids special situations arising from SUSY cascade decays due to a spread in the sfermion masses, but also keeps the scenario above board by suppressing flavour-changing neutral currents (FCNC) [25]. Such close degeneracy can also be motivated in a GMSB scenario. The Higgsino mass parameter μ , too, is a free parameter here. The mass parameters of the Higgs sector are determined once μ , the neutral pseudoscalar mass (m_A) and $\tan\beta$ (the ratio of the two Higgs vev's) are specified.

Side by side, we also present an analysis pertaining to a non-universal SUGRA scenario where the low energy supersymmetric spectrum is generated from a common scalar mass m_0 , common trilinear coupling A_0 and $\text{sgn}(\mu)$, with non-universal gaugino masses M_i at high scale arising from various non-singlet representations of $SU(5)$. While this allows a spread in the low-energy sfermion masses, it also gives one the opportunity to compare the predicted collider results with those in the phenomenological scalar spectrum mentioned above. It has been made sure that in both this case and the previous one, the parameter choices are consistent with the LEP bounds, as far as the neutral Higgs mass, the lighter chargino mass etc. are concerned [26].

The spectrum in the first case is generated by the option **pMSSM** in the code `SuSpect v2.3` [27]. It should be remembered that our goal here is to generate a phenomenological low-energy spectrum with degenerate scalar masses, but with the three gaugino mass parameters related not by high-scale universality but by the specific conditions answering to various non-singlet GUT representations. In order to implement this, we resort to a two-step process. The first step is to give as inputs non-universal gaugino masses at the GUT scale, and evolve them

down to low scale through one-loop renormalization group equations (which do not involve scalar masses). This yields a phenomenological gaugino spectrum which, to a reasonable approximation, corresponds to the specific non-singlet GUT representation under scrutiny. In the second step, we feed the thus obtained gaugino masses, together with the degenerate scalar masses (and the free parameters in the Higgs sector) at the electroweak symmetry breaking (EWSB) scale, into SuSpect as low energy inputs in the **pMSSM** option. The subsequent running of SuSpect yields a low-energy spectrum which is basically phenomenological, but ensures gauge coupling unification at high scale (see discussion in the previous section), and is nonetheless consistent with laboratory constraints on a SUSY scenario. We have used the low-energy value of $\alpha_3(M_Z)^{\overline{MS}} = 0.1172$ for this calculation which is default in SuSpect. Throughout the analysis we have assumed the top quark mass to be 171.4 GeV. Electroweak symmetry breaking at the ‘default scale’ $\sqrt{m_{\tilde{t}_L} m_{\tilde{t}_R}}$ has been ensured in this procedure, together with the requirement of no tachyonic modes for sfermions. No radiative correction to gaugino masses has been considered, which does not affect the main flow of our analysis in any significant way. Full one-loop and the dominant two-loop corrections to the Higgs masses are incorporated. And finally, consistency with low-energy constraints $b \rightarrow s\gamma$ and muon anomalous magnetic moment are checked for every combination of parameters used in the analysis. Preferring to be strictly confined to accelerator signals, we have not considered dark matter constraints in our analysis. For studies in this direction, we refer the reader to [7, 28–30] where the issues related to dark matter in non-universal gaugino scenarios have been discussed. It should also be remembered that, although we shall henceforth refer to this case as **pMSSM** for convenience, the low-energy spectrum is not purely ‘phenomenological’, since the gaugino masses at low energy actually correspond to specific high-scale GUT-breaking conditions.

We attempt a representative analysis of the above situation by taking all possible combinations of parameters, arising out of the following choices, for each type of GUT breaking scheme:

$$m_{\tilde{g}} = [500 \text{ GeV}, 1000 \text{ GeV}, 1500 \text{ GeV}]$$

$$m_{\tilde{f}} = [500 \text{ GeV}, 1000 \text{ GeV}]$$

$$\mu = [300 \text{ GeV}, 1000 \text{ GeV}]$$

$$\tan \beta = [5, 40]$$

where by $m_{\tilde{f}}$ we denote all the degenerate squark and slepton masses. This gives

us a total of 24 combinations which include the most important kinematics regions in terms of $m_{\tilde{g}}$ and $m_{\tilde{q}}$ namely, (i) $m_{\tilde{g}} \gg m_{\tilde{f}}$, (ii) $m_{\tilde{q}} \gg m_{\tilde{g}}$ and (iii) $m_{\tilde{q}} \simeq m_{\tilde{g}}$ which crucially controls the final state scenario at the collider. Also the variation in μ changes the chargino and neutralino compositions which affect the various decay branching fractions involved in the cascades. We have also taken two values of $\tan \beta$, one close to the limit coming from $e^+ e^-$ collider data, and the other on the high side, since they also control the chargino-neutralino sector. For all these points we keep all the trilinear coupling constants $A_0 = 0$ and the pseudoscalar Higgs mass $m_A = 1000$ GeV. The chargino and neutralino mass spectra corresponding to the **pMSSM** parameter points are provided in Table A1-A8 in Appendix A of this chapter.

For studying the other scenario, namely, gaugino mass non-universality in a **SUGRA** setting, the spectrum is generated with the help of ISASUGRA v7.75 [31]. As mentioned earlier, here one uses as the inputs a common scalar mass m_0 , a common trilinear coupling A_0 , $\tan \beta$ and $\text{sgn}(\mu)$, along with non-universal gaugino masses m_i at the GUT scale (with ratios as appropriate for various GUT-breaking representations) and run down to low scale via two-loop renormalization group equations. The chargino and neutralino spectra are given in Table A9, Appendix A. We select a smaller number of samples than in the case of **pMSSM**, taking $A_0 = 0$, $\text{sgn}(\mu)$ as positive and $\tan \beta = 5$. We choose m_0 at the GUT scale such that, for $m_{\tilde{g}} = 1000$ GeV at the low scale, the first two generations of squark masses are clubbed around 1000 GeV. We know that the scalar mass thus obtained at the electroweak symmetry breaking scale with a high scale input by renormalisation group equation (RGE) has almost 90 % contribution from gauginos due to the running [32]. This value turns out to be 506 GeV at the GUT scale. As is done earlier, we tune the $SU(3)$ gaugino mass M_3 at the high scale to get $m_{\tilde{g}} = 500$ GeV, 1000 GeV and 1500 GeV. We stick to $m_0 = 506$ GeV at the GUT scale for all these cases. The low-energy spectrum is consistent with radiative electroweak symmetry breaking as well as all other phenomenological constraints [33].

4.3.2 Collider simulation

The spectra generated as described in the previous section are fed into the event generator Pythia 6.405 [34] by SLHA interface [35] for the simulation of pp collision with centre-of-mass energy $E_{CM} = 14$ TeV.

We have used CTEQ5L [36] parton distribution functions, the QCD renormalisation and factorisation scales being both set at the subprocess centre-of-mass energy $\sqrt{\hat{s}}$. All possible SUSY processes and decay chains have been kept open. In the illustrative study presented here, we have switched off initial and final state radiation as well as multiple interactions. However, we take hadronisation into account using the fragmentation functions inbuilt in Pythia. We have checked our analysis code against earlier studies done at the parton level in the MSSM framework [3]. We also checked our code in the context of Tevatron using [37]. We checked all the cross-sections with CalcHEP also [38].

The standard final states in connection with R -parity conserving SUSY have been looked for. All of these have been discussed in the literature in different contexts [3,39]. These are

- Opposite sign dilepton (OSD) : $(\ell^\pm \ell^\mp) + (\geq 2) jets + E_{\cancel{\ell}}$
- Same sign dilepton (SSD) : $(\ell^\pm \ell^\pm) + (\geq 2) jets + E_{\cancel{\ell}}$
- Single lepton ($(1\ell + jets)$): $1\ell + (\geq 2) jets + E_{\cancel{\ell}}$
- Trilepton ($(3\ell + jets)$): $3\ell + (\geq 2) jets + E_{\cancel{\ell}}$
- Inclusive jet ($jets$): $(\geq 3) jets + E_{\cancel{\ell}}$

where ℓ stands for electrons or muons. The cuts used are as follows:

- Missing transverse momentum $E_{\cancel{\ell}} \geq 100$ GeV.
- $p_{T\ell} \geq 20$ GeV and $|\eta_\ell| \leq 2.5$.
- An isolated lepton should have lepton-lepton separation $\Delta R_{\ell\ell} \geq 0.2$, lepton-jet separation $\Delta R_{\ell j} \geq 0.4$, the energy deposit due to jet activity around a lepton E_T within $\Delta R \leq 0.2$ of the lepton axis should be ≤ 10 GeV.
- $E_{Tjet} \geq 100$ GeV and $|\eta_{jet}| \leq 2.5$.

where $\Delta R = \sqrt{\Delta\eta^2 + \Delta\phi^2}$ is the separation in pseudorapidity and azimuthal angle plane.

Jets are formed in Pythia using PYCELL jet formation criteria with $|\eta_{jet}| \leq 5.0$ in the calorimeter, $N_{\eta_{bin}} = 100$ and $N_{\phi_{bin}} = 64$. For a partonic jet to be considered as a jet initiator $E_T > 2$ GeV is required while a cluster of partonic jets to be called a hadron-jet $\sum_{parton} E_{Tjet}$ is required to be more than 20 GeV. For a formed jet the maximum ΔR from the jet initiator is 0.4.

4.3.3 Backgrounds

We have generated all dominant standard model (SM) events in Pythia for the same final states, using the same factorisation scale, parton distributions and cuts. It has been found that $t\bar{t}$ production gives the most serious backgrounds in all channels excepting in the trilepton channel, for which the electroweak backgrounds are rather effectively removed by our event selection criteria.

The signal and background events have been all calculated for an integrated luminosity of $300 fb^{-1}$. As has been already mentioned, the ratios of events in the different final states have been presented, which presumably reduces some uncertainties in prediction. Cases where the number of signal events in any of the channels used in the ratio(s) is less than three have been left out. Also, in the histograms (to be discussed in the next section), cases where any of the entries in the ratio has $\sigma = S/\sqrt{B} \leq 2$ (S, B being the number of signal and background events) have been specially marked with a '#', since our observations on them may become useful if statistics can be improved.

4.4 Prediction for different GUT representations in $SU(5)$

We discuss here the possibility of interpreting non-universality arising in various $SU(5)$ representations, namely **24**, **75**, **200**, and compare them with the universal case. For the **pMSSM** kind of framework, and adhering to the approach outlined already, we present in Figures 4.1-4.8 the ratios of the various types of signals for each of the above schemes of non-universality. Figure 4.9 contains our prediction for $SU(5)$ SUGRA. We have taken the ratio of the number of each type of signal event to the number of OSD events at the corresponding point in the parameter space. Thus each panel shows four ratios, namely, SSD/OSD , $(1\ell + jets)/OSD$, $(3\ell + jets)/OSD$ and $jets/OSD$ in the form of histograms. For reasons already mentioned, the ratio space is a rather reliable discriminator in the signature space. However, as we shall see, there are regions where all the ratios turn out to be of similar values for different GUT representations. In order to address such cases and make the presentation complete, we also present the absolute values of the cross-sections for each type of signal in Appendix B, while the chargino and neutralino spectra in different cases are found in Appendix A.

We plot a particular ratio (eg. SSD/OSD) along the y-axis for all non-singlet

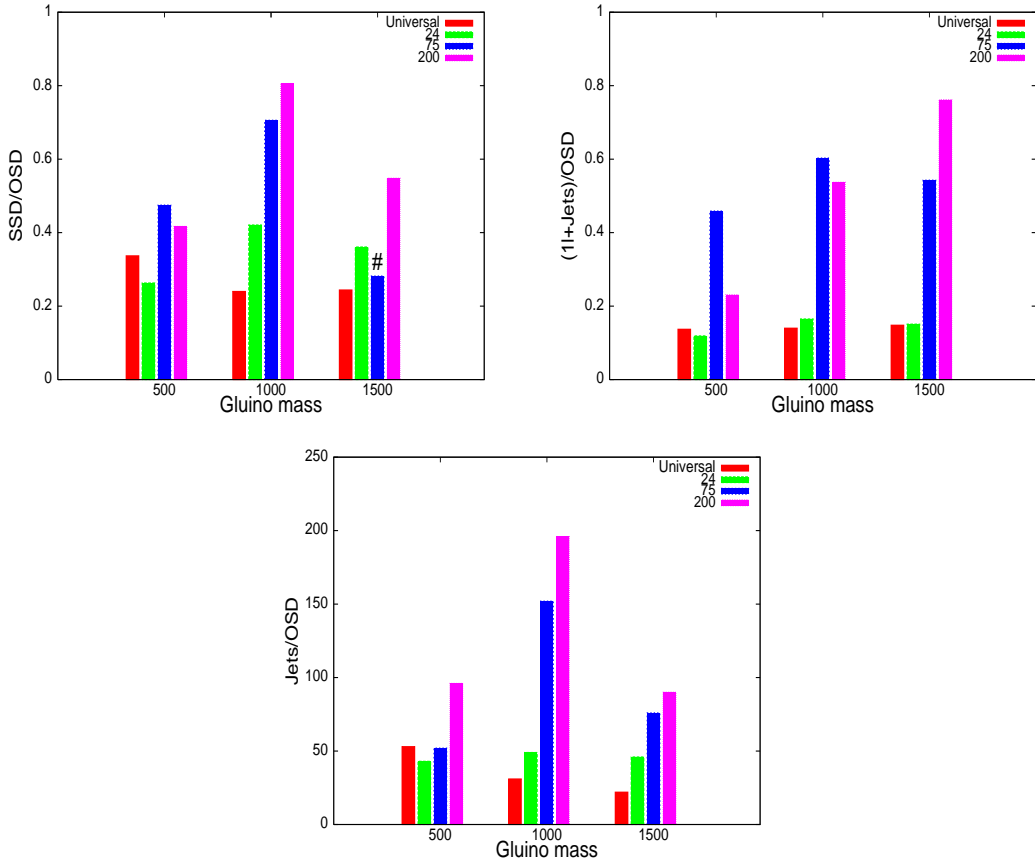


Figure 4.1: Event ratios for **pMSSM** in **SU(5)**: $m_{\tilde{f}} = 500 \text{ GeV}$, $\mu = 300 \text{ GeV}$, $\tan \beta = 5$

representations along with the universal one at three gluino masses 500 GeV, 1000 GeV and 1500 GeV in the x-axis with fixed sfermion mass $m_{\tilde{f}}$, μ and $\tan \beta$. We club all the different ratio plots in one panel and discuss the outcome as a whole.

It can perhaps be assumed that, if SUSY signals are seen at the LHC, their kinematic distributions in variables such as $p_{\cancel{H}}$ or effective mass will yield some useful information about the range of the gluino and sfermion masses. Adding to this the information extracted from the Higgs sector, one may be in a position to examine the aforementioned ratios, and compare them with our sample results.

In general, the wide multiplicity of parameters makes the variation of different rates with GUT representations far from transparent. However, a few features are broadly noticeable from Figures 4.1-4.9, and we list them below, before giving a brief account of each individual figure.

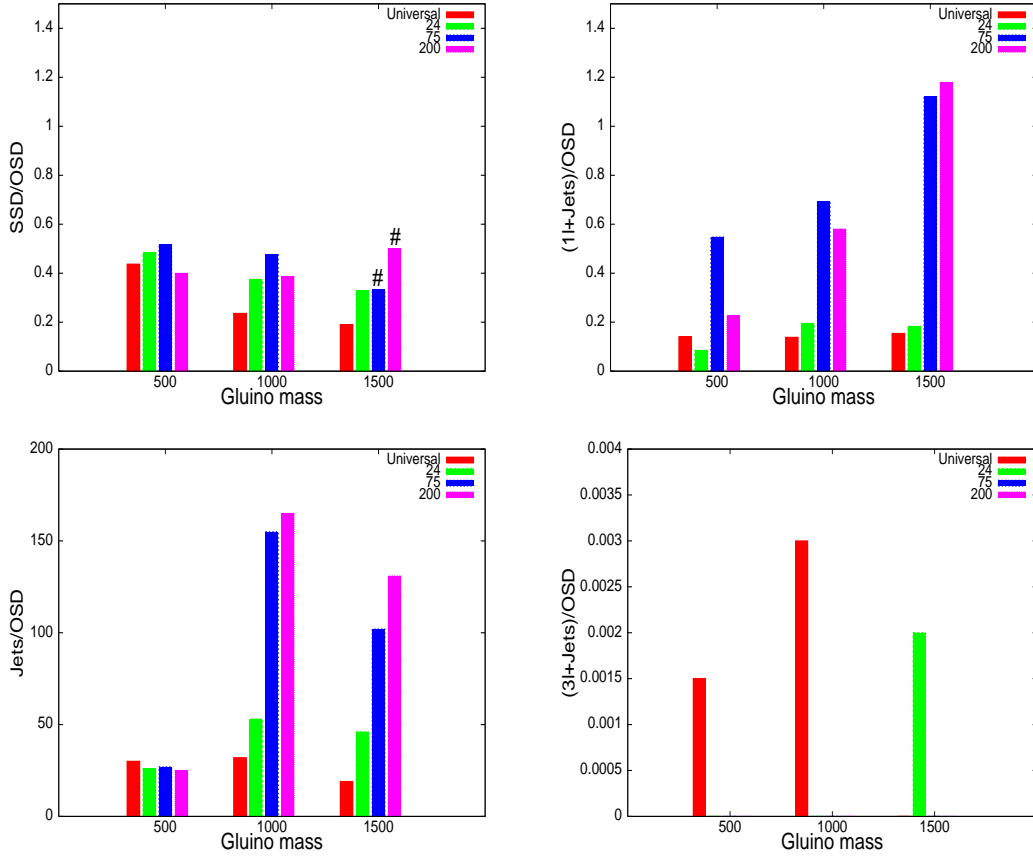


Figure 4.2: Event ratios for pMSSM in SU(5): $m_{\tilde{f}} = 500 \text{ GeV}$, $\mu = 300 \text{ GeV}$, $\tan\beta = 40$

1. The event ratios for the representations **75** and **200** are mostly bigger than those for **24** and the universal case. These correspond to the cases where the chargino and neutralino masses are relatively large compared to the gluino mass, which in turn is an artifact of larger M_1 and M_2 compared to M_3 at the GUT scale. The two worst sufferers due to this are the OSD and SSD events; of which the former suffers more. This is due to the different masses and compositions of χ_2^0 and χ_1^\pm (see next para), which are principally responsible for the OSD and SSD events respectively. The ratios for **200** are also separable from the others in at least one channel for a large number of cases. In contrast, **24** and the universal case often behave similarly in the SSD/OSD, $(1l + jets)/OSD$ and $jets/OSD$ ratios. While this indicates a partially available handle for discrimination over a substantial region of

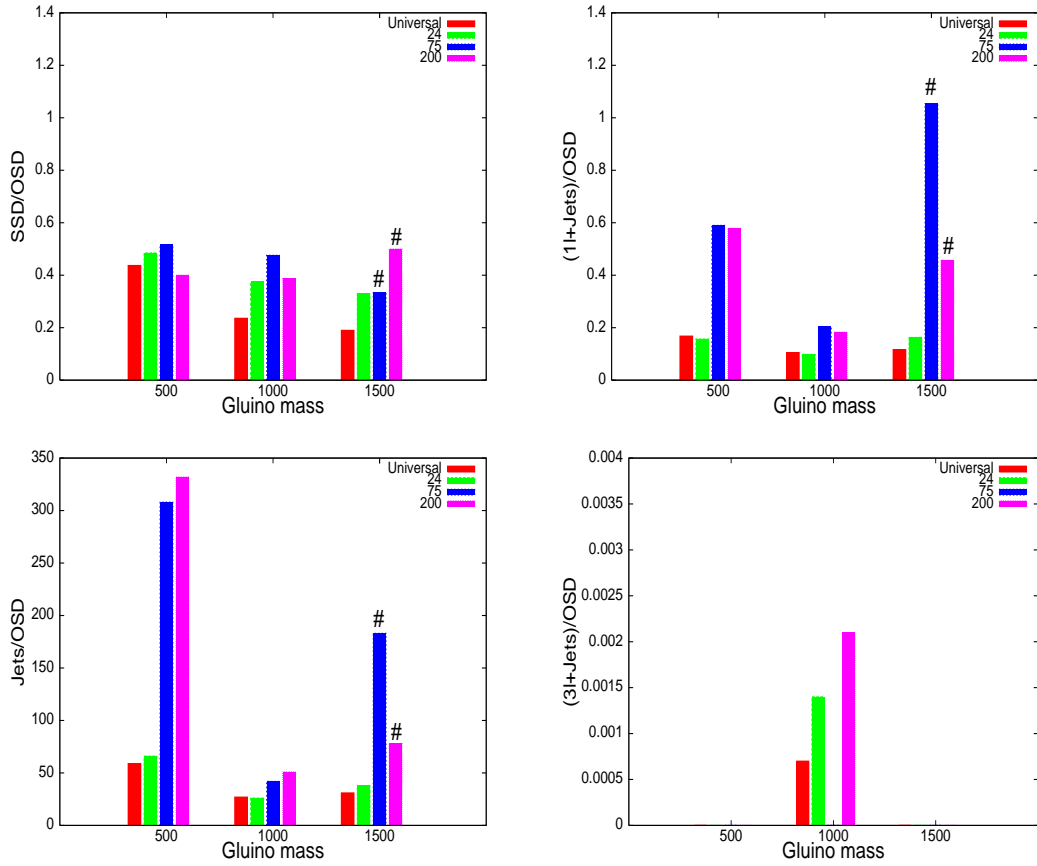


Figure 4.3: Event ratios for pMSSM in SU(5): $m_{\tilde{f}} = 1000 \text{ GeV}$, $\mu = 300 \text{ GeV}$, $\tan\beta = 5$

the parameter space, distinction between **24** and the universal case is possible relatively easily through absolute values of the event rates. However, in cases where distinguishing **75** and **200** from the ratios are difficult, distinction from absolute number of events are more challenging, because of the rather low rates of events in such cases.

- In general, the $(3\ell + jets)$ channel is a rather useful discriminator. This is because in the non-universal cases, especially for **75** and **200**, the masses of χ_2^0 and χ_1^\pm are rather widely spaced, as opposed to the case of universality. This can be attributed to the fact that the ratio M_2/M_1 is different from the universal case, and, while the gaugino contribution to χ_1^\pm comes exclusively from the Wino, χ_2^0 has Bino contributions as well with the altered mass ratios. For **24**, too, the spacing between χ_2^0 and χ_1^0 is different from the uni-

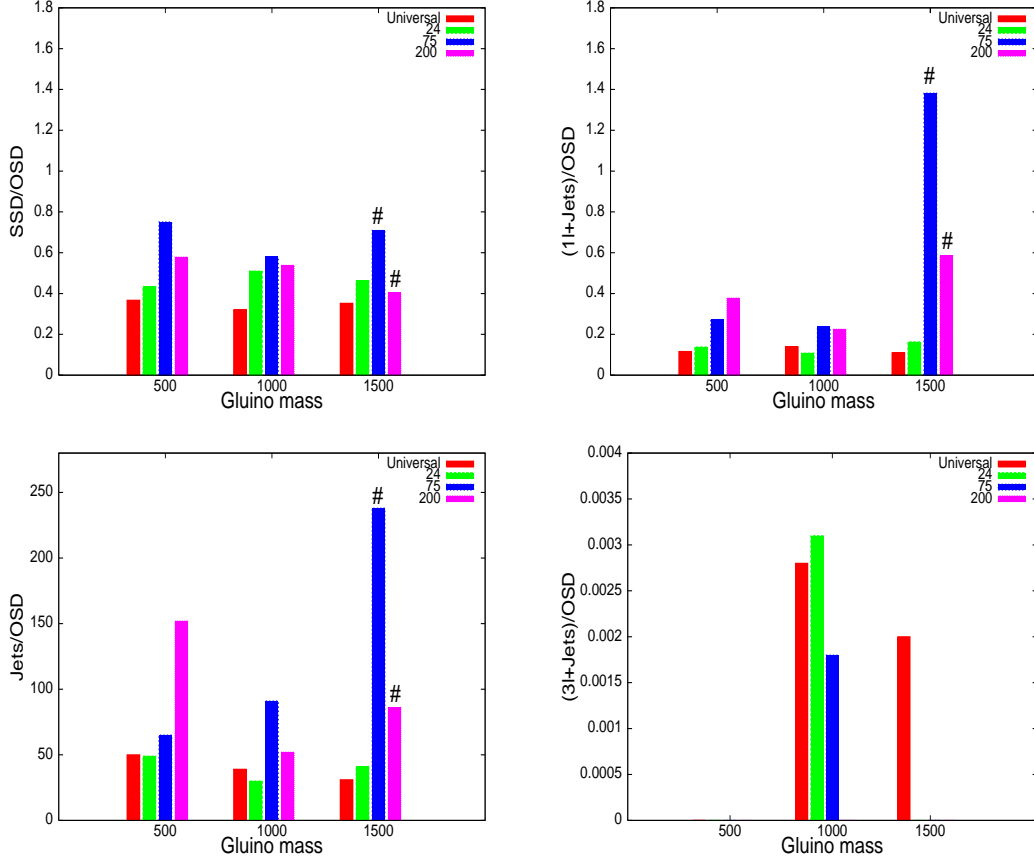


Figure 4.4: Event ratios for **pMSSM** in $SU(5)$: $m_{\tilde{f}} = 1000 \text{ GeV}$, $\mu = 300 \text{ GeV}$, $\tan \beta = 40$

versal case. Thus the suppression of trileptons for 75 and 200 can be useful, while the maximum number of such events can be obtained in the universal case. All these affect the branching ratios for $\chi_2^0 \chi_1^\pm \rightarrow 3\ell + E_{\cancel{f}}$. However, events rates tend to be low in this channel, as a result of which its ratio with the OSD rates can not be presented in a number of cases. However, the rates are in general on the higher side for $\tan \beta = 40$ than 5, because of the lower mass of the lighter sbottom state in the former case, which enhances its production and subsequent cascades to χ_1^\pm and χ_2^0 . Besides, the compositions of χ_1^\pm and χ_2^0 also is somewhat altered by a different $\tan \beta$.

3. SSD/OSD is usually less useful in distinguishing among the different cases of non-universality. This is because the modified gaugino mass ratios at high scale due to non-singlet GUT-breaking representations usually tend to

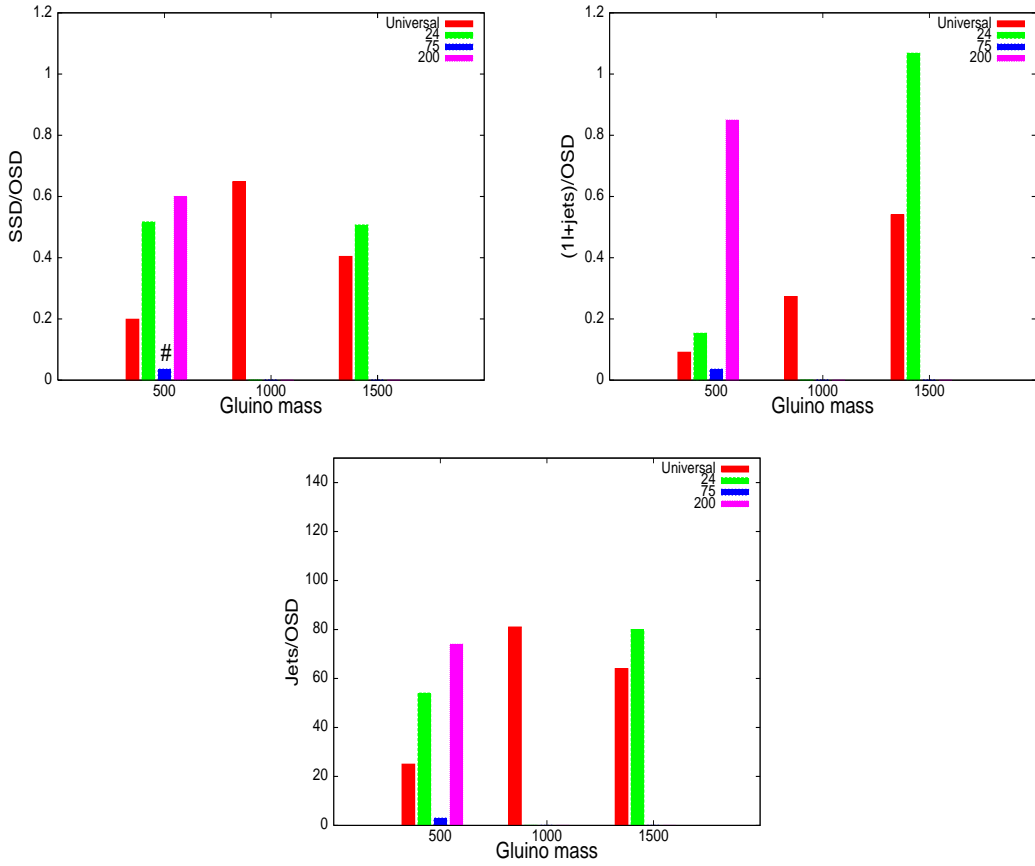


Figure 4.5: Event ratios for pMSSM in SU(5): $m_{\tilde{f}} = 500 \text{ GeV}$, $\mu = 1000 \text{ GeV}$, $\tan \beta = 5$

affect $m_{\chi_1^\pm}$ and $m_{\chi_2^0}$ similarly, thus having the same impact on both the SSD and OSD rates.

4. The rates for single lepton events, as in the case of trileptons, are affected significantly once the isolation cut between leptons and jets is turned on.
5. The absolute rates for events with jets in the final state are always way above the backgrounds with the cuts adopted here. However, the suppression of OSD, SSD and single-lepton channels for (a) high gluino/squark masses and (b) relatively higher chargino/neutralino masses for cases such as 75 and 200 often tend to drown them with backgrounds, as a result of which the ratios are likely to be useful only when statistics can be significantly improved. The trilepton events are rather easy to keep above backgrounds, due to the rather stiff jet p_T cut and the missing- E_T cut.

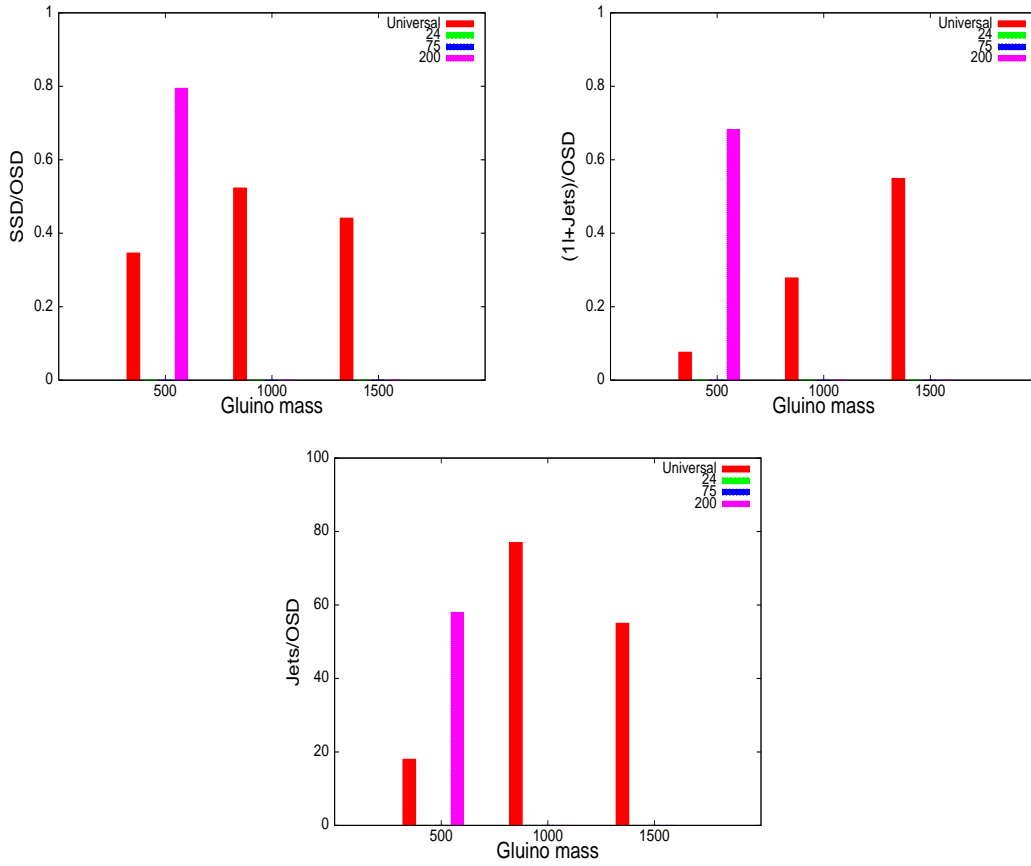


Figure 4.6: Event ratios for **pMSSM** in $SU(5)$: $m_{\tilde{f}} = 500$ GeV, $\mu = 1000$ GeV, $\tan\beta = 40$

6. The SSD and single lepton events (and sometimes the OSD events) for $m_{\tilde{f}}=1000$ GeV, and gluino mass in the range of 1000 GeV or higher, are relatively background-prone for **75** and **200**. The reason for this is higher values of the chargino and neutralino masses and the suppression of leptonic final states by heavy sleptons.
7. For $\mu=1000$ GeV, $m_{\tilde{f}}=500$ GeV and $m_{\tilde{g}} \gg 500$ GeV, most of the non-universal scenarios give inconsistent spectrum, because both the gaugino and Higgsino components of the lightest neutralino tend to make it heavier than some sfermion(s). For $m_{\tilde{g}}=500$ GeV, too, this happens for $\tan\beta=40$, as it lowers the lighter stau mass below that of χ_1^0 .
8. For μ increased from 300 GeV to 1000 GeV in the universal case, particularly with gauginos on the lower side, the Higgsino component in the lighter

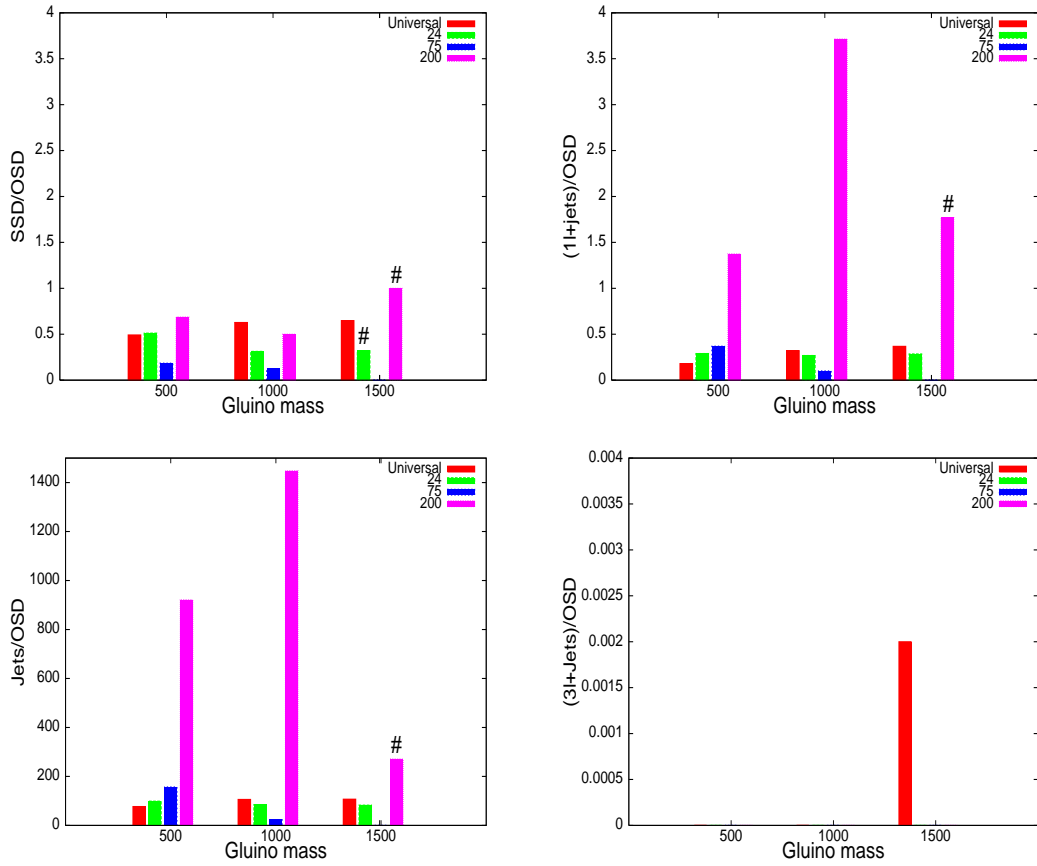


Figure 4.7: Event ratios for pMSSM in SU(5): $m_{\tilde{f}} = 1000 \text{ GeV}$, $\mu = 1000 \text{ GeV}$, $\tan\beta = 5$

charginos/neutralinos decreases and enhances the probability of leptons arising from cascades. Thus, say, the ratio $jets/OSD$ is smaller for higher μ . This feature, however, is not always there (for example for non-universality, ostensibly due to the more complicated gaugino mass ratios as well as the different hierarchy between the gluino and chargino/neutralino masses).

- It should be noted that no observation is predicted in $(3\ell + jets)$ channel for certain representations and in certain regions of the parameter space (see NULL points in Appendix B). Such ‘null observations’, however, can themselves be of use in distinguishing among scenarios.

In the region of the parameter space illustrated in Figure 4.1, the $(3\ell + jets)$ channel search gives null result for all the representations (Table B1 in Appendix B). For $m_{\tilde{g}}=500 \text{ GeV}$, one can distinguish the case of 75 from others from the ra-

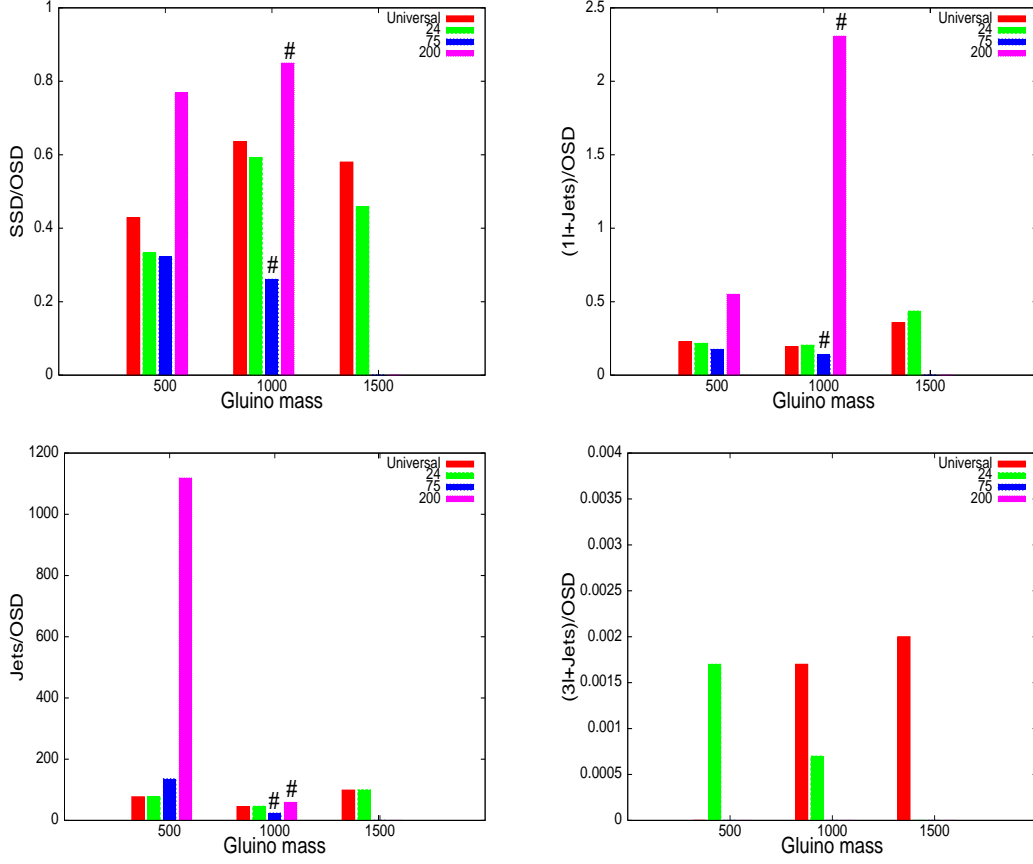


Figure 4.8: Event ratios for pMSSM in SU(5): $m_{\tilde{g}} = 1000 \text{ GeV}$, $\mu = 1000 \text{ GeV}$, $\tan\beta = 40$

ratio $(1\ell + jets)/\text{OSD}$, and **200** from $jets/\text{OSD}$. It is very difficult to distinguish the universal and **24** from any of the plots. However, as has been mentioned already, one can do so from the absolute number in the OSD channel search where **24** gives a significantly larger number. For $m_{\tilde{g}}= 1000 \text{ GeV}$, the ratios for both **75** and **200** are distinctly larger than those for **24** and the universal case, when one considers SSD/OSD , $(1\ell + jets)/\text{OSD}$ and $jets/\text{OSD}$. However, distinguishing between **75** and **200** is difficult not only in this ratio space but also from the absolute rates. Distinction between the remaining two representation is possible through SSD/OSD and also through the absolute rates in the OSD channel, where the universal case gives sufficiently larger number than **24**. This is because the charginos and higher neutralinos become sufficiently heavy in the latter case. For $m_{\tilde{g}}= 1500 \text{ GeV}$, the leptonic signals corresponding to **75** are beset with

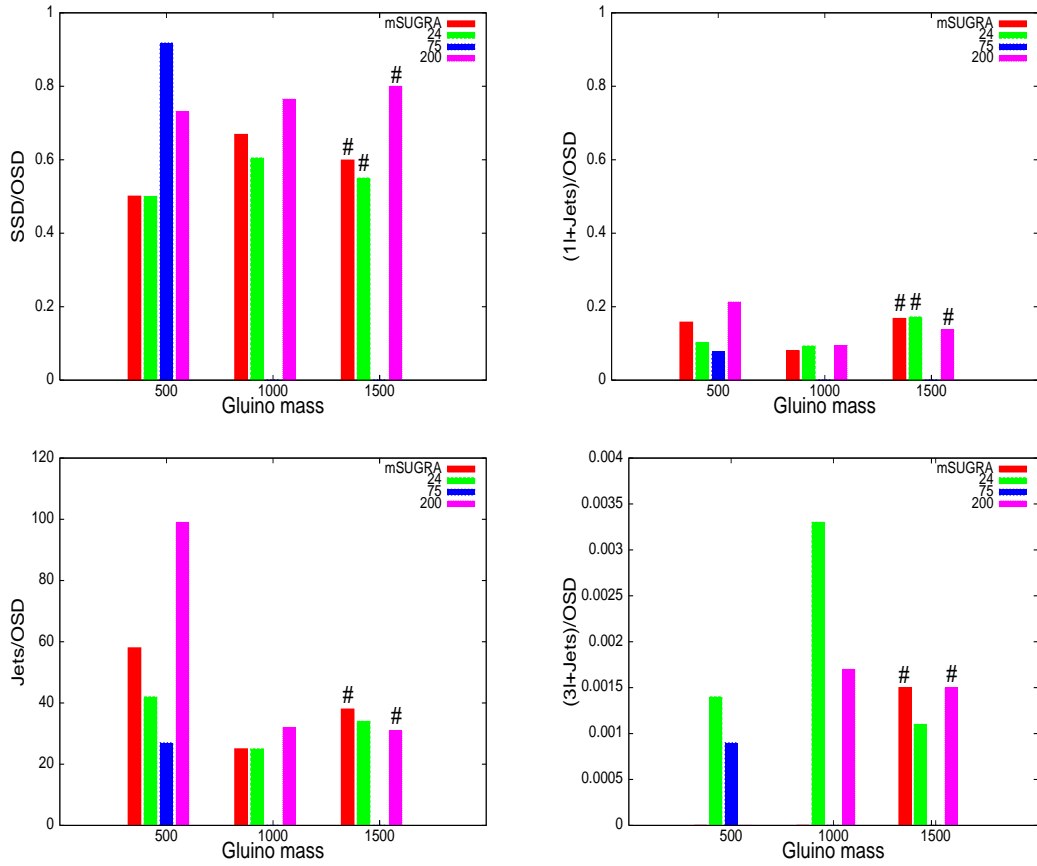


Figure 4.9: Event ratios for $SU(5)$ **SUGRA** with non-universal gaugino masses: $m_0 = 506$ GeV, $\tan \beta = 5$, $\text{sgn}(\mu) = +$, $A_0 = 0$

backgrounds, thus putting the ratio SSD/OSD at the mercy of statistics. **200** can be separated through SSD/OSD or $(1\ell + jets)/\text{OSD}$, while **75** is distinguishable from **1** and **24** quite clearly with the help of $(1\ell + jets)/\text{OSD}$. However, the distinction between **24** and the universal case is still difficult. Figure 4.2 differs from the Figure 4.1 only in $\tan \beta$, whose effect on $(3\ell + jets)/\text{OSD}$ has already been discussed. The SSD/OSD values in this case show a different behaviour from $\tan \beta = 5$ for $m_{\tilde{g}} = 1000$ GeV, the ratio showing a rather flat character with respect to gluino mass variation. Moreover, the ratio $(1\ell + jets)/\text{OSD}$ also shows a significant enhancement for **75**.

Figures 4.3 and 4.4 differ from Figures 4.1 and 4.2 in terms of $m_{\tilde{f}}$ only. For $m_{\tilde{g}} = 500$ GeV, the ratios $(1\ell + jets)/\text{OSD}$ and $jets/\text{OSD}$ for **75** and **200** are well separated from others for $\tan \beta = 5$, while the distinction between these two rep-

representations from the ratios is difficult. For $\tan\beta = 40$, however, SSD/OSD and $jets/OSD$ make such distinction possible. Similar conclusions can be drawn for higher gluino masses as well, except that the $(3\ell + jets)$ channel emerges as a successful discriminator for $m_{\tilde{g}} = 1000$ GeV.

The predictions corresponding to a high value of μ are shown in Figure 4.5 and Figure 4.6. This scenario often does not allow a consistent spectrum except for a low gluino mass, because, with sfermion masses on the low side, the lightest neutralino is mostly not the LSP. The situation is found to be worse for $\tan\beta = 40$. However, all the aforementioned ratios provide rather easy ways of discrimination among the different representations for those cases which survive.

Figures 4.7 and 4.8 show predictions with both the sfermion masses and μ at 1000 GeV. For both the values of $\tan\beta$, **200** is clearly differentiable, for cases where consistent spectra that can rise above the background are possible. While the ratio SSD/OSD can act as a fair discriminator for $\tan\beta = 40$, the *single – lepton* channel or $jets/OSD$ do better for $\tan\beta = 5$. The signals for **24** and the universal case still require knowledge of the absolute event rates. For $\tan\beta = 40$, these two representations can be distinguished through $(3\ell + jets)/OSD$, which does not give sufficient event rates for the universal case for $m_{\tilde{g}} = 500$ GeV, while the same thing happens to **24** for $m_{\tilde{g}} = 1500$ GeV. Both of these cases yield measurable $(3\ell + jets)/OSD$ rates for $m_{\tilde{g}} = 1000$ GeV, but are sufficiently apart numerically.

Figure 4.9 contains some illustrative numbers for SUGRA with non-universal gaugino masses at high scale. It may be noted that, corresponding to $m_{\tilde{g}} = 1000$ GeV, the values of the lighter charginos/neutralinos become too small to be allowed by LEP results, whereas for $m_{\tilde{g}} = 1500$ GeV, no spectrum is generated for **75** since it can not implement radiative electroweak symmetry breaking (the gaugino contributions being responsible for rendering all scalar mass-squared values positive). For $m_{\tilde{g}} = 500$ GeV, **75** is allowed, and can easily be distinguished from either the SSD/OSD or the $jets/OSD$ ratio. Identification of **200** is also possible through $jets/OSD$. **24** and **75** may be separated from **200** and the universal case with the help of the ratio $(3\ell + jets)/OSD$. On the whole, for gluino mass on the lower side, all the four GUT breaking schemes can be distinguished from each other through the ratios SSD/OSD , in conjunction with non-observation (or otherwise) of $(3\ell + jets)/OSD$. This is in a sense a gratifying conclusion, since one can make useful inference even while avoiding the overall uncertainties of events containing jets only. $(1\ell + jets)/OSD$ is quite suppressed in all the cases

and are numerically quite uniform, so that it is not of much help. For $m_{\tilde{g}}=1000$ GeV, **24** and **200** can be separated quite visibly from $(3\ell + jets)/OSD$, while non-observation of $(3\ell + jets)$ events (with the other final states observed) will point towards **75** since **75** is inadmissible for the reason mentioned above and observations in all other channels indicate **24**. The results presented for $m_{\tilde{g}}=1500$ GeV are not numerically very different from each other; however, for all representations excepting **24**, the OSD events do not rise beyond 2σ above the backgrounds for an integrated luminosity of $300 fb^{-1}$. For **24**, all of the *jets*, OSD and *trilepton* channels rise above backgrounds, and thus the ratios $jets/OSD$ and $(3\ell + jets)/OSD$ should be able to make it stand out.

4.5 Summary and conclusions

We have carried out a multichannel analysis of SUSY signals, including $jets + \cancel{E}_T$, SSD, OSD, $trileptons + jets + \cancel{E}_T$ and $single lepton + jets + \cancel{E}_T$, for a number of non-universal representations breaking the $SU(5)$ GUT group, and compared them with those corresponding to universal gaugino masses. Both a phenomenological SUSY spectrum for the remaining particles and one arising from a SUGRA scenario have been studied in this context.

We have found it most useful to discriminate among the various cases with the help of ratios of event rates for the various signals mentioned above, although the absolute event rates have also been presented, and can be used for specific cases. In any case the absolute event rates provide additional information which can be gainfully used in ones analysis. In general, it is found that the GUT-breaking representations are rather clearly differentiable over a substantial region of the parameter space in the case of **75** and **200**. For the **24** and the universal case, such distinction is relatively difficult in many cases from the event ratios, and one may have to use the absolute event rates for them. However, even in these cases the ratio $(3\ell + jets)/OSD$ can be useful in discrimination, especially in separating the universal case. In general, distinction is relatively easy for high values of μ , since a low μ enhances the Higgsino component of low-lying charginos and neutralinos, thus tending to partially obliterate the clear stamps of various gaugino mass patterns as manifested in the physical states. It is also interesting to note that for the non-minimal SUGRA scenario, at $m_{\tilde{g}}=1500$ GeV, only **24** give excess signal over background in almost all channels, while others including mSUGRA

are always overwhelmed by background in OSD channel.

In the effort to learn about gaugino non-universality, one is also required to have an idea of the gluino and sfermion masses, and it is expected that various kinematic distributions (ranging from p_T to effective mass) will throw light on them in such a study. The role of such distributions (especially of missing p_T and lepton p_T) is also important when judgment has to be made on the basis of the mass separation between the two lightest neutralinos, which is a possible discriminator between **24** and the universal case. While the value of $\tan\beta$, another quantity affecting the observables, can be obtained from studies of the SUSY Higgs sector and Yukawa couplings, extraction of the value of the μ is a more challenging task. One is likely to face this challenge in ascertaining the nature of gaugino non-universality, if any, unless the magnitude μ is determined by radiative electroweak symmetry breaking, as is expected in a SUGRA scenario.

It should also be noted that, in an illustrative study like this, we have used leading order cross-sections only. Higher order effects need to be taken into account in order to complete the study, although the use of ratios suggested by us can cancel the K -factors. However, our preliminary investigation serves to show that, once data from the LHC are available, a detailed look at them can indeed indicate whether some SUSY signals are consistent with specific scenarios embedded in a GUT setting. Our study is thus commensurate with the 'inverse problem' approach to LHC data.

On the whole, the exploration of gaugino non-universality is an extremely important task in understanding the underlying nature of a SUSY scenario. Therefore, further elaborate studies in this direction need to be undertaken in a signal-based manner.

Bibliography

- [1] S. P. Martin, arXiv:hep-ph/9709356.
- [2] P. Nath and R. Arnowitt, Phys. Lett. B **56**, 177 (1975); R. Arnowitt, P. Nath and B. Zumino, Phys. Lett. B **56**, 81 (1975); S. Ferrara, D.Z. Freedman and P. van Nieuwenhuizen, Phys. Rev. D **13**, 3214 (1976); S. Deser and B. Zumino, Phys. Lett. B **62**, 335 (1976); D.Z. Freedman and P. van Nieuwenhuizen, Phys. Rev. D **14**, 912 (1976); E. Cremmer et al., Nucl. Phys. B **147**, 105 (1979); J. Bagger, Nucl. Phys. B **211**, 302 (1983); A. Chamseddin, R. Arnowitt and P. Nath, *'Applied N=1 Supergravity'*, World Scientific, Singapore (1984).
- [3] A. Datta, G. L. Kane and M. Toharia, arXiv:hep-ph/0510204.
- [4] J. R. Ellis, C. Kounnas and D. V. Nanopoulos, Nucl. Phys. B **247**, 373 (1984); J. R. Ellis, K. Enqvist, D. V. Nanopoulos and K. Tamvakis, Phys. Lett. B **155**, 381 (1985).
- [5] M. Drees, Phys. Lett. B **158**, 409 (1985).
- [6] N. Chamoun, C. S. Huang, C. Liu and X. H. Wu, Nucl. Phys. B **624**, 81 (2002) [arXiv:hep-ph/0110332].
- [7] A. Corsetti and P. Nath, Phys. Rev. D **64**, 125010 (2001) [arXiv:hep-ph/0003186].
- [8] B. Ananthanarayan and P. N. Pandita, Int. J. Mod. Phys. A **22**, 3229 (2007) [arXiv:0706.2560 [hep-ph]]; D. Suematsu, Eur. Phys. J. C **52**, 211 (2007) [arXiv:0706.3241 [hep-ph]].
- [9] H. Abe, T. Kobayashi and Y. Omura, Phys. Rev. D **76**, 015002 (2007) [arXiv:hep-ph/0703044].
- [10] S. Profumo and C. E. Yaguna, Nucl. Phys. B **681**, 247 (2004) [arXiv:hep-ph/0307225].
- [11] S. Komine and M. Yamaguchi, Phys. Rev. D **63**, 035005 (2001) [arXiv:hep-ph/0007327].

- [12] S. Khalil, *Phys. Lett. B* **484**, 98 (2000) [arXiv:hep-ph/9910408].
- [13] G. Anderson, H. Baer, C. h. Chen and X. Tata, *Phys. Rev. D* **61**, 095005 (2000) [arXiv:hep-ph/9903370].
- [14] K. Huitu, Y. Kawamura, T. Kobayashi and K. Puolamaki, *Phys. Rev. D* **61**, 035001 (2000) [arXiv:hep-ph/9903528].
- [15] K. Huitu, J. Laamanen, P. N. Pandita and S. Roy, *Phys. Rev. D* **72**, 055013 (2005) [arXiv:hep-ph/0502100].
- [16] K. Choi and H. P. Nilles, *JHEP* **0704**, 006 (2007) [arXiv:hep-ph/0702146].
- [17] S. I. Bityukov and N. V. Krasnikov, *Phys. Atom. Nucl.* **65**, 1341 (2002) [*Yad. Fiz.* **65**, 1374 (2002)] [arXiv:hep-ph/0102179].
- [18] S. I. Bityukov and N. V. Krasnikov, arXiv:hep-ph/0210269; S. I. Bityukov and N. V. Krasnikov, *Nuovo Cim. A* **112**, 913 (1999) [arXiv:hep-ph/9903519]; *Phys. Lett. B* **469**, 149 (1999) [*Phys. Atom. Nucl.* **64**, 1315 (2001 YAFIA,64,1391-1398.2001)] [arXiv:hep-ph/9907257].
- [19] S. Bhattacharya, A. Datta and B. Mukhopadhyaya, *JHEP* **0710** (2007) 080 [arXiv:0708.2427 [hep-ph]].
- [20] A. Datta, A. Datta and M. K. Parida, *Phys. Lett. B* **431**, 347 (1998) [arXiv:hep-ph/9801242]; A. Datta, A. Datta, M. Drees and D. P. Roy, *Phys. Rev. D* **61**, 055003 (2000) [arXiv:hep-ph/9907444].
- [21] H. Baer, C. h. Chen, F. Paige and X. Tata, *Phys. Rev. D* **53**, 6241 (1996) [arXiv:hep-ph/9512383].
- [22] N. Arkani-Hamed, G. L. Kane, J. Thaler and L. T. Wang, *JHEP* **0608**, 070 (2006) [arXiv:hep-ph/0512190]; N. Arkani-Hamed, P. Schuster, N. Toro, J. Thaler, L. T. Wang, B. Knuteson and S. Mrenna, arXiv:hep-ph/0703088.
- [23] E. Cremmer, B. Julia, J. Scherk, P. van Nieuwenhuizen, S. Ferrara and L. Girardello, *Phys. Lett. B* **79**, 231 (1978); E. Cremmer, B. Julia, J. Scherk, S. Ferrara, L. Girardello and P. van Nieuwenhuizen, *Nucl. Phys. B* **147**, 105 (1979); E. Cremmer, S. Ferrara, L. Girardello and A. Van Proeyen, *Phys. Lett. B* **116**, 231 (1982); E. Cremmer, S. Ferrara, L. Girardello and A. Van Proeyen, *Nucl. Phys. B* **212**, 413 (1983).
- [24] C. T. Hill, *Phys. Lett. B* **135**, 47 (1984); Q. Shafi and C. Wetterich, *Phys. Rev. Lett.* **52**, 875 (1984).

- [25] F. Gabbiani, E. Gabrielli, A. Masiero and L. Silvestrini, Nucl. Phys. B **477**, 321 (1996) [arXiv:hep-ph/9604387].
- [26] W. M. Yao *et al.* [Particle Data Group], J. Phys. G **33**, 1 (2006).
- [27] A. Djouadi, J. L. Kneur and G. Moultaka, Comput. Phys. Commun. **176**, 426 (2007) [arXiv:hep-ph/0211331].
- [28] S. F. King, J. P. Roberts and D. P. Roy, JHEP **0710**, 106 (2007) [arXiv:0705.4219 [hep-ph]].
- [29] D. G. Cerdeno and C. Munoz, JHEP **0410**, 015 (2004) [arXiv:hep-ph/0405057]; G. Belanger, F. Boudjema, A. Cottrant, A. Pukhov and A. Semenov, Nucl. Phys. B **706**, 411 (2005) [arXiv:hep-ph/0407218].
- [30] A. Birkedal-Hansen and B. D. Nelson, Phys. Rev. D **67**, 095006 (2003) [arXiv:hep-ph/0211071]; U. Chattopadhyay and D. P. Roy, Phys. Rev. D **68**, 033010 (2003) [arXiv:hep-ph/0304108].
- [31] F. E. Paige, S. D. Protopopescu, H. Baer and X. Tata, arXiv:hep-ph/0312045.
- [32] S. P. Martin and P. Ramond, Phys. Rev. D **48**, 5365 (1993) [arXiv:hep-ph/9306314].
- [33] A. Djouadi, M. Drees and J. L. Kneur, JHEP **0603**, 033 (2006) [arXiv:hep-ph/0602001].
- [34] T. Sjostrand, S. Mrenna and P. Skands, JHEP **0605**, 026 (2006) [arXiv:hep-ph/0603175].
- [35] P. Skands *et al.*, JHEP **0407**, 036 (2004) [arXiv:hep-ph/0311123].
- [36] H. L. Lai *et al.* [CTEQ Collaboration], Eur. Phys. J. C **12**, 375 (2000) [arXiv:hep-ph/9903282].
- [37] S. Chakrabarti, A. Datta and N. K. Mondal, Pramana **63**, 1355 (2004).
- [38] A. Pukhov, arXiv:hep-ph/0412191.
- [39] H. Baer, C. h. Chen, M. Drees, F. Paige and X. Tata, Phys. Rev. D **59**, 055014 (1999) [arXiv:hep-ph/9809223].

APPENDIX A

Here we list the neutralino and chargino masses in the region of the parameter space covered by us for all the representations. Tables A1-A8 represent mass spectra in **pMSSM** framework in $SU(5)$, while table A9 is for the **SUGRA** framework. In tables A1-A8, we depict the spectra for three gluino masses namely $m_{\tilde{g}}=500$ GeV, 1000 GeV and 1500 GeV and fixed μ , $m_{\tilde{f}}$ and $\tan\beta$. The entries marked NA do not give consistent spectra having a neutralino LSP or are disallowed by LEP limits.

Table A1 : Neutralino and Chargino spectra (GeV) for $SU(5)$ **pMSSM**

$$m_{\tilde{f}} = 500 \text{ GeV}, \mu = 300 \text{ GeV}, \tan\beta = 5$$

(Figure 4.1)

$m_{\tilde{g}}$	Model	$m_{\tilde{\chi}_1^0}$	$m_{\tilde{\chi}_2^0}$	$m_{\tilde{\chi}_3^0}$	$m_{\tilde{\chi}_4^0}$	$m_{\tilde{\chi}_1^\pm}$	$m_{\tilde{\chi}_2^\pm}$
500	universal	66.80	128.30	305.90	330.20	126.80	329.50
500	24	37.60	209.80	312.20	323.00	210.80	328.30
500	75	276.00	294.00	371.10	474.10	276.40	474.20
500	200	232.73	303.83	365.66	729.01	235.36	369.37
1000	universal	140.40	243.10	304.50	373.60	238.20	372.30
1000	24	75.50	291.20	309.30	474.80	294.40	475.00
1000	75	294.10	300.30	751.70	927.70	294.40	927.70
1000	200	285.47	302.46	631.27	1509.18	288.47	631.47
1500	universal	211.42	293.78	303.64	491.75	278.76	491.42
1500	24	114.81	298.36	307.56	718.07	299.73	718.10
1500	75	296.86	300.48	1155.07	1413.08	297.09	1413.08
1500	200	292.48	301.79	951.77	2322.19	294.64	951.81

Table A2: Neutralino and Chargino spectra (GeV) for $SU(5)$ pMSSM

$$m_{\tilde{f}} = 1000 \text{ GeV}, \mu = 300 \text{ GeV}, \tan \beta = 5$$

(Figure 4.3)

$m_{\tilde{g}}$	Model	$m_{\tilde{\chi}_1^0}$	$m_{\tilde{\chi}_2^0}$	$m_{\tilde{\chi}_3^0}$	$m_{\tilde{\chi}_4^0}$	$m_{\tilde{\chi}_1^\pm}$	$m_{\tilde{\chi}_2^\pm}$
500	universal	68.80	131.60	305.70	330.40	130.00	329.60
500	24	38.60	213.90	312.00	323.50	215.00	328.60
500	75	277.40	295.10	379.20	481.80	277.80	482.00
500	200	235.87	303.71	368.42	746.27	238.55	371.84
1000	universal	142.30	245.10	304.40	374.90	240.10	373.50
1000	24	76.50	291.70	309.20	479.30	294.80	479.50
1000	75	294.20	300.30	760.10	935.90	294.50	935.90
1000	200	285.83	302.39	636.12	1524.92	288.76	636.30
1500	universal	212.88	294.61	303.56	494.02	279.26	493.70
1500	24	115.53	298.38	307.51	713.30	299.75	713.33
1500	75	296.92	300.46	1161.27	1419.11	297.13	1419.11
1500	200	292.6	301.75	955.63	233.44	294.72	955.67

Table A3: Neutralino and Chargino spectra (GeV) for $SU(5)$ pMSSM

$$m_{\tilde{f}} = 500 \text{ GeV}, \mu = 1000 \text{ GeV}, \tan \beta = 5$$

(Figure 4.5)

$m_{\tilde{g}}$	Model	$m_{\tilde{\chi}_1^0}$	$m_{\tilde{\chi}_2^0}$	$m_{\tilde{\chi}_3^0}$	$m_{\tilde{\chi}_4^0}$	$m_{\tilde{\chi}_1^\pm}$	$m_{\tilde{\chi}_2^\pm}$
500	universal	73.00	148.00	1002.20	1006.60	147.90	1006.90
500	24	37.70	228.60	1003.10	1004.90	228.60	1006.10
500	75	371.00	449.00	1002.00	1009.10	449.00	1009.50
500	200	299.19	738.18	1001.81	1011.24	299.21	1007.88
1000	universal	149.60	302.70	1002.00	1007.90	302.70	1007.90
1000	24	NA	NA	NA	NA	NA	NA
1000	75	NA	NA	NA	NA	NA	NA
1000	200	NA	NA	NA	NA	NA	NA
1500	universal	228.81	461.31	1001.78	1009.98	461.26	1009.63
1500	24	116.03	700.85	1003.8	1007.11	700.89	1009.06
1500	75	NA	NA	NA	NA	NA	NA
1500	200	NA	NA	NA	NA	NA	NA

Table A4 : Neutralino and Chargino spectra (GeV) for $SU(5)$ pMSSM

$$m_{\tilde{f}} = 1000 \text{ GeV}, \mu = 1000 \text{ GeV}, \tan \beta = 5$$

(Figure 4.7)

$m_{\tilde{g}}$	Model	$m_{\tilde{\chi}_1^0}$	$m_{\tilde{\chi}_2^0}$	$m_{\tilde{\chi}_3^0}$	$m_{\tilde{\chi}_4^0}$	$m_{\tilde{\chi}_1^\pm}$	$m_{\tilde{\chi}_2^\pm}$
500	universal	74.10	149.80	1002.20	1006.60	149.80	1006.80
500	24	38.20	231.40	1003.00	1004.80	465.50	1006.50
500	75	376.40	454.40	1002.20	1009.10	454.40	1009.40
500	200	302.60	748.21	1001.77	1011.38	302.62	1007.80
1000	universal	150.90	305.00	1001.90	1007.90	305.00	1007.80
1000	24	76.80	465.50	1004.10	1004.20	465.5	1006.5
1000	75	763.20	894.00	1003.30	1042.30	894.00	1042.50
1000	200	614.03	1001.39	1009.07	1536.64	614.09	1012.64
1500	universal	230.06	463.39	1001.75	1009.92	463.34	1009.54
1500	24	116.59	703.66	1003.76	1007.03	703.69	1008.95
1500	75	NA	NA	NA	NA	NA	NA
1500	200	904.54	1001.14	1045.98	2344.38	905.13	1047.34

Table A5 : Neutralino and Chargino spectra (GeV) for $SU(5)$ pMSSM

$$m_{\tilde{f}} = 500 \text{ GeV}, \mu = 300 \text{ GeV}, \tan \beta = 40$$

(Figure 4.2)

$m_{\tilde{g}}$	Model	$m_{\tilde{\chi}_1^0}$	$m_{\tilde{\chi}_2^0}$	$m_{\tilde{\chi}_3^0}$	$m_{\tilde{\chi}_4^0}$	$m_{\tilde{\chi}_1^\pm}$	$m_{\tilde{\chi}_2^\pm}$
500	universal	69.30	134.50	309.20	323.70	134.20	326.20
500	24	35.30	198.80	309.30	332.20	199.20	334.80
500	75	281.30	291.20	373.60	468.10	283.50	468.50
500	200	241.96	306.0	356.96	722.48	245.05	361.29
1000	universal	143.30	250.30	307.00	364.70	248.60	364.80
1000	24	73.10	286.60	307.10	478.50	286.90	478.70
1000	75	295.50	300.50	750.80	925.50	297.10	925.50
1000	200	288.96	303.85	626.87	1501.91	292.89	627.07
1500	universal	216.13	294.81	305.68	486.87	285.51	486.81
1500	24	112.51	297.31	305.75	710.55	295.87	710.58
1500	75	297.63	300.75	1153.72	1411.23	298.74	1411.23
1500	200	294.32	302.81	948.35	2314.19	297.22	948.39

Table A6 : Neutralino and Chargino spectra (GeV) for $SU(5)$ pMSSM

$$m_{\tilde{f}} = 1000 \text{ GeV}, \mu = 300 \text{ GeV}, \tan \beta = 40$$

(Figure 4.4)

$m_{\tilde{g}}$	Model	$m_{\tilde{\chi}_1^0}$	$m_{\tilde{\chi}_2^0}$	$m_{\tilde{\chi}_3^0}$	$m_{\tilde{\chi}_4^0}$	$m_{\tilde{\chi}_1^\pm}$	$m_{\tilde{\chi}_2^\pm}$
500	universal	71.30	137.80	309.00	323.90	137.50	326.20
500	24	36.30	202.90	309.10	332.90	203.30	335.40
500	75	282.50	292.50	381.70	476.30	284.70	476.60
500	200	254.40	305.84	360.00	741.60	248.60	364.00
1000	universal	144.70	251.80	306.90	365.40	250.00	365.40
1000	24	73.90	287.20	307.00	482.10	287.50	482.30
1000	75	295.70	300.70	758.30	932.90	297.20	932.90
1000	200	289.26	302.18	1279.90	3148.39	298.50	1279.90
1500	universal	217.50	295.43	305.6	488.9	285.91	488.83
1500	24	112.73	297.44	305.67	713.34	295.97	713.37
1500	75	297.54	301.07	1416.72	1577.18	298.76	1416.72
1500	200	294.43	302.77	952.30	2326.64	297.28	952.34

Table A7 : Neutralino and Chargino spectra (GeV) for $SU(5)$ pMSSM

$$m_{\tilde{f}} = 500 \text{ GeV}, \mu = 1000 \text{ GeV}, \tan \beta = 40$$

(Figure 4.6)

$m_{\tilde{g}}$	Model	$m_{\tilde{\chi}_1^0}$	$m_{\tilde{\chi}_2^0}$	$m_{\tilde{\chi}_3^0}$	$m_{\tilde{\chi}_4^0}$	$m_{\tilde{\chi}_1^\pm}$	$m_{\tilde{\chi}_2^\pm}$
500	universal	73.0	149.0	1003.5	1005.0	149.0	1006.5
500	24	NA	NA	NA	NA	NA	NA
500	75	NA	NA	NA	NA	NA	NA
500	200	299.23	732.41	1002.83	1008.35	299.25	1007.09
1000	universal	149.40	303.70	1003.10	1005.90	303.70	1007.10
1000	24	NA	NA	NA	NA	NA	NA
1000	75	NA	NA	NA	NA	NA	NA
1000	200	NA	NA	NA	NA	NA	NA
1500	universal	228.57	462.53	1002.78	1007.48	462.52	1008.27
1500	24	NA	NA	NA	NA	NA	NA
1500	75	NA	NA	NA	NA	NA	NA
1500	200	NA	NA	NA	NA	NA	NA

Table A8 : Neutralino and Chargino spectra (GeV) for $SU(5)$ pMSSM

$$m_{\tilde{f}} = 1000 \text{ GeV}, \mu = 1000 \text{ GeV}, \tan \beta = 40$$

(Figure 4.8)

$m_{\tilde{g}}$	Model	$m_{\tilde{\chi}_1^0}$	$m_{\tilde{\chi}_2^0}$	$m_{\tilde{\chi}_3^0}$	$m_{\tilde{\chi}_4^0}$	$m_{\tilde{\chi}_1^\pm}$	$m_{\tilde{\chi}_2^\pm}$
500	universal	74.20	151.10	1003.40	1005.90	151.10	1006.50
500	24	37.30	227.40	1003.60	1004.80	227.40	1006.60
500	75	327.70	454.20	1003.50	1006.80	454.20	1008.10
500	200	303.39	744.63	1002.79	1008.48	303.4	1007.02
1000	universal	150.80	306.10	1003.00	1005.90	306.10	1007.00
1000	24	75.07	460.10	1003.20	1006.50	460.60	1007.80
1000	75	758.40	899.70	1005.20	1033.50	900.00	1034.30
1000	200	615.17	1002.19	1006.76	1528.79	615.21	1010.41
1500	universal	229.98	464.89	1002.76	1007.45	464.89	1008.22
1500	24	115.55	697.57	1002.82	1010.87	697.59	1011.80
1500	75	NA	NA	NA	NA	NA	NA
1500	200	NA	NA	NA	NA	NA	NA

Table A9 : Neutralino and Chargino spectra (GeV) for $SU(5)$ SUGRA

$$m_{\tilde{f}} = 506 \text{ GeV at } M_{GUT}, \tan \beta = 5$$

(Figure 4.9)

$m_{\tilde{g}}$	Model	$m_{\tilde{\chi}_1^0}$	$m_{\tilde{\chi}_2^0}$	$m_{\tilde{\chi}_3^0}$	$m_{\tilde{\chi}_4^0}$	$m_{\tilde{\chi}_1^\pm}$	$m_{\tilde{\chi}_2^\pm}$
500	universal	70.74	129.16	289.03	316.94	127.91	314.65
500	24	42.54	199.39	252.60	288.42	200.04	289.92
500	75	136.36	147.69	400.26	470.33	138.90	467.43
500	200	202.80	249.30	348.56	792.82	207.99	348.32
1000	universal	171.20	321.40	555.60	574.93	321.55	573.38
1000	24	92.52	420.53	445.10	545.27	413.17	538.06
1000	75	NA	NA	NA	NA	NA	NA
1000	200	414.84	433.79	686.93	1767.96	421.96	680.06
1500	universal	275.57	519.73	819.60	834.40	520.22	833.47
1500	24	145.87	624.14	638.06	831.61	608.20	818.44
1500	75	NA	NA	NA	NA	NA	NA
1500	200	592.68	603.33	1059.96	2804.17	602.40	1048.06

APPENDIX B

In this appendix we tabulate the cross-sections in each channel for all representations in the region of parameter space studied and depicted in Figures 4.1-4.9. The cross-sections are named as follows: σ_1 for OSD, σ_2 for SSD, σ_3 for $(1\ell + jets)$, σ_4 for $jets$ and σ_5 for $(3\ell + jets)$. The points for which we do not get consistent spectra are denoted by NA as earlier and the points which give null result (for $(3\ell + jets)$ channel only) is written as NULL. Bold faced entries correspond to cross-sections which are less than 2σ above the background for an integrated luminosity of $300 fb^{-1}$.

Table B1 : Cross-sections (pb) **pMSSM**

$$m_{\tilde{f}} = 500 \text{ GeV}, \mu = 300 \text{ GeV}, \tan \beta = 5$$

(Figure 4.1)

$m_{\tilde{g}}$	Model	σ_1	σ_2	σ_3	σ_4	σ_5
500	universal	0.3434	0.1157	0.0472	18.3140	NULL
500	24	0.4648	0.1223	0.0552	20.2893	NULL
500	75	0.0388	0.0185	0.0178	2.0555	NULL
500	200	0.0576	0.0240	0.0133	5.5483	NULL
1000	universal	0.1086	0.0261	0.0152	3.4062	NULL
1000	24	0.0808	0.0340	0.0133	4.0154	NULL
1000	75	0.0089	0.0063	0.0054	1.3613	NULL
1000	200	0.0090	0.0072	0.0048	1.4017	NULL
1500	universal	0.0346	0.0845	0.0512	0.7688	NULL
1500	24	0.0265	0.0096	0.0040	1.2308	NULL
1500	75	0.0037	0.0010	0.0020	0.2852	NULL
1500	200	0.0034	0.0019	0.0026	0.3110	NULL

Table B2 : Cross-sections (pb) **pMSSM**

$$m_{\tilde{f}} = 1000 \text{ GeV}, \mu = 300 \text{ GeV}, \tan \beta = 5$$

(Figure 4.3)

$m_{\tilde{g}}$	Model	σ_1	σ_2	σ_3	σ_4	σ_5
500	universal	0.1400	0.0440	0.0230	8.3310	NULL
500	24	0.1317	0.0463	0.0207	8.7260	NULL
500	75	0.0108	0.0048	0.0064	3.3280	NULL
500	200	0.0137	0.0068	0.0079	4.5549	NULL
1000	universal	0.0310	0.0132	0.0033	0.8462	2.0×10^{-5}
1000	24	0.0350	0.0196	0.0034	0.9417	5.0×10^{-5}
1000	75	0.0197	0.0137	0.0040	0.8528	NULL
1000	200	0.0145	0.0091	0.0027	0.7410	3.0×10^{-5}
1500	universal	0.0091	0.0032	0.0010	0.2788	NULL
1500	24	0.0089	0.0037	0.0015	0.3422	NULL
1500	75	0.0006	0.0003	0.0006	0.1023	NULL
1500	200	0.0016	0.0006	0.0007	0.1259	NULL

Table B3 : Cross-sections (pb) **pMSSM**

$$m_{\tilde{f}} = 500 \text{ GeV}, \mu = 1000 \text{ GeV}, \tan \beta = 5$$

(Figure 4.5)

$m_{\tilde{g}}$	Model	σ_1	σ_2	σ_3	σ_4	σ_5
500	universal	0.7456	0.1483	0.0680	18.8841	NULL
500	24	0.3510	0.1814	0.0537	19.1663	NULL
500	75	0.0356	0.0013	0.0013	0.1100	NULL
500	200	0.0125	0.0075	0.0106	0.9345	NULL
1000	universal	0.0453	0.0293	0.0124	3.6705	NULL
1000	24	NA	NA	NA	NA	NA
1000	75	NA	NA	NA	NA	NA
1000	200	NA	NA	NA	NA	NA
1500	universal	0.0090	0.0036	0.0049	0.5811	NULL
1500	24	0.0062	0.0031	0.0066	0.4968	NULL
1500	75	NA	NA	NA	NA	NA
1500	200	NA	NA	NA	NA	NA

Table B4 : Cross-sections (pb) **pMSSM**

$$m_{\tilde{f}} = 1000 \text{ GeV}, \mu = 1000 \text{ GeV}, \tan \beta = 5$$

(Figure 4.7)

$m_{\tilde{g}}$	Model	σ_1	σ_2	σ_3	σ_4	σ_5
500	universal	0.1022	0.0503	0.0185	7.9664	NULL
500	24	0.0878	0.0449	0.0255	8.7054	NULL
500	75	0.0047	0.0009	0.0017	0.7335	NULL
500	200	0.0028	0.0019	0.0038	2.5958	NULL
1000	universal	0.0098	0.0062	0.0032	1.0422	NULL
1000	24	0.0119	0.0037	0.0032	1.0220	NULL
1000	75	0.0044	0.0005	0.0004	0.1052	NULL
1000	200	0.0002	0.0001	0.0006	0.2546	NULL
1500	universal	0.0026	0.0017	0.0009	0.2781	0.5×10^{-5}
1500	24	0.0036	0.0012	0.0010	0.3007	NULL
1500	75	NA	NA	NA	NA	NA
1500	200	6.0×10^{-5}	6.0×10^{-5}	0.0001	0.0172	NULL

Table B5 : Cross-sections (pb) **pMSSM**

$$m_{\tilde{f}} = 500 \text{ GeV}, \mu = 300 \text{ GeV}, \tan \beta = 40$$

(Figure 4.2)

$m_{\tilde{g}}$	Model	σ_1	σ_2	σ_3	σ_4	σ_5
500	universal	0.5220	0.2281	0.0729	16.0476	0.0008
500	24	0.6831	0.3310	0.0581	18.3674	NULL
500	75	0.0393	0.0203	0.0215	1.0915	NULL
500	200	0.0983	0.0393	0.0222	2.4881	NULL
1000	universal	0.1033	0.0244	0.0142	3.3959	0.0003
1000	24	0.0800	0.0300	0.0156	4.2959	NULL
1000	75	0.0089	0.0041	0.0060	1.3822	NULL
1000	200	0.0083	0.0032	0.0048	1.3759	NULL
1500	universal	0.0374	0.0071	0.0058	0.7133	NULL
1500	24	0.0306	0.0101	0.0056	1.4278	0.0001
1500	75	0.0027	0.0009	0.0030	0.2765	NULL
1500	200	0.0023	0.0012	0.0027	0.3046	NULL

Table B6 : Cross-sections (pb) **pMSSM**

$$m_{\tilde{f}} = 1000 \text{ GeV}, \mu = 300 \text{ GeV}, \tan \beta = 40$$

(Figure 4.4)

$m_{\tilde{g}}$	Model	σ_1	σ_2	σ_3	σ_4	σ_5
500	universal	0.1602	0.0059	0.0019	8.1530	NULL
500	24	0.1714	0.0745	0.0236	8.4541	NULL
500	75	0.0312	0.0234	0.0085	2.8467	NULL
500	200	0.0258	0.0139	0.0097	3.9270	NULL
1000	universal	0.0214	0.0069	0.0030	0.8446	6.0×10^{-5}
1000	24	0.0343	0.0175	0.0037	1.0486	0.0001
1000	75	0.0182	0.0106	0.0043	0.8455	3.0×10^{-5}
1000	200	0.0120	0.0063	0.0027	0.7075	NULL
1500	universal	0.0088	0.0031	0.0009	0.2799	2.0×10^{-5}
1500	24	0.0082	0.0038	0.0013	0.3403	NULL
1500	75	0.0004	0.0003	0.0006	0.0981	NULL
1500	200	0.0015	0.0006	0.0008	0.1272	NULL

Table B7 : Cross-sections (pb) **pMSSM**

$$m_{\tilde{f}} = 500 \text{ GeV}, \mu = 1000 \text{ GeV}, \tan \beta = 40$$

(Figure 4.6)

$m_{\tilde{g}}$	Model	σ_1	σ_2	σ_3	σ_4	σ_5
500	universal	0.9410	0.3260	0.0715	17.3778	NULL
500	24	NA	NA	NA	NA	NA
500	75	NA	NA	NA	NA	NA
500	200	0.0283	0.0225	0.0193	1.6686	NULL
1000	universal	0.0467	0.0245	0.0130	3.6043	NULL
1000	24	NA	NA	NA	NA	NA
1000	75	NA	NA	NA	NA	NA
1000	200	NA	NA	NA	NA	NA
1500	universal	0.0100	0.0044	0.0055	5.5373	NULL
1500	24	NA	NA	NA	NA	NA
1500	75	NA	NA	NA	NA	NA
1500	200	NA	NA	NA	NA	NA

Table B8 : Cross-sections (pb) **pMSSM**

$$m_{\tilde{f}} = 1000 \text{ GeV}, \mu = 1000 \text{ GeV}, \tan \beta = 40$$

(Figure 4.8)

$m_{\tilde{g}}$	Model	σ_1	σ_2	σ_3	σ_4	σ_5
500	universal	0.1027	0.0440	0.0233	7.9509	NULL
500	24	0.1123	0.0373	0.0243	8.7752	0.0002
500	75	0.0059	0.0019	0.0010	0.8054	NULL
500	200	0.0023	0.0018	0.0053	2.5620	NULL
1000	universal	0.0204	0.0130	0.0039	0.9343	3.0×10^{-5}
1000	24	0.0209	0.0124	0.0043	0.9690	1.5×10^{-5}
1000	75	0.0314	0.0001	0.0004	0.0771	NULL
1000	200	0.0018	0.0016	0.0010	0.1095	NULL
1500	universal	0.0028	0.0016	0.0010	0.2775	0.6×10^{-5}
1500	24	0.0030	0.0014	0.0013	0.3063	NULL
1500	75	NA	NA	NA	NA	NA
1500	200	NA	NA	NA	NA	NA

Table B9 : Cross-sections (pb) **SUGRA**

$$m_{\tilde{f}} = 506 \text{ GeV at } M_{GUT}, \tan \beta = 5$$

(Figure 4.9)

$m_{\tilde{g}}$	Model	σ_1	σ_2	σ_3	σ_4	σ_5
500	universal	0.2818	0.1411	0.0445	16.5239	NULL
500	24	0.3807	0.1900	0.0390	16.1696	0.0007
500	75	0.3685	0.3382	0.0282	10.1572	0.0003
500	200	0.0912	0.0667	0.0194	9.0323	NULL
1000	universal	0.0397	0.0266	0.0032	1.0060	NULL
1000	24	0.0315	0.0191	0.0029	0.8035	0.0001
1000	75	NA	NA	NA	NA	NA
1000	200	0.0137	0.0105	0.0013	0.4504	2.0×10^{-5}
1500	universal	0.0019	0.0011	0.0003	0.0735	3.0×10^{-5}
1500	24	0.0022	0.0012	0.0004	0.0750	2.0×10^{-5}
1500	75	NA	NA	NA	NA	NA
1500	200	0.0012	0.0009	0.0002	0.0368	2.0×10^{-5}

Chapter 5

Non-universal gaugino masses in $SO(10)$: a signal-based analysis for the Large hadron Collider

5.1 Introduction

Although the issue of GUT-motivated non-universality in gaugino masses has been explored in earlier works, particularly in the context of $SU(5)$ [1–3], there had been very few efforts [4] to study the same in the context of $SO(10)$. In this chapter [5], we calculate the non-universal gaugino mass ratios for the non-singlet representations **54** and **770**, based on the results obtained in [6], for the intermediate gauge group, namely, Pati-Salam gauge group $SU(4)_c \otimes SU(2)_L \otimes SU(2)_R$ (G_{422}) with conserved D -parity [7]. In order to understand the low-energy phenomenology of such high scale breaking patterns, which is indeed essential in the context of the LHC and dark matter searches, we scan a wide region of parameter space using the renormalisation group equations (RGEs) and discuss the consequences in terms of various low-energy constraints. For example, we discuss the consistency of such low-energy spectra with the radiative electroweak symmetry breaking (REWSB), Landau pole, tachyonic masses etc. We

also point out the constraints from stau-LSP (adhering to a situation with conserved R -parity and hence lightest neutralino-LSP), and flavour constraints like $b \rightarrow s\gamma$ for all possible combination of the parameter space points. Here, we assume the breaking of the $SO(10)$ to the intermediate gauge group and that to SM takes place at the GUT scale. To study the collider signatures in the context of the LHC, we choose some benchmark points (BP) consistent with the cold dark matter (CDM) relic density constraint obtained from the WMAP data [8]. We perform the so-called ‘multilepton channel analysis’ [9, 10] in *same – sign dilepton*, *opposite – sign dilepton*, *trilepton*, *inclusive four – lepton* channels associated with *jets*, as well as in *hadronically quiet trilepton* channel at these benchmark points. We compare our results with WMAP allowed points in mSUGRA, tuned at the same gluino masses ¹.

There has been a lot of effort in discussing various phenomenological aspects [11–15] of such high scale non-universality and its effect in terms of collider signatures [16–18], our analysis is remarkable in the following aspects:

- Apart from noting some errors in the earlier available calculations of non-universal gaugino mass ratio for the representation **54**, we present the hitherto unknown ratio for the representation **770** for the intermediate breaking chain G_{422} . Our work [5] was completed at the same time as by Martin [19], where similar conclusions were independently reached.
- While we discuss the consistency of the low-energy spectra obtained from such high scale non-universality in a wide region of the parameter space, we study the collider aspects as well in some selected BPs in context of the LHC.
- In order to distinguish such non-universal schemes from the universal one, we compare our results at these chosen BPs with WMAP allowed points in mSUGRA tuned at the same gluino masses. We identify a remarkable distinction between the two, which might be important in pointing out the departure in ‘signature-space’ [20–23] in context of the LHC for different input schemes at the GUT scale.

This chapter is organized as follows. In the following section, we calculate

¹We are benchmarking a potentially faking SUGRA scenario in terms of the gluino mass, which has a very important role in the final state event rates. The corresponding sfermion masses are fixed by requiring the fulfillment of WMAP constraints.

the non-universal gaugino mass ratios. The low-energy spectra, their consistency with various constraints and subsequently the choices of the benchmark points have been discussed in Section 5.3. Section 5.4 contains the strategy for the collider simulation and the numerical results obtained. We conclude in Section 5.5.

5.2 Non-universal Gaugino mass ratios for $SO(10)$

Here we calculate the non-universal gaugino mass ratios for non-singlet Higgses belonging to the representations **54** and **770** under $SO(10)$ SUSY-GUT scenario.

We adhere to a situation where all soft SUSY breaking effects arise via hidden sector interactions in an underlying supergravity (SUGRA) framework, specifically, in $SO(10)$ gauge theories with an arbitrary chiral matter superfield content coupled to $N = 1$ supergravity. Non-universality arises due to the non-trivial extension of the gauge kinetic function $f_{\alpha\beta}(\Phi^j)$ in terms of the non-singlet components of the chiral superfields Φ^N as discussed in the earlier chapter:

$$f_{\alpha\beta}(\Phi^j) = f_0(\Phi^S)\delta_{\alpha\beta} + \sum_N \zeta_N(\Phi^S) \frac{\Phi^N_{\alpha\beta}}{M} + \mathcal{O}\left(\frac{\Phi^N}{M}\right)^2 \quad (5.1)$$

where f_0 and ζ^N are functions of chiral singlet superfields, essentially determining the strength of the interaction and M is the reduced Planck mass = $M_{Pl}/\sqrt{8\pi}$.

In Equation (5.1), the contribution to the gauge kinetic function from Φ^N has to come through symmetric products of the adjoint representation of the associated GUT group, since $f_{\alpha\beta}$ on the left side of Equation (5.1) has such transformation property for the sake of gauge invariance. For $SO(10)$, contributions to $f_{\alpha\beta}$ comes from all possible non-singlet irreducible representations to which Φ^N can belong :

$$(45 \otimes 45)_{symm} = 1 \oplus 54 \oplus 210 \oplus 770 \quad (5.2)$$

As mentioned earlier, we calculate here, non-universal contribution to the gaugino masses, for the non-singlet chiral superfields, Φ^N 's ² belonging to representations **54** and **770** which break $SO(10)$ to the intermediate gauge group,

²Higgs here, that breaks Pati-Salam gauge group to SM, doesn't contribute to gaugino masses.

Representations	$M_3 : M_2 : M_1$ at M_{GUT}
1	1:1:1
54	1:(-3/2):(-1/2)
770	1:(2.5):(1.9)

Table 5.1: High scale gaugino mass ratios for the representations **54** and **770**.

namely, the Pati-Salam gauge group with unbroken D -parity, $SU(4)_C \otimes SU(2)_L \otimes SU(2)_R$ (usually denoted as G_{422P}).

The representations of $SO(10)$ [24], decomposed into that of the Pati-Salam gauge group

$$SO(10) \rightarrow G_{422} = SU(4)_C \otimes SU(2)_L \otimes SU(2)_R \quad (5.3)$$

combining that with the subsequent breaking of $SU(4)_C$ to $SU(3)_C \otimes U(1)_{B-L}$ and at the same time, $SU(2)_R$ to $U(1)_{T_{3R}}$ yields a gaugino mass relation at the intermediate scale :

$$M_1 = \frac{3}{5} M_{2R} + \frac{2}{5} M_{4C} \quad (5.4)$$

Identifying $M_3 = M_{4C}$, $M_2 = M_{2R} = M_{2L}$ ³ and using specific values obtained corresponding to M_{4C} and $M_{2L} = M_{2R}$ for representations **54** and **770** as a result of subsequent breaking into the SM at the GUT scale itself M_{GUT} , we obtain gaugino mass ratios $M_3 : M_2 : M_1$ as shown in Table 5.1. For details see [5]. Obviously, M_i ($i = 1, 2, 3, 4c, 2L, 2R$)s here, denote gaugino masses corresponding to the specific gauge groups.

The cases with *odd* D -parity (specifically representation **210**), yield high-scale $M_3 = 0$, which is not favourable from the phenomenological point of view and hence we refrain from discussing that.

5.2.1 Implication of the Intermediate Scale

We have an underlying assumption that the breaking of $SO(10)$ GUT group to the intermediate gauge group and that to the SM takes place at the GUT scale

³This is an outcome of even D -parity.

itself, which is of course a simplification. But more interesting question to ask is *how things will change if the intermediate scale is different from the GUT scale (which is usually the most realistic one)?* Although we do not address this question in this analysis, we prefer to mention the crucial consequences of choosing an intermediate scale distinctly different from GUT scale:

- In this case, the choice of the non-singlet Higgses will be restricted. Now, only those Higgses will contribute which have a singlet direction under the intermediate gauge group. Hence, the Higgses that break $SO(10)$ directly to the SM at the GUT scale are disallowed. The choices of the non-singlet Higgses, in our analysis, are compatible even if the intermediate scale is different from the GUT scale.
- The mass relation in Equation 5.4 is indeed independent of the intermediate scale as it is an outcome of purely group theoretical analysis. But the gaugino mass ratios will change depending on the choice of the intermediate scale due to the running of the gaugino masses from the GUT scale.

5.3 Low energy spectra, Consistency and Benchmark

Points

Before we discuss in details the low-energy spectra for the non-universal inputs, we would like to mention a few points regarding the evolution of these gaugino mass ratios with different RGE specifications. As we know, in the one-loop RGE, the gaugino mass parameters do not involve the scalar masses [25], the ratios obtained at the low scale are independent of the high scale scalar mass input m_0 . In addition, if we also assume no radiative corrections (RC)⁴ to the gaugino masses, the ratios at the EWSB scale are also independent of the choice of the gaugino mass parameters at the high scale. Instead, if one uses the two-loop RGE (scalars contributing to the gauginos), the values of the gaugino masses at the EWSB scale tend to decrease compared to the values obtained with one-loop RGE. Now, independently, the inclusion of RC to the gaugino masses, makes M_3 lighter, but M_1 and M_2 become heavier compared to the case of one-loop results with no RC. When, one uses both the two-loop RGE and RC to the gauginos, it is

⁴The radiative corrections to the gauginos have been incorporated in calculating the physical masses after the RGE using the reference [26].

Representations	$M_3 : M_2 : M_1$ One-loop with No RC	$M_3 : M_2 : M_1$ Two-loop with RC
1 (mSUGRA)	1:0.27:0.13	1:0.35:0.19
54	1:(-0.40):(-0.06)	1:(-0.55):(-0.10)
770	1:0.67:0.24	1:0.91:0.37

Table 5.2: *Low scale (EWSB) gaugino mass ratios for representations 54 and 770 breaking through G_{422P} .*

a competition between these two effects. In short, the gaugino mass ratios at the EWSB scale crucially depend on the choice of the RGE specifications. However, the dependence on the high scale mass parameters m_0 and/or M_3 is very feeble⁵.

We present in Table 5.2, the gaugino mass ratios at the EWSB scale for two different RGE conditions:

- One-loop RGE with no RC to the gaugino masses
- Two-loop RGE with RC to the gaugino masses⁶

The numerical results have been obtained using the spectrum generator `SuSpect v2.3` [27] with the **pMSSM** option. For the rest of our analysis we adhere to the second type of RGE specifications, *two-loop RGE + RC to the gauginos* as mentioned earlier. The other broad specifications used for the scanning are listed below.

- Full one-loop and the dominant two-loop corrections to the Higgs masses are incorporated.
- Gauge coupling constant unification at the high scale have been ensured and the corresponding scale has been chosen as the 'high scale' or 'GUT-scale' to start the running by RGE. All the non-universal inputs are provided at this scale using the **pMSSM** option. This is an artifact of choosing the intermediate scale set at the GUT scale itself.

⁵In particular, with change in M_3 from 300-1000 GeV, with $m_0=1000$ GeV, the change in the ratios is within 10%, where as the ratios remain almost the same with change in m_0 .

⁶The case with two-loop RGE + RC to the gaugino masses have been obtained with $m_0 = M_3 = 500$ GeV.

- Electroweak symmetry breaking at the ‘default scale’ $\sqrt{m_{\tilde{t}_L} m_{\tilde{t}_R}}$ has been set.
- We have used the strong coupling $\alpha_3(M_Z)^{\overline{MS}} = 0.1172$ for this calculation which is again the default option in SuSpect.
- Throughout the analysis we have assumed the top quark mass to be 171.4 GeV.
- All the scalar masses have been set to a universal value of m_0 and radiative electroweak symmetry breaking has been taken into account by setting high scale Higgs mass parameter $M_{H_u}^2 = M_{H_d}^2 = m_0^2$ and specifying $\text{sgn}(\mu)$, which has been taken to be positive throughout the analysis.
- All the trilinear couplings have been set to zero.
- Tachyonic modes for sfermions and other inconsistencies in RGE, like Landau pole have been taken into account.
- As we work in a R -parity conserving scenario, stau-LSP regions have been identified as disfavoured.
- Consistency with low-energy FCNC constraints such as those from $b \rightarrow s\gamma$ has been noted for each combination of the parameter space. We have used a 3σ level constraint from $b \rightarrow s\gamma$ with the following limits [28].

$$2.77 \times 10^{-4} < Br(b \rightarrow s\gamma) < 4.33 \times 10^{-4}. \quad (5.5)$$

However, we must point out that we have taken all those regions as allowed where the value of $b \rightarrow s\gamma$ is lower or within the constraint.

- Regions allowed by all these constraints have been studied for the relic density constraint of the cold dark matter (CDM) candidate (lightest neutralino in our case) and referred to the WMAP data [8] within 3σ limit

$$0.091 < \Omega_{CDM} h^2 < 0.128. \quad (5.6)$$

where $\Omega_{CDM} h^2$ is the dark matter relic density in units of the critical density and $h = 0.71 \pm 0.026$ is the Hubble constant in units of $100 \text{ Km s}^{-1} \text{ Mpc}^{-1}$.

We have used the code `microOMEGA v2.0.7` [29] for computing the relic density.

With these inputs, we scan the parameter space for a wide range of values of m_0 and M_3 ⁷ for the non-universal gaugino mass ratios advocated above.

⁷Choice of M_3 automatically determines the values of M_1 and M_2 for a choice of non-universality.

The ratios obtained for **54** at the high scale (see Table 5.1) are actually the same as the one for the representation **24** in case of $SU(5)$ (see [1–3, 17]). This observation differs from the earlier result available in [4]. The low-energy spectrum and its consistency for the case of **24** have been well-studied [14]. Without the inclusion of the intermediate breaking scale in case of $SO(10)$, the case of **54** is difficult to distinguish from the one in $SU(5)$. Anyway we do not address any such situations here and hence, refrain from illustrating the case of **54**.

In Figure 5.1, we depict the results of the scan in the $M_3 - m_0$ parameter space for the representation **770**, i.e. breaking through G_{422} . Along the x-axis, high scale M_3 is varied from 100-2000 GeV and along the y-axis, high scale universal scalar mass m_0 is varied in the same range. Our limit of the scan is motivated by the fact that we cover the low scale parameters well beyond the reach of the LHC. The figure on the left hand side is for $\tan \beta = 5$ and on the right hand side is for $\tan \beta = 40$.

For $\tan \beta = 5$, full parameter space is allowed by REWSB, $b \rightarrow s\gamma$ and other RGE constraints. The black region at the bottom (for $M_3 = 400$ -1100 GeV and for very small values of m_0) is disfavoured by the stau-LSP constraint. Hence, there is a large region of the parameter space (shown in red) which satisfies all the constraints and it is definitely within the reach of the LHC. We study the dark-matter constraints in this allowed region of parameter space and our conclusion is as follows:

- For $M_3 = 200$ GeV, the allowed range of m_0 spans around 200 GeV
- For $M_3 = 400$ GeV, the allowed region is extremely narrow (because of the stau-LSP constraint) and is around $m_0 = 140$ GeV
- For $M_3 = 600$ GeV, $m_0 = 300$ GeV is allowed
- For $M_3 = 800$ GeV, the value of m_0 goes as high as 1100 GeV

We choose three benchmark points (BP1, BP2 and BP3, see Table 5.3 and 5.4) from here and study the collider signature.

The figure on the right hand side of Figure 5.1 is with $\tan \beta = 40$ and is quite different from the one with $\tan \beta = 5$. In this figure, the red region is allowed by REWSB while the area in blue at small m_0 is disfavoured by the stau-LSP constraint. Hence, here also, there exists a large region of parameter space, sandwiched between these two, allowed by all the constraints for the study of dark-matter and collider search. Excepting for a very narrow region at the left bottom

corner spanning 100-200 GeV of M_3 or m_0 value (in green), the whole region is under the $b \rightarrow s\gamma$ upper limit. The dark matter study in this case, yields something special. We find almost all the regions to be lying below the lower bound of the WMAP data⁸. We choose a couple of benchmark points (BP4 and BP5, see Table 5.3 and 5.4) from here for the collider study.

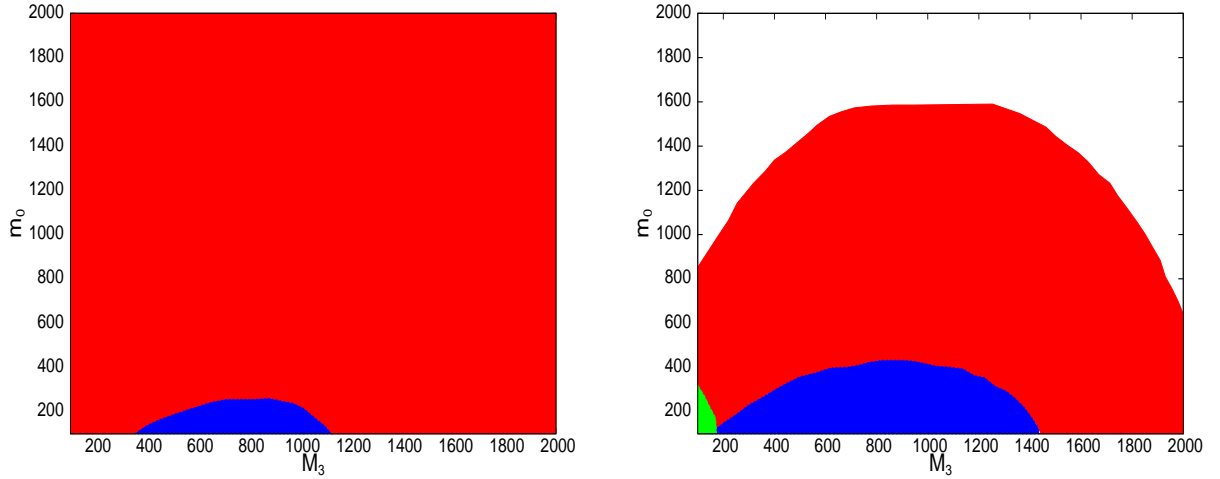


Figure 5.1: *Parameter space scan for the representation 770 (breaking through G_{422}) at high scale $M_3 - m_0$ plane (in GeV), showing the regions allowed by various constraints. Figure on the left hand side: $\tan\beta=5$. The red region is allowed and the blue region at the bottom is disfavoured by stau-LSP. Figure on the right hand side: $\tan\beta=40$. The region in red is allowed by all constraints. Region in white is disfavoured by REWSB, the low- m_0 region, in blue, is disfavoured by stau-LSP and the left corner of the graph in green with small M_3 and m_0 is disfavoured by $b \rightarrow s\gamma$.*

Figure 5.2, shows similar parameter space scan for the case of mSUGRA, for $\tan\beta=5$ (left) and $\tan\beta=40$ (right). These are presented to show the difference in the low-energy parameter space consistency patterns for different high scale gaugino mass inputs. These cases have been studied well and need not require much illustration. Our scan seems to match with the earlier available results [12] and show the robustness of our analysis. However, it is worth mentioning that

⁸This is not strictly disfavoured as some other scenarios beyond the SM can co-exist and contribute.

the red region, excepting for the blue region at small m_0 (disfavoured by stau-LSP), is allowed for $\tan \beta=5$. For $\tan \beta=40$, a small region at the upper left corner with high values of m_0 (1200-2000 GeV) and small M_3 (100-400 GeV) (in white) is disfavoured by REWSB. The blue region at the bottom is disfavoured for stau-LSP.

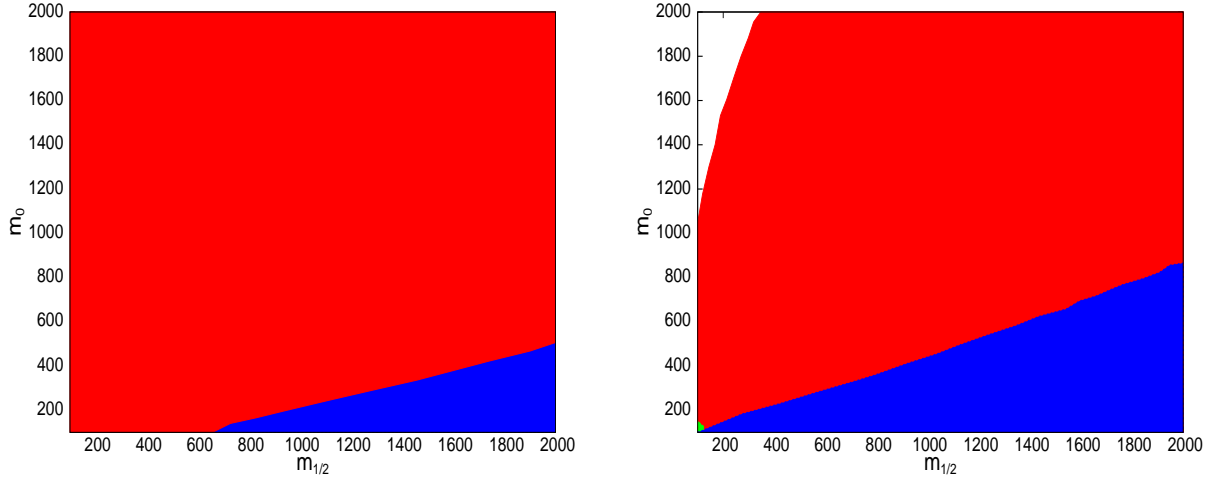


Figure 5.2: *Parameter space scan for mSUGRA at high scale $M_3 - m_0$ plane (in GeV), showing the regions allowed by various constraints. Figure on the left side: $\tan \beta=5$. The red region is allowed. The blue region at the bottom with low m_0 is disfavoured by stau-LSP. Figure on the right side: $\tan \beta=40$. The red region is allowed. The region in white at the left corner with high values of m_0 (1200-2000 GeV) is disallowed by REWSB and the bottom of the figure in blue with low values of m_0 (100-600 GeV), is disfavoured by stau-LSP.*

The benchmark points (BPs) chosen from Figure 5.1, to study the collider signature in context of the LHC, are presented in Table 5.3 and 5.4. In Table 5.3, we mention the high scale input parameters, while the low-energy spectra corresponding to these points have been mentioned in Table 5.4. The points have been chosen for two different values of $\tan \beta$, 5 (BP1, BP2, BP3) and 40 (BP4, BP5) and have gluino masses around 500 GeV and 1000 GeV. These points for $\tan \beta=5$ satisfy the WMAP data for the cold dark matter relic density search, while the points for $\tan \beta=40$ are all below the lower limit quoted by WMAP. The corresponding

Benchmark Points	Model	M_3	m_0	$\tan \beta$	$\Omega_{CDM}h^2$
BP1	770-422	200	200	5	0.124
BP2	770-422	400	140	5	0.125
BP3	770-422	600	300	5	0.126
BP4	770-422	200	200	40	0.0002
BP5	770-422	400	700	40	0.0162

Table 5.3: *Benchmark Points: Models, High scale input parameters (in GeV), $\tan \beta$ and $\Omega_{CDM}h^2$.*

values of $\Omega_{CDM}h^2$ have also been mentioned in Table 5.3. These points also obey the LEP bounds [30]. The model under scrutiny has been referred as 770-422 in Table 5.3 and will be referred so in the following text.

In Table 5.4, we note the gluino mass ($m_{\tilde{g}}$), average of the first two generation squark masses ($m_{\tilde{q}_{1,2}}$), average of the first two generation slepton masses ($m_{\tilde{l}_{1,2}}$), lighter stau mass ($m_{\tilde{\tau}_1}$), lighter stop ($m_{\tilde{t}_1}$), lightest neutralino ($m_{\tilde{\chi}_1^0}$), lighter chargino ($m_{\tilde{\chi}_1^\pm}$), 2nd lightest neutralino ($m_{\tilde{\chi}_2^0}$) as well as the value of μ , generated by REWSB at the BPs. It can also be noted that BP1, BP2, BP3 have bino dominated $\tilde{\chi}_1^0$, while it is mixed and higgsino dominated in case of BP4 and BP5 respectively. The $\tilde{\chi}_2^0$ is mixed in case of BP1 and higgsino dominated in all the other cases. The lighter chargino is mostly higgsino dominated and degenerate with $\tilde{\chi}_2^0$, excepting for the case of BP1. We would like to mention that, the composition (gaugino dominated, higgsino dominated or mixed) and the mass difference of the neutralinos and charginos get altered for different high scale gaugino non-universality. Given the similar values of squark and gluino masses in different non-universal schemes (actually similar choices of M_3 and m_0 at the high scale), the electroweak gauginos become instrumental for a possible distinction between different GUT-breaking schemes, which might also get reflected at the collider signature in a favourable region of parameter space.

To see such distinction in collider signature, we choose two points from mSUGRA scenario with suitable values of $M_{1/2}$ such that the low scale gluino

Benchmark Points	$m_{\tilde{g}}$	$m_{\tilde{q}_{1,2}}$ $m_{\tilde{t}_1}$	$m_{\tilde{l}_{1,2}}$ $m_{\tilde{\tau}_1}$	$m_{\tilde{\chi}_1^0}$	$m_{\tilde{\chi}_1^\pm}$ $m_{\tilde{\chi}_2^0}$	μ
BP1	499.95	524 305.26	319.5 246.79	138.43	203.5 219.56	221.4
BP2	938.8	928 551.83	495 313.93	303.53	375.96 386.92	381.18
BP3	1368.48	1366 815.14	770.5 513.84	464.3	515.65 522.39	515.27
BP4	499.5	524.5 315	320 172.25	132.23	170.45 187.51	178.36
BP5	966.58	1145 699.06	857 597.87	246.73	262.11 269.58	261.83

Table 5.4: *Low-energy spectra for the chosen benchmark points (in GeV).*

masses are around 500 GeV and 1000 GeV (similar to the benchmark points selected above) in a region of parameter space that satisfies the WMAP data for cold dark matter constraint. It should be noted that once these points respect the CDM constraint, the value of m_0 automatically get restricted for a particular choice of $M_{1/2}$ for a specific $\tan\beta$. Similar is the situation here where we have taken $\tan\beta = 5$ for illustration. The chosen points are named as MSG1 and MSG2. The high scale parameters along with the $\Omega_{CDM}h^2$ at these points are mentioned in Table 5.5, while the corresponding low scale spectra are noted in Table 5.6.

5.4 Collider Simulation and Numerical Results

We would like to discuss the collider signature now, of the benchmark points advocated in the preceding section.

We first discuss the strategy for the simulation which includes the final state observables and the cuts employed therein. In the next subsection we discuss the numerical results obtained from this analysis.

Points	Model	$m_{1/2}$	m_0	$\tan \beta$	$\Omega_{\text{CDM}} h^2$
MSG1	mSUGRA	480	100	5	0.111
MSG2	mSUGRA	200	70	5	0.128

Table 5.5: *mSUGRA points* : Models, High scale input parameters (in GeV), $\tan \beta$ and $\Omega_{\text{CDM}} h^2$.

Points	$m_{\tilde{g}}$	$m_{\tilde{q}_{1,2}}$ $m_{\tilde{t}_1}$	$m_{\tilde{l}_{1,2}}$ $m_{\tilde{\tau}_1}$	$m_{\tilde{\chi}_1^0}$	$m_{\tilde{\chi}_1^\pm}$ $m_{\tilde{\chi}_2^0}$	μ
MSG1	1104.1	992 768.6	272 205.1	195.66	367.1 367.4	622.1
MSG2	493.25	452 323.6	129 101.3	73.2	131.4 133.6	281.4

Table 5.6: *Low-energy spectra for the chosen mSUGRA points (in GeV).*

5.4.1 Strategy for Simulation

The spectrum generated by SuSpect v2.3 as described in the earlier section, at the benchmark points are fed into the event generator Pythia 6.4.16 [31] by SLHA interface [32] for the simulation of pp collision with centre of mass energy 14 TeV.

We have used CTEQ5L [33] parton distribution functions, the QCD renormalization and factorization scales being both set at the subprocess centre-of-mass energy $\sqrt{\hat{s}}$. All possible SUSY processes and decay chains consistent with conserved R -parity have been kept open. We have kept initial and final state radiations on. The effect of multiple interactions has been neglected. However, we take hadronisation into account using the fragmentation functions inbuilt in Pythia.

The final states studied here are :

- Opposite sign dilepton (OSD) : $(\ell^\pm \ell^\mp) + (\geq 2) jets + E_{\cancel{t}}$
- Same sign dilepton (SSD) : $(\ell^\pm \ell^\pm) + (\geq 2) jets + E_{\cancel{t}}$
- Trilepton ($3\ell + jets$): $3\ell + (\geq 2) jets + E_{\cancel{t}}$
- Hadronically quiet trilepton (3ℓ): $3\ell + (0) jets + E_{\cancel{t}}$

- Inclusive 4-lepton (4ℓ): $4\ell + X + E_{\cancel{f}}$

where ℓ stands for final state isolated electrons and or muons, $E_{\cancel{f}}$ depicts the missing energy, X indicates any associated jet production.

We will discuss these objects in details, that constitute the final state observables. The nomenclature assigned to the final state events in parentheses will be referred in the following text.

As defined in some earlier works [17], the absence of any jets with $E_T^{jet} \geq 100$ GeV qualifies the event as hadronically quiet. This avoids unnecessary removing of events along with jets originating from underlying events, pile up effects and initial state radiation/final state radiation (ISR/FSR). The 4ℓ events have been defined without putting an exclusive jet veto.

Before we mention the selection cuts, we would like to discuss the resolution effects of the detectors, specifically of the ECAL, HCAL and that of the muon chamber, which have been incorporated in our analysis. This is particularly important for reconstructing $E_{\cancel{f}}$, which is a key variable for discovering physics beyond the standard model.

All the charged particles with transverse momentum, $p_T > 0.5$ GeV⁹ that are produced in a collider, are detected due to strong B-field within a pseudorapidity range $|\eta| < 5$, excepting for the muons where the range is $|\eta| < 2.5$, due to the characteristics of the muon chamber. Experimentally, the main 'physics objects' that are reconstructed in a collider, are categorised as follows:

- Isolated leptons identified from electrons and muons
- Hadronic Jets formed after identifying isolated leptons
- Unclustered Energy made of calorimeter clusters with $p_T > 0.5$ GeV (ATLAS) and $|\eta| < 5$, not associated to any of the above types of high- E_T objects (jets or isolated leptons).

Below we discuss the 'physics objects' described above in details.

- *Isolated leptons (iso ℓ):*

Isolated leptons are identified as electrons and muons with $p_T > 10$ GeV and $|\eta| < 2.5$. An isolated lepton should have lepton-lepton separation $\Delta R_{\ell\ell} \geq 0.2$, lepton-jet separation (jets with $E_T > 20$ GeV) $\Delta R_{\ell j} \geq 0.4$, the energy deposit $\sum E_T$ due to low- E_T hadron activity around a lepton within $\Delta R \leq 0.2$ of the

⁹This is specifically for ATLAS, while for CMS, $p_T > 1$ GeV is used.

lepton axis should be ≤ 10 GeV, where $\Delta R = \sqrt{\Delta\eta^2 + \Delta\phi^2}$ is the separation in pseudo rapidity and azimuthal angle plane. The smearing functions of isolated electrons, photons and muons are described below.

- *Jets (jet):*

Jets are formed with all the final state particles after removing the isolated leptons from the list with PYCELL, an inbuilt cluster routine in Pythia. The detector is assumed to stretch within the pseudorapidity range $|\eta|$ from -5 to +5 and is segmented in 100 pseudorapidity (η) bins and 64 azimuthal (ϕ) bins. The minimum E_T of each cell is considered as 0.5 GeV, while the minimum E_T for a cell to act as a jet initiator is taken as 2 GeV. All the partons within $\Delta R=0.4$ from the jet initiator cell is considered for the jet formation and the minimum $\sum_{parton} E_T^{jet}$ for a collected cell to be considered as a jet is taken to be 20 GeV. We have used the smearing function and parameters for jets that are used in PYCELL in Pythia.

- *Unclustered Objects (Unc.O):*

Now, as has been mentioned earlier, all the other final state particles, which are not isolated leptons and separated from jets by $\Delta R \geq 0.4$ are considered as unclustered objects. This clearly means all the particles (electron/photon/muon) with $0.5 < E_T < 10\text{GeV}$ and $|\eta| < 5$ (for muon-like track $|\eta| < 2.5$) and jets with $0.5 < E_T < 20\text{GeV}$ and $|\eta| < 5$, which are detected at the detector, are considered as unclustered energy and their resolution function have been considered separately and mentioned below.

- *Electron/Photon Energy Resolution :*

$$\sigma(E)/E = a/\sqrt{E} \oplus b \oplus c/E^{10} \quad (5.7)$$

Where,

$$\begin{aligned} a &= 0.03 [\text{GeV}^{1/2}], & b &= 0.005 \ \& \ c = 0.2 [\text{GeV}] & \text{for } |\eta| < 1.5 \\ &= 0.055 & &= 0.005 & = 0.6 & \text{for } 1.5 < |\eta| < 5 \end{aligned}$$

- *Muon P_T Resolution :*

¹⁰ \oplus indicates addition in quadrature

$$\sigma(P_T)/P_T = a \quad \text{if } P_T < 100\text{GeV} \quad (5.8)$$

$$= a + b \log(P_T/100) \quad \text{if } P_T > 100\text{GeV} \quad (5.9)$$

Where,

$$\begin{aligned} a &= 0.008 \quad \& \quad b = 0.037 \quad \text{for } |\eta| < 1.5 \\ &= 0.02 \quad \quad \quad = 0.05 \quad \text{for } 1.5 < |\eta| < 2.5 \end{aligned}$$

- Jet Energy Resolution :

$$\sigma(E_T)/E_T = a/\sqrt{E_T} \quad (5.10)$$

Where,

$$a = 0.55 [\text{GeV}^{1/2}], \text{ default value used in PYCELL.}$$

- Unclustered Energy Resolution :

$$\sigma(E_T) = \alpha \sqrt{\sum_i E_T^{(Unc.O)i}} \quad (5.11)$$

Where, $\alpha \approx 0.55$. One should keep in mind that the x and y component of $E_T^{Unc.O}$ need to be smeared independently with same smearing parameter.

All the smearing parameters that have been used are mostly in agreement with the ATLAS detector specifications and also have been discussed in details in [34]

Once we have identified the 'physics objects' as described above, we sum vectorially the x and y components of the smeared momenta separately for isolated leptons, jets and unclustered objects in each event to form visible transverse momentum $(p_T)_{vis}$,

$$(p_T)_{vis} = \sqrt{(\sum p_x)^2 + (\sum p_y)^2} \quad (5.12)$$

where, $\sum p_x = \sum (p_x)_{iso \ell} + \sum (p_x)_{jet} + \sum (p_x)_{Unc.O}$ and similarly for $\sum p_y$. We identify the negative of the $(p_T)_{vis}$ as missing energy $E_{\cancel{E}}$:

$$E_{\cancel{E}} = -(p_T)_{vis} \quad (5.13)$$

Finally the selection cuts that are used in our analysis are as follows:

- Missing transverse energy $E_{\cancel{E}} \geq 100 \text{ GeV}$.

- $p_T^\ell \geq 20$ GeV for all isolated leptons.
- $E_T^{jet} \geq 100$ GeV and $|\eta_{jet}| \leq 2.5$
- For OSD, hadronically quiet trilepton (3ℓ) and also for inclusive 4ℓ events we have used, in addition, invariant mass cut on the same flavour opposite sign lepton pair as $|M_Z - M_{\ell_+\ell_-}| \geq 10$ GeV.

We have checked the hard scattering cross-sections of various production processes with CalcHEP [35]. All the final states with jets at the parton level have been checked against the results available in [21]. The calculation of hadronically quiet trilepton rates have been checked against [36], in the appropriate limits.

We have generated dominant SM events in Pythia for the same final states with same cuts. $t\bar{t}$ production gives the most serious backgrounds. We have multiplied the corresponding events in different channels by proper K -factor ($= 2.23$) to obtain the usually noted next to leading order (NLO) and next to leading log resummed (NLL) cross-section of $t\bar{t}$ production at the LHC, 908 pb (without taking the PDF and scale uncertainty), for m_t around 171 GeV [37]. The other sources of background include WZ production, ZZ production etc. The contribution of each of these processes to the various final states are mentioned in the Table 5.9.

5.4.2 Numerical Results

Figure 5.3 shows the *effective mass* distribution at the benchmark points and the corresponding mSUGRA ones in OSD events. Effective mass is defined as

$$Effective\ mass = \sum(p_T)_{iso\ \ell} + \sum(p_T)_{jets} + E_{\cancel{t}} \quad (5.14)$$

Figure 5.3 has been organised following the model inputs. Top left figure shows the distributions at BP1, BP2 and BP3 chosen from 770-422 with $\tan\beta=5$, whereas the top right one contains BP4 and BP5 chosen from the same scenario with $\tan\beta=40$ and the one from $t\bar{t}$ production, the dominant process for the background. The bottom one is for mSUGRA, containing MSG1 and MSG2 with $\tan\beta=5$. The peak of the effective mass distribution corresponds to the threshold energy of the hard scattering process which is dominantly responsible for the final state under scrutiny. For OSD events, processes responsible are mostly the $\tilde{g}\tilde{g}$, $\tilde{g}\tilde{q}$ and $\tilde{q}\tilde{q}$ productions due to their $SU(3)$ interactions, provided they are accessible to the LHC center of mass energy. In such cases, the threshold energy is around $2m_{\tilde{g}}$ or $(m_{\tilde{g}} + m_{\tilde{q}})$ or $2m_{\tilde{q}}$. Now, in each of the BPs advocated here,

$m_{\tilde{g}} = m_{\tilde{q}}$ and the threshold is approximately at $2m_{\tilde{g}}$. Our figures magnificently depict the correspondence with such threshold. For example, the peaks of BP1, BP4 and MSG2 are greater than 1000 GeV (where the gluino and squark masses are around 500 GeV). The reason that these distributions peak at higher values than the threshold, can be attributed to the fact that the final state considered here, has a very large $E_{\cancel{T}}$ cut, (p_T) cut on associated jets and leptons. While this indicates the robustness of our analysis, this also points to the deficiency in distinguishing these non-universal models from the mSUGRA one with similar gluino masses. However, a possible way that could have been exploited is perhaps the effective mass distribution in 3ℓ events. This is expected as the dominant production process for this final state is $\tilde{\chi}_2^0$ and $\tilde{\chi}_1^\pm$ and these electroweak gauginos actually carry the information of different non-universal gaugino mass inputs at the GUT scale. However, this was not very successful in our case due to small event rates.

The missing energy distributions in OSD events at all the benchmark points have been shown in Figure 5.4. The organisation of the points remain the same as in Figure 5.3. In each case, the distribution starts from 100 GeV, as the event selection itself had this missing energy cut. As a result, all the points show a similar falling feature which indicates that the peak of the distribution is either small or around 100 GeV. The difference in the distributions is in the tail and is due to the hierarchy of the lightest neutralino masses. The heavier is the neutralino, the flatter is the distribution. Although this gives a nice distinction between the points with different gluino masses (and hence with different LSP masses), it is again, difficult to distinguish points with similar gluino masses.

The numerical values of the event rates at the benchmark points are presented in Table 5.7, while Table 5.8 contains the results in similar channels for the mSUGRA ones. We note the contributions to these channels from the SM background in Table 5.8. While we note that the results are widely different from each other for different BPs, we also point out the distinction with corresponding mSUGRA ones with similar gluino masses. For example, when we compare BP1, BP4 and MSG2 (all with gluino masses around 500 GeV), we note that the mSUGRA point yields much more events in almost all channels. This primarily has two reasons: one, the choice of the scalar mass parameter is very low for the mSUGRA one, compared to the non-universal case to obey CDM constraint and two, the non-universal scenario studied here, have higher values of M_1 and M_2

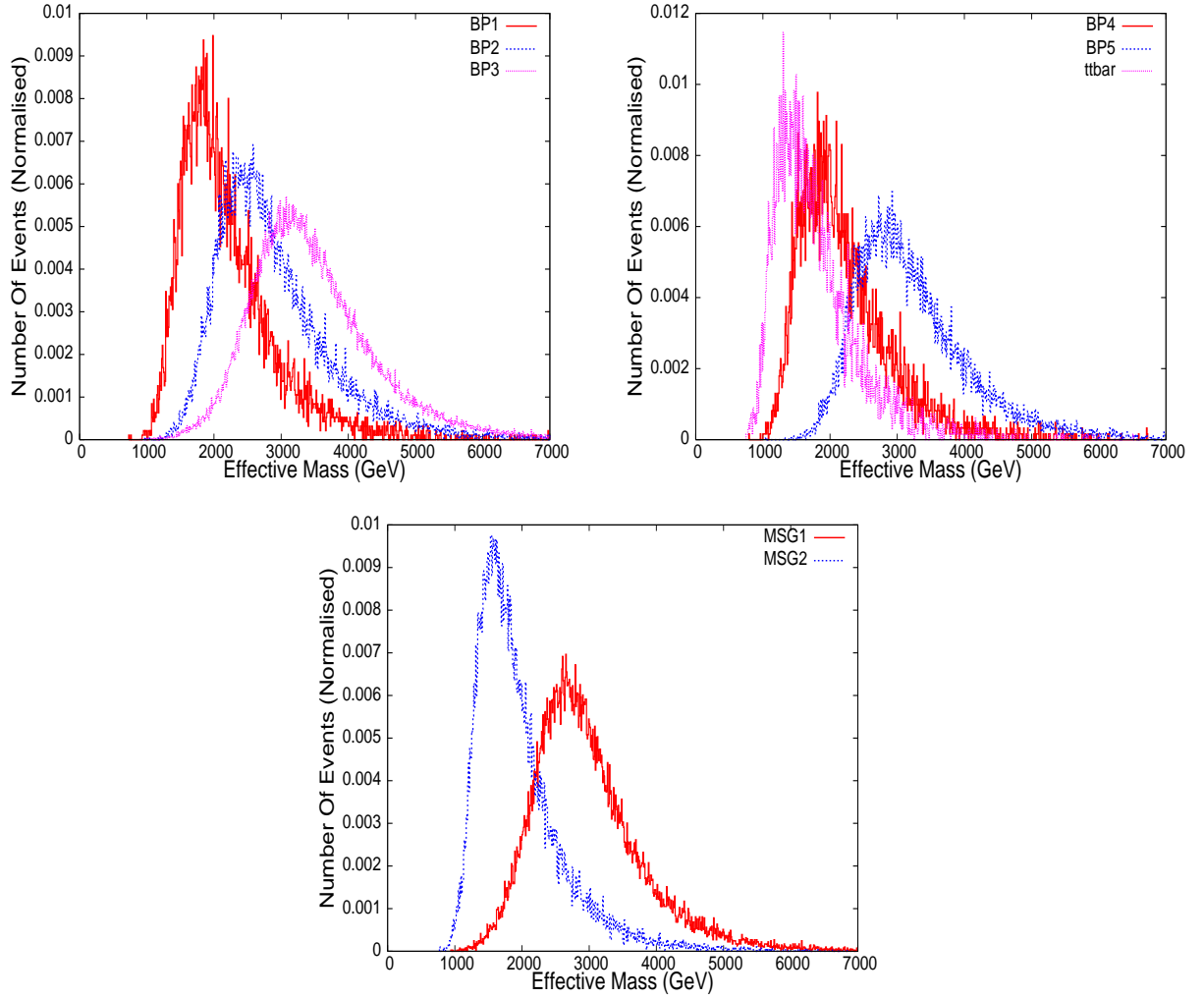


Figure 5.3: *Effective mass distribution in OSD events. Top left: BP1 (Red), BP2 (Blue) and BP3 (Pink) chosen from 770-422 with $\tan \beta=5$ have been plotted. Top right: BP4 (Red) and BP5 (Blue) chosen from 770-422 with $\tan \beta=40$ and $t\bar{t}$ (Pink) have been plotted. Bottom: MSG1 (Red) and MSG2 (Blue) chosen from $mSUGRA$ with $\tan \beta=5$ have been plotted. CTEQ5L pdfset was used. Factorisation and Renormalisation scale has been set to $\mu_F = \mu_R = \sqrt{\hat{s}}$, sub-process centre of mass energy.*

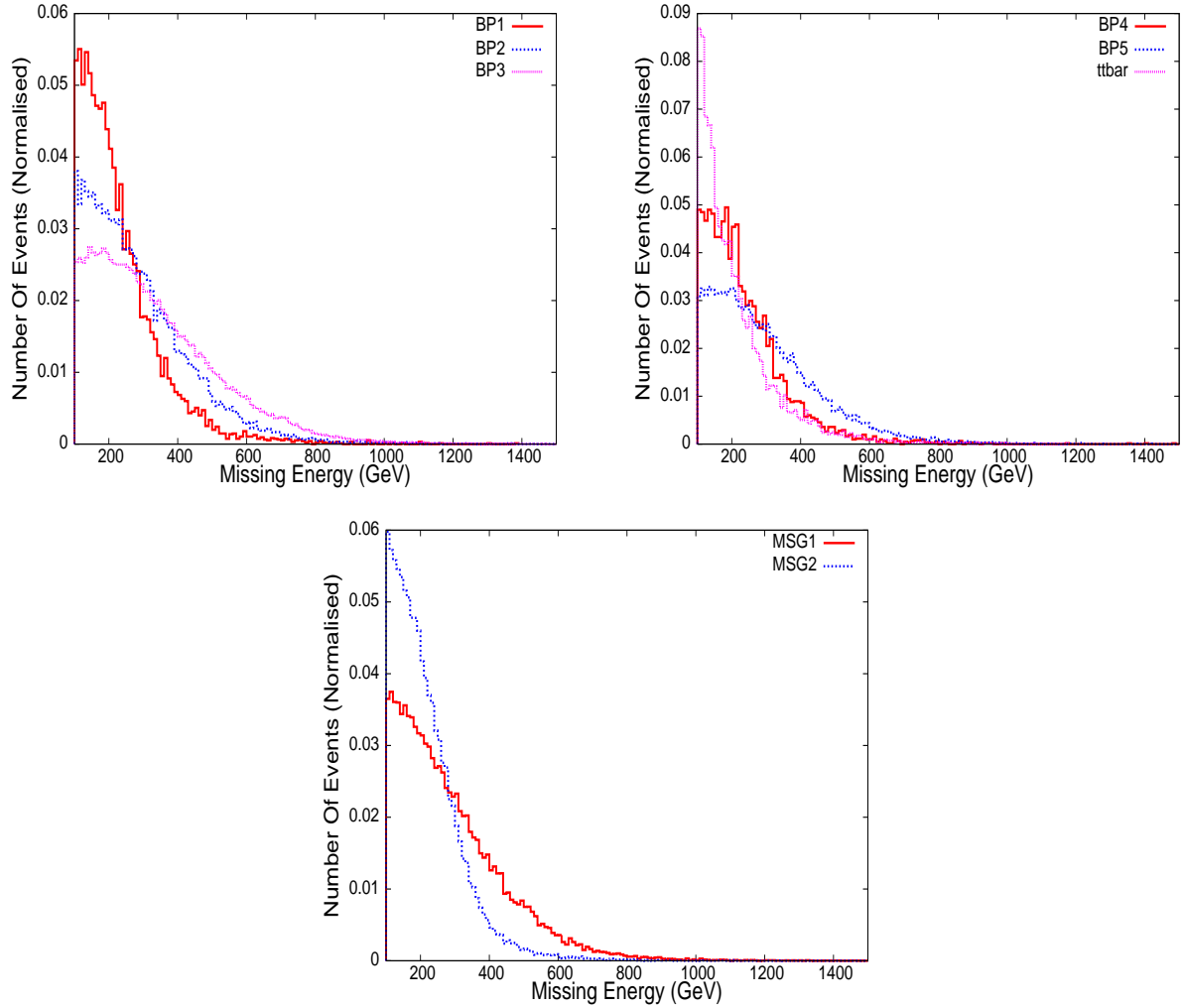


Figure 5.4: Missing energy distribution in OSD events. Top left: BP1 (Red), BP2 (Blue) and BP3 (Pink) chosen from 770-422 with $\tan \beta=5$ have been plotted. Top right: BP4 (Red) and BP5 (Blue) chosen from 770-422 with $\tan \beta=40$ and $t\bar{t}$ (Pink) have been plotted. Bottom: MSG1 (Red) and MSG2 (Blue) chosen from $mSUGRA$ with $\tan \beta=5$ have been plotted. CTEQ5L pdfset was used. Factorisation and Renormalisation scale has been set to $\mu_F = \mu_R = \sqrt{\hat{s}}$, sub-process centre of mass energy.

at the high scale, which make the low-lying charginos and neutralinos heavier and correspondingly lower decay branching fraction through these to the leptonic final states. Similar observation can be made in an attempt to compare the event rates of BP2, BP3, BP5 and MSG1 ($m_{\tilde{g}} \simeq 1000$ GeV). The reason that BP2 has slightly higher event rates than MSG1 can be attributed to the fact that $m_{\tilde{g}} = 938.8$ GeV for BP1, which is smaller to be compared to MSG1 ($m_{\tilde{g}} = 1104$ GeV).

While we see that almost all the channels at the BPs rise sufficiently over the background fluctuations, the hadronically quiet trilepton channel gets submerged in to the background even for an integrated luminosity $100fb^{-1}$ at the points BP2, BP3, BP5 and MSG1. This is because of the very high values of $m_{\tilde{\chi}_2^0}$ and $m_{\tilde{\chi}_1^\pm}$ with very small $\Delta m_{(\tilde{\chi}_2^0/\tilde{\chi}_1^\pm - \tilde{\chi}_1^0)}$. The significance in most of these points, in most of the channels (excepting the 3ℓ), are so high that it is very unlikely to be affected by the systematic errors. We would also like to point out that all the channels in BP1, BP4 and MSG2 rise over the background even for an integrated luminosity of $10fb^{-1}$ (only exception being the $\sigma_{3\ell}$ for BP4), while others are suppressed by the background. In Table 5.10, we summarise this information for each of the channels and parameter points, for an integrated luminosity of $30fb^{-1}$.

In the tables, the cross-sections are named as follows: σ_{OSD} for OSD, σ_{SSD} for SSD, $\sigma_{3\ell+jets}$ for ($3\ell + jets$), $\sigma_{3\ell}$ for (3ℓ) and $\sigma_{4\ell}$ for inclusive 4 lepton events 4ℓ .

We also compare these results in the ratio space of events which is demonstrated in Figure 5.5 in form of barplot. The advantage of going to the ratio space is the uncertainties due to the choice of pdfsets, jet energy scale get reduced. Here we take the ratios of all events with respect to the OSD and referred as SSD/OSD, 3L+JETS/OSD, 3L/OSD and 4L/OSD along the x-axis of the barplot. As earlier, we divide the BPs and the MSGs in two categories: one, with BP1, BP4 and MSG2 ($m_{\tilde{g}} \simeq 500$ GeV), which is shown in the left panel of the Figure 5.5; two, BP2, BP3, BP5 and MSG1 ($m_{\tilde{g}} \simeq 1000$ GeV), which is shown in the right panel of the Figure 5.5. We note that BP1, BP4 and MSG2 are well distinguished from

Benchmark Points	σ_{OSD}	σ_{SSD}	$\sigma_{3\ell+jets}$	$\sigma_{3\ell}$	$\sigma_{4\ell}$
BP1	597.7	102.9	57.6	13.10	10.30
BP2	70.1	15.7	11.6	0.09	1.64
BP3	17.9	2.2	4.0	0.01	1.16
BP4	398.4	120.8	30.8	4.50	3.28
BP5	26.5	12.2	3.9	0.05	0.33

Table 5.7: Event-rates (fb) in multilepton channels at the chosen benchmark points. CTEQ5L pdfset was used. Factorisation and Renormalisation scale has been set to $\mu_F = \mu_R = \sqrt{\hat{s}}$, subprocess centre of mass energy.

mSUGRA Points	σ_{OSD}	σ_{SSD}	$\sigma_{3\ell+jets}$	$\sigma_{3\ell}$	$\sigma_{4\ell}$
MSG1	50.9	16.4	10.6	0.08	1.34
MSG2	2781.8	175.9	285.1	12.26	99.89

Table 5.8: Event-rates (fb) in multilepton channels at the mSUGRA points. CTEQ5L pdfset was used. Factorisation and Renormalisation scale has been set to $\mu_F = \mu_R = \sqrt{\hat{s}}$, subprocess centre of mass energy.

SM Processes	σ_{OSD}	σ_{SSD}	$\sigma_{3\ell+jets}$	$\sigma_{3\ell}$	$\sigma_{4\ell}$
$t\bar{t}$	1102	18.1	2.7	5.3	0.0
$ZZ, WZ, ZH, Z\gamma$	16.3	0.3	0.5	1.1	0.4
Total	1118.3	18.4	3.2	6.4	0.4

Table 5.9: Event-rates after cut (fb) in multilepton channels from the dominant SM backgrounds. The event rates in different channels for $t\bar{t}$ production have been multiplied by proper K-factor (2.23) to obtain the usually noted NLO+NLL cross-section of $t\bar{t}$ [37]. CTEQ5L pdfset was used. Factorisation and Renormalisation scale has been set to $\mu_F = \mu_R = \sqrt{\hat{s}}$, subprocess centre of mass energy.

Model Points	OSD	SSD	$3\ell + jets$	3ℓ	4ℓ
BP1	✓	✓	✓	✓	✓
BP2	✓	✓	✓	×	✓
BP3	×	×	✓	×	✓
BP4	✓	✓	✓	✓	✓
BP5	✓	✓	✓	×	×
MSG1	✓	✓	✓	×	✓
MSG2	✓	✓	✓	✓	✓

Table 5.10: 5σ visibility of various signals for an integrated luminosity of $30fb^{-1}$. A ✓ indicates a positive conclusion while a × indicates a negative one.

SSD/OSD, $3L/OSD$ and $4L/OSD$. While BP2 and MSG1 can not be distinguished very well from each other, identification of BP3, BP5 and MSG1 is quite apparent from SSD/OSD and $4L/OSD$ events.

In a nutshell we can summarise that, it is indeed possible to distinguish the non-universal gaugino mass scenario advocated here, from the mSUGRA ones with similar gluino masses. This is possible in both the absolute event rates or from the ratio plots shown here. However, the distinguishability reduces with increasing gluino mass.

5.5 Summary and Conclusions

We have derived non-universal gaugino mass ratios for the representations **54** and **770** for the breaking chain $SU(4)_C \otimes SU(2)_L \otimes SU(2)_R$ (G_{422}) in a $SO(10)$ SUSY-GUT scenario. We have assumed that the breaking of $SO(10)$ to the intermediate gauge group and the latter in turn to the SM gauge group takes place at the GUT scale itself. We point out some errors in the earlier calculation and derive new results on the gaugino mass ratios. We scan the parameter space with different low-energy constraints taken into account and point out the allowed region of the parameter space. We also study the dark matter constraint in these models and study collider simulation at some selected benchmark points in context

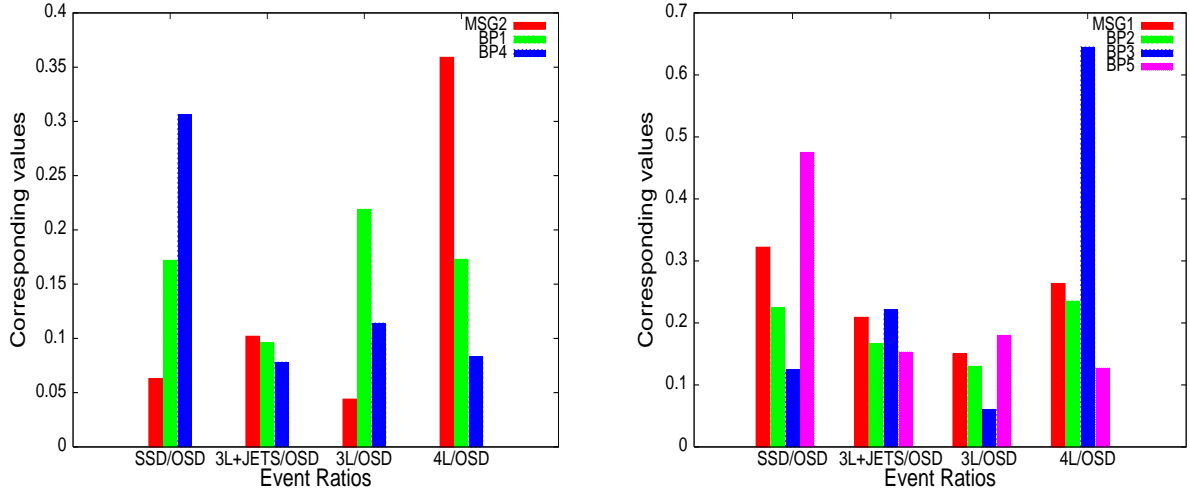


Figure 5.5: Event ratios of different benchmark points compared with $mSUGRA$. Along the x -axis, ratios of events with respect to OSD have been taken. The relative values of these ratios for different benchmark points are indicated along the y -axis. Figure on the left: MSG2 (Red), BP1 (Green) and BP4 (Blue) are compared. $m_{\tilde{g}}$ is around 500 GeV in each case. 3L/OSD and 4L/OSD have been multiplied by 10. Figure on the right: MSG1 (Red), BP2 (Green), BP3 (Blue) and BP5 (Pink) are compared. $m_{\tilde{g}}$ is around 1000 GeV in each case. 3L/OSD has been multiplied by 100 and 4L/OSD has been multiplied by 10 to accommodate them in the same figure. CTEQ5L pdfset was used. Factorisation and Renormalisation scale has been set to $\mu_F = \mu_R = \sqrt{\hat{s}}$, sub-process centre of mass energy.

of the LHC. The scans presented, have many interesting features that might help us in understanding the correlation between high scale input and low-energy spectra. We must mention here that the study is limited by the assumption that the series of symmetry breaking occurs at the GUT scale itself. It is essentially a simplification, although we know that the mass relation in Equation (5.4) is not going to change with different choices of the intermediate scale, while the running of the masses from the GUT scale to the intermediate scale will eventually change the gaugino mass ratios. However, our choice of the non-singlet Higgses, apart from conserving D -parity, are compatible even if the intermediate scale is different from the GUT scale. Within such a framework we have performed a collider study which is more illustrative than exhaustive. It nonetheless elicits some characteristics of the signature space for such high scale ratios in context of the LHC. It is worth mentioning in this context that the comparison between the non-universal inputs with the mSUGRA ones yields a significant distinction in the multilepton channel parameter space in context of the LHC. This feature might be important in pointing out the departure of the 'signature space' with the inclusion of non-universality at the high scale.

Around the time we completed this study, we came across the reference [19], where the issue of gaugino mass non-universality in the context of $SO(10)$ and $E(6)$ has been addressed. While we agree completely with the corrected gaugino mass ratios for G_{422} , our analysis in addition, point out the phenomenologically viable situations where the choices of the Higgses get restricted with D -parity conservation and inclusion of the intermediate scale different from the GUT scale. Furthermore, the low-energy particle spectra in different cases have been derived in a comparative manner and the allowed regions of the parameter space consistent with low-energy and dark matter constraints are obtained in each case. In addition, we have predicted event-rates for such a breaking chain in a multichannel study pertinent to the LHC. The distinguishability of relative rates in different channels has also been explicitly demonstrated by us.

Bibliography

- [1] J. R. Ellis, C. Kounnas and D. V. Nanopoulos, Nucl. Phys. B **247**, 373 (1984);
J. R. Ellis, K. Enqvist, D. V. Nanopoulos and K. Tamvakis, Phys. Lett. B **155**,
381 (1985).
- [2] M. Drees, Phys. Lett. B **158**, 409 (1985).
- [3] A. Corsetti and P. Nath, Phys. Rev. D **64**, 125010 (2001) [arXiv:hep-
ph/0003186].
- [4] N. Chamoun, C. S. Huang, C. Liu and X. H. Wu, Nucl. Phys. B **624**, 81 (2002)
[arXiv:hep-ph/0110332].
- [5] S. Bhattacharya and J. Chakraborty, Phys. Rev. D **81**, 015007 (2010)
[arXiv:0903.4196 [hep-ph]].
- [6] J. Chakraborty and A. Raychaudhuri, Phys. Lett. B **673** (2009) 57
[arXiv:0812.2783 [hep-ph]].
- [7] D. Chang, R. N. Mohapatra and M. K. Parida, Phys. Rev. Lett. **52** (1984)
1072.
- [8] E. Komatsu *et al.* [WMAP Collaboration], Astrophys. J. Suppl. **180**, 330
(2009) [arXiv:0803.0547 [astro-ph]].
- [9] A. Datta, A. Datta and M. K. Parida, Phys. Lett. B **431**, 347 (1998) [arXiv:hep-
ph/9801242]; A. Datta, A. Datta, M. Drees and D. P. Roy, Phys. Rev. D **61**,
055003 (2000) [arXiv:hep-ph/9907444].
- [10] H. Baer, C. h. Chen, F. Paige and X. Tata, Phys. Rev. D **53**, 6241 (1996)
[arXiv:hep-ph/9512383].
- [11] S. Khalil, Phys. Lett. B **484**, 98 (2000) [arXiv:hep-ph/9910408]; S. Komine
and M. Yamaguchi, Phys. Rev. D **63**, 035005 (2001) [arXiv:hep-ph/0007327].
- [12] K. Huitu, Y. Kawamura, T. Kobayashi and K. Puolamaki, Phys. Rev. D **61**,
035001 (2000) [arXiv:hep-ph/9903528]; K. Huitu, J. Laamanen, P. N. Pan-
dita and S. Roy, Phys. Rev. D **72**, 055013 (2005) [arXiv:hep-ph/0502100];

- U. Chattopadhyay, D. Das and D. P. Roy, Phys. Rev. D **79**, 095013 (2009) [arXiv:0902.4568 [hep-ph]].
- [13] K. Choi and H. P. Nilles, JHEP **0704**, 006 (2007) [arXiv:hep-ph/0702146].
- [14] S. F. King, J. P. Roberts and D. P. Roy, JHEP **0710** (2007) 106 [arXiv:0705.4219 [hep-ph]]; K. Huitu, R. Kinnunen, J. Laamanen, S. Lehti, S. Roy and T. Salminen, Eur. Phys. J. C **58** (2008) 591 [arXiv:0808.3094 [hep-ph]].
- [15] K. Huitu and J. Laamanen, Phys. Rev. D **79**, 085009 (2009) [arXiv:0901.0668 [hep-ph]].
- [16] S. I. Bityukov and N. V. Krasnikov, Phys. Lett. B **469**, 149 (1999) [Phys. Atom. Nucl. **64**, 1315 (2001) YAFIA,64,1391-1398.2001] [arXiv:hep-ph/9907257]; G. Anderson, H. Baer, C. h. Chen and X. Tata, Phys. Rev. D **61**, 095005 (2000) [arXiv:hep-ph/9903370]; S. I. Bityukov and N. V. Krasnikov, Phys. Atom. Nucl. **65**, 1341 (2002) [Yad. Fiz. **65**, 1374 (2002)] [arXiv:hep-ph/0102179].
- [17] S. Bhattacharya, A. Datta and B. Mukhopadhyaya, JHEP **0710** (2007) 080 [arXiv:0708.2427 [hep-ph]]; S. Bhattacharya, A. Datta and B. Mukhopadhyaya, Phys. Rev. D **78** (2008) 115018 [arXiv:0809.2012 [hep-ph]].
- [18] P. Bandyopadhyay, A. Datta and B. Mukhopadhyaya, Phys. Lett. B **670** (2008) 5 [arXiv:0806.2367 [hep-ph]]; P. Bandyopadhyay, JHEP **0907**, 102 (2009) [arXiv:0811.2537 [hep-ph]].
- [19] S. P. Martin, Phys. Rev. D **79**, 095019 (2009) [arXiv:0903.3568 [hep-ph]].
- [20] A. A. Affolder *et al.* [CDF Collaboration], Phys. Rev. Lett. **88**, 041801 (2002) [arXiv:hep-ex/0106001]; P. Binetruy, G. L. Kane, B. D. Nelson, L. T. Wang and T. T. Wang, Phys. Rev. D **70**, 095006 (2004) [arXiv:hep-ph/0312248]; J. L. Bourjaily, G. L. Kane, P. Kumar and T. T. Wang, arXiv:hep-ph/0504170; G. L. Kane, P. Kumar, D. E. Morrissey and M. Toharia, Phys. Rev. D **75**, 115018 (2007) [arXiv:hep-ph/0612287].
- [21] A. Datta, G. L. Kane and M. Toharia, arXiv:hep-ph/0510204.
- [22] V. D. Barger, W. Y. Keung and R. J. N. Phillips, Phys. Rev. Lett. **55**, 166 (1985); H. Baer, X. Tata and J. Woodside, Phys. Rev. D **41**, 906 (1990); H. Baer, X. Tata and J. Woodside, Phys. Rev. D **45**, 142 (1992); R. M. Barnett, J. F. Gunion and H. E. Haber, Phys. Lett. B **315**, 349 (1993) [arXiv:hep-ph/9306204]; A. Datta, K. Kong and K. T. Matchev, Phys. Rev. D **72**, 096006 (2005) [Erratum-ibid. D **72**, 119901 (2005)] [arXiv:hep-ph/0509246].

- [23] G. Duckeck *et al.* [ATLAS Collaboration].
- [24] R. Slansky, *Phys. Rept.* **79** (1981) 1.
- [25] S. P. Martin and P. Ramond, *Phys. Rev. D* **48**, 5365 (1993) [arXiv:hep-ph/9306314].
- [26] D. M. Pierce, J. A. Bagger, K. T. Matchev and R. j. Zhang, *Nucl. Phys. B* **491** (1997) 3 [arXiv:hep-ph/9606211].
- [27] A. Djouadi, J. L. Kneur and G. Moultaka, *Comput. Phys. Commun.* **176**, 426 (2007) [arXiv:hep-ph/0211331].
- [28] S. Chen *et al.* [CLEO Collaboration], *Phys. Rev. Lett.* **87**, 251807 (2001) [arXiv:hep-ex/0108032]; P. Koppenburg *et al.* [Belle Collaboration], *Phys. Rev. Lett.* **93**, 061803 (2004) [arXiv:hep-ex/0403004]; B. Aubert *et al.* [BaBar Collaboration], arXiv:hep-ex/0207076.
- [29] G. Belanger, F. Boudjema, A. Pukhov and A. Semenov, *Comput. Phys. Commun.* **176**, 367 (2007) [arXiv:hep-ph/0607059].
- [30] W. M. Yao *et al.* [Particle Data Group], *J. Phys. G* **33**, 1 (2006).
- [31] T. Sjostrand, S. Mrenna and P. Skands, *JHEP* **0605**, 026 (2006) [arXiv:hep-ph/0603175].
- [32] P. Skands *et al.*, *JHEP* **0407**, 036 (2004) [arXiv:hep-ph/0311123].
- [33] H. L. Lai *et al.* [CTEQ Collaboration], *Eur. Phys. J. C* **12**, 375 (2000) [arXiv:hep-ph/9903282].
- [34] S. Biswas and B. Mukhopadhyaya, *Phys. Rev. D* **79**, 115009 (2009) [arXiv:0902.4349 [hep-ph]].
- [35] A. Pukhov, arXiv:hep-ph/0412191.
- [36] H. Baer, C. H. Chen, F. Paige and X. Tata, *Phys. Rev. D* **50** (1994) 4508 [arXiv:hep-ph/9404212].
- [37] S. Moch and P. Uwer, *Phys. Rev. D* **78** (2008) 034003 [arXiv:0804.1476 [hep-ph]].

Chapter 6

Non-universal masses, hadronically quiet trileptons and the Large Hadron Collider

6.1 Introduction

The predicted signals of SUSY at the LHC depend largely on the production of strongly interacting superparticles, namely, the squarks and gluinos, via the annihilation of quarks, antiquarks and gluons. Their subsequent decays culminate into the lightest SUSY particle (LSP)– the lightest neutralino in most scenarios– which is stable and a dark matter candidate when R-parity is conserved. The resulting signals of SUSY consist in a large amount of missing transverse energy (\cancel{E}_T), together with hard central jets and leptons of various multiplicities [1, 2]. Of course, hadronically quiet events, such as trileptons arising from the direct production of charginos and neutralinos have also been studied as useful supporting signals which can help in probing the non-strongly interacting sector of the theory [3]. Still, the final states arising from squark/gluino cascades have overwhelming importance in general, for the sheer level of copiousness that they associate.

How about a situation where the squarks and gluinos are so heavy (say, $\gtrsim 5$ TeV) that their production rate is too low to support the cascades? In such a case, most of the signals that depend on strongly interacting superparticles will not be easy to see at the LHC. Keeping such a situation in mind, it is important in one's preparation for the LHC to check how the 'hadronically quiet events' fare. One needs to know exactly over which ranges in the parameter space of SUSY, for example, *the hadronically quiet trilepton events can act as the harbinger of new physics, not as a supplementary search channel but as the main one.* The present chapter [4] is aimed at answering such a question, by making an elaborate survey of the SUSY parameter space, especially in terms of M_1 and M_2 , the $U(1)$ and $SU(2)$ gaugino masses which dictate the rate of the hadronically trilepton rates. In other words, although hadronically quiet trileptons in the context of the LHC have been already studied, here we wish to make the study specifically focused on cases where squarks and gluinos tend to decouple.

Hadronically quiet trileptons occur mostly from the production $pp \rightarrow \chi_2^0 \chi_1^\pm$, where χ_2^0 is the second lightest neutralino and χ_1^\pm is the lighter chargino. The hadronically quiet trilepton events have the best chance when the squarks are very heavy compared to the sleptons and decays of charginos and neutralinos to on-shell sleptons and leptons are allowed. From this point of view, the decoupled nature of squarks favours the trilepton final states. On the other hand, they have less of a chance when the decay modes $\chi_2^0 \rightarrow \chi_1^0 h^0$ or $\chi_2^0 \rightarrow \chi_1^0 Z$ have substantial branching ratios.

An exhaustive investigation of the SUSY parameter space in this light has to go beyond universality of gauginos and scalars at high scale. We outline some ways of theoretically motivating non-universality in the next section. However, we wish to re-iterate that, in the absence of any concrete knowledge of high scale physics as well as whether a 'grand desert' exists, it is really important in the context of collider studies to go beyond specific theoretical schemes. *We rather propose to establish a new benchmark of non-universal SUSY breaking masses, distinguished by the suppression of final states arising from strong production.* The remaining part of the paper is an exercise in this direction and therefore in our collider studies we treat the strong versus electroweak gaugino and scalar masses essentially as phenomenological inputs.

In Section 6.2 we first outline some standard GUT-based schemes of achieving non-universal SUSY breaking masses. Then it is shown that the situation with

heavy squarks and gluinos may require one to go beyond such schemes, and establish our benchmark based on this consideration. A detailed discussion of the hadronically quiet trilepton signal, and the main backgrounds, is presented in Section 6.3. In section 6.4 we present numerical predictions for leptonic final states of various multiplicity, with accompanying hard jets. We conclude in section 6.5.

6.2 Non-universality and hadronically quiet signals

The kind of spectrum that we use for our study can be motivated from the non-universality of gaugino and scalar masses at high scale.

As is well known, universality of gaugino masses at high scale is not a necessity even in GUT-based scenarios. A number of non-universal ratios among $M_{1,2,3}$ can arise, say, in $SU(5)$ and $SO(10)$ scenarios, with general gauge kinetic functions

$$f_{\alpha\beta}(\Phi^j) = f_0(\Phi^S)\delta_{\alpha\beta} + \sum_N \xi_N(\Phi^S) \frac{\Phi^N_{\alpha\beta}}{M} + \mathcal{O}\left(\frac{\Phi^N}{M}\right)^2 \quad (6.1)$$

where f_0 and ξ^N are functions of chiral singlet superfields, and M is the reduced Planck mass $= M_{Pl}/\sqrt{8\pi}$. Here Φ^S and Φ^N are Higgs multiplets that are, respectively, singlets and non-singlets under the GUT group. Different non-singlet representations leading to the breaking of the GUT group, arising from symmetric products of the adjoint representations, lead to different ratios among the high-scale values of the three gaugino masses [5–7]. However, in neither of the cases pertaining to the two GUT groups mentioned above can one have $M_3 \gg M_{1,2}$ at the electroweak scale. One can not achieve the above hierarchy by breaking the GUT group via linear combinations of various non-singlet representations unless there is strong cancellation among various contributing multiplets. For example, in case of $SU(5)$, the Higgs belonging to the representation **24** or, for $SO(10)$, the the representation **54** breaking through the Pati-Salam gauge group G_{224} , yield a non-universal gaugino mass ratio $M_3 : M_2 : M_1 = 2 : -3 : -1$ (See Chapter 4 and 5). Under such circumstances, the GUT group may break through a linear combination of the singlet with either of the non-singlet Higgs representations. In the process, one can not rule out the possibility of getting $M_{1,2} \simeq 0$, thanks

$m_{\tilde{\ell}}$ in GeV	(M_1, M_2) in GeV	OSD	SSD	$3\ell + jets$	$\geq 3 jets$	3ℓ
200	(150,300)	1.25	0.04	0.11	2.82	5.99
300	(232,350)	0.55	0.07	0.10	1.79	2.39
400	(179,200)	0.24	0.07	0.01	3.37	0.11

Table 6.1: *Different final state rates (fb) with cuts at the LHC with $M_3 = m_{\tilde{g}} = 5$ TeV, $m_{\tilde{q}} = 5$ TeV, $\mu = 1$ TeV, $m_A = 500$ GeV, $A = 0$, $\tan \beta = 10$, where μ , A and $\tan \beta$ are respectively the Higgsino mass parameter, the trilinear soft SUSY breaking parameter and the ratio of the vacuum expectation values of the two Higgs doublets. All the parameters are at the electroweak scale with appropriate mixing in the third family. ℓ stands for electrons and muons. CTEQ5L PDFset used with $\mu_F = \mu_R = \sqrt{s}$.*

to the negative sign that arises in the non-universal ratio of **24** (or **54** of $SO(10)$). This, in turn, can yield a hierarchy of the type $M_3 \gg M_{1,2}$.

Nonetheless, as has been already mentioned, a hierarchy of the gluino and electroweak gaugino masses can arise from hitherto unknown effects, such as the presence of intermediate scale(s) as well as the evolution between the Planck and the GUT scales.

In the scalar sector, while certain SUSY-GUT effects like $SO(10)$ D -terms can lead to non-universality of mass parameters at high scale [8–11], it is generally difficult to accommodate squarks much heavier than sleptons in such a framework. One can not however rule out, for example, additional $U(1)$ symmetries under which the squarks and sleptons have widely disparate charges, and which breaks to make the squarks much heavier than sleptons via D -terms. In addition, if a large hierarchy exists in the gaugino sector, making the $SU(3)$ gaugino mass much higher than those of the $SU(2)$ and $U(1)$ gauginos at high scale, then even a universal scalar mass scenario can make the squarks much heavier at the electroweak scale, through the large gluino contribution in the process of running.

In the rest of our study we take the low-energy spectrum as a phenomeno-

logical input, and look at regions where large squark and gluino masses prevent strong processes from contributing significantly to SUSY signals at the LHC. We wish to see SUSY signals when, in the above situation, the sleptons and electroweak gauginos are well within the reach of the machine.

We show in Table 6.1 three sample points in situations of the above type. These points are consistent with the cold dark matter relic density indicated by the WMAP results ($0.091 < \Omega_{CDM}h^2 < 0.128$ within 3σ limit) [12]. The relic density for these points have been computed using the SLHA output of the low-energy SUSY spectra from `Suspect v2.3` [13] and feeding it to the code `micrOMEGAs v2.0` [14]. Corresponding to these points, rates are presented for opposite-sign dileptons (OSD), same-sign dileptons (SSD) and trilepton final states ($3\ell + jets$) each associated with hard central jets, as also for the inclusive jets ($\geq 3 jets$). Lastly, the hadronically quiet trilepton (3ℓ) rate is presented, each case being characterized by missing E_T . Acceptance cuts as specified in our earlier works [7,11] have been used in computing these rates. It can be seen that all these rates are suppressed in this region of the parameter space. Compared to them, the rate for hadronically quiet trileptons arising from purely electroweak processes turns out to be higher, though they are still somewhat small in the absolute sense. The points chosen in Table 6.1 are samples, where the statistical significance of the signals over backgrounds is not as much the issue as the relative strengths of the hadronically quiet trileptons vis-a-vis other signals. We show after a detailed scan of the parameter space that the hadronically quiet trilepton signal, largely the result of $\chi_1^\pm \chi_2^0$ production, is still significant over a noticeable region of the parameter space.

It is in general seen that the signals are appreciable, and simultaneously the WMAP bound can be satisfied with relative ease, if the slepton mass is on the low side ($\lesssim 300$ GeV). For $m_{\tilde{\nu}} = 200$ GeV, the WMAP-allowed region spans over M_1 in the range between 103 GeV and $\gtrsim 175$ GeV, while M_2 varies in the range 120 - 300 GeV. For larger slepton masses, the allowed band shifts to larger values of M_1 (approximately 170 - 235 GeV for a slepton mass of 300 GeV) for the same M_2 . The allowed band includes regions of lower M_1 and M_2 for lower values of μ where, however, the hadronically quiet signals become more intractable, as the enhanced Higgsino components in χ_1^\pm and χ_2^0 reduce their couplings to leptons of the first two families.

While the sample points shown in Table 6.1 are fully consistent with the

GUT-Scale input	M_1	M_2	M_3	$m_{0\tilde{\ell}}$	$m_{0\tilde{q}}$	$\text{sgn}(\mu)$
	300	300	2400	300	300	+ve
Low-Scale Output	M_1	M_2	$m_{\tilde{g}}$	$m_{\tilde{\ell}}$	$m_{\tilde{q}}$	μ
	113.8	194.0	4961.4	$\simeq 300$	$\simeq 4200$	2630

Table 6.2: *Spectrum (in GeV) generated with Suspect v2.3 by having high scale gaugino mass non-universality. $\tan\beta=10$, $A_0=0$. Radiative electroweak symmetry breaking is ensured. High scale Higgs mass parameters $m_{H_u}^2$ and $m_{H_d}^2$ are kept degenerate with universal scalar masses ($m_{0\tilde{\ell}} = m_{0\tilde{q}}$) at the same scale.*

WMAP constraints, and serve to illustrate the efficacy of the hadronically quiet trilepton channel, we feel that a scan over a large region of the parameter space should be made in an analysis pertaining to the LHC. In this spirit, we have calculated the signal rates in the entire region over the $M_1 - M_2$ space allowed by terrestrial experiments, with various values of the slepton mass, assuming that the squark and gluino masses are 5 TeV (where they contribute little to the cascades). Apart from the values of M_1 , M_2 and the slepton mass, all the other SUSY parameters are fixed at values used in Table 6.1 for most of our analysis. Variation with squark/gluino mass and $\tan\beta$ are shown only at the end of the next section, to demonstrate how they affect the predictions.

We indicate in Table 6.2 some sample high scale parameters that generate a representative SUSY spectrum in our benchmark scenario, running two loop renormalisation group equation (RGE) with radiative corrections to all squark and gaugino masses in Suspect v2.3. It has been obtained by using the pMSSM option of the code. It is demonstrated that non-universality in the gaugino sector can be responsible for the kind of spectrum phenomenologically adopted by us. It should be noted that the non-universality of M_3 with $M_{1,2}$ required here, can be produced within the ambit of familiar SUSY-GUT, but with a strong cancellation between different contributing non-singlet representations, as mentioned earlier.

6.3 Signal and backgrounds: hadronically quiet trileptons

We have used the event generator Pythia v6.4.16 [15] for the generation of low-energy SUSY spectra. The consistency of parameter combinations under investigation have been checked with the programme Suspect v2.3, where all the low-energy constraints from $b \rightarrow s\gamma$, muon anomalous magnetic moment etc. are taken into account [16]. The Higgsino mass parameter μ is used as a free parameter in the numerical study.

Pythia v6.4.16 has also been used for the simulation of pp collision with the centre-of-mass energy of 14 TeV, with hadronisation effects turned on. We have used CTEQ5L [17] parton distribution functions, the QCD renormalization and factorization scales (μ_R, μ_F) being both set at the subprocess centre-of-mass energy $\sqrt{\hat{s}}$. As we shall show later, the overall conclusions are rather insensitive to the choice of scales.

All possible SUSY processes and decay chains consistent with conserved R -parity have been kept open. We have switched on initial and final state radiations (ISR and FSR respectively) with the functions built within Pythia v6.4.16, but otherwise confined ourselves to the lowest order matrix elements for the signal. The effect of multiple interactions has been neglected.

Jets are formed in Pythia using PYCELL jet formation criteria with $|\eta_{jet}| \leq 5$ in the calorimeter, $N_{\eta_{bin}} = 100$ and $N_{\phi_{bin}} = 64$. For a partonic jet to be considered as a jet initiator, $E_T > 2$ GeV is required, while a cluster of partonic jets is branded as a hadron-jet when $\sum_{parton} E_T^{jet}$ is more than 20 GeV. The maximum ΔR from the initiator jet is taken to be 0.4. We have cross-checked the hard scattering cross-sections of various production processes with CalCHEP [18]. All the final states with jets at the parton level have been checked against the results available in [19]. The calculation of hadronically quiet trilepton rates have been checked against other standard works, in the appropriate limits [3].

While the minimum E_T or trigger for jet formation is 20 GeV, hadronically quiet trilepton events (with $\ell = e, \mu$) have been defined by the absence of any accompanying central jet ($|\eta_{jet}| \leq 2.5$) with $E_T^{jet} \geq 100$ GeV qualifies the event as hadronically quiet. This avoids unnecessary vetoing of trilepton events along with jets originating from ISR/FSR, underlying events and pile-up effects. Strong cascades with events leading to relatively soft jets also add to the signal. The same definition of hadronically quiet trilepton is retained in [11], discussed in the

following chapter.

The background to the proposed signal can come from a number of processes including $WZ/Z^*/\gamma^*$, $t\bar{t}$ as well as heavy flavours. The $WZ^*/W\gamma^*$ and heavy flavour (mostly b) channels are brought under control with a large missing- E_T cut [20]. Furthermore, we have demanded the three leptons to be isolated, according to the criteria listed below. In addition, at least one pair of opposite charged leptons (electrons/muons) have to be of the same flavour. This finally leaves us with $t\bar{t}$ and WZ production. Of the latter channel, whatever survives the missing- E_T cut is suppressed by imposing an invariant mass cut on opposite-sign, same flavour dileptons. Thus it is the $t\bar{t}$ channel that really constitutes the irreducible background, mostly due to the overwhelmingly large rate of top-quark pair production at the LHC.

We have generated all dominant SM events in Pythia for the same final states, using the same renormalization/factorization scale, parton distributions and cuts. The WZ and $t\bar{t}$ channels are dominant among the backgrounds. While the former is effectively suppressed through an invariant mass cut on the same flavour, opposite-sign lepton pairs, the $t\bar{t}$ background is of an irreducible nature, since, with the huge production cross-section at the LHC, jets that do not satisfy either the trigger or our imposed cuts can masquerade as hadronically quiet events. An enhancement of statistical significance of the signal over such backgrounds is attempted with the help of the missing E_T cut. As we shall see in the numerical results, a higher degree of significance is expected when the mass differences between the χ_1^0 and each of the χ_2^0 and the χ_1^\pm are on the higher side, thus allowing a harder p_T spectrum for the leptons. The other backgrounds, namely, the ones from virtual Z /photons, are found to be under control after imposing the cuts, which are as follows [21]:

- Missing transverse energy $E_T \geq 100$ GeV
- $p_T^\ell \geq 20$ GeV and $|\eta_\ell| \leq 2.5$
- Lepton isolation, such that lepton-lepton separation $\Delta R_{\ell\ell} \geq 0.2$, lepton-jet separation $\Delta R_{\ell j} \geq 0.4$. The E_T deposit due to jet activity around a lepton E_T within a cone of $\Delta R \leq 0.2$ of the lepton axis should be < 10 GeV
- No jet with $E_T^{jet} \geq 100$ GeV and $|\eta_{jet}| \leq 2.5$ (Vetoing central hard jets)
- Invariant mass of any same flavour, opposite sign lepton pair with $|m_Z - M_{\ell_+\ell_-}| \geq 10$ GeV

Cuts	$\sigma_{\tilde{t}\tilde{t}} \rightarrow 3\ell$	$\sigma_{WZ} \rightarrow 3\ell$	$\sigma_{3\ell(\text{total})}$
p_T, η cut (on ℓ, jets)	2.428	0.130	2.557
+lepton isolation	0.473	0.031	0.504
+ E_T^{miss} cut	0.267	0.010	0.277
+invariant mass cut	0.129	0.008	0.137

Table 6.3: Cross-sections (pb) for leading sources of SM background after successive application of different cuts, $m_t = 171.4$ GeV. CTEQ5L PDFset used with $\mu_F = \mu_R = \sqrt{\hat{s}}$. $\sigma_{\tilde{t}\tilde{t}} \rightarrow 3\ell$ is presented after multiplying by appropriate K-factor (2.04).

where $\Delta R = \sqrt{\Delta\eta^2 + \Delta\phi^2}$ is the so-called isolation parameter which is the separation in the pseudo-rapidity and the azimuthal angle plane.

The cross-sections for the backgrounds from the dominant sources, subjected to the cuts that are used in the signal-analysis, are presented in Table 6.3. The effectiveness of cuts at successive levels have been shown.

The numbers of signal and background events have been calculated for an integrated luminosity of 100 fb^{-1} . The significance is obtained in the Gaussian limit, using $\sigma = S/\sqrt{B}$ where S and B denote the number of signal and the background events respectively.

In Figure 6.1 we plot the significance of hadronically quiet trileptons in the $M_1 - M_2$ plane, for three different slepton masses which are all kept to be degenerate at 200 GeV, 300 GeV and 400 GeV. Of course, the lighter stau is somewhat lighter than the other sleptons, and we truncate the value of M_1 accordingly in each plot, so as to disallow a scenario with stau as the lightest SUSY particle (LSP). In each case, the gluino and squark masses are kept at 5 TeV, with $\mu = 1$ TeV and $\tan\beta = 10$. While regions with less than 2σ have not been marked, regions marked in red correspond to significance more than 5, blue, to significance in the $3-5\sigma$ range and black, to the $2-3\sigma$ range, while in black-and-white print light grey, grey and black implies above significance respectively.

For a slepton mass of 200 GeV (the top left plot), there is a large region of

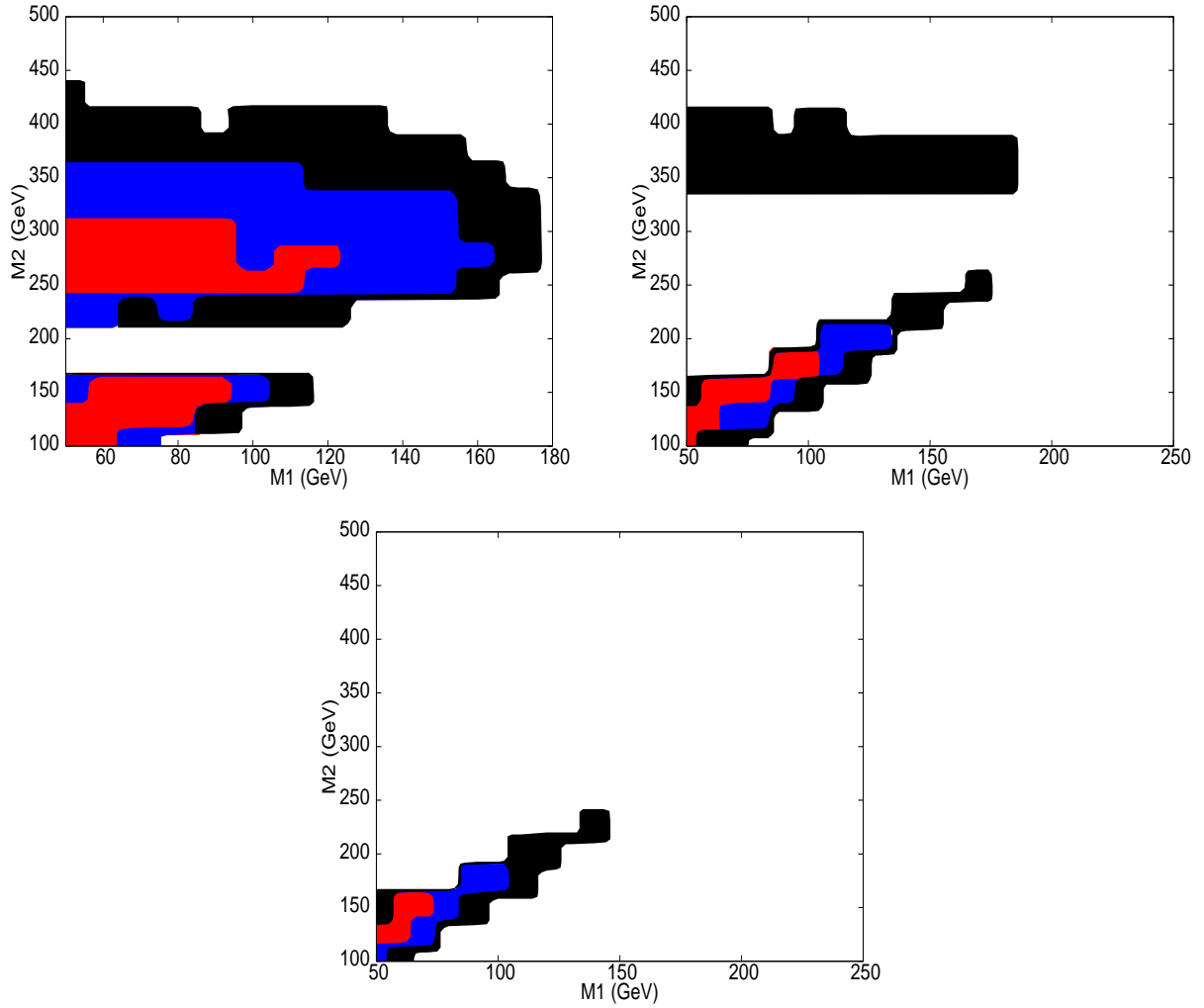


Figure 6.1: Significance contours for hadronically quiet trilepton events, for an integrated luminosity of 100 fb^{-1} in $M_1 - M_2$ plane. Colour Code: Black: $2 \leq \sigma < 3$, Blue: $3 \leq \sigma < 5$, Red: $\sigma \geq 5$ (in black-and-white print: Black: $2 \leq \sigma < 3$, Grey: $3 \leq \sigma < 5$, Light Grey: $\sigma \geq 5$). Top left: Slepton mass = 200 GeV, Top right: Slepton mass = 300 GeV, Bottom: Slepton mass = 400 GeV. CTEQ5L PDFset used with $\mu_F = \mu_R = \sqrt{s}$.

parameter space for M_1 between 50 GeV and 125 GeV and M_2 between 240 GeV and 300 GeV with significance more than 5σ . There also exists a small region at the bottom left portion of the graph for M_1 between 50 GeV and 90 GeV and for low M_2 (between 100 GeV and 140 GeV) which has significance more than 5σ . The regions of significance between $3-5\sigma$ and $2-3\sigma$ lie around the region of $\sigma \geq 5$. The statistical significance in various regions can be explained by remembering that the rate of $\chi_1^\pm \chi_2^0$ production is large for smaller chargino and neutralino masses, thus giving higher overall rates. At the same time, there is a complementary trend of a larger number of events surviving the hardness cut once one has larger M_2 , thus creating a rather large region in the parameter space with higher significance of the signal. In addition, there is a dynamical effect [22], namely, the destructive interference between the Z -and slepton-mediated diagrams in χ_2^0 decays, when on-shell sleptons are not produced. The observed pattern of significance contours is a consequence of such effects as well.

For higher slepton masses, namely, $m_{\tilde{\ell}} = 300$ or 400 GeV, the region of the parameter space depicting $\sigma \geq 5$ for $m_{\tilde{\ell}} = 200$ GeV shrinks. Only the small region at the bottom left corner of the graph shows $\sigma \geq 5$, although it also shrinks to a considerable extent compared to the case of $m_{\tilde{\ell}} = 200$ GeV.

However, for the case of $m_{\tilde{\ell}} = 300$ GeV, although the $3-5\sigma$ region is absent in the upper segment, the region of $2-3\sigma$ extends up to $M_1 = 180$ GeV, and for M_2 slightly on the higher side (340 GeV to 400 GeV). This is because, with the degenerate slepton masses going up, the allowed region with neutralino LSP is larger, and at the same time the leptons in the final state tend to be harder. The regions with $\sigma \geq 5$ correspond to regions with very low M_2 (110 GeV to 160 GeV) for a slepton mass of 400 GeV. The erstwhile regions of high significance for larger values of M_2 are gone for heavier sleptons. In such cases, as has been mentioned earlier, the $\chi_1^0 h$ and $\chi_1^0 Z$ channels tend to dominate in the decays of χ_2^0 , thus reducing the significance of the triplepton signals.

We have also checked the dependence of our predictions on the QCD renormalization/factorization scales by setting, for instance, both the scales at the average mass of the final state particles in the hard scattering. While this affects both signal and background rates, the significance contours remain very similar to the corresponding case with the scale set at the subprocess centre-of-mass energy. This shows the robustness of the expected significance levels.

We also plot in Figure 6.3 the variation in rates for hadronically quiet triplep-

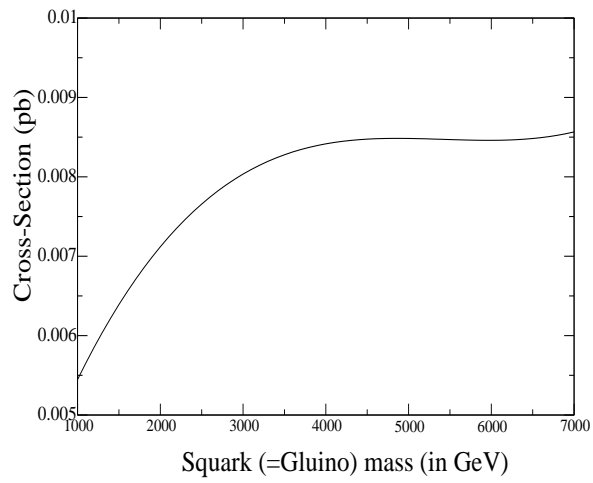


Figure 6.2: Variation of rates (pb) with cuts for hadronically quiet trilepton events with degenerate squark-gluino mass. Other relevant parameters are at the following values: $m_{\tilde{\chi}} = 200$ GeV, $M_1 = 100$ GeV and $M_2 = 300$ GeV, $\mu = 1$ TeV, and $\tan \beta = 10$. CTEQ5L PDFset used with $\mu_F = \mu_R = \sqrt{\hat{s}}$.

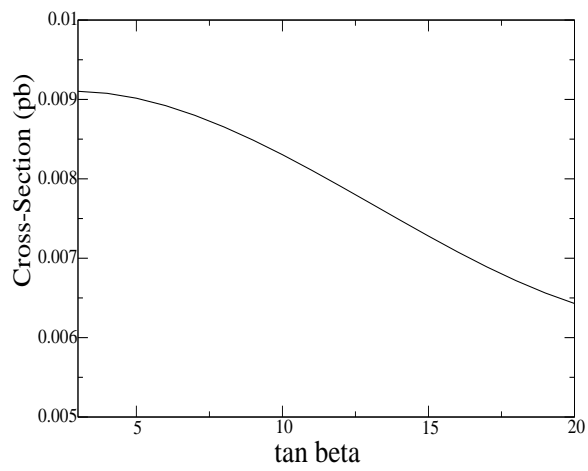


Figure 6.3: Variation of rates (pb) with cuts for hadronically quiet trilepton events with $\tan \beta$. Other relevant parameters are at the following values: $m_{\tilde{g}} = m_{\tilde{q}} = 5$ TeV, $m_{\tilde{\chi}} = 200$ GeV, $M_1 = 100$ GeV, $M_2 = 300$ GeV, and $\mu = 1$ TeV. CTEQ5L PDFset used with $\mu_F = \mu_R = \sqrt{\hat{s}}$.

ton (3ℓ) events with $m_{\tilde{g}} = m_{\tilde{q}}$ varying from 1 to 7 TeV for $m_{\tilde{\chi}} = 200$ GeV, $M_1 = 100$ GeV, $M_2 = 300$ GeV, $\mu = 1$ TeV with $\tan\beta = 10$. The rate for hadronically quiet trileptons increases gradually with the coloured sparticle mass going up, due to the interference between the s - and squark-mediated t -channel diagrams. The effect dwindles as the squark and gluino mass reaches 3 TeV, and a plateau is clear from about 5 TeV onwards.

We also show the variation with $\tan\beta$ from 3 to 20 in Figure 6.3 in the same region of parameter space with $m_{\tilde{g}} = m_{\tilde{q}} = 5$ TeV where the cross-section decreases sharply. Beyond 20 one ends up with a stau LSP, which turns into tachyonic stau state as $\tan\beta$ grows larger. The signal rate goes down for higher $\tan\beta$. This is because the lighter stau eigenstate becomes gradually lighter with respect to the other sleptons, and the decays of the lighter chargino and the second lightest neutralino take place more into the tau-channels. Again, smaller values of μ will affect the signal adversely, since the lighter chargino/neutralino eigenstates then have enhanced Higgsino components. This either tends to open their decays into a Higgs, or causes them to decay into final states involving τ 's.

We have discussed above the viability of the hadronically quiet trilepton signals at the LHC in terms of statistical significance in specific situations. It should be noted that we have left out the effects of systematic errors here. When the signal is a few percent of the background, one may have problems due to systematic shift in the background, especially if the background is large [23]. How well the signals can fare under such circumstances depends on whether the systematics affect the signal and the background strengths in a similar way or not. In addition, the ultimate success of probes in such a final state will depend on the accurate estimate of backgrounds, possibly in the light of initial data available at the LHC. Since this is an open issue, which is serious in much wider context, we would just like to keep the reader aware of the need to be cautious on this matter.

6.4 Other signals

It may be worthwhile to check whether our benchmark scenario has accessibility by other types of signals. Table 6.1 shows the advantage of the hadronically quiet trilepton signal. However, a scan over the parameters is required to establish a general conclusion on the scenario where the coloured superparticles are too

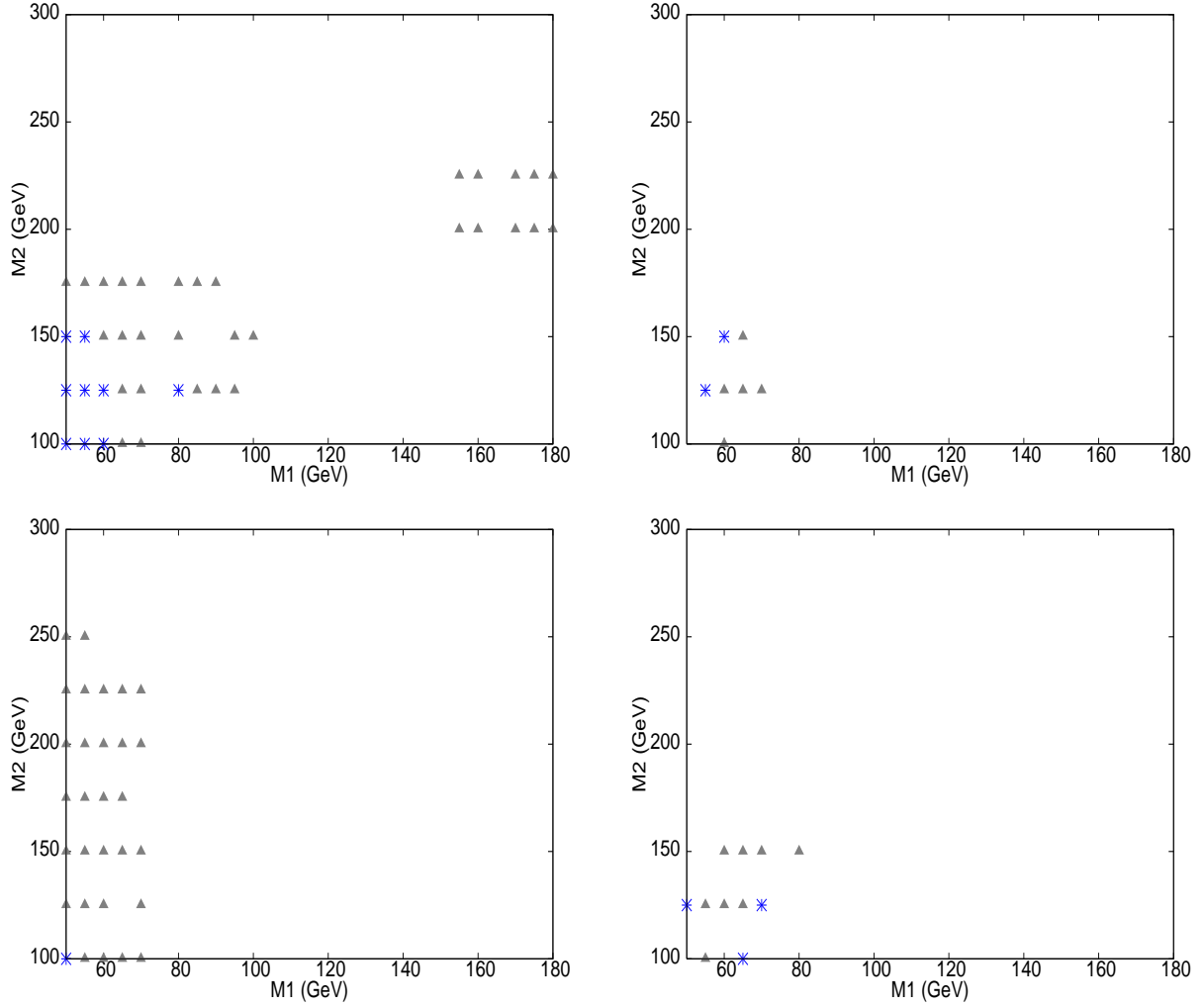


Figure 6.4: Scattered plot of the significance of single-lepton events (on the left side) and dilepton events (on the right side) for an integrated luminosity of 100 fb^{-1} in $M_1 - M_2$ plane. Significance Code: Triangular points: $1 \leq \sigma < 1.5$, Star marked points: $\sigma \geq 1.5$. Top row: Slepton mass = 200 GeV, Bottom row: Slepton mass = 400 GeV, Left Column: Single-lepton events, Right Column: Dilepton events. CTEQ5L PDFset used with $\mu_F = \mu_R = \sqrt{\hat{s}}$.

massive to have any significant contribution to final states at the LHC. With this in view, we have studied signals with $n\ell + \geq 2 \text{ hard jets} + \cancel{E}_T$ across the $M_1 - M_2$ plane, with the slepton mass set at 200 and 400 GeV respectively. The various panels in Figure 6.3 contain the results of this scan. Each of the hard jets is required to have $E_T \geq 100$ GeV and $|\eta| \leq 2.5$, the cuts on leptons and \cancel{E}_T being the same as in the case of hadronically quiet trileptons.

The figure shows that the single- and dilepton signals both fail to achieve significance higher than 2σ in the entire region of relevance, with an integrated luminosity of 100 fb^{-1} . For the trilepton channel with associated hard jets, it is even less than 1 and has not been presented pictorially. Thus in general the other channels are always of less advantage than hadronically quiet trileptons, as was suggested at the beginning of the paper. The reason behind this is the low event rate from gluino/squark production when both of them are very heavy. Thus we are essentially dependent on electroweak processes, where the demand of at least two hard central jets has a negative effect. Without such jets, on the other hand, one has rather large backgrounds which could be handled in the case of hadronically quiet trileptons with the help of an invariant mass cut.

We have also checked the effect of reducing the p_T cut on the hard jets to 75 and 50 GeV in succession. It is found that the significance increases at best by about a factor of two in the favourable situations. However, the uncertainty in backgrounds increases considerably in such cases.

6.5 Conclusions

In summary, SUSY scenarios with non-universality in both gaugino and scalar masses, can envision regions in the parameter space where the usual signals from the cascade decays of strongly interacting superparticles involving hard multi-jets drop below the threshold of observability. We demonstrate that hadronically quiet trileptons can be of significant help in these cases. As a numerical study presented here indicates, other signals such as single- or dileptons, for which additional hard jets are required for background suppression, are decidedly less advantageous for such a scenario. Most favourable in this respect are regions with slepton masses not too far above 200 GeV, and either both M_1 and M_2 in the 100 - 200 GeV range, with relatively large production rates, or with a large separation

between them so as to enable the decay- leptons to be harder. These two effects yield a substantial region in the parameter space with 5σ or better statistics, while a still larger region with $3-5\sigma$ effects can be identified for an integrated luminosity of 100 fb^{-1} . With higher accumulated luminosity, of course, the reach of the signal increases. The effects can be expected to be experimentally favourable for $\tan \beta \lesssim 15 - 20$, and with gaugino-dominated low-lying neutralino and chargino states.

Bibliography

- [1] A. A. Affolder *et al.* [CDF Collaboration], Phys. Rev. Lett. **88**, 041801 (2002) [arXiv:hep-ex/0106001].
- [2] H. Baer, C. h. Chen, F. Paige and X. Tata, Phys. Rev. D **53**, 6241 (1996) [arXiv:hep-ph/9512383].
- [3] H. Baer, C. H. Chen, F. Paige and X. Tata, Phys. Rev. D **50** (1994) 4508 [arXiv:hep-ph/9404212].
- [4] S. Bhattacharya, A. Datta and B. Mukhopadhyaya, Phys. Rev. D **78** (2008) 115018 [arXiv:0809.2012 [hep-ph]].
- [5] J. R. Ellis, C. Kounnas and D. V. Nanopoulos, Nucl. Phys. B **247**, 373 (1984); J. R. Ellis, K. Enqvist, D. V. Nanopoulos and K. Tamvakis, Phys. Lett. B **155**, 381 (1985); M. Drees, Phys. Lett. B **158**, 409 (1985); A. Corsetti and P. Nath, Phys. Rev. D **64**, 125010 (2001) [arXiv:hep-ph/0003186]; N. Chamoun, C. S. Huang, C. Liu and X. H. Wu, Nucl. Phys. B **624**, 81 (2002) [arXiv:hep-ph/0110332].
- [6] S. I. Bityukov and N. V. Krasnikov, Phys. Lett. B **469**, 149 (1999) [Phys. Atom. Nucl. **64**, 1315 (2001 YAFIA,64,1391-1398.2001)] [arXiv:hep-ph/9907257]; G. Anderson, H. Baer, C. h. Chen and X. Tata, Phys. Rev. D **61**, 095005 (2000) [arXiv:hep-ph/9903370]; K. Huitu, Y. Kawamura, T. Kobayashi and K. Puolamaki, Phys. Rev. D **61**, 035001 (2000) [arXiv:hep-ph/9903528]; K. Huitu, J. Laamanen, P. N. Pandita and S. Roy, Phys. Rev. D **72**, 055013 (2005) [arXiv:hep-ph/0502100].
- [7] S. Bhattacharya, A. Datta and B. Mukhopadhyaya, JHEP **0710** (2007) 080 [arXiv:0708.2427 [hep-ph]].
- [8] M. Drees, Phys. Lett. B **181** (1986) 279; J. S. Hagelin and S. Kelley, Nucl. Phys. B **342**, 95 (1990).
- [9] Y. Kawamura, H. Murayama and M. Yamaguchi, Phys. Lett. B **324** (1994) 52

- [arXiv:hep-ph/9402254]; Y. Kawamura, H. Murayama and M. Yamaguchi, Phys. Rev. D **51** (1995) 1337 [arXiv:hep-ph/9406245].
- [10] A. Datta, A. Datta and M. K. Parida, Phys. Lett. B **431**, 347 (1998) [arXiv:hep-ph/9801242]; A. Datta, A. Datta, M. Drees and D. P. Roy, Phys. Rev. D **61**, 055003 (2000) [arXiv:hep-ph/9907444]; I. Gogoladze, R. Khalid, N. Okada and Q. Shafi, arXiv:0811.1187 [hep-ph].
- [11] S. Bhattacharya, A. Datta and B. Mukhopadhyaya, Phys. Rev. D **78** (2008) 035011 [arXiv:0804.4051 [hep-ph]].
- [12] E. Komatsu *et al.* [WMAP Collaboration], Astrophys. J. Suppl. **180**, 330 (2009) [arXiv:0803.0547 [astro-ph]].
- [13] A. Djouadi, J. L. Kneur and G. Moultaka, Comput. Phys. Commun. **176**, 426 (2007) [arXiv:hep-ph/0211331].
- [14] G. Belanger, F. Boudjema, A. Pukhov and A. Semenov, Comput. Phys. Commun. **176** (2007) 367 [arXiv:hep-ph/0607059].
- [15] T. Sjostrand, S. Mrenna and P. Skands, JHEP **0605**, 026 (2006) [arXiv:hep-ph/0603175].
- [16] A. Djouadi, M. Drees and J. L. Kneur, JHEP **0603**, 033 (2006) [arXiv:hep-ph/0602001].
- [17] H. L. Lai *et al.* [CTEQ Collaboration], Eur. Phys. J. C **12**, 375 (2000) [arXiv:hep-ph/9903282].
- [18] A. Pukhov, arXiv:hep-ph/0412191.
- [19] A. Datta, G. L. Kane and M. Toharia, arXiv:hep-ph/0510204.
- [20] Z. Sullivan and E. L. Berger, Phys. Rev. D **78**, 034030 (2008) [arXiv:0805.3720 [hep-ph]].
- [21] G. Duckeck *et al.* [ATLAS Collaboration], CITATION = ATLAS-TRD-017.
- [22] H. Baer and X. Tata, Phys. Rev. D **47** (1993) 2739.
- [23] G. L. Bayatian *et al.* [CMS Collaboration], J. Phys. G **34** (2007) 995.

Chapter 7

Non-universal scalar masses: a signal-based analysis for the Large Hadron Collider

7.1 Introduction

In earlier studies, we have investigated the effects of departure from gaugino universality (within the ambit of a SUSY-GUT scenario) on various signals at the LHC, and identified situations where a multichannel analysis can reveal traces of such departure [1]. In the present chapter [2], we take up a similar investigation of departure of the squark and slepton spectrum from that predicted by mSUGRA. A number of theoretical scenarios have already been investigated in this connection. These include, for example, scenarios with heavy scalars [3–6] or some superstring-inspired models [7]. In addition, one finds studies on the phenomenological implications of non-universal scalars [8,9], particularly relating to dark matter [10]. The special thrust of the present work lies in its generality as well as the emphasis on the relative strengths of different signals in eliciting a non-universal scalar mass pattern.

The most important signals of R -parity conserving SUSY consist in large

missing transverse energy E_T , accompanied with energetic jets and leptons of various multiplicity in the central region. While the signal strengths, kinematics and event topology of a given final state yield information of the mass scale of new particles, it is emphasized that *the relative strengths of different signals corresponding to the spectrum of a given type often tells us more*. In particular, the departure from the mSUGRA scenario can crucially affect some particular final state. Hence we advocate the detailed exploration of the ‘signature space’ [1, 11–17] as a whole, and illustrate such exploration for some representative cases through a multichannel analysis [18].

Our (restricted) signature space consists of the following final states: *jets + E_T , same-sign* as well as *opposite-sign dileptons*, and *trileptons* along with *jets + E_T* . In addition, we include the so-called ‘hadronically quiet’ trilepton events in our analysis. The event rates predicted are after the imposition of cuts aimed at reducing the SM backgrounds. We present the ratios of various types of final states, thus also reducing uncertainties due to parton distributions, factorization scales, jet energy resolutions etc. These ratios, presented as bar graphs, demonstrate the departure (or otherwise) from what is predicted in mSUGRA, for superparticle masses in different combinations. They can be supplemented by the absolute rates, too, for (a) information on the overall SUSY masses, and (b) cases where the rate of one type of event is either too small or submerged in backgrounds.

In the mSUGRA models, all low-scale parameters are derived from a universal gaugino mass ($M_{1/2}$), a universal scalar mass (m_0), the trilinear soft SUSY-breaking parameter (A_0) and the sign of the Higgsino mass parameter ($\text{sgn}(\mu)$) for each value of $\tan\beta$, the ratio of the two Higgs vacuum expectation values (vev). Since the consequence of gaugino non-universality [1, 19–23] has been probed in our earlier work, the gauginos have been taken to have a universal mass at high scale in this study.

Specifically, we consider three different types of non-universal scenarios. These are (a) non-universality of the squark and slepton masses, (b) non-universality of the third family sfermions with respect to the first two, and (c) non-universality due to high-scale D -terms, pertinent to an $SO(10)$ model. While the first scenario is purely phenomenological, the second one is motivated by the so-called ‘inverted hierarchy’ at a high scale, which is advocated as a solution to the flavour problem [24–28]. The third case concerns a particular theoretical picture where physics between the Planck and GUT scales affects the masses of

sfermions in different sub-representations of $SO(10)$, leading to different low-energy mass patterns [29–31].

The approach advocated here can be useful in so called ‘inverse problem’ approach [32], where one aims to construct an underlying theory from a multi-channel assortment of data.

The paper is organized as follows. In the following section, we outline the general strategies of our collider simulation, including the main event selection criteria. We discuss the non-universality of squark-slepton masses and the different predictions in the signature space in section 7.3. Section 7.4 contains a comparative study of different signals at the LHC, when the non-universality is limited to scalars in the third family. Signatures of $SO(10)$ D -terms leading to non-universality is discussed in section 7.5, where we also discuss the variation of the mass spectrum with the D -term contribution treated as a free parameter. We summarize and conclude in section 7.6. Salient features of the particle spectra in the different cases, and the absolute rates of predicted events, are presented in Appendices A and B, respectively.

7.2 Strategy for simulation

Before we proceed to analyze specific scenarios, let us summarize the collider simulation procedure that has been adopted in all the cases. The spectrum generated by SuSpect v2.3 [33] as described in each scenario is fed into the event generator Pythia 6.405 [34] by SLHA interface [35] for the simulation of pp collision with centre of mass energy 14 TeV.

We have used CTEQ5L [36] parton distribution functions, the QCD renormalization and factorization scales being both set at the subprocess centre-of-mass energy $\sqrt{\hat{s}}$. Other options such as the scales set at the average mass of the particles produced in the initial hard scattering are not found to alter the qualitative features of our results. All possible SUSY processes and decay chains consistent with conserved R -parity have been kept open. In the illustrative study presented here, we have switched off initial and final state radiations. This does not affect the major conclusions, as events with ≥ 2 jets are mostly considered and jet counting is not of any crucial significance here. The effect of multiple interactions has been neglected. However, we take hadronisation into account using the fragmen-

tation functions inbuilt in Pythia.

The final states studied here are [13,17,37]:

- Opposite sign dilepton (*OSD*): $(\ell^\pm \ell^\mp) + (\geq 2) jets + E_{\cancel{H}}$
- Same sign dilepton (*SSD*): $(\ell^\pm \ell^\pm) + (\geq 2) jets + E_{\cancel{H}}$
- Trilepton ($3\ell + jets$): $3\ell + (\geq 2) jets + E_{\cancel{H}}$
- Hadronically quiet trilepton (3ℓ): $3\ell + E_{\cancel{H}}$
- Inclusive jets (*jets*): $(\geq 3) jets + X + E_{\cancel{H}}$

where ℓ stands for electrons and or muons.

It should be noted that hadronically quiet trileptons have been introduced as a separate channel of study here, contrary, for example, to the one presented in reference [1]. The reason for our optimism about this channel is the fact that the very notion of sfermion non-universality entails scenarios with sleptons that are light with respect to charginos and neutralinos, a feature that serves to enhance the rates of final states with high lepton multiplicity arising from decays of the latter. The numerical results presented in the following sections show that, with exceptions, this optimism is not entirely misplaced.

We have generated all dominant SM events in Pythia for the same final states, using the same factorization scale, parton distributions and cuts. $t\bar{t}$ production gives the most serious backgrounds in all channels excepting in the trilepton channels, for which electroweak backgrounds can be serious. For the inclusive jet signals, the final states without any isolated, central, hard leptons are also prone to large QCD backgrounds, where, for example, jet energy mismeasurement can lead to a tail with missing- E_T . The maximum reduction of such QCD backgrounds is very challenging (especially due to uncertainties in the prediction and interpretation of multi jets). In our theoretical study, keeping the above problem in mind, we have tried to be conservative by imposing a cut of 100 GeV on *each jet* and not choosing to order their hardness cuts. While one can further improve on this by making the $E_{\cancel{H}}$ cut even higher, our main message, namely, the sensitivity of the ratios of various signals to different non-universal scenarios, still retains its relevance after such improvements.

The signal and background events have been all calculated for an integrated luminosity of $300 fb^{-1}$. As noted earlier, the event ratios which are the primary objects of our analysis help in avoiding uncertainties in prediction. Cases where

the number of signal events in any of the channels used in the ratio(s) is less than three have been left out. Also, in the histograms (to be discussed in the next section), cases where any of the entries in the ratio has a significance less than 2σ have been specially marked with a # in the bar graphs. since our observations on them may still be useful if statistics can be improved.

The cuts used in our analysis are as follows:

- Missing transverse energy $E_{\cancel{T}} \geq 100$ GeV.
- $p_T^l \geq 20$ GeV and $|\eta_\ell| \leq 2.5$.
- An isolated lepton should have lepton-lepton separation $\Delta R_{\ell\ell} \geq 0.2$, lepton-jet separation $\Delta R_{\ell j} \geq 0.4$, the energy deposit due to jet activity around a lepton E_T within $\Delta R \leq 0.2$ of the lepton axis should be ≤ 10 GeV.
- $E_T^{jet} \geq 100$ GeV and $|\eta_{jet}| \leq 2.5$
- For the hadronically quiet trilepton events, we have used in addition, invariant mass cut on the same flavour opposite sign lepton pair as $|M_Z - M_{l_+l_-}| \geq 10$ GeV.

where $\Delta R = \sqrt{\Delta\eta^2 + \Delta\phi^2}$ is the separation in pseudo rapidity and azimuthal angle plane.

Jets are formed in Pythia using PYCELL jet formation criteria with $|\eta_{jet}| \leq 5$ in the calorimeter, $N_{\eta_{bin}} = 100$ and $N_{\phi_{bin}} = 64$. For a partonic jet to be considered as a jet initiator $E_T > 2$ GeV is required while a cluster of partonic jets to be called a hadron-jet $\sum_{parton} E_T^{jet}$ is required to be more than 20 GeV. For a formed jet the maximum ΔR from the jet initiator is 0.4.

We have checked the hard scattering cross-sections of various production processes with CalCHEP [38]. All the final states with jets at the parton level have been checked against the results available in [13]. The calculation of hadronically quiet trilepton rates have been checked against [39], in the appropriate limits.

7.3 Squark-slepton Non-universality

Here we select a scenario where the squarks and slepton masses at low-energy are results of evolution from mutually uncorrelated mass parameters ($m_{0\tilde{q}}$ and $m_{0\tilde{l}}$ respectively) at a high scale. Although this is a purely phenomenological approach, it is helpful in the sense that it embodies the complete independence of

the coloured and uncoloured scalar masses at the high scale, while still achieving some simplification of the parameter space, by avoiding a random proliferation of low-energy masses. The choice of parameters made in this manner takes all collider and low-energy constraints into account, as summarized in the subsection below.

7.3.1 Choice of SUSY parameters

As has been already indicated, we have confined ourselves to R -parity conserving supersymmetry where the lightest neutralino is the LSP. The squark-slepton spectrum is generated by SuSpect v2.3 [33] with the **pMSSM** option, where a separate mass parameter for squarks and sleptons is assumed at the high scale. The Higgs mass parameters $m_{H_u}^2$ & $m_{H_d}^2$ are also taken to evolve from the high-scale slepton mass. We tune the non-universal scalar masses and gaugino masses at the GUT scale such that the following combinations arise:

$(m_{\tilde{g}}, m_{\tilde{q}^{1,2}}) = (500, 500), (500, 1000)$ and $(1000, 1000)$ where $m_{\tilde{g}}$ is the gluino mass and $m_{\tilde{q}^{1,2}}$ denote the (approximately degenerate) squark masses of the first two families at the electroweak symmetry breaking (EWSB) scale defined by the ‘default option’ in SuSpect, i.e. $\sqrt{m_{\tilde{t}_L} m_{\tilde{t}_R}}$. All the above masses are in GeV. All the aforementioned sets are studied for three non-universal slepton masses of the first two families $m_{\tilde{l}^{1,2}}$ (approximately degenerate) at the low-scale, namely, 250 GeV, 500 GeV and 750 GeV with $\tan\beta = 5$ and 40 for each choice. The high-scale value of the soft trilinear parameter (A_0) has been set at zero, a practice that has been followed in the subsequent sections, too (For details see table A1 and A2).

Radiative electroweak symmetry breaking has been ensured in each case, after which the positive value of μ has been chosen for illustration, in this section as well as in the subsequent ones. One also achieves gauge coupling unification at high scale and consistency with laboratory constraints on a SUSY scenario. Consistency with low-energy FCNC constraints such as those from $b \rightarrow s\gamma$, and also with the data on muon anomalous magnetic moment are checked for every combination of parameters [40, 41] used in the analysis. No constraints from dark matter have been included here. We have used the strong coupling $\alpha_3(M_Z)^{\overline{MS}} = 0.1172$ for this calculation which is again the default option in SuSpect. Throughout the analysis we have assumed the top quark mass to be 171.4 GeV. No tachyonic modes for sfermions are allowed at any energy scale.

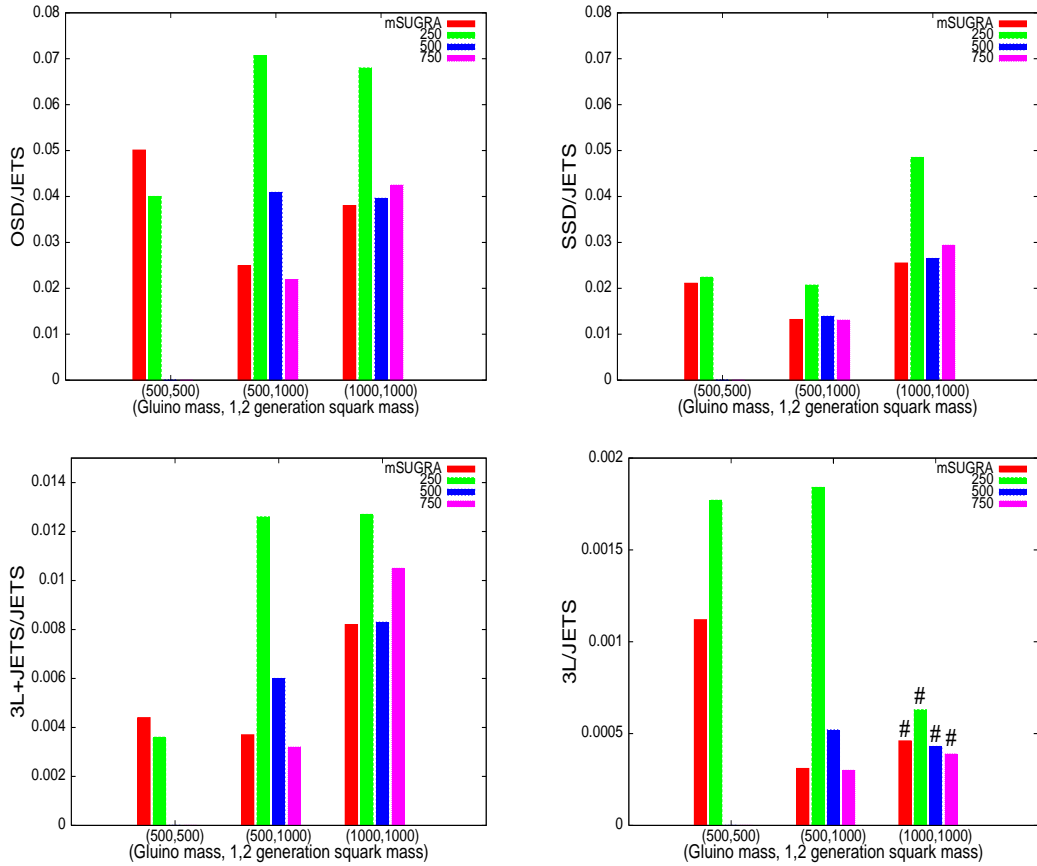


Figure 7.1: Event ratios for Squark-Slepton Non-universality: $\tan \beta = 5$

Gaugino masses have been treated as universal at high scale for simplification.

In this study the low energy sfermion masses vis-a-vis those of charginos and neutralinos primarily dictate the phenomenology. Relating them to high scale parameters is done for the purpose more in the way of illustration, and achieving a very high degree of precision in the relationship among low and high scale parameters is not of primary importance here. Thus, in the running of parameters, one-loop renormalization group equations (RGE) have been used. No low-energy radiative corrections to the chargino and neutralino masses matrices have been taken, which does not affect our analysis in any significant way [42]. Full one-loop and the dominant two-loop corrections to the Higgs masses are incorporated.

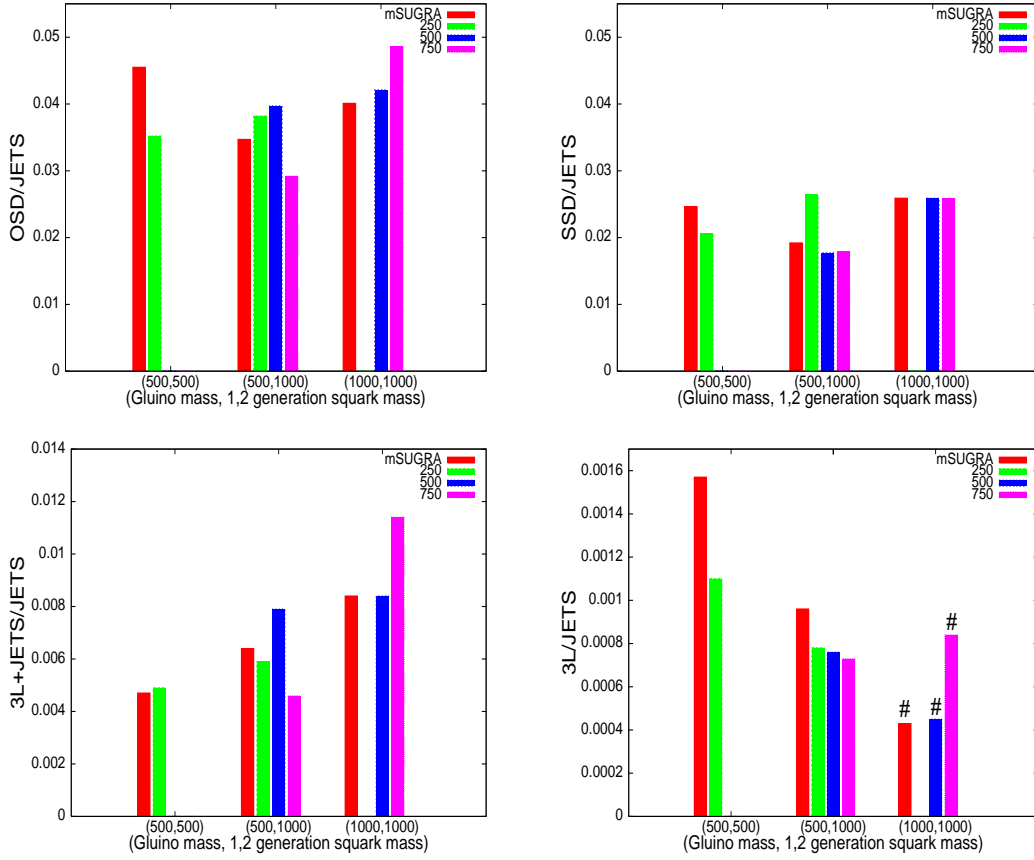


Figure 7.2: Event ratios for Squark-Slepton Non-universality: $\tan \beta = 40$

7.3.2 Numerical results

In Figure 7.1 and 7.2, we have presented four ratios, namely, $OSD/jets$, $SSD/jets$, $(3\ell + jets)/jets$ and $3\ell/jets$. For $(m_{\tilde{g}}, m_{\tilde{q}^{1,2}}) = (500, 500)$ GeV, electroweak symmetry breaking conditions are not satisfied when the low-energy slepton mass is 500 or 750 GeV. This is because, with gaugino masses on the lower side, such large slepton masses require a rather large high-scale value for the slepton-Higgs mass parameter, which prevents $m_{H_u}^2$ from being driven to a negative value at the electroweak scale. For low slepton and high gaugino masses, on the other hand, the lighter stau eigenstate becomes the LSP for $\tan \beta = 40$.

A survey of Figure 7.1 and 7.2 reveals the following general features for the case with squark-slepton non-universality:

- The case with the lowest choice of slepton masses, namely, $m_{\tilde{l}_{1,2}} = 250$ GeV, is fairly distinguishable from the others, especially for the squark masses on the higher side. This is primarily because low-lying sleptons participate in the chargino and neutralino cascades to yield more events with leptons in the final state. Such an effect is noticeable for $\tan\beta = 5$. One has to remember here that the chargino and neutralino mass matrices whose textures govern the cascades are also controlled by μ which is related to $m_{\tilde{l}_{1,2}}$. Thus the final rates depend on a crucial interplay of the slepton mass parameter, the gaugino masses and $\tan\beta$, over and above the enhanced probability of on-shell decays of charginos and neutralinos into sleptons.
- Cases with $m_{\tilde{l}_{1,2}} = 500$ GeV are by and large difficult to differentiate from a spectrum with universal scalar mass.
- The $3\ell + jets$ events allow one to distinguish cases with the slepton mass on the high side, such as 750 GeV. This effect is more prominent for high gluino mass and large $\tan\beta$.
- The hadronically quiet trilepton signals give us sufficient distinction in cases where the background is not forbidding. This channel gets drowned in backgrounds only for $(m_{\tilde{g}}, m_{\tilde{q}_{1,2}}) = (1000, 1000)$ GeV. The universal case is best distinguished with one where the slepton mass of the first two families assumes the lowest chosen value (250 GeV). This is because these would help on-shell slepton production in two-body decays of charginos and neutralinos. Naturally, higher gluino masses hurt this channel because they mean higher chargino/neutralino masses and thus lower production rates with gaugino universality (see table B1 and B2). Moreover, the distinction is more prominent for $\tan\beta$ on the lower side.
- In general (including the difficult case mentioned above), trileptons in the final state are the most useful signals in distinguishing among different scenarios.

7.4 Non-universality in the third family

In order to address the FCNC problem that continues to haunt SUGRA-type models, it has sometimes been proposed that the first two families of squarks and sleptons are very heavy. This suppresses FCNC in most cases. At the same time,

a third family of sfermions within a TeV suffices to provide a solution to the naturalness problem. Such scenarios have been theoretically motivated, for example, in string-inspired models, assuming flavour-dependent coupling to modular fields, or postulating that the masses of the third family scalars arise from a separate F -term vev. D -terms of an anomalous $U(1)$ symmetry have also been suggested for implementing such ‘inverted hierarchy’ [24–28].

Since this is a rather representative case of scalar non-universality, we have subjected the resulting spectra to the multichannel analysis outlined earlier. However, we do not confine ourselves to any special theoretical scenario, except assuming that scalar masses in the third family evolve from a separate high-scale mass parameter m_0^3 , while a different parameter $m_0^{(1,2)}$ is the origin of scalar masses in the first two families.

7.4.1 Choice of parameters

As has been already mentioned, we have assumed the third family scalar masses to arise out of a separate parameter at high scale (m_0^3). The SUSY breaking mass parameters m_{H_u} & m_{H_d} in the Higgs sector are also assumed to originate in same parameter m_0^3 . Otherwise, in cases where $m_0^{(1,2)}$ is very high and essentially decoupled, a correspondingly high value of the Higgs mass parameter(s) will make it difficult to obtain electroweak symmetry breaking in a consistent manner.

This allows one to fix the magnitude of the μ -parameter, which we have taken to be of positive sign throughout our analysis. As in the previous section, we have taken $A_0 = 0$. The unification of gaugino masses and gauge couplings at high scale has been ensured. As before, the **pMSSM** option in SuSpect has been used, and m_0^3 as well as the high-scale gaugino mass parameter has been tuned in such a way as to yield specific values of the gluino mass and the lighter stop mass ($m_{\tilde{t}_1}$) at low-energy. The chosen combinations of $(m_{\tilde{g}}, m_{\tilde{t}_1})$ are (500,500), (500, 1000) and (1000,1000), all masses being expressed in GeV. These values are used in the labels of the x-axis in Figure 7.3 and 7.4.

For each combination mentioned above, two choices of $m_0^{(1,2)}$ have been made, corresponding to the average squark mass in the first two families equal to 1 TeV and 10 TeV, respectively, at the electroweak scale. It should be mentioned here that a parameter combination with $m_0^{(1,2)}$ of the order of a few TeV’s and the third family squark masses around a few hundred GeV’s is admissible even in an

mSUGRA scenario, where the first two families of squarks can be missed at the LHC [43]. The results for such choices are juxtaposed with the universal SUGRA scenario tuned in such a way as to yield the same $(m_{\tilde{g}}, m_{\tilde{t}_1})$, in the bar graphs shown in figures 7.3 and 7.4. Two values of $\tan\beta$, namely, 5 and 40, have been used for every combination of masses (see Table A3 and A4 in Appendix A).

The procedure adopted in running the parameters is the same as that described in the previous section. All constraints on the low-energy parameters, including those from FCNC, have been satisfied in each case.

7.4.2 Numerical results

The general format of presentation of the numerical results in this case is similar to that adopted in the previous section. All the parameter combinations here are found to lead to consistent sparticle spectra, satisfying the electroweak symmetry breaking conditions and other necessary requirements.

The various event rates are influenced by some salient features of the spectrum. First of all, the high value of $m_0^{(1,2)}$ required to make the first two squark families as heavy as 10 TeV leaves little significance for gaugino corrections at low scale, resulting in the close degeneracy of squark and sleptons in the first two families. For the squark masses around 1 TeV for the first two families, on the other hand, one has to take a much smaller $m_0^{(1,2)}$, which leads to relatively light sleptons. For the third family, the effects of mixing and Yukawa coupling bring the lighter stop below all other sfermions, the difference being more pronounced for low $\tan\beta$ (see table in B3 and B4).

The following broad features can be seen in the results:

- The rate of leptonic events relative to the all-jet final state goes up significantly for higher masses for the first two generations, i.e. $m_{\tilde{q}^{1,2}} = 10$ TeV. This is because final states in the cases of decoupled first two families are dominated by the stop, which leads to more avenues of lepton production via top decay. The relative suppression of all-jet events from squark pairs (of the first two families) is also responsible for lower values of the denominators in different ratios.
- The leptonic final states for the non-universal case with $m_{\tilde{q}^{1,2}} = 1$ TeV get considerably depleted with respect to the corresponding universal cases,

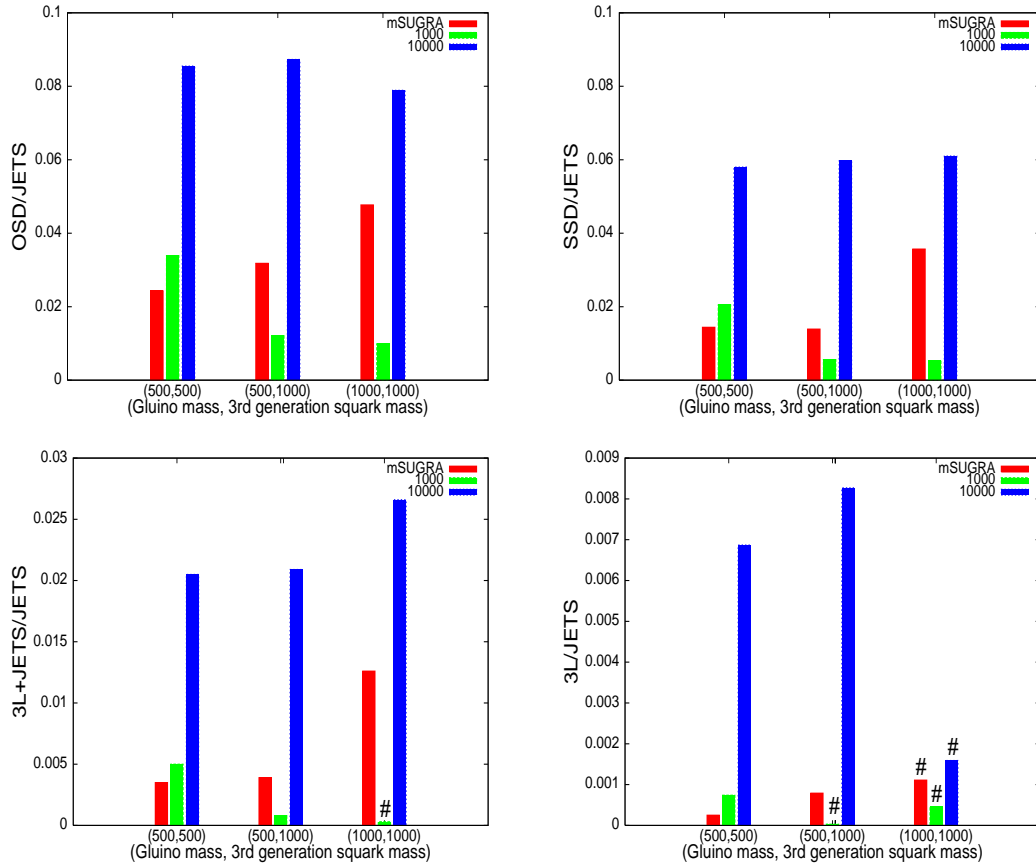


Figure 7.3: Event ratios for 3rd family scalar Non-universality: $\tan \beta = 5$

especially for relatively high third family squark masses. This happens as a result of our parametrization where we are matching the mass of the lighter stop between the two cases. While this means heavier squarks of the first two families in universal case, the non-universal case with $m_{\tilde{q}^{1,2}} = 1$ TeV gives such squarks in the same mass range. Therefore, they contribute more effectively to all-jet final states, leading to a depletion of leptonic signals. This feature is reflected not only in the various ratios but also in the absolute values of the events rates.

- The difference between $m_{\tilde{q}^{1,2}} = 1$ TeV $m_{\tilde{q}^{1,2}} = 10$ TeV is most clearly noticeable for the trilepton channel.
- In a way similar to the other ratios, higher values of third family scalar masses facilitate distinction via the hadronically quiet channels. However,

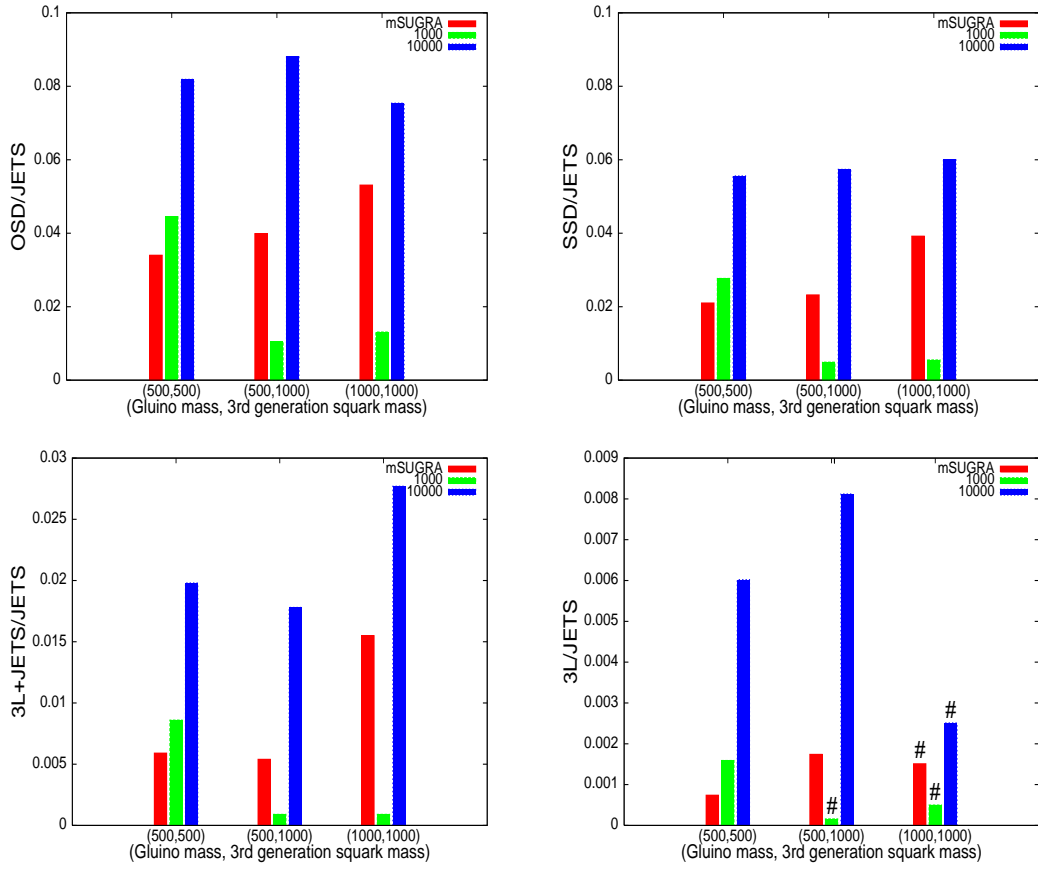


Figure 7.4: Event ratios for 3rd family scalar Non-universality: $\tan \beta = 40$

this channel does not really serve as a better discriminator than OSD , SSD , and inclusive trilepton final states for this type of non-universality. The underlying reason for this is again the enhancement of the latter through frequent occurrence of the top quark in SUSY cascades. Also, just as for squark-slepton non-universality, the hadronically quiet trileptons are suppressed by backgrounds for $(m_{\tilde{g}}, m_{\tilde{t}_1}) = (1000, 1000)$ GeV.

- Unlike the other cases of non-universality studied in this paper the observed features bear very little imprint on the value of $\tan \beta$.

7.5 Non-universality due to $SO(10)$ D -terms

In the two previous sections, scenarios reflecting scalar non-universality have been considered in a purely phenomenological ways. Now we take up a specific theoretical model, namely one based on an $SO(10)$ SUSY-GUT [44].

In an $SO(10)$ framework, the matter fields belong to the representation **16**, and can be further classified into sub-multiplets, depending on the representations of $SU(5)$ to which they belong. In this classification, expressing the (s)fermions generically to include all families, the superfields D^c and L belong to $\bar{\mathbf{5}}$, while Q , U^c and E^c belong to **10**, where Q and L denote $SU(2)$ doublets and the others, singlets. The breakdown of $SO(10)$ (without any intermediate scale) to the SM gauge group, which amounts to a reduction of rank, will therefore endow the scalars in these different $SU(5)$ representations with different D -terms [29]. Consequently, the high-scale scalar mass parameters will be different for the two multiplets respectively for $\bar{\mathbf{5}}$ and **10**: [30, 31]

$$m_{\bar{\mathbf{5}}}^2 = m_0^2 - 1.5Dm_0^2 \quad (\text{for } D^c \text{ \& } L) \quad (7.1)$$

$$m_{\mathbf{10}}^2 = m_0^2 + 0.5Dm_0^2 \quad (\text{for } E^c, U^c \text{ \& } Q) \quad (7.2)$$

$$(7.3)$$

thus leading to a predestined non-universality in the GUT scale itself. Here D is a dimensionless parameter quantifying the added contribution to the SUSY breaking terms in terms of the ‘universal’ high-scale mass parameter m_0 .

7.5.1 Choice of parameters

We have restricted the value of D in order to avoid tachyonic modes at high scale. Thus $D = 0.5, -0.5$ and -1.25 have been taken, m_0 being fixed at 300 GeV. $M_{1/2}$ has been chosen in such a way as to obtain the low-scale gluino mass at 500 GeV, 1 TeV and 1.5 TeV.

While the sign of μ has been kept positive in each case, we have again chosen $\tan \beta$ to be 5 and 40. The low-energy spectrum is the result of one-loop RGE following Suspect, with the **pMSSM** option (see Table A5 and A6).

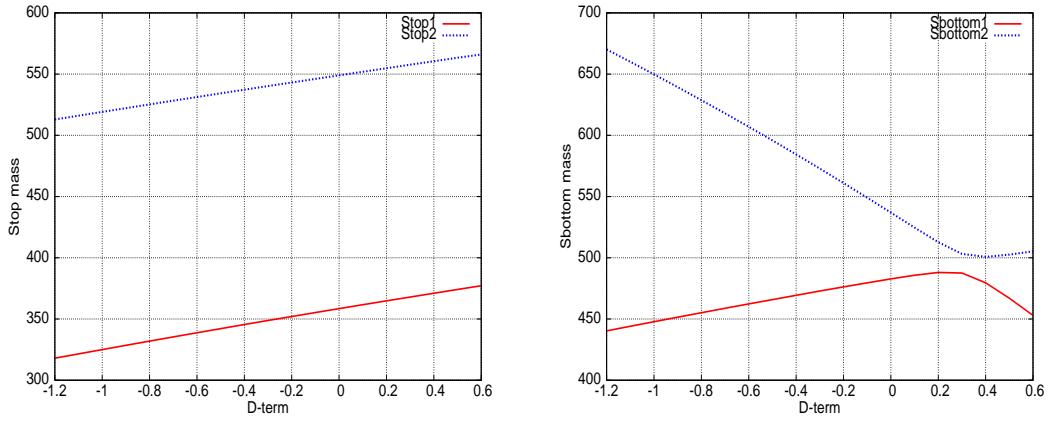


Figure 7.5: Variation of stop and sbottom mass with D-term: $\tan \beta = 5$

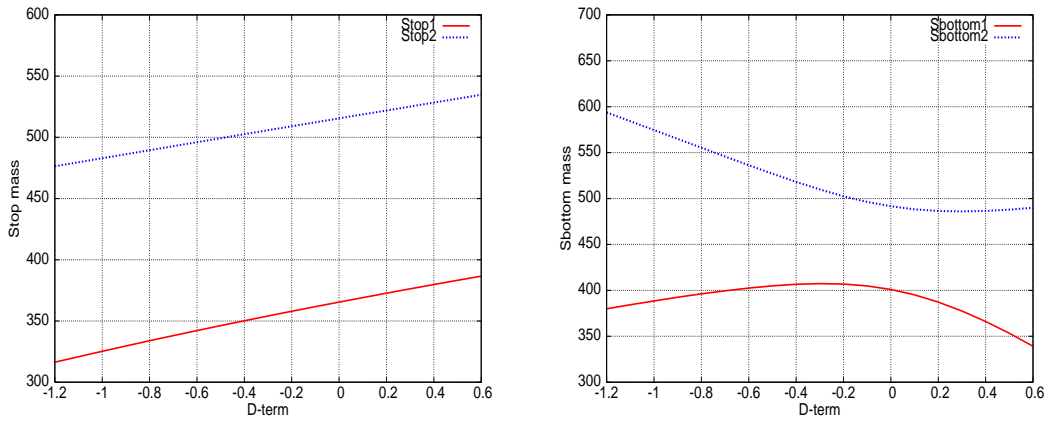


Figure 7.6: Variation of stop and sbottom mass with D-term: $\tan \beta = 40$

7.5.2 Numerical results

The low-energy masses of the right-chiral down-type squarks and left-chiral charged leptons fall as D is varied from the minimum to the maximum allowed value in the permissible range. In particular, the masses of the physical states in the third family as a function of D are shown in Figure 7.5 and Figure 7.6 for both $\tan \beta = 5$ and 40, because they bring in more complex behaviour due to mixing. It should be noted that the parabolic D -dependence of the masses are flattened out considerably due to running, since gauginos contribute to the low-energy scalar masses [42]. The two stop mass eigen-states vary in the same way with D , since

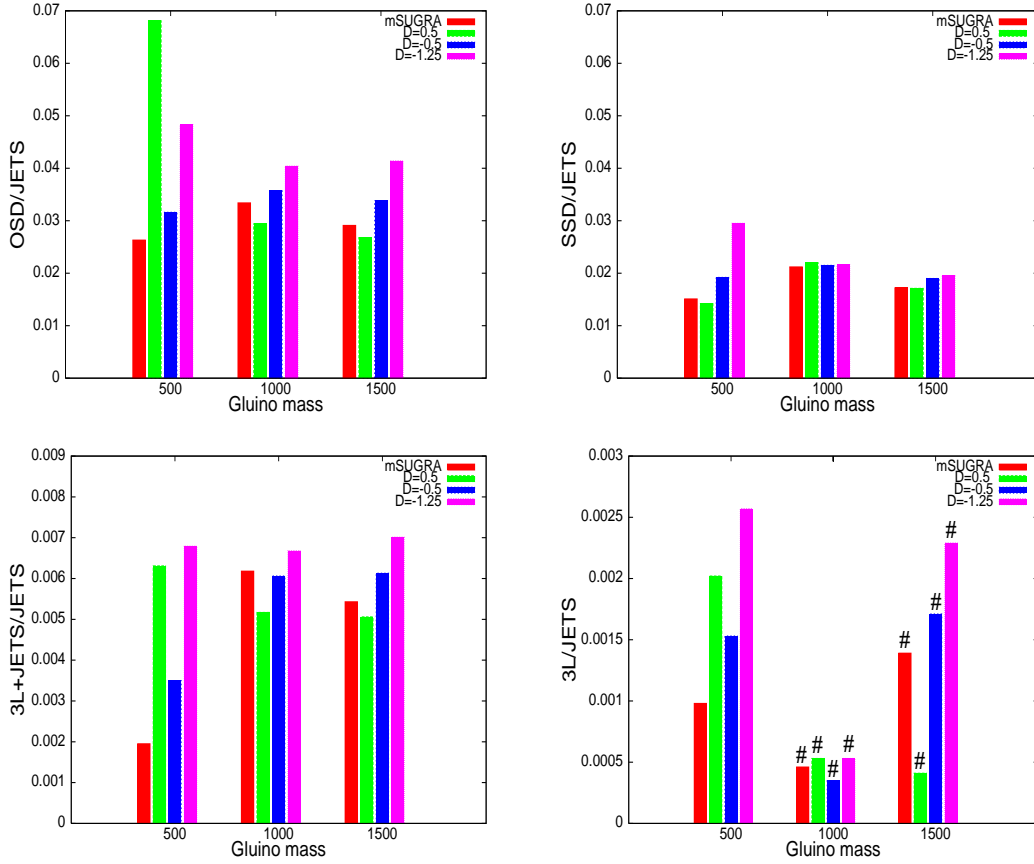


Figure 7.7: Event ratios for $SO(10)$ D -term Non-universality: $\tan \beta = 5$

both the t_L and t_R superfields belong to $\mathbf{10}$ of $SU(5)$, while b_R , unlike b_L , belongs to $\bar{\mathbf{5}}$. The last mentioned effect is responsible for different variation patterns of the two sbottom mass eigen-states.

In any case, the nature of non-universality is different from the two cases investigated earlier.

The same ratios as those studied previously are presented in this context, in figures 7.7 and 7.8. The three values of D mentioned above lead to the three non-universal bar graphs in each case, $D = 0$ being the corresponding mSUGRA scenario. It may be noted that for $D = -1.25$, one ends up with a stau LSP for $m_{\tilde{g}} = 1$ TeV, 1.5 TeV and $\tan \beta = 40$. The reason this does not happen for $m_{\tilde{g}} = 500$ GeV is because the lowering of the lighter mass eigenstate is stalled by the low value of μ in the first case.

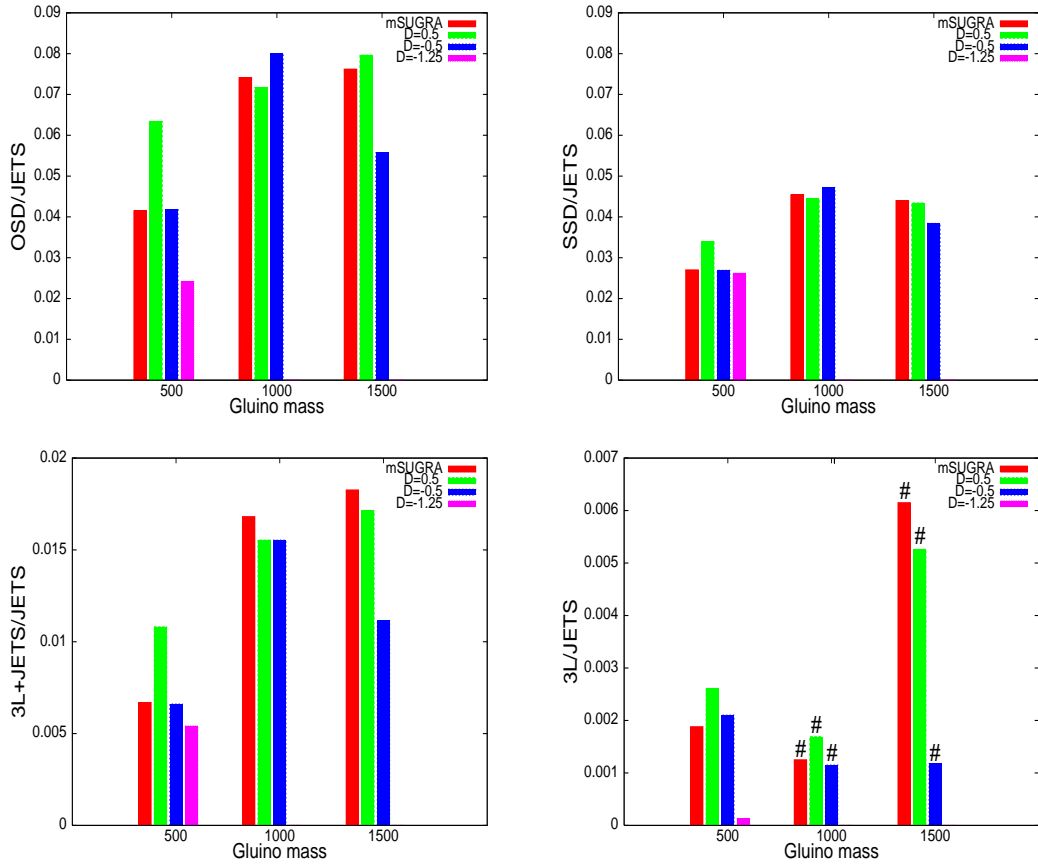


Figure 7.8: Event ratios for $SO(10)$ D -term Non-universality: $\tan \beta = 40$

The main features that emerge from the ratio as well as the absolute rates are as follows:

- For high gluino masses such as $m_{\tilde{g}} = 1$ TeV and 1.5 TeV, the distinction between various non-universality for $D = 0.5, -0.5$ and -1.25 becomes difficult from the ratio plot. This is because, for high value of $M_{1/2}$, the low energy squark-slepton masses are dominated by gaugino contributions, the effect of non-universal inputs to the scalar masses through D -terms being thus imperceptible. An exception to this occurs for $m_{\tilde{g}} = 1.5$ TeV and $\tan \beta = 40$, due to the same reason as above, namely, the contribution to the off-diagonal term in the sbottom mass matrix through the μ -parameter determined by such gaugino masses.
- For $m_{\tilde{g}} = 1$ TeV and 1.5 TeV (particularly for $\tan \beta = 5$), the only channels that

partly distinguish among various values of the $SO(10)$ D -term are $3\ell + jets$. This happens because whatever mass hierarchy between squarks and sleptons due to the D -terms is there is accentuated with the largest detectable number of leptons in the final state.

- For $m_{\tilde{g}} = 500$ GeV, $OSD/jets$ is a good discriminator along with the trileptonic channels. In particular, the cases of $D=0.5$ and $D=-1.25$ are easily distinguishable from the ratios. The ratio $SSD/jets$, on the other hand, is relatively flat, because these are initiated by the production of gluinos, where the effects of scalars are more often washed out.
- The hadronically quiet trilepton events are largely washed out by backgrounds, excepting for $m_{\tilde{g}} = 500$ GeV.
- For $D=-1.25$, the leptonic final states give almost always the largest fraction of events for $\tan\beta = 5$, while for $\tan\beta = 40$ the fraction is the smallest.
- The absolute numbers in various channels are also very efficient discriminators in this type of non-universal scenarios particularly for low gluino mass (see table B5 and B6).

7.6 Summary and conclusions

We have considered three representative scenarios where the scalar mass spectrum in SUSY can deviate from the predictions of a universal SUGRA model. These are situations with (a) high-scale non-universality of squarks and sleptons, (b) a separate high-scale mass parameter for the third family sfermions, and (c) the effect of $SO(10)$ D -terms. In each case, we have made a detailed scan of the parameter space, in terms of the gluino and squark masses which set the scale of the hard scattering leading to superparticle production. While the value of the μ parameter (up to a sign) has been mostly fixed from radiative electroweak symmetry breaking, we have chosen two representative values of $\tan\beta$ for our analysis, namely 5 and 40.

In essence, relatively low values of slepton masses in various schemes and in different regions of the parameter space buttress the leptonic final states. With this in view, a multichannel analysis including various leptonic final states has been performed in each case, comparing the different degrees of non-universality with the mSUGRA case. The ratios of the like- and opposite-sign dilepton rates

as well as trileptons (with and without accompanying hard jets) with respect to the inclusive jet signal.

The case where the most conspicuous effects are seen in terms of the ratios is one where the the first two family squarks have masses on the order of 10 TeV. In addition, the absolute number of events for this situation is rather low compared to the other cases, which can serve as another distinguishing feature.

For the first two family squarks still within 1 TeV or so, however, the distinction with the case of squark-slepton universality gets somewhat blurred. This is because the masses of the first two families of squarks and sleptons are often in the same range, and thus the cascades leading to the leptonic final states are similar in nature. A marginal, though not spectacular, improvement is achieved by considering the absolute event rates. However, the ratios are more sensitive to the mass ranges of the squarks and gluinos within a given pattern of non-universality, and as such they can provide useful clues to the level at which a departure from universality has taken place. The distinction is even more difficult for $SO(10)$ D -terms, except for $D = -1.25$. For these values of D , distinction among various cases as well as with the universal case can be problematic.

The effect of $\tan \beta$ can also have important bearing on the various ratios an exception being in case of third family non-universality. Therefore, the independent extraction of $\tan \beta$ from Higgs boson signals is going to be useful in establishing scalar non-universality.

It is also seen that the trilepton events can be most useful in making distinction among different situations. So are hadronically quiet trileptons, so long as they are able to rise above backgrounds. Next in the order is the importance of opposite-sign dileptons. Thus the investigation of leptonic final states with increasing multiplicity, apart from the enhancing 'clean' character of the events, is likely to enlighten us on the issue of non-universality.

In addition to the different kinds of sfermion non-universality discussed in the previous sections, one could also think of the Higgs mass parameters evolving from a different common high-scale value compared to that determining the squark and slepton masses [45]. While this can affect Higgs phenomenology considerably, our multichannel analysis gets appreciably affected by such non-universality only when the charged Higgs state can be made very light. In such case, too, the rates in leptonic channels which are our main concern are altered if

the charged Higgs can be produced on-shell in the decay of the stop or the sbottom, or of a chargino/neutralino. Although the charged Higgs mass is lowered around or below 200 GeV for some combinations of parameters including a large $\tan\beta$, effects of the above type are rare.

It should be noted at the end that, unlike in the case of gaugino non-universality, the schemes of parametrising scalar non-universality are more non-uniform. Therefore, different schemes often lead to overlapping portions in the spectrum, where signals may turn out to be of similar nature. The most significant departure from universality in terms of overall event rates can occur through the variation of masses of the first two family squarks, whereas the lepton-to-jet event ratios are influenced more substantially when the first two family sleptons have masses that are different from what is predicted in mSUGRA. These generic features of the scalar spectrum, rather than different theoretical schemes, are likely to be exposed more easily at the LHC.

Bibliography

- [1] S. Bhattacharya, A. Datta and B. Mukhopadhyaya, JHEP **0710** (2007) 080 [arXiv:0708.2427 [hep-ph]].
- [2] S. Bhattacharya, A. Datta and B. Mukhopadhyaya, Phys. Rev. D **78**, 035011 (2008) [arXiv:0804.4051 [hep-ph]].
- [3] N. Arkani-Hamed and S. Dimopoulos, JHEP **0506**, 073 (2005) [arXiv:hep-th/0405159].
- [4] G. F. Giudice and A. Romanino, Nucl. Phys. B **699**, 65 (2004) [Erratum-ibid. B **706**, 65 (2005)] [arXiv:hep-ph/0406088]; N. Arkani-Hamed, S. Dimopoulos, G. F. Giudice and A. Romanino, Nucl. Phys. B **709**, 3 (2005) [arXiv:hep-ph/0409232]; S. K. Gupta, B. Mukhopadhyaya and S. K. Rai, Phys. Rev. D **73**, 075006 (2006) [arXiv:hep-ph/0510306].
- [5] J. L. Feng, K. T. Matchev and F. Wilczek, Phys. Lett. B **482** (2000) 388 [arXiv:hep-ph/0004043]; J. L. Feng and K. T. Matchev, Phys. Rev. D **63** (2001) 095003 [arXiv:hep-ph/0011356]; U. Chattopadhyay, T. Ibrahim and D. P. Roy, Phys. Rev. D **64** (2001) 013004 [arXiv:hep-ph/0012337].
- [6] N. Bernal, A. Djouadi and P. Slavich, JHEP **0707**, 016 (2007) [arXiv:0705.1496 [hep-ph]].
- [7] L. E. Ibanez and D. Lust, Nucl. Phys. B **382** (1992) 305 [arXiv:hep-th/9202046]; B. de Carlos, J. A. Casas and C. Munoz, Phys. Lett. B **299** (1993) 234 [arXiv:hep-ph/9211266]; T. Kobayashi, D. Suematsu, K. Yamada and Y. Yamagishi, Phys. Lett. B **348** (1995) 402 [arXiv:hep-ph/9408322].
- [8] M. Olechowski and S. Pokorski, Phys. Lett. B **344** (1995) 201 [arXiv:hep-ph/9407404];
- [9] A. Lleyda and C. Munoz, Phys. Lett. B **317** (1993) 82 [arXiv:hep-ph/9308208]; A. Datta, M. Guchait and N. Parua, Phys. Lett. B **395** (1997) 54 [arXiv:hep-ph/9609413].

- [10] V. Berezhinsky, A. Bottino, J. R. Ellis, N. Fornengo, G. Mignola and S. Scopel, *Astropart. Phys.* **5** (1996) 1 [arXiv:hep-ph/9508249]; D. G. Cerdeno and C. Munoz, *JHEP* **0410** (2004) 015 [arXiv:hep-ph/0405057]; A. De Roeck, J. R. Ellis, F. Gianotti, F. Moortgat, K. A. Olive and L. Pape, *Eur. Phys. J. C* **49** (2007) 1041 [arXiv:hep-ph/0508198].
- [11] P. Binetruy, G. L. Kane, B. D. Nelson, L. T. Wang and T. T. Wang, *Phys. Rev. D* **70**, 095006 (2004) [arXiv:hep-ph/0312248]; J. L. Bourjaily, G. L. Kane, P. Kumar and T. T. Wang, arXiv:hep-ph/0504170; G. L. Kane, P. Kumar, D. E. Morrissey and M. Toharia, *Phys. Rev. D* **75**, 115018 (2007) [arXiv:hep-ph/0612287].
- [12] A. A. Affolder *et al.* [CDF Collaboration], *Phys. Rev. Lett.* **88**, 041801 (2002) [arXiv:hep-ex/0106001].
- [13] A. Datta, G. L. Kane and M. Toharia, arXiv:hep-ph/0510204.
- [14] V. D. Barger, W. Y. Keung and R. J. N. Phillips, *Phys. Rev. Lett.* **55**, 166 (1985); H. Baer, X. Tata and J. Woodside, *Phys. Rev. D* **41**, 906 (1990).
- [15] A. Datta, K. Kong and K. T. Matchev, *Phys. Rev. D* **72**, 096006 (2005) [Erratum-ibid. *D* **72**, 119901 (2005)] [arXiv:hep-ph/0509246].
- [16] H. Baer, X. Tata and J. Woodside, *Phys. Rev. D* **45**, 142 (1992); R. M. Barnett, J. F. Gunion and H. E. Haber, *Phys. Lett. B* **315**, 349 (1993) [arXiv:hep-ph/9306204].
- [17] G. Duckeck *et al.* [ATLAS Collaboration].
- [18] H. Baer, C. h. Chen, F. Paige and X. Tata, *Phys. Rev. D* **53**, 6241 (1996) [arXiv:hep-ph/9512383].
- [19] J. R. Ellis, C. Kounnas and D. V. Nanopoulos, *Nucl. Phys. B* **247**, 373 (1984); J. R. Ellis, K. Enqvist, D. V. Nanopoulos and K. Tamvakis, *Phys. Lett. B* **155**, 381 (1985); M. Drees, *Phys. Lett. B* **158**, 409 (1985); A. Corsetti and P. Nath, *Phys. Rev. D* **64**, 125010 (2001) [arXiv:hep-ph/0003186]; N. Chamoun, C. S. Huang, C. Liu and X. H. Wu, *Nucl. Phys. B* **624**, 81 (2002) [arXiv:hep-ph/0110332].
- [20] S. Khalil, *Phys. Lett. B* **484**, 98 (2000) [arXiv:hep-ph/9910408]; S. Komine and M. Yamaguchi, *Phys. Rev. D* **63**, 035005 (2001) [arXiv:hep-ph/0007327].
- [21] G. Anderson, H. Baer, C. h. Chen and X. Tata, *Phys. Rev. D* **61**, 095005 (2000) [arXiv:hep-ph/9903370]; K. Huitu, Y. Kawamura, T. Kobayashi and K. Puo-

- lamaki, Phys. Rev. D **61**, 035001 (2000) [arXiv:hep-ph/9903528]; K. Huitu, J. Laamanen, P. N. Pandita and S. Roy, Phys. Rev. D **72**, 055013 (2005) [arXiv:hep-ph/0502100].
- [22] K. Choi and H. P. Nilles, JHEP **0704**, 006 (2007) [arXiv:hep-ph/0702146].
- [23] S. I. Bityukov and N. V. Krasnikov, Phys. Lett. B **469**, 149 (1999) [Phys. Atom. Nucl. **64**, 1315 (2001 YAFIA,64,1391-1398.2001)] [arXiv:hep-ph/9907257]; S. I. Bityukov and N. V. Krasnikov, Phys. Atom. Nucl. **65**, 1341 (2002) [Yad. Fiz. **65**, 1374 (2002)] [arXiv:hep-ph/0102179].
- [24] V. D. Barger, C. Kao and R. J. Zhang, Phys. Lett. B **483** (2000) 184 [arXiv:hep-ph/9911510].
- [25] Y. Nir and N. Seiberg, Phys. Lett. B **309** (1993) 337 [arXiv:hep-ph/9304307]; M. Dine, A. E. Nelson and Y. Shirman, Phys. Rev. D **51** (1995) 1362 [arXiv:hep-ph/9408384]; L. Randall and R. Sundrum, Nucl. Phys. B **557** (1999) 79 [arXiv:hep-th/9810155].
- [26] S. Dimopoulos and G. F. Giudice, Phys. Lett. B **357** (1995) 573 [arXiv:hep-ph/9507282]; A. Pomarol and D. Tommasini, Nucl. Phys. B **466** (1996) 3 [arXiv:hep-ph/9507462]; A. G. Cohen, D. B. Kaplan and A. E. Nelson, Phys. Lett. B **388** (1996) 588 [arXiv:hep-ph/9607394].
- [27] P. Binetruy and E. Dudas, Phys. Lett. B **389** (1996) 503 [arXiv:hep-th/9607172]; G. R. Dvali and A. Pomarol, Phys. Rev. Lett. **77** (1996) 3728 [arXiv:hep-ph/9607383].
- [28] J. Bagger, J. L. Feng and N. Polonsky, Nucl. Phys. B **563** (1999) 3 [arXiv:hep-ph/9905292]; J. A. Bagger, J. L. Feng, N. Polonsky and R. J. Zhang, Phys. Lett. B **473** (2000) 264 [arXiv:hep-ph/9911255]; H. Baer, P. Mercadante and X. Tata, Phys. Lett. B **475** (2000) 289 [arXiv:hep-ph/9912494].
- [29] M. Drees, Phys. Lett. B **181** (1986) 279; J. S. Hagelin and S. Kelley, Nucl. Phys. B **342** (1990) 95.
- [30] Y. Kawamura, H. Murayama and M. Yamaguchi, Phys. Lett. B **324** (1994) 52 [arXiv:hep-ph/9402254]; Y. Kawamura, H. Murayama and M. Yamaguchi, Phys. Rev. D **51** (1995) 1337 [arXiv:hep-ph/9406245].
- [31] A. Datta, A. Datta and M. K. Parida, Phys. Lett. B **431**, 347 (1998) [arXiv:hep-ph/9801242]; A. Datta, A. Datta, M. Drees and D. P. Roy, Phys. Rev. D **61**, 055003 (2000) [arXiv:hep-ph/9907444].

- [32] N. Arkani-Hamed, G. L. Kane, J. Thaler and L. T. Wang, JHEP **0608**, 070 (2006) [arXiv:hep-ph/0512190]; N. Arkani-Hamed, P. Schuster, N. Toro, J. Thaler, L. T. Wang, B. Knuteson and S. Mrenna, arXiv:hep-ph/0703088.
- [33] A. Djouadi, J. L. Kneur and G. Moultaka, Comput. Phys. Commun. **176**, 426 (2007) [arXiv:hep-ph/0211331].
- [34] T. Sjostrand, S. Mrenna and P. Skands, JHEP **0605**, 026 (2006) [arXiv:hep-ph/0603175].
- [35] P. Skands *et al.*, JHEP **0407**, 036 (2004) [arXiv:hep-ph/0311123].
- [36] H. L. Lai *et al.* [CTEQ Collaboration], Eur. Phys. J. C **12**, 375 (2000) [arXiv:hep-ph/9903282].
- [37] H. Baer, C. h. Chen, M. Drees, F. Paige and X. Tata, Phys. Rev. D **59**, 055014 (1999) [arXiv:hep-ph/9809223].
- [38] A. Pukhov, arXiv:hep-ph/0412191.
- [39] H. Baer, C. H. Chen, F. Paige and X. Tata, Phys. Rev. D **50** (1994) 4508 [arXiv:hep-ph/9404212];
- [40] A. Djouadi, M. Drees and J. L. Kneur, JHEP **0603**, 033 (2006) [arXiv:hep-ph/0602001].
- [41] W. M. Yao *et al.* [Particle Data Group], J. Phys. G **33**, 1 (2006).
- [42] S. P. Martin and P. Ramond, Phys. Rev. D **48**, 5365 (1993) [arXiv:hep-ph/9306314].
- [43] H. Baer, P. Mercadante and X. Tata, Phys. Lett. B **475** (2000) 289 [arXiv:hep-ph/9912494]; U. Chattopadhyay, A. Datta, A. Datta, A. Datta and D. P. Roy, Phys. Lett. B **493** (2000) 127 [arXiv:hep-ph/0008228].
- [44] P. Langacker, Phys. Rept. **72** (1981) 185.
- [45] S. Codoban, M. Jurcisin and D. Kazakov, Phys. Lett. B **477** (2000) 223 [arXiv:hep-ph/9912504]; J. R. Ellis, K. A. Olive and Y. Santoso, Phys. Lett. B **539** (2002) 107 [arXiv:hep-ph/0204192]; J. R. Ellis, T. Falk, K. A. Olive and Y. Santoso, Nucl. Phys. B **652** (2003) 259 [arXiv:hep-ph/0210205]; H. Baer, A. Mustafayev, S. Profumo, A. Belyaev and X. Tata, JHEP **0507** (2005) 065 [arXiv:hep-ph/0504001].

APPENDIX A

In this appendix we list the relevant masses in the spectrum. Specifically, we provide the high scale scalar inputs (which is specific to the kind of non-universal model) to generate the low energy scalar mass parameters. We provide the low lying chargino-neutralino masses as well. The tables are organised as follows: squark-Slepton non-universal case in A1 and A2, third generation scalar non-universality and in A3 and A4, and non-universality arising due to $SO(10)$ D -term in A5 and A6.

We would like to mention that for low energy $m_{\tilde{g}} = 500$ GeV, 1000 GeV, or 1500 GeV, high scale universal input for the gaugino masses $m_{1/2}$ are 166.9 GeV, 333.65 GeV and 500.5 GeV for 1-loop RGE and this is obviously independent of what kind of scalar non-universal model we are looking at.

NA indicates that the spectrum generated is inconsistent due to the reasons mentioned in the text accordingly.

Table A1 : Mass Spectrum (GeV) for squark-slepton non-universality
 $\tan \beta = 5$
(Figure 7.1)

$(m_{\tilde{g}}, m_{\tilde{q}^{1,2}})$	$m_{\tilde{l}^{1,2}}$	$m_{0\tilde{q}}$	$m_{0\tilde{l}}$	$m_{\tilde{\chi}_2^\pm}$	$m_{\tilde{\chi}_1^\pm}$	$m_{\tilde{\chi}_2^0}$	$m_{\tilde{\chi}_1^0}$	$m_{\tilde{\tau}_1}$	$m_{\tilde{b}_1}$	$m_{\tilde{t}_1}$
(500,500)	225*	200	200	344	117	118	60	336	450	212
(500,500)	250	200	220	337	116	117	60	333	449	231
(500,500)	500	NA	NA	NA	NA	NA	NA	NA	NA	NA
(500,500)	750	NA	NA	NA	NA	NA	NA	NA	NA	NA
(500,1000)	906*	900	900	546	126	127	62	558	818	900
(500,1000)	250	900	230	867	130	130	63	705	876	234
(500,1000)	500	900	490	799	130	130	63	672	862	491
(500,1000)	750	900	740	674	128	128	62	613	838	740
(1000,1000)	450*	400	400	668	259	259	126	709	896	421
(1000,1000)	250	400	0	736	261	261	126	734	907	133
(1000,1000)	500	400	431	657	259	259	126	705	894	450
(1000,1000)	750	400	705	499	252	252	125	652	871	716

* marked cases correspond to mSUGRA

($m_{0\tilde{q}}$ and $m_{0\tilde{l}}$ are high scale non-universal inputs of squark and slepton mass)

Table A2 : Mass Spectrum (GeV)for squark-slepton non-universality

$$\tan \beta = 40$$

(Figure 7.2)

$(m_{\tilde{g}}, m_{\tilde{q}^{1,2}})$	$m_{\tilde{l}^{1,2}}$	$m_{0\tilde{q}}$	$m_{0\tilde{l}}$	$m_{\tilde{\chi}_2^\pm}$	$m_{\tilde{\chi}_1^\pm}$	$m_{\tilde{\chi}_2^0}$	$m_{\tilde{\chi}_1^0}$	$m_{\tilde{t}_1}$	$m_{\tilde{b}_1}$	$m_{\tilde{\tau}_1}$
(500,500)	225*	200	200	320	122	122	62	344	371	134
(500,500)	250	200	220	312	121	122	62	341	371	156
(500,500)	500	NA	NA	NA	NA	NA	NA	NA	NA	NA
(500,500)	750	NA	NA	NA	NA	NA	NA	NA	NA	NA
(500,1000)	906*	900	900	457	129	129	63	578	684	731
(500,1000)	250	900	230	827	132	132	63	719	750	921
(500,1000)	500	900	490	752	132	132	63	687	734	381
(500,1000)	750	900	740	611	131	131	63	631	707	599
(1000,1000)	450*	400	400	620	262	262	127	718	788	317
(1000,1000)	250	NA	NA	NA	NA	NA	NA	NA	NA	NA
(1000,1000)	500	400	431	607	262	262	127	714	787	344
(1000,1000)	750	400	705	423	251	251	126	661	769	572

* marked cases correspond to mSUGRA

($m_{0\tilde{q}}$ and $m_{0\tilde{l}}$ are high scale non-universal inputs of squark and slepton mass)

Table A3 : Mass Spectrum(GeV) for Third family scalar non-universality

$$\tan \beta = 5$$

(Figure 7.3)

$(m_{\tilde{g}}, m_{\tilde{t}_1})$	$m_{\tilde{q}^{1,2}}$	m_0^3	$m_0^{(1,2)}$	$m_{\tilde{\chi}_2^\pm}$	$m_{\tilde{\chi}_1^\pm}$	$m_{\tilde{\chi}_2^0}$	$m_{\tilde{\chi}_1^0}$	$m_{\tilde{l}^{1,2}}$	$m_{\tilde{\tau}_1}$	$m_{\tilde{b}_1}$
(500,500)	876*	750	750	490	125	125	62	758	751	720
(500,500)	1000	750	900	490	125	125	62	906	751	720
(500,500)	10000	750	9990	490	125	125	62	9990	751	720
(500,1000)	2050*	2000	2000	1024	131	131	63	2000	1995	1611
(500,1000)	1000	2000	900	1024	131	131	63	906	1995	1611
(500,1000)	10000	2000	9990	1024	131	131	63	9990	1995	1611
(1000,1000)	1765*	1510	1510	973	263	263	126	1525	1512	1444
(1000,1000)	1000	1510	400	973	263	263	126	450	1512	1444
(1000,1000)	10000	1510	9990	973	263	263	126	9990	1512	1444

* marked cases correspond to mSUGRA

(m_0^3 and $m_0^{(1,2)}$ are high scale inputs of 3rd and 1,2 family non-universal scalar mass)

Table A4 : Mass Spectrum(GeV) for Third family scalar non-universality

$$\tan \beta = 40$$

(Figure 7.4)

$(m_{\tilde{g}}, m_{\tilde{t}_1})$	$m_{\tilde{q}^{1,2}}$	m_0^3	$m_0^{(1,2)}$	$m_{\tilde{\chi}_2^\pm}$	$m_{\tilde{\chi}_1^\pm}$	$m_{\tilde{\chi}_2^0}$	$m_{\tilde{\chi}_1^0}$	$m_{\tilde{t}_{1,2}}$	$m_{\tilde{\tau}_1}$	$m_{\tilde{b}_1}$
(500,500)	876*	750	750	418	128	128	63	758	608	604
(500,500)	1000	750	900	418	128	128	63	906	608	604
(500,500)	10000	750	9990	418	128	128	63	9990	608	604
(500,1000)	2050*	2000	2000	811	132	132	63	2000	1626	1331
(500,1000)	1000	2000	900	811	132	132	63	906	1626	1331
(500,1000)	10000	2000	9990	811	132	132	63	9990	1626	1331
(1000,1000)	1765*	1510	1510	827	265	265	127	1525	1230	1236
(1000,1000)	1000	1510	400	827	265	265	127	450	1230	1236
(1000,1000)	10000	1510	9990	927	265	265	127	9990	1230	1236

* marked cases correspond to mSUGRA

(m_0^3 and $m_0^{(1,2)}$ are high scale inputs of 3rd and 1,2 family non-universal scalar mass)

Table A5 : Mass Spectrum(GeV) for $SO(10)$ D-term scalar Non-universality

High scale scalar mass input $m_0=300$ GeV

$$\tan \beta = 5$$

(Figure 7.7)

$m_{\tilde{g}}$	D-term	$m_{\tilde{\chi}_2^\pm}$	$m_{\tilde{\chi}_1^\pm}$	$m_{\tilde{\chi}_2^0}$	$m_{\tilde{\chi}_1^0}$	$m_{\tilde{e}_L}$	$m_{\tilde{u}_L}$	$m_{\tilde{d}_R}$	$m_{\tilde{t}_1}$	$m_{\tilde{b}_1}$	$m_{\tilde{\tau}_1}$
500	0.0*	361	118	119	60	328	548	537	358	483	308
500	0.5	386	120	121	60	201	568	470	374	467	200
500	-0.5	334	116	117	59	419	527	597	342	466	270
500	-1.25	291	110	112	58	526	494	676	316	438	198
1000	0.0*	656	259	259	126	394	968	939	695	872	328
1000	0.5	670	259	259	126	297	980	903	703	880	287
1000	-0.5	641	259	259	126	472	956	975	686	863	292
1000	-1.25	619	258	258	126	569	939	1025	673	849	227
1500	0.0*	965	396	396	190	485	1414	1368	1052	1281	359
1500	0.5	975	396	396	190	409	1422	1344	1057	1287	384
1500	-0.5	955	396	396	190	550	1406	1393	1047	1275	326
1500	-1.25	940	396	396	190	635	1394	1429	1039	1265	270

* marked cases correspond to mSUGRA

Table A6 : Mass Spectrum(GeV) for $SO(10)$ D -term scalar Non-universality

High scale scalar mass input $m_0=300$ GeV

$\tan \beta= 40$

(Figure 7.8)

$m_{\tilde{g}}$	D-term	$m_{\tilde{\chi}_2^\pm}$	$m_{\tilde{\chi}_1^\pm}$	$m_{\tilde{\chi}_2^0}$	$m_{\tilde{\chi}_1^0}$	$m_{\tilde{e}_L}$	$m_{\tilde{u}_L}$	$m_{\tilde{d}_R}$	$m_{\tilde{t}_1}$	$m_{\tilde{b}_1}$	$m_{\tilde{\tau}_1}$
500	0.0*	330	123	123	62	329	547	537	365	401	229
500	0.5	358	125	125	62	202	568	470	383	353	139
500	-0.5	301	120	121	62	419	526	597	346	405	184
500	-1.25	252	112	113	60	526	493	676	314	378	305
1000	0.0*	612	262	262	127	395	968	940	704	767	229
1000	0.5	628	262	262	127	297	980	903	713	746	204
1000	-0.5	596	261	261	127	472	956	975	694	775	189
1000	-1.25	NA	NA	NA	NA	NA	NA	NA	NA	NA	NA
1500	0.0*	905	398	398	191	485	1414	1369	1065	1151	250
1500	0.5	916	398	398	191	409	1422	1344	1071	1138	259
1500	-0.5	894	398	398	191	550	1406	1393	1059	1159	211
1500	-1.25	NA	NA	NA	NA	NA	NA	NA	NA	NA	NA

* marked cases correspond to mSUGRA

APPENDIX B

Here we provide cross sections for all the channels in the three non-universal scenarios studied a) Squark-Slepton Non-universal case, b) 3rd generation scalar non-universality and c) Non-universality arising due to $SO(10)$ D -term respectively in three tables a) B1, B2 b) B3, B4 c) B5, B6. The SM background cross section is tabulated in B7.

The cross-sections are named as follows: σ_{OSD} for OSD, σ_{SSD} for SSD, $\sigma_{3\ell+jets}$ for $(3\ell + jets)$, $\sigma_{(3\ell)}$ for (3ℓ) and σ_{jets} for $jets$.

The cross-sections in bold font indicate that it is submerged in the background as defined in text.

NA indicates that the spectrum is inconsistent as discussed early.

Table B1 : Cross-sections (pb) for squark-slepton non-universality
 $\tan \beta = 5$
(Figure 7.1)

$(m_{\tilde{g}}, m_{\tilde{q}^{1,2}})$	$m_{\tilde{t}_{1,2}}$	σ_{OSD}	σ_{SSD}	$\sigma_{(3\ell+jets)}$	$\sigma_{(3\ell)}$	σ_{jets}
(500,500)	mSUGRA	0.4972	0.2100	0.0437	0.00111	9.3302
(500,500)	250	0.4144	0.2316	0.0367	0.01836	10.351
(500,500)	500	NA	NA	NA	NA	NA
(500,500)	750	NA	NA	NA	NA	NA
(500,1000)	mSUGRA	0.1782	0.0948	0.0266	0.00224	7.1574
(500,1000)	250	0.5218	0.1526	0.0931	0.01357	7.3764
(500,1000)	500	0.2989	0.1019	0.0440	0.00380	7.3032
(500,1000)	750	0.1593	0.0955	0.0231	0.00220	7.2698
(1000,1000)	mSUGRA	0.0277	0.0185	0.0060	0.00034	0.7277
(1000,1000)	250	0.0261	0.0186	0.0049	0.00024	0.3838
(1000,1000)	500	0.0289	0.0193	0.0060	0.00032	0.7285
(1000,1000)	750	0.0333	0.0231	0.0082	0.00031	0.7851

Table B2 : Cross-sections (pb) for squark-slepton non-universality

$$\tan \beta = 40$$

(Figure 7.2)

$(m_{\tilde{g}}, m_{\tilde{q}^{1,2}})$	$m_{\tilde{q}^{1,2}}$	σ_{OSD}	σ_{SSD}	$\sigma_{(3\ell+jets)}$	$\sigma_{(3\ell)}$	σ_{jets}
(500,500)	mSUGRA	0.6267	0.3466	0.0665	0.02215	14.0742
(500,500)	250	0.5079	0.2971	0.0713	0.01585	14.4145
(500,500)	500	NA	NA	NA	NA	NA
(500,500)	750	NA	NA	NA	NA	NA
(500,1000)	mSUGRA	0.2388	0.1317	0.0441	0.00657	6.8736
(500,1000)	250	0.2730	0.1886	0.0422	0.00561	7.1379
(500,1000)	500	0.2798	0.1248	0.0556	0.00532	7.0394
(500,1000)	750	0.2037	0.1246	0.0319	0.00509	6.9650
(1000,1000)	mSUGRA	0.0314	0.0203	0.0066	0.00034	0.7839
(1000,1000)	250	NA	NA	NA	NA	NA
(1000,1000)	500	0.03323	0.0205	0.0066	0.00036	0.7900
(1000,1000)	750	0.0393	0.0209	0.0093	0.00068	0.8101

Table B3 : Cross-sections (pb) for Third family scalar non-universality

$$\tan \beta = 5$$

(Figure 7.3)

$(m_{\tilde{g}}, m_{\tilde{q}^3})$	$m_{\tilde{q}^{1,2}}$	σ_{OSD}	σ_{SSD}	$\sigma_{(3\ell+jets)}$	$\sigma_{(3\ell)}$	σ_{jets}
(500,500)	mSUGRA	0.2190	0.1301	0.0316	0.00222	9.0107
(500,500)	1000	0.2365	0.1428	0.0351	0.00518	6.9707
(500,500)	10000	0.2535	0.1720	0.0608	0.02036	2.9642
(500,1000)	mSUGRA	0.1317	0.0574	0.0160	0.00325	4.1353
(500,1000)	1000	0.0949	0.0442	0.0067	0.00027	7.8590
(500,1000)	10000	0.2411	0.1649	0.0577	0.02284	2.7613
(1000,1000)	mSUGRA	0.0092	0.0069	0.0024	0.00021	0.1921
(1000,1000)	1000	0.0052	0.0028	0.0002	0.00024	0.5255
(1000,1000)	10000	0.0103	0.0080	0.0035	0.00021	0.1309

Table B4 : Cross-sections (pb) for Third family scalar non-universality

$$\tan \beta = 40$$

(Figure 7.4)

$(m_{\tilde{g}}, m_{\tilde{q}^3})$	$m_{\tilde{q}^{1,2}}$	σ_{OSD}	σ_{SSD}	$\sigma_{(3\ell+jets)}$	$\sigma_{(3\ell)}$	σ_{jets}
(500,500)	mSUGRA	0.2971	0.1841	0.0515	0.00652	8.7476
(500,500)	1000	0.2894	0.1800	0.0563	0.01036	6.5057
(500,500)	10000	0.2557	0.1737	0.0617	0.01879	3.1213
(500,1000)	mSUGRA	0.1517	0.0882	0.0206	0.00663	3.8034
(500,1000)	1000	0.0835	0.0386	0.0068	0.00131	7.9259
(500,1000)	10000	0.2512	0.1639	0.0509	0.02318	2.8557
(1000,1000)	mSUGRA	0.0103	0.0076	0.0030	0.00029	0.1947
(1000,1000)	1000	0.0069	0.0029	0.0005	0.00026	0.5256
(1000,1000)	10000	0.0103	0.0082	0.0038	0.00034	0.1362

Table B5 : Cross-sections (pb) for $SO(10)$ D -term non-universality

$$\tan \beta = 5$$

(Figure 7.7)

$m_{\tilde{g}}$	D-term	σ_{OSD}	σ_{SSD}	$\sigma_{(3\ell+jets)}$	$\sigma_{(3\ell)}$	σ_{jets}
500	mSUGRA	0.3720	0.2136	0.0276	0.01380	14.1440
500	0.5	0.3762	0.0782	0.0349	0.01120	5.5250
500	-0.5	0.3955	0.2402	0.0438	0.01916	12.5007
500	-1.25	0.5638	0.3438	0.0792	0.02999	11.6682
1000	mSUGRA	0.0251	0.0160	0.0046	0.00035	0.7530
1000	0.5	0.0221	0.0165	0.0039	0.00040	0.7519
1000	-0.5	0.0287	0.0173	0.0049	0.00028	0.8043
1000	-1.25	0.0341	0.0182	0.0056	0.00045	0.8456
1500	mSUGRA	0.0020	0.0012	0.0003	0.00001	0.0702
1500	0.5	0.0018	0.0012	0.0003	0.00003	0.0689
1500	-0.5	0.0024	0.0013	0.0004	0.00012	0.0709
1500	-1.25	0.0030	0.0014	0.0005	0.00016	0.0720

Table B6 : Cross-sections (pb) for $SO(10)$ D -term non-universality
 $\tan \beta = 40$
(Figure 7.8)

$m_{\tilde{g}}$	D-term	σ_{OSD}	σ_{SSD}	$\sigma_{(3\ell+jets)}$	$\sigma_{(3\ell)}$	σ_{jets}
500	mSUGRA	0.5467	0.3360	0.0882	0.02482	13.1779
500	0.5	0.8111	0.4336	0.1383	0.03341	12.7985
500	-0.5	0.5552	0.3565	0.0898	0.02789	13.2670
500	-1.25	0.5731	0.6209	0.1283	0.0030	23.6538
1000	mSUGRA	0.0494	0.0303	0.0112	0.00083	0.6668
1000	0.5	0.0447	0.0278	0.0097	0.00105	0.6240
1000	-0.5	0.0505	0.0298	0.0098	0.00073	0.6309
1000	-1.25	NA	NA	NA	NA	NA
1500	mSUGRA	0.0041	0.0023	0.0010	0.00033	0.0532
1500	0.5	0.0043	0.0023	0.0009	0.00028	0.0537
1500	-0.5	0.0026	0.0018	0.0005	0.00005	0.0460
1500	-1.25	NA	NA	NA	NA	NA

Table B7 : Cross-sections (pb) for SM background

σ_{OSD}	σ_{SSD}	$\sigma_{(3\ell+jets)}$	$\sigma_{(3\ell)}$	σ_{jets}
0.1991	0.0900	0.0041	0.1920	2.1015

Chapter 8

Non-universal scalar mass scenario with Higgs funnel region of SUSY dark matter: a signal-based analysis for the Large Hadron Collider

8.1 Introduction

The mSUGRA scenario has a remarkable simplicity of principle, an economy of parameters and features that at least partially ameliorate potentially disastrous consequences in low energy physics. From a more agnostic standpoint, however, there is no strong reason to restrict ourselves to such universal models as has been discussed in different contexts in the earlier chapters. For one, even with gravity conveying supersymmetry breaking, the soft SUSY-breaking terms need not be universal at the supergravity scale, but would depend on the structure of the Kähler potential. Similarly, large non-universal corrections may accrue to the soft parameters as a result of the evolution between the Planck scale and the gauge-coupling unification scale ($M_G \simeq 2 \times 10^{16}$ GeV) [1]. These and other related issues have led to several studies of non-universal scalar [2–12] and gaugino

mass [13, 14] models. Non-universal scalar masses may appear due to a non-flat Kähler metric [15], or, for example, from $SO(10)$ D -terms [9–11]. However, any such non-universality, at the electroweak scale, would lead to low-energy flavor changing neutral current (FCNC) processes (through SUSY loops) [16]. The existing data on flavor physics thus impose severe constraints on any non-universality in scalar masses, in particular for the first two families. The restrictions on the third generation scalars (and the Higgses) from FCNC data are not too severe though.

It turns out that both FCNC and CP-violation constraints may be best tackled if one assumes the first two generations of scalars to be multi-TeV and (quasi-)degenerate in masses [17]¹. Clearly, allowing universal scalar masses at the gauge coupling unification scale would not satisfy the above objective because either (i) the REWSB constraint would prohibit such large scalar masses for a reasonable set of values of the gluino masses, or (ii) one must have very large gaugino masses, so as to allow very large scalar masses, thereby worsening the fine tuning problem [18]. We recall that, within the MSSM, the naturalness problem and its solution revolve around the third family, as well as the gaugino and Higgs scalar mass parameters. As long as the third generation scalars and the electroweak gauginos are on the lighter side, any quantitative measure of naturalness would stay within an acceptable domain. Furthermore, constraints from FCNC and CP-violation are relatively weak in such a scenario with an inverted mass hierarchy [19, 20].

In this chapter [21], we consider a particular non-universal scalar mass scenario (NUSM), namely that of Ref. [2]. The model addresses the FCNC issue by invoking very large masses for the first two generations of squarks and sleptons. As is well-known, such a solution is difficult to achieve within the mSUGRA scenario as the requirement of REWSB prevents the scalar masses from being too large. In the present context, this is circumvented by allowing the third generation squark masses and the Higgs scalar mass parameters to be small. This very smallness also serves to keep the degree of fine-tuning within control.

As far as the third generation sleptons are concerned, a very small SUSY-breaking mass at the GUT scale is not phenomenologically viable since the larger

¹We remind the reader that satisfying constraints imposed by electric dipole moments of electron and neutron would require very large scalar masses if we like to have finite values for the CP-violating SUSY phases.

Yukawa coupling serves to drive down the mass of the lighter stau, thereby rendering it the lightest of the supersymmetric partners (LSP) at the electroweak scale. Consequently, the SUSY-breaking mass in this sector has to be sizable². Rather than introducing a new parameter, we shall assume it to be same as that of first two generations of squarks or sleptons. To summarize, at the GUT scale, all sfermion masses are diagonal; and, apart from those pertaining to the stop and the sbottom, are universal. The last-mentioned, along with the Higgs scalars, have a vanishing mass at this scale. While this construction might seem artificial, note that this accords a special status to only those fields that are expected to play a direct role in EWSB. Interestingly, the model satisfies the WMAP constraint [24] on neutralino relic density for a large region of the parameter space without requiring any delicate mixing of Binos and Higgsinos. For simplicity, we confine ourselves to a universal gaugino mass and a vanishing trilinear soft-breaking parameter (A_0) at M_G .

We investigate how such a scenario can leave its fingerprint on numbers measured at the Large Hadron Collider (LHC). Such fingerprints are of value if ways can be devised to distinguish this scenario from an mSUGRA one with, say, similar gluino masses. For this, one has to perform a multichannel analysis [12, 14, 25, 26] studying several final states simultaneously.

A promising signal of supersymmetry (with a conserved R-parity) comprises large missing transverse energy, accompanied by jets and leptons with varying multiplicities. An analysis in different channels, compared with that of a similar mSUGRA scenario may lead to a significant hint of the non-universality. In the present analysis, we assess the accessibility of our non-universal scalar mass model (NUSM) at the LHC. We find that the direct pair production of stops and sbottoms as well as their cascading down from gluino decays lead to the possibility of four-lepton final states as a distinct signature of this scenario. Additionally, we also analyse the two-lepton and the three-lepton final states. This includes opposite sign dilepton, same-sign dilepton and trilepton final states. All these analyses are done also for mSUGRA so that the multipronged approach of analysing for different channels may become more conclusive.

²However, in analyses with Higgs-exempt no-scale SUSY model [22] or in a model with gaugino mediation [23] one may avoid such charged LSPs at the electro-weak scale by using non-zero Higgs scalar masses at the unification scale. In these scenarios the no scale boundary conditions are also valid for sleptons.

This chapter is organized as follows. In Section 8.2 we describe the NUSM model, apply cosmological constraints on neutralino dark matter and use low energy constraints such as those from $b \rightarrow s + \gamma$ or $B_s \rightarrow \mu^+ \mu^-$. We also identify benchmark points for our analyses of collider signals at the LHC. In Section 8.3, we pinpoint our strategies for collider simulations and report the numerical results. Finally, in Section 8.4, we summarize our results and conclude.

8.2 The Non-Universal Scalar Mass model (NUSM) and benchmark points

8.2.1 The NUSM parameter space

The NUSM model [2], at the scale M_G , is characterized by five parameters, namely,

$$\tan \beta, m_{1/2}, m_0, A_0 \text{ and } \text{sign}(\mu). \quad (8.1)$$

The parameters here play rôles similar to those in mSUGRA except for a subtle and important difference in the scalar sector. *Masses of the first two generations of scalars (squarks and sleptons) and the third generation of sleptons are assigned the value m_0 . However, the Higgs scalars and the third family of squarks have vanishing mass values at M_G .* Here, m_0 is allowed to be up to tens of TeVs. As has already been stated, we limit ourselves to vanishing A_0 . We have considered $\mu > 0$ in this analysis.

The NUSM admits a smaller pseudoscalar Higgs boson mass m_A on account of the Large Slepton Mass (LSM) renormalization group effect [2] for large m_0 . With such a m_0 , the LSM effect causes $m_{H_D}^2$ to become large and negative and this may happen for even a small $\tan \beta$. This, in turn, reduces the masses of the pseudoscalar Higgs boson (A), the CP-even heavy Higgs boson (H) and the charged Higgs bosons (H^\pm). In this scenario, μ is quite insensitive to a change in m_0 [2], since the Higgs and the third-generation squark masses at M_G are free of the latter. In fact, μ is completely independent of m_0 up to one-loop, whereas the two-loop contributions to its RGEs result in only a tiny dependence on m_0 . Recall that, in mSUGRA on the contrary, $|\mu|$ decreases significantly with an increase in m_0 . Whereas this led to a very small $|\mu|$ for a large m_0 in mSUGRA, giving the so called Hyperbolic Branch/Focus point (HB/FP) [27, 28] region that is close to the upper limit of m_0 satisfying REWSB for a given $m_{1/2}$, there is no HB/FP type of

effect in NUSM and μ stays reasonably independent of m_0 . It turns out that the lightest neutralino is highly Bino-dominated (with a small Higgsino admixture) throughout virtually the entire parameter space of NUSM. Along with the resonance condition, namely, $2 m_{\tilde{\chi}_1^0} \simeq m_A (m_H)$, the small Higgsino content allows the LSP to have the right degree of pair-annihilation via s -channel Higgs-exchanges, so as to satisfy the WMAP limits on the neutralino relic density. It is important to note that, excepting for LSP-stau coannihilation, the Higgs-pole annihilation mechanism is the only one in NUSM that reduces the relic density from overabundance to an acceptable degree of abundance. Thus, unlike in models such as the mSUGRA, here one does not need any delicate mixing between a Bino and Higgsinos in order to satisfy the WMAP data. Such Higgs-pole annihilations that occur for large $\tan \beta$ in mSUGRA is typically known as the funnel region [29,30]. NUSM has an extended funnel region that spans from low to high $\tan \beta$.

8.2.2 Cosmological and low energy constraints in NUSM

Assuming that dark matter was generated thermally, the limits on the cosmological relic density from the WMAP data [24] impose severe constraints on supergravity type of models wherein the lightest neutralino $\tilde{\chi}_1^0$ becomes the LSP for most of the parameter space [31,32]. We now perform an analogous analysis for the NUSM. For a given set of parameter (vide eq.(8.1)) values, the supersymmetric particle spectrum is generated using `SuSpect v2.34` [33]. This, then, is used as an input to `micrOMEGAs` [34] for computing the neutralino relic density. The recent WMAP data [24] stipulates that, at the 3σ level,

$$0.091 < \Omega_{CDM} h^2 < 0.128 , \quad (8.2)$$

where Ω_{CDM} is the dark matter relic density in units of the critical density and $h = 0.71 \pm 0.026$ is the reduced Hubble constant (namely, in units of $100 \text{ km s}^{-1} \text{ Mpc}^{-1}$).

In Fig.8.1, we display the allowed regions in the $m_{1/2} - m_0$ plane for three values of the ratio of the Higgs vacuum expectation values, namely $\tan \beta = 10, 15$ and 40 . The thin (cyan) sliver at the bottom is ruled out as, for such values of the parameters, the lighter stau becomes the LSP. The upper (cyan) region is rejected primarily on account of the failure in the breaking of the electroweak symmetry via radiative means. In other words, for such parameter values, m_A^2 does not acquire a positive value through RG flow. Close to the boundary of this region, several other phenomenological constraints become important. The most

important of these pertain to (i) the LEP2 and Tevatron lower bounds for sparticle masses, (ii) sfermions turning tachyonic, or (iii) the appearance of charge and color breaking (CCB) minima. To be allowed, a parameter point must evade all these and other such constraints. Specific details may be found in Ref. [2].

Highlighted (in bold—red—dots) in Fig.8.1 are examples of parameter points that satisfy the WMAP data. There are two distinct regions with acceptable relic density as already mentioned in Sec.8.2.1. (a) The Higgs pole annihilation region (also known as the funnel region) is characterised by $2m_{\tilde{\chi}_1^0} \simeq m_A, m_H$. In this particular scenario, it extends over the full range of $m_{1/2}$ under consideration. The Higgs pole annihilations may occur through s -channel pseudoscalar Higgs boson (A) or CP-even neutral H or h -bosons. NUSM has a bino-dominated LSP similar to what occurs in mSUGRA in its funnel region that satisfies the WMAP data. Similar to the case in mSUGRA, the WMAP satisfied parameter regions of NUSM is also dominantly characterized by the pseudoscalar Higgs boson mediated resonance annihilation. The exact or near-exact resonance regions have very large

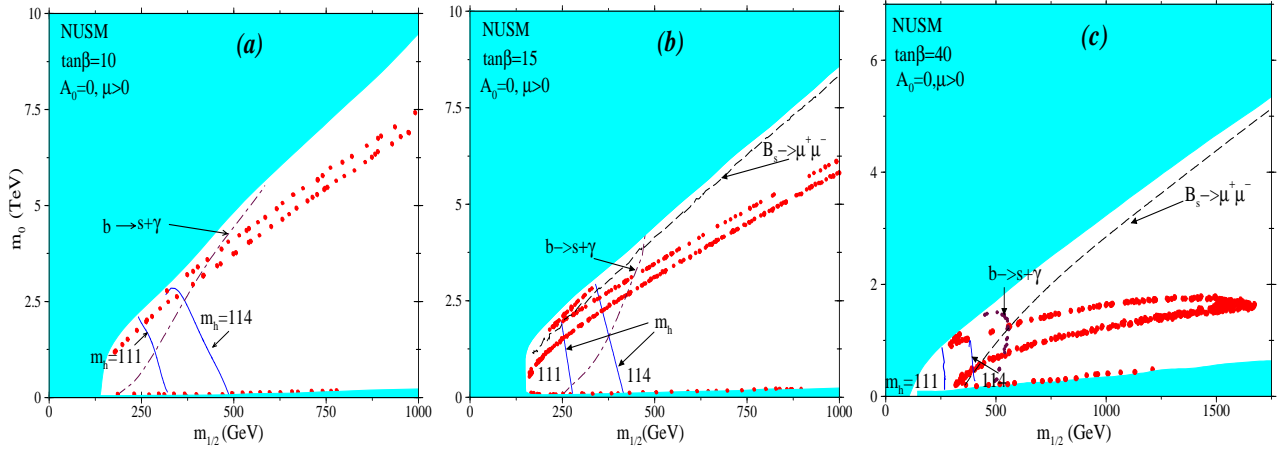


Figure 8.1: (a) WMAP allowed regions in the $m_{1/2} - m_0$ plane for $\tan \beta = 10$ and $A_0 = 0$ with $\mu > 0$ for NUSM are shown in red dots. Lighter Higgs boson mass limits are represented by solid lines. Dot-dashed line refers to $b \rightarrow s\gamma$ limit. The entire region is allowed by $B_s \rightarrow \mu^+\mu^-$ data. (b) Same as (a) except that $\tan \beta = 15$. The $B_s \rightarrow \mu^+\mu^-$ bound is shown as a long-dashed line. This eliminates a small strip of region below the discarded top (cyan) region. (c) Same as (b) except that $\tan \beta = 40$.

annihilation cross sections resulting in a high degree of under-abundance of dark matter. The resonance region that satisfies the WMAP data may be a few $\Gamma_{A/H}$ away from exact resonance. The widths $\Gamma_{A/H}$ (of A/H bosons) can be fairly large (e.g. $\Gamma_{A/H} \sim 10\text{-}50$ GeV). The WMAP satisfied regions fall on either side of the exact resonance condition thus showing two branches in the figure. (b) The second region, just above the lower ruled-out part, corresponds to the case where the lighter stau is nearly degenerate with the LSP, leading to very efficient LSP-stau coannihilation, thereby reducing the relic abundance to acceptable levels.

Also imposed on Fig.8.1 are the pertinent low-energy constraints. Whereas non-observance at LEP2 impose a strict bound of 114.4 GeV on the SM Higgs [35], with recent negative results from Tevatron [36] ruling out even somewhat heavier Higgses, the translation of this bound to the MSSM case needs careful consideration. Apart from the parameter-dependence of the cross-sections at LEP2/Tevatron, one needs to account for the uncertainties in computing the mass of light Higgs boson [37], originating primarily from momentum-independent as well as momentum-dependent two-loop corrections, higher loop corrections from the top-stop sector etc. Numerically, this amounts to about 3 GeV, and we have taken that into account in drawing the solid lines representing this constraint. Additionally, a part of the NUSM parameter space is associated with very light m_A even for a small $\tan\beta$ and this may lower the lighter Higgs boson lower bound to a value much smaller than that of the SM Higgs boson limit. We will revert to this while discussing the NUSM benchmark points.

A low energy observable of particular importance is the decay rate for $b \rightarrow s\gamma$ rate [38,39], which, at the 3σ level, reads [40]

$$2.77 \times 10^{-4} < Br(b \rightarrow s\gamma) < 4.33 \times 10^{-4}. \quad (8.3)$$

We used micrOMEGAs [34] for computation of $b \rightarrow s\gamma$ that in turn refers to Refs. [38,39] for actual computation. Typically, $b \rightarrow s\gamma$ disfavors the small $m_{1/2}$ region where the rate is below the lower limit. Note, however, that the usual estimation assumes a perfect alignment at high energies between the quark and squark mass matrices. In other words, the (super-)Cabibbo-Kobayashi-Maskawa matrix operative for supersymmetric diagrams is assumed to be identical to the usual CKM matrix. However, if one relaxes the above assumption and considers even a moderate amount of $\tilde{b} - \tilde{s}$ mixing at the GUT scale, Eq.8.3 is no longer an effective constraint for high scale models like mSUGRA. This, on the other hand, will not

cause any significant change in the sparticle mass spectra or in the flavor conserving process of neutralino annihilation. We refer the reader to Refs. [41,42] for further discussions on the amount of model-dependence in computing $Br(b \rightarrow s\gamma)$ in this context.

Since the NUSM scenario may contain a light pseudoscalar Higgs, it is necessary to consider the constraints from $B_s \rightarrow \mu^+\mu^-$. Within the MSSM, the above branching ratio is proportional to m_A^{-4} and $\tan^6\beta$ [43]. The recent CDF [44] limit for $Br(B_s \rightarrow \mu^+\mu^-)$ is given by

$$Br(B_s \rightarrow \mu^+\mu^-) < 5.8 \times 10^{-8}. \quad (8.4)$$

The branching ratio of $B_s \rightarrow \mu^+\mu^-$ is evaluated by using `micrOMEGAs` [34] that in turn implemented Ref. [45] for the computation. The computation involves inclusion of loop contributions due to chargino, sneutrino, stop and Higgs exchanges. The upper limit of this branching ratio is shown in dashed lines in Fig.8.1. The white regions above the dashed lines in Figs.8.1(b,c) are thus discarded. As mentioned in Ref. [2], the intense coupling region of Higgs bosons that appears when m_A is very small is also ruled out in NUSM for the same reason.

8.2.3 Benchmark points

The NUSM has a large volume of allowed parameter space, especially because REWSB does not prohibit m_0 from assuming a very large value. We focus here on a few characteristic parameter points that satisfy WMAP as well as low energy constraints. As seen in Figs.8.1(a-c), for a given $m_{1/2}$, the upper limit on m_0 decreases with an increase in $\tan\beta$. As an example, for $m_{1/2} = 1$ TeV, m_0 may well be as large as 7 TeV for $\tan\beta = 10$, 6 TeV for $\tan\beta = 15$, and 1.6 TeV for $\tan\beta = 40$.

Here, we have preferentially explored those regions in the parameter space which give distinctly different low energy and cosmological signatures as compared to mSUGRA. As we have mentioned before, the Higgs funnel region for mSUGRA is found only for large values of $\tan\beta$. The NUSM is characteristically different from mSUGRA in the sense that funnel regions exist even for small $\tan\beta$. Hence, we choose to explore two benchmark points with small $\tan\beta$. The next point to note is that NUSM, typically, has heavier spectra for the first two generations of scalars and the third generation of sleptons. Sfermions become

parameter	A	B
$\tan \beta$	10	15
$m_{1/2}$	270	255
m_0	2050	2000
A_0	0	0
$\text{sign}(\mu)$	1	1
μ	312	291
$m_{\tilde{g}}$	709	674
$m_{\tilde{u}_L}$	2100	2050
$m_{\tilde{t}_1}$	276	248
$m_{\tilde{t}_2}$	493	465
$m_{\tilde{b}_1}$	390	354
$m_{\tilde{b}_2}$	434	403
$m_{\tilde{e}_L}$	2050	2000
$m_{\tilde{\tau}_1}$	2040	1970
$m_{\tilde{\chi}_1^\pm}$	196	183
$m_{\tilde{\chi}_2^\pm}$	347	327
$m_{\tilde{\chi}_2^0}$	197	185
$m_{\tilde{\chi}_1^0}$	108	101
m_A	259	148
m_{H^+}	272	169
m_h	111	111
$\Omega_{\tilde{\chi}_1^0} h^2$	0.105	0.102
$Br(b \rightarrow s\gamma)$	1.59×10^{-4}	4.65×10^{-5}
$Br(B_s \rightarrow \mu^+ \mu^-)$	4.02×10^{-9}	2.81×10^{-8}
Δa_μ	9.31×10^{-11}	1.59×10^{-10}

Table 8.1: NUSM Benchmark points A and B (masses are in GeVs). The first five parameters define the model, while the rest are predictions.

heavier with increase in $m_{1/2}$. Therefore, if we like to probe the model in the early phase of the LHC, we would rather select $m_{1/2}$ to be relatively small for the benchmark points.

Table 8.1 lists two benchmark points for NUSM. Point A (for $\tan\beta = 10$, $A_0 = 0$, $m_{1/2} = 270$ GeV, $m_0 = 2.05$ TeV and $\text{sign}(\mu) = 1$), is associated with reasonably small masses for stop, sbottom, charginos as well as neutralinos. Furthermore, it has a light Higgs spectrum. All these are promising from the viewpoint of early LHC results.

Point B of Table 8.1 refers to a special parameter point ($\tan\beta = 15$, $A_0 = 0$, $m_{1/2} = 255$ GeV, $m_0 = 2.0$ TeV and $\text{sign}(\mu) = 1$), for which the Higgs sector is not in the decoupling [46,47] region. Thus, here we obtain a reduced lower limit for m_h (close to M_Z). We point out that we have relaxed the $b \rightarrow s\gamma$ constraint for these points. This is in keeping with the discussion in the paragraph following Eq.8.3. However, with a small displacement of the parameter point, we would be able to respect the constraint at the cost of having a benchmark point with an upwardly shifted spectrum. Both points A and B obey the constraints from $B_s \rightarrow \mu^+\mu^-$.

We also study the collider signatures for mSUGRA scenario at points with the same (or very similar) gluino mass and $\tan\beta$ corresponding to the points A and B. These have been denoted by mSUGRA-A and mSUGRA-B. We must mention that the requirements of obeying the stringent WMAP data as well as the lower bound of the lighter chargino mass did not allow us to choose exactly identical values of the masses of the gluino in each case of the mSUGRA points. This is true for both of the mSUGRA-A and mSUGRA-B that fall in the HB/FP zone. The high scale parameters as well as the low scale soft masses for these points are listed in Table 2, all of them being consistent with the constraint from WMAP. $\text{sign}(\mu)$ is taken to be positive and the trilinear coupling A_0 is taken to be zero, as mentioned earlier. The corresponding low-energy spectra have also been generated via SuSpect v2.34 using two-loop RGEs. Full one-loop and the dominant two-loop corrections to the Higgs masses are incorporated. We have used the strong coupling $\alpha_3(M_Z)^{\overline{MS}} = 0.1172$ for this calculation, adopting the default option in SuSpect. We have assumed the top quark mass to be 172.7 GeV throughout the analysis, and no tachyonic sfermion mode has been allowed at any scale. We now comment on the differences in spectra between the NUSM and mSUGRA benchmark points. For reasons that have been already stated, the

parameter	mSUGRA-A	mSUGRA-B
$\tan \beta$	10	15
$m_{1/2}$	253	252
m_0	2740	2300
A_0	0	0
$sign(\mu)$	1	1
μ	149	135
$m_{\tilde{g}}$	740	725
$m_{\tilde{u}_L}$	2745	2320
$m_{\tilde{t}_1}$	1636	1391
$m_{\tilde{t}_2}$	2258	1898
$m_{\tilde{b}_1}$	2255	1895
$m_{\tilde{b}_2}$	2730	2282
$m_{\tilde{e}_L}$	2731	2294
$m_{\tilde{\tau}_1}$	2714	2255
$m_{\tilde{\chi}_1^\pm}$	114	113
$m_{\tilde{\chi}_2^\pm}$	255	251
$m_{\tilde{\chi}_2^0}$	136	134
$m_{\tilde{\chi}_1^0}$	82	81
m_A	2704	2212
m_{H^+}	2706	2214
m_h	118	118
$\Omega_{\tilde{\chi}_1^0} h^2$	0.128	0.120
$Br(b \rightarrow s\gamma)$	3.62×10^{-4}	3.57×10^{-4}
$Br(B_s \rightarrow \mu^+ \mu^-)$	3.12×10^{-9}	3.11×10^{-9}
Δa_μ	4.60×10^{-11}	1.14×10^{-10}

Table 8.2: *mSUGRA Benchmark points A and B (masses are in GeVs). The first five parameters define the model, while the rest are predictions.*

high scale scalar mass parameters need to be chosen differently in the two cases. Consequently, the value of μ in NUSM is larger than that in mSUGRA, simply because the mSUGRA benchmark points are within or very close to the HB/FP zones. We must note that there is no HB/FP like effect in NUSM that would reduce μ . As a result, the chargino and neutralino masses in mSUGRA benchmark points are smaller than their counterparts in NUSM.

Finally, in regard to the mass of gluino it is important to clarify the role of radiative corrections in the benchmark points of the two scenarios namely mSUGRA- i and NUSM's point i , where $i \equiv A, B$. Radiative corrections comprising of gluon-gluino and quark-squark loops may be estimated as in Eq.8.5 [48].

$$\begin{aligned}
m_{\tilde{g}} &= m_3(Q^2) + \frac{3\alpha_s}{4\pi} m_3 \left(5 - 3 \ln \left(\frac{m_3^2}{Q^2} \right) \right) \\
&- \sum_{q=u,\dots,t} \frac{\alpha_s}{4\pi} m_3 \operatorname{Re} \left[\hat{B}_1(m_3^2, m_q^2, m_{\tilde{q}_1}^2) + \hat{B}_1(m_3^2, m_q^2, m_{\tilde{q}_2}^2) \right] \\
&+ \sum_{q=t,b} \frac{\alpha_s}{4\pi} m_q \sin(2\theta_q) \operatorname{Re} \left[B_0(m_3^2, m_q^2, m_{\tilde{q}_1}^2) - B_0(m_3^2, m_q^2, m_{\tilde{q}_2}^2) \right]. \quad (8.5)
\end{aligned}$$

The Passarino-Veltman functions B_0 , \hat{B}_1 and further useful details may be seen in Ref. [48]. The choice of the scale Q is not unambiguous and, in general, is defined by an appropriate mass scale in the theory. In SuSpect, for example, this is set equal to the geometric average of the values of the two stop squark masses. As we can see from Table 8.3, this average varies widely between mSUGRA- i and the corresponding NUSM's benchmark point i . As a result the running mass $m_3(Q^2)$ for mSUGRA- i is smaller where Q is higher compared to point i of NUSM, where the corresponding scale is smaller because the masses of the third generation of squarks in NUSM are quite smaller³. In general, for the given benchmark points under consideration, a point mSUGRA- i has a smaller running mass $m_3(Q^2)$ but has a much larger contribution from radiative corrections (*vide* Eq.8.5) compared to the corresponding point i of NUSM. We note that the radiative correction amounts that arise from gluon-gluino and quark-squark loops are quite different in the two scenarios. With a heavier average squark mass, a benchmark point mSUGRA- i has a much smaller contribution from quark-squark loops compared to that of NUSM point i . On the other hand, the logarithmic term in Eq.8.5 is such that for mSUGRA- i the term is negative because of the fact that $m_3^2(Q^2) < Q^2$ owing to a heavier average SUSY mass scale. This leads to a large

³ $m_3(Q^2)$ increases with a decreasing Q : see for example Ref. [49].

Points	m_0	$m_{1/2}$	Q	$m_3(Q^2)$	$m_{\tilde{g}}$	Radiative Correction
	GeV	GeV	GeV	GeV	GeV	
A	2050	270	357	633	709	12%
mSUGRA-A	2740	253	1917	548	740	35%
B	2000	255	329	602	674	12%
mSUGRA-B	2300	252	1619	551	725	32%

Table 8.3: *Running mass, radiative correction in percentage and pole mass of gluino in mSUGRA and NUSM benchmark points. The scale Q refers to geometric mean of the two stop squark mass eigenvalues.*

contribution from the second term of the same equation for mSUGRA-*i*. This, however is not true for NUSM where one has $m_3^2(Q^2) > Q^2$ owing to a lighter average stop mass or a lighter SUSY mass scale in general. NUSM points also have significant amount of quark-squark contributions for the same reason. The final effect is such that smaller values of $m_3(Q^2)$ are overrun by radiative corrections in mSUGRA-A and mSUGRA-B leading to larger values of the pole masses $m_{\tilde{g}}$ in comparison to the values of $m_{\tilde{g}}$ for NUSM benchmark points A and B.

8.3 Collider Signatures

8.3.1 The general strategy

The collider signatures, and hence the optimal search strategies, of the NUSM would naturally depend on the particular point in the parameter space that nature may have chosen. Rather than attempting a general, and hence non-optimal, analysis, we choose to illustrate the various features, concentrating largely on the three representative points identified in the preceding section. To start with, we summarize, in brief, the generic simulation procedure that has been adopted here. The spectrum generated by SuSpect v2.34 as described earlier is fed into the event generator Pythia 6.4.16 [50] through a standard SLHA [51] interface for the simulation of pp collisions with a centre-of-mass energy of 14 TeV.

We have used the CTEQ5L [52] parton distribution functions, the QCD renor-

malization and factorization scales both being set at the subprocess centre-of-mass energy $\sqrt{\hat{s}}$. All possible SUSY processes and decay chains consistent with conserved R -parity have been kept open. We have kept initial and final state radiations (ISR/FSR) on. The effect of multiple interactions has been neglected though. We, however, take hadronisation into account using the fragmentation functions built into Pythia.

In Table 8.4, we list the total supersymmetric particle production cross-sections for each of the benchmark points. Also listed are the individual cross sections for some of the important processes, namely, $\tilde{g}\tilde{g}$, $\tilde{t}_{1(2)}\tilde{t}_{1(2)}^*$ and $\tilde{b}_{1(2)}\tilde{b}_{1(2)}^*$ and processes with at least one chargino or neutralino denoted by “ $\tilde{\chi}_i^0/\tilde{\chi}_{1,2}^\pm$ ”. We note that, for points A and B, dominant production accrues from stop pairs. The other important processes include associated stop and sbottom production along with gluinos as well as charginos and neutralinos. It should be noted that while the mSUGRA and the NUSM benchmark points are quite similar as far as the gluino-pair production or the total supersymmetric particle production cross sections are concerned, they differ markedly in the dominant production modes. For the mSUGRA points, it is the lighter neutralinos and charginos that dominate overwhelmingly, whereas for the NUSM points, this rôle is usurped by stop-pairs and sbottom pairs.

mSUGRA				NUSM				
Point	Total	$\tilde{\chi}_i^0/\tilde{\chi}_{1,2}^\pm$	$\tilde{g}\tilde{g}$	Point	Total	$\tilde{t}_1\tilde{t}_1^* + \tilde{t}_2\tilde{t}_2^*$	$\tilde{b}_1\tilde{b}_1^* + \tilde{b}_2\tilde{b}_2^*$	$\tilde{g}\tilde{g}$
mSUGRA-A	11.86	10.67	1.18	A	12.42	6.77	1.73	1.28
mSUGRA-B	12.49	11.18	1.25	B	19.92	11.73	2.79	1.78

Table 8.4: Total supersymmetric particle production cross-sections (in pb) as well as the leading contributions for each of the NUSM and mSUGRA benchmark points.

Before we discuss the signals, it behoves us to briefly discuss the major decay modes (see 8.5 and 8.6), for the structure of the cascades would determine the final state configurations. Starting with the major produce, namely the stop, for each of points A and B, it has almost a 100% decay branching fraction to b and $\tilde{\chi}_1^+$. The $\tilde{\chi}_1^\pm$ decays, in turn, into W^\pm and the LSP again with nearly a 100% branching fraction. As for the sbottoms, they have sizable branching fractions into both

Decay modes (squark/gluino)	A	B
$\tilde{g} \rightarrow \tilde{b}_1 b$	31.0	33.0
$\tilde{g} \rightarrow \tilde{b}_2 b$	26.0	26.0
$\tilde{g} \rightarrow \tilde{t}_1 t$	22.0	21.0
$\tilde{g} \rightarrow \tilde{t}_2 t$	21.0	20.0
$\tilde{b}_1 \rightarrow \tilde{\chi}_1^0 b$	8.0	13.0
$\tilde{b}_1 \rightarrow \tilde{\chi}_2^0 b$	42.0	52.0
$\tilde{b}_1 \rightarrow \tilde{\chi}_1^\pm t$	11.0	0.0
$\tilde{b}_1 \rightarrow \tilde{t}_1 W^-$	37.0	33.0
$\tilde{t}_1 \rightarrow \tilde{\chi}_1^+ b$	100.0	100.0
$\tilde{\chi}_2^0 \rightarrow \tilde{\chi}_1^0 q \bar{q}$	69.0	71.0
$\tilde{\chi}_2^0 \rightarrow \tilde{\chi}_1^0 l \bar{l}$	10.0	10.0
$\tilde{\chi}_2^0 \rightarrow \tilde{\chi}_1^0 \nu \bar{\nu}$	20.0	18.0
$\tilde{\chi}_2^0 \rightarrow \tilde{\chi}_1^0 h$	0.0	0.0
$\tilde{\chi}_1^+ \rightarrow \tilde{\chi}_1^0 W^+$	100.0	100.0

Table 8.5: *The branching ratios(%)of the dominant decay modes of the gluinos, squarks and lighter electroweak gauginos for NUSM for the different benchmark points.*

the top–chargino and the bottom–neutralino modes. The former, though slightly suppressed on account of phase space considerations, is particularly interesting in that it leads to tops in final states. With the stop and sbottom being so light in this scenario, it is obvious that the gluino decay branching fractions into stop and sbottom (accompanied by a top or a bottom, as the case may be) are significantly enhanced as compared to the typical mSUGRA case. In fact, these modes, all of comparable magnitudes, together turn out to be overwhelmingly dominant. This, obviously, results in an enhanced scope of having top and/or bottom quarks with a high multiplicity. This, in turn, makes it likely to have several leptons in the final state (typically from the top quark decays). This particular character of

Decay modes (squark/gluino)	mSUGRA-A	mSUGRA-B
$\tilde{g} \rightarrow \tilde{\chi}_1^\pm tb$	26.6	27.4
$\tilde{g} \rightarrow \tilde{\chi}_2^\pm tb$	19.0	19.0
$\tilde{g} \rightarrow \tilde{\chi}_i^0 t\bar{t}$	22.0	22.0
$\tilde{\chi}_2^0 \rightarrow \tilde{\chi}_1^0 q\bar{q}$	33.0	35.4
$\tilde{\chi}_2^0 \rightarrow \tilde{\chi}_1^\pm ud$	32.4	32.0
$\tilde{\chi}_2^0 \rightarrow \tilde{\chi}_1^\pm l\nu_l$	10.0	15.4
$\tilde{\chi}_1^+ \rightarrow \tilde{\chi}_1^0 ud$	66.6	66.6
$\tilde{\chi}_1^+ \rightarrow \tilde{\chi}_1^0 l\nu_l$	33.0	33.0

Table 8.6: The branching ratios(%)of the dominant decay modes of the gluinos, lighter neutralino and chargino states for mSUGRA for the different benchmark points.

the spectrum, thus, raises hopes for 4ℓ (with $\ell = e, \mu$) final states as a viable signal of SUSY. We, nonetheless, do not limit ourselves to these alone, but consider each of the following final states:

- Opposite sign dilepton (OSD): $(\ell^\pm \ell'^\mp) + (\geq 2) jets + \cancel{E}_T$,
- Same sign dilepton (SSD): $(\ell^\pm \ell'^\pm) + (\geq 2) jets + \cancel{E}_T$,
- Trilepton ($3\ell + jets$): $3\ell + (\geq 2) jets + \cancel{E}_T$,
- Hadronically quiet trilepton⁴ (3ℓ): $3\ell + \cancel{E}_T$,
- Inclusive 4-lepton ($4\ell + X$): $4\ell + X + \cancel{E}_T$,

where ℓ stands for final state electrons and/or muons, \cancel{E}_T denotes missing transverse energy and X denotes any associated jet(s).

Of the various final states listed above, only the hadronically quiet trileptons have their origin in electroweak processes such as $\tilde{\chi}_2^0 \tilde{\chi}_1^\pm$ production. However, as can be seen from our event selection criteria set down in section 8.3.2, strong processes which do not give rise to hard enough jets can also be responsible for such final states. The large rate of $t\bar{t}$ and $b\bar{b}$ production in NUSM thus

⁴These get contributions from electroweak production of a chargino and a neutralino.

leads to relatively higher rates for hadronically quiet tripletons. On the whole, rates are never found to exceed a few percent of those with accompanying hard jets.

As is well known, in the LHC environment, even if the hard scattering process were to lead to a purely non-hadronic final state, the actual observable final state would, nonetheless, still include typically a few jets, originating from underlying events, pile up effects and ISR/FSR. In view of this, we define a hadronically quiet event to be one devoid entirely of any jet with $E_T^{jet} \geq 100$ GeV. This avoids unnecessary removal of events accompanied by relatively soft jets.

8.3.2 Detection and Kinematical Requirements

Before we mention the selection cuts, we would like to discuss the resolutions of the detectors, specifically those applicable to the ECAL, the HCAL and the muon chamber that have been incorporated in our analysis [53]. This is particularly important for reconstructing missing- E_T , which is a key variable for discovering physics beyond the Standard Model.

We assume that all charged particles with $p_T > 0.5$ GeV are detected⁵ as long as they emanate within the pseudorapidity range $|\eta| < 5$. For muons though, the applicable pseudorapidity range is determined by the geometry of the muon chamber to be⁶ $|\eta| < 2.5$. All the particles thus detected constitute the “physics objects” that are reconstructed in a collider experiments, and are further classified as

- isolated leptons;
- hadronic jets formed after identifying isolated leptons;
- unclustered energy comprised of calorimetric clusters with $p_T > 0.5$ GeV (ATLAS) and $|\eta| < 5$, that are not associated with any of the above types of high- E_T objects

Electrons and muons with $p_T > 10$ GeV and $|\eta| < 2.5$ may be identified as

⁵This threshold is specific to ATLAS, while for CMS, $p_T > 1$ GeV is applicable. Our results, though, are largely insensitive to the exact figure.

⁶Although it seems that muons in the range $2.5 < |\eta| < 5$ would leave their footprints in the tracker, we deliberately choose to be consistent with the above criteria. Once again, the inclusion of such muons would make little quantitative difference.

isolated leptons. In order to be deemed isolated, the lepton should be sufficiently separated from any other lepton in that it must satisfy $\Delta R_{\ell\ell} \geq 0.2$, where $\Delta R = \sqrt{(\Delta\eta)^2 + (\Delta\phi)^2}$ is the separation in the pseudorapidity–azimuthal angle plane. Similarly, it must be far away ($\Delta R_{\ell j} \geq 0.4$) from all putative jets with $E_T > 20$ GeV. And, finally, the total energy deposit from all hadronic activity within a cone of $\Delta R \leq 0.2$ around the the lepton axis should be ≤ 10 GeV.

Jets are formed with all the final state particles after removing the isolated leptons from the list with PYCELL, the inbuilt cluster routine in Pythia. The detector is assumed to stretch over the pseudorapidity range $|\eta| \leq 5$ and is segmented into 100 equal-sized (in η -spread) strips. Similarly, the entire 2π azimuthal spread is again segmented into 64 equal-sized strips resulting in a 100×64 grid of cells. To register a signal, a minimum E_T of 0.5GeV needs to be deposited in a cell, while the minimum E_T for a cell to act as a jet initiator is assumed to be 2 GeV. All objects within a cone of $\Delta R=0.4$ around the jet initiator cell are considered for jet formation, and for a conglomeration to be considered a jet, it must satisfy $\sum_{\text{objects}} E_T > 20\text{GeV}$.

Now, as has been mentioned earlier, all the other final state particles, which are not isolated leptons and are yet separated from jets by $\Delta R \geq 0.4$ are considered as unclustered objects. This includes all electromagnetic objects (muons) with $0.5\text{GeV} < E_T < 10\text{GeV}$ and $|\eta| < 5$ (2.5) as well as hadronic energy deposits with $0.5\text{GeV} < E_T < 20\text{GeV}$ and $|\eta| < 5$. Such unclustered energy deposits need to be taken into account in order to properly reconstruct any missing- E_T .

Any detector suffers from finite resolutions and collider detectors are no exception. To approximate the attendant experimental effects, we smear the energies (transverse momenta) with Gaussian functions. Nominally, the widths of the distributions have different contributions (accruing from different sources), each with a characteristic energy dependence and with these being added in quadrature. To wit (all energies are measured in units of GeV),

- electron/photon energy resolution:

$$\frac{\sigma(E)}{E} = \frac{a}{\sqrt{E}} \oplus b \oplus \frac{c}{E} \quad (8.6a)$$

where

$$(a, b, c) = \begin{cases} (0.030, 0.005, 0.2) & |\eta| < 1.5 \\ (0.055, 0.005, 0.6) & 1.5 < |\eta| < 5 \end{cases} \quad (8.6b)$$

- muon p_T resolution :

$$\frac{\sigma(P_T)}{P_T} = \begin{cases} a & |\eta| < 1.5 \\ a + b \log \frac{p_T}{100\text{GeV}} & 1.5 < |\eta| < 2.5 \end{cases} \quad (8.7a)$$

with

$$(a, b) = \begin{cases} (0.008, 0.037) & |\eta| < 1.5 \\ (0.020, 0.050) & 1.5 < |\eta| < 2.5 \end{cases} \quad (8.7b)$$

- jet energy resolution :

$$\frac{\sigma(E_T)}{E_T} = \frac{a}{\sqrt{E_T}} \quad (8.8)$$

with $a = 0.55$ being the default value used in PYCELL

- unclustered energy resolution :

$$\sigma(E_T) = \alpha \sqrt{\sum_i E_T^{(Unc.E)_i}} \quad (8.9)$$

where $\alpha \approx 0.55$. One should keep in mind here that the x - and y -components of $E_T^{Unc.E}$ need to be smeared independently (with identical widths).

Once we have identified the ‘physics objects’ as described above, we sum vectorially the transverse components of all the momenta smeared thus to obtain the total visible transverse momentum. Clearly, the missing transverse energy is nothing but the magnitude of the visible transverse momentum, namely

$$\cancel{E}_T = \sqrt{(\sum p_x)^2 + (\sum p_y)^2} \quad (8.10)$$

where the sum goes over all the isolated leptons, the jets as well as the unclustered energy deposits. At this stage, we are in a position to impose the selection cuts, namely

- Missing transverse energy $\cancel{E}_T \geq 100\text{GeV}$,
- $p_T^\ell \geq 20\text{ GeV}$ for all isolated leptons,
- $E_T^{\text{jet}} \geq 100\text{ GeV}$ and $|\eta_{jet}| \leq 2.5$,
- For the hadronically quiet trilepton events, as also for inclusive 4ℓ events, we reject, in addition, any event with a same flavour opposite sign lepton pair satisfying $|M_Z - M_{\ell^+\ell^-}| \leq 10\text{ GeV}$. Such events are characterised by the requirement of having no central jet with $E_T > 100\text{ GeV}$.

We have generated the corresponding SM backgrounds (with identical kinematical cuts) using `Pythia`. The bulk of the contribution comes from $t\bar{t}$ events. To take into account the next to leading order (NLO) and next to leading log resummed (NLL) corrections—not included in `Pythia`—we rescale the results by the appropriate K -factor [54] viz. 2.23. Exclusive diboson (WW , WZ , ZZ) production constitutes another potential background, but it is easy to see that except for the hadronically quite trilepton channel, these contributions are very sub-dominant. Furthermore, these are reduced drastically by the cuts imposed, especially by the one on the leptonic invariant mass. Inclusive, i.e. including (multi-)jets, gauge boson production is another very serious background, but can be estimated with a high accuracy using `ALPGEN` [55]. The combination of a large missing E_T along with the requirement of at least two high- p_T leptons reduces even this to innocuous levels.

8.3.3 Results

The event rates in the various channels discussed in the preceding section would, of course, differ amongst themselves and also depend on the point in the parameter space, both on account of the differing production cross sections and branching fractions as well as the kinematical restrictions imposed. In Table 8.7, we tabulate the event rates in different channels obtained for the points A and B of the NUSM scenario as well as those for the corresponding mSUGRA ones. Also shown are the respective SM backgrounds.

For the NUSM benchmark points, the gluino decays dominantly into top-stop and bottom-sbottom (see table 4). The source of leptons in the final state can thus be both the stop and the sbottom which can lead to the top and chargino in the next stage of the cascade. Of course, appropriate branching and combinatoric factors are to be used in each case. For the mSUGRA benchmark points, on the other hand, the gluino (which is the lightest strongly interacting superparticle) decays primarily into the three-body channels such as $t\bar{t}\tilde{\chi}_i^0$ and $tb\tilde{\chi}_i^\pm$ (see table 5). It should be remembered, however, that gluino decays mediated by light squark flavours are not entirely negligible and in fact, can account for up to one-third of the decays. This causes an effective enhancement, in the NUSM cases, of decays into the intermediate states containing top/chargino.

Another crucial difference is the splitting between the $\tilde{\chi}_1^\pm$ and $\tilde{\chi}_1^0$ states.

Model Points	σ_{OSD}	σ_{SSD}	$\sigma_{3\ell+jets}$	$\sigma_{3\ell}$	$\sigma_{4\ell}$
A	103	24.0	14.9	3.1	3.1
mSUGRA-A	33.7	15.4	8.1	0.4	1.3
B	135	28.7	19.0	4.4	3.8
mSUGRA-B	38.9	16.9	9.1	0.4	1.5
SM Backgrounds					
$t\bar{t}$	1.10×10^3	18.1	2.7	5.3	0.0
$ZZ, WZ, ZH, Z\gamma$	16.3	0.3	0.5	1.1	0.4
Total Background	1.12×10^3	18.4	3.2	6.4	0.4

Table 8.7: Event-rates (fb) after cuts for non-universal scalar mass points and corresponding mSUGRA points with same gluino mass. CTEQ5L parton distribution functions used with $\mu_F = \mu_R = \sqrt{\hat{s}}$.

With the splitting being large in the NUSM case, the W^\pm from $\tilde{\chi}_1^\pm$ can be nearly on-shell (as opposed to an off-shell one in the mSUGRA case), thereby resulting in typically harder leptons. Together, these features are responsible for effectively reducing the rates for leptonic final states for mSUGRA in comparison with the NUSM benchmark points consistent with the dark matter constraints. Of course, the already mentioned difference in gluino masses has also a small role to play.

Based on the above observations, the following features in the results are noted.

- For each of OSD , 3ℓ and 4ℓ final states, the difference in the absolute rates between the NUSM points and the corresponding mSUGRA ones is remarkably large. As has been argued at the beginning of Section 3.1, this can be understood in terms of the relative lightness of the third-generation squarks in the NUSM scenario. While it might be tempting to aver that this alone would serve to distinguish NUSM from mSUGRA scenarios, a little reflection shows that just the absolute rates are not enough for this purpose and a combination of observables would be required.
- For the same sign dilepton final state (a manifestation of the Majorana nature of the gauginos), the signal to background ratio (S/B) exceeds unity for

both points A and B. This, though, is not surprising, for *SSD* is well known for its efficacy in SUSY search. Note though that the *SSD* rate can not really distinguish between NUSM and its mSUGRA counterpart.

- While $S/B \gtrsim 1$ for the 4-lepton final state as well, the smaller rates for this signal significantly reduces its potential as a discovery channel. However, this could potentially serve as a very efficient discriminator between scenarios.
- The situation for the $3\ell + \text{jets}$ is somewhat better than the 4ℓ one. The rates are larger while maintaining the difference between NUSM and mSUGRA.
- As for the *OSD* and the hadronically-quiet 3ℓ final states, generically, $S/B < 1$. The former though boasts of the largest event rates. For points A and B, this signal begins to stand well over the background fluctuation for an integrated luminosity of as little as 1fb^{-1} whereas 2fb^{-1} would allow a discovery claim. For the hadronically-quiet trilepton mode, the required luminosity is $\sim 10\text{fb}^{-1}$ for points A and B. Qualitatively, these two points are very similar to each other, especially as far as the superpartner masses are concerned. The main difference lies in the Higgs sector, which has not been explored here.
- It is obvious that, for an integrated luminosity of 30fb^{-1} , many of these channels would allow us to register a 5σ discovery claim⁷. In Table 8.8, we summarise this information for each of the channels and parameter points, both in the NUSM scenario as well as their mSUGRA counterparts.

Model Points	<i>OSD</i>	<i>SSD</i>	$3\ell + \text{jets}$	3ℓ	4ℓ
A	✓	✓	✓	✓	✓
mSUGRA-A	✓	✓	✓	×	✓
B	✓	✓	✓	✓	✓
mSUGRA-B	✓	✓	✓	×	✓

Table 8.8: 5σ visibility of various signals for an integrated luminosity of 30fb^{-1} . A ✓ indicates a positive conclusion while a × indicates a negative one.

We now discuss the profile of the dominant (though not necessarily the

⁷The required luminosity is much smaller for some channels and parameter points.

most background-free) signal mode, namely events with opposite sign dileptons. The quest is to see if quantitative features in the same could be used to either accentuate the discovery potential or as discriminators between models and/or parameter points. In Fig.8.2, we display the normalized (to unity) distributions of missing transverse energy, a most crucial aspect of supersymmetry signals. As a comparison of the first two panels shows, the \cancel{E}_T distributions for parameter points A and B look very similar, which is but a consequence of the aforementioned similarity between the corresponding spectra. Furthermore, all of them are discernibly different from those for the corresponding mSUGRA points⁸. That the latter are softer can be understood by realizing that the main production channel for the mSUGRA spectrum is $pp \rightarrow \tilde{g}\tilde{g}$ and that, unlike in the NUSM case, the gluino undergoes a three body decay, resulting in relatively less momentum imparted to the LSP. Note also that the the dominant ($t\bar{t}$) background—as displayed in the first panel—is almost as soft as the mSUGRA signals, and thus a hardening of the \cancel{E}_T cut would have considerably improved the S/B ratio for the NUSM cases, while worsening it for the mSUGRA ones.

Another kinematical variable often used advantageously in searches for new physics involving \cancel{E}_T is the “effective mass” defined to be the scalar sum of the transverse momenta of the isolated leptons and jets and the missing transverse energy, viz.

$$m_{\text{eff}} \equiv \sum (p_T)_{\text{iso.}\ell} + \sum (p_T)_{\text{jets}} + \cancel{E}_T . \quad (8.11)$$

In Fig.8.3, we display the corresponding distributions, again for both the NUSM points and their mSUGRA counterparts. As the first panel shows, as far as point A is concerned, there is little to choose between this distribution and that for the corresponding mSUGRA point. Similar is the case for point B (second panel). Note, furthermore, that the peak in either case is at a fairly large value of m_{eff} . While this, at first sight, might seem contradictory to the oft-repeated claim that this distribution should peak roughly at twice the mass of the dominant particle being produced, the reason for this discrepancy is easy to appreciate. First and foremost, with the strong demands made on the transverse momenta of the two leading jets, the contribution from stop-pair production reduces drastically. This is understandable since the relatively small difference between the stop mass and

⁸Note that we are concerned here about the *shape* of the curve, not the absolute magnitude, which, of course, are different (*vide* Table 8.7.)

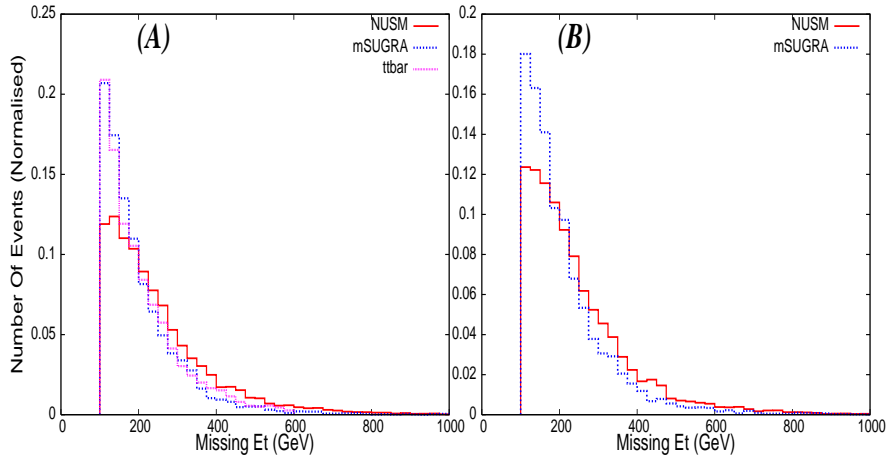


Figure 8.2: Missing transverse energy distribution (normalized to unit area) for opposite sign dilepton (OSD) events. The eponymous panels refer to the respective representative points in the parameter space. Also shown are the analogous distributions for the corresponding $mSUGRA$ points. The first panel also shows the distribution accruing from the overwhelmingly dominant SM background, namely $t\bar{t}$ production.

those of the lighter chargino implies that the b from stop decay tends to be softer. With the stop-pair contribution thus being effectively decimated⁹, this also offers hints as to why the NUSM and $mSUGRA$ distributions look so similar. And, with the gluinos themselves being produced with a considerable transverse momentum, it is easy to understand why the distribution peaks at a high value of m_{eff} .

Having discussed the prospects of refining and/or using the kinematical variables in the *OSD* sample towards discriminating between scenarios, we now consider a set of observables, namely the ratios of events seen in various channels. As is well known, there is a great advantage to the use of such variables in that it almost entirely eliminates some systematic uncertainties such as that in the luminosity and drastically reduces others such as those corresponding to the

⁹It might seem paradoxical that we are altogether sacrificing the signal from the light stop, a cornerstone of this scenario. However, including the stop contribution would require softening the p_T requirements, a process fraught with danger in the context of the LHC. In the absence of a full-scale simulation including multiple scattering and underlying events, we deliberately desist from this.

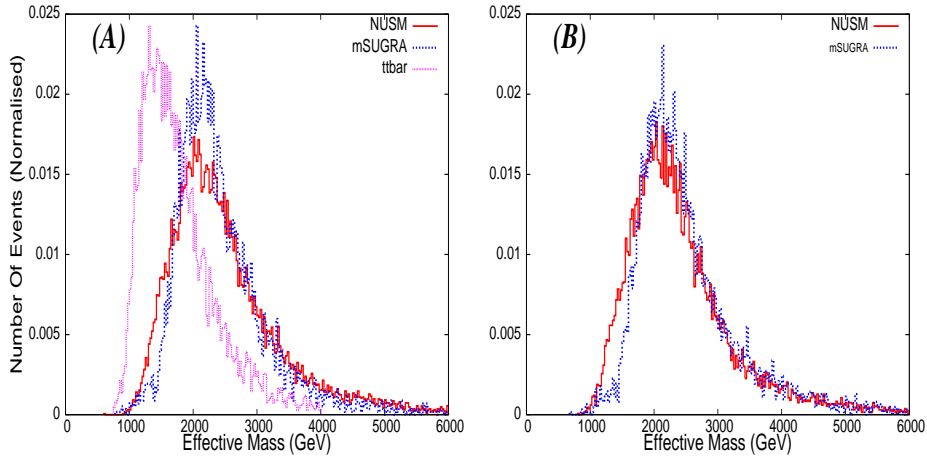


Figure 8.3: As in Fig.8.2, but for the effective mass instead.

choice of the parton distributions, the choice of renormalization and fragmentation scales etc. In Fig.8.4, we present the ratio of the subordinate channels with the dominant (*OSD*) channel for each of the parameter points.

At this stage, we can easily formulate the means of discriminating between a NUSM point and the corresponding mSUGRA one, namely

- ★ For parameters points (such as A and B) with a relatively smaller $m_{1/2}$ but large m_0 (i.e., when the gluino is considerably heavier than the stop/sbottom but sufficiently lighter than the first two generation squarks and sleptons), the NUSM scenario would typically result in a smaller proportion of same sign dilepton events, as is clear from Fig.8.4(a), when compared to the *OSD* rates. This can be attributed to the fact that the *OSD*-rate increases significantly for the gluinos decaying through stop-top (with, consequently, *OSD* being possible even from the decay of a single gluino, irrespective of how the other one decays), whereas the *SSD* relies on the good old fact of the gluino being a Majorana spinor, with only a slight increment to the leptonic branching fraction due to the decays through third generation.
- ★ The mSUGRA-A and mSUGRA-B points have sufficiently small values of μ and these points indeed fall in the HB/FP region. This implies that there is more of Higgsino in the lighter chargino ($\tilde{\chi}_1^\pm$) and the second lightest neutralino ($\tilde{\chi}_2^0$). Therefore, the leptonic signals are weakened compared to

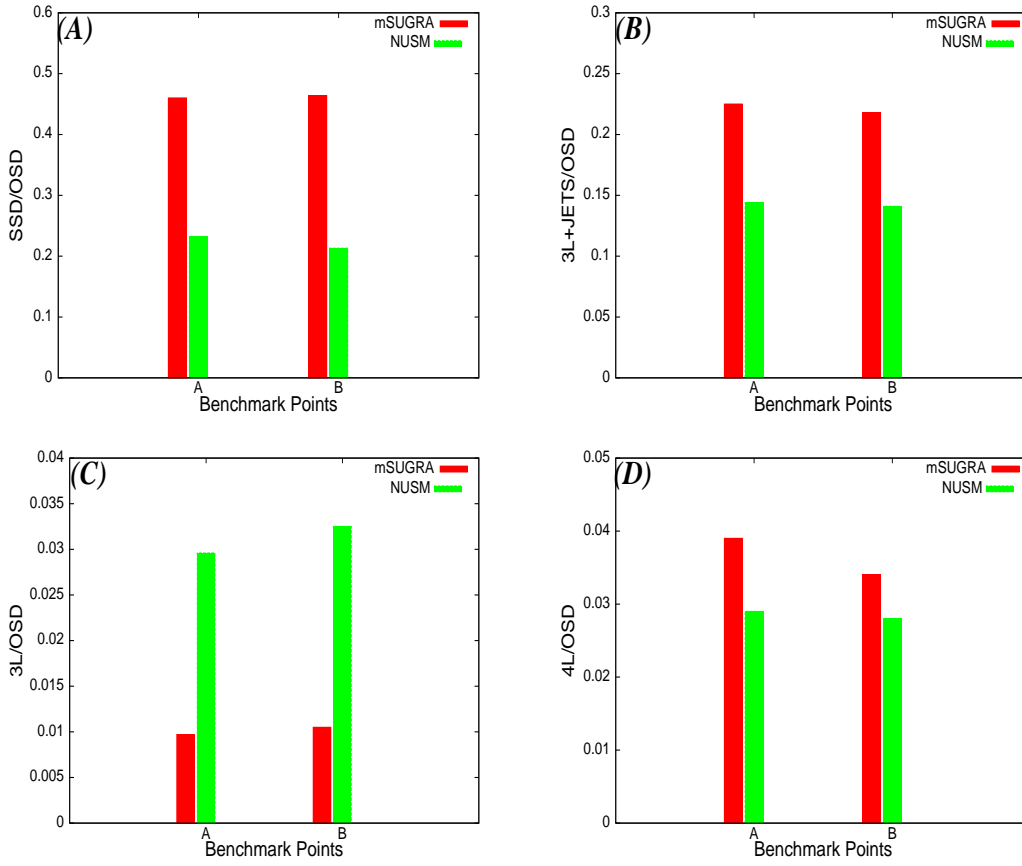


Figure 8.4: Event ratios with respect to opposite-sign dilepton(OSD) events for NUSM and mSUGRA cases at the points A and B mentioned in the text. Colour Code: Red: mSUGRA, Green: NUSM scenario.

what we predict in NUSM.

- ★ Again, for points with a small $m_{1/2}$ but large m_0 (such as A and B), the rates (absolute and relative) for the hadronically quiet trilepton mode are markedly higher for the NUSM case. This can be attributed to the aforementioned feature of the NUSM spectrum which renders it easier to have large- p_T isolated leptons.
- ★ Overall, it is self-evident that a combination of these ratios would serve to easily distinguish between the two scenarios.
- ★ And, finally, the relative lightness of the stop and the sbottom (and the con-

sequent fact of the gluinos decaying through these), renders the NUSM signal b -rich. Invoking b -tagging (which we had not done in the results presented so far) would thus present us with a very useful discriminator. With this in view, we perform a study in OSD channel associated with two or more partonic b -jets ($\geq 2b + OSD$). We assume a b -tagging efficiency [56] of $\epsilon_b = 0.5$ for $p_T > 40$ GeV and $|\eta| < 2.5$. The OSD event selection criteria remain the same. As expected, we see a clear distinction between the NUSM and the corresponding mSUGRA ones in the absolute event rates as shown in Table 6. With the NUSM sample being particularly rich in b 's, the suppression in rates as compared to those in Fig.8.7 is understandably less severe than ϵ_b^2 .

Model Points	A	mSUGRA-A	B	mSUGRA-B	$t\bar{t}$
$\geq 2b + OSD$	36.6	6.3	46.4	10.2	148.7

Table 8.9: Event rates (fb) at different benchmark points and for the $t\bar{t}$ background for a final state $\geq 2b + OSD$.

8.4 Summary and Conclusions

We have studied a case of non-universal scalar masses, wherein the first two families of squarks as well as sleptons of all generations are much heavier than the third family of squarks and the Higgs scalars. The universality of gaugino masses has been adhered to. We confine ourselves only to that region of the parameter space where one achieves a relic density consistent with the WMAP data. LSP annihilation is efficiently mediated by the pseudoscalar Higgs, with the ‘funnel region’ being significantly extended toward small values of $\tan \beta$ when compared to mSUGRA. Having ensured that the region of SUSY parameter space thus isolated is consistent with all constraints from FCNC and CP-violation, we have proceeded to investigate the signals of this scenario at the LHC.

Although stop-pair production is the dominant SUSY process in such scenarios, the stringent cuts that we choose to impose results in stop-cascades being suppressed. Rather, the dominant contribution to the signal rates turns out to be gluino pair-production. The relatively large multiplicity of top quarks pro-

duced in the cascades results in enhanced rates for two, three and four-lepton final states, together with missing- E_T and hard jets. In particular, the usefulness of four-lepton final states is highlighted through this analysis.

Based on the study of a few benchmark points (corresponding to different gluino masses and $\tan \beta$), we find that, using the criteria chosen by us, it is possible to probe the above scenario with an integrated luminosity of 30fb^{-1} for gluino masses up to about 1.2 TeV. (Indeed, for certain significant parts of the parameter space, even 2fb^{-1} would be enough.) The reach can be potentially extended further once more luminosity accrues. We also demonstrate that it is possible to distinguish this scenario from an mSUGRA-one tuned at the same gluino mass and satisfying the WMAP constraints. The usefulness of the ratios of events in various channels is clearly elicited from our study. Moreover, such distinction is facilitated by the effective mass distribution of events for gluino masses on the higher side, i.e. above a TeV. Thus, we succeed in illustrating that a multichannel analysis is not only able to probe such non-universal SUSY scenarios satisfying the relic density constraints, but can also highlight notable differences with a simple-minded model based on universal SUGRA.

Bibliography

- [1] N. Polonsky and A. Pomarol, Phys. Rev. D **51**, 6532 (1995) [arXiv:hep-ph/9410231]; R. Barbieri, L. J. Hall and A. Strumia, Nucl. Phys. B **445**, 219 (1995) [arXiv:hep-ph/9501334]; R. L. Arnowitt and P. Nath, Phys. Rev. D **56**, 2833 (1997) [arXiv:hep-ph/9701325].
- [2] U. Chattopadhyay and D. Das, Phys. Rev. D **79**, 035007 (2009) [arXiv:0809.4065 [hep-ph]].
- [3] V. Berezhinsky, A. Bottino, J. R. Ellis, N. Fornengo, G. Mignola and S. Scopel, Astropart. Phys. **5**, 1 (1996) [arXiv:hep-ph/9508249].
- [4] P. Nath and R. L. Arnowitt, Phys. Rev. D **56**, 2820 (1997) [arXiv:hep-ph/9701301]; D. Feldman, Z. Liu and P. Nath, JHEP **0804**, 054 (2008) [arXiv:0802.4085 [hep-ph]]; C. F. Berger, J. S. Gainer, J. L. Hewett and T. G. Rizzo, JHEP **0902**, 023 (2009) [arXiv:0812.0980 [hep-ph]].
- [5] D. G. Cerdeno and C. Munoz, JHEP **0410**, 015 (2004), [arXiv:hep-ph/0405057].
- [6] J. R. Ellis, T. Falk, K. A. Olive and Y. Santoso, Nucl. Phys. B **652**, 259 (2003) [arXiv:hep-ph/0210205]; J. R. Ellis, K. A. Olive, Y. Santoso and V. C. Spanos, Phys. Lett. B **603**, 51 (2004) [arXiv:hep-ph/0408118]; A. De Roeck, J. R. Ellis, F. Gianotti, F. Moortgat, K. A. Olive and L. Pape, Eur. Phys. J. C **49**, 1041 (2007) [arXiv:hep-ph/0508198]; J. R. Ellis, K. A. Olive and P. Sandick, Phys. Rev. D **78**, 075012 (2008) [arXiv:0805.2343 [hep-ph]].
- [7] H. Baer, A. Mustafayev, E. K. Park, S. Profumo and X. Tata, JHEP **0604**, 041 (2006) [arXiv:hep-ph/0603197]; H. Baer, A. Mustafayev, E. K. Park and X. Tata, JHEP **0805**, 058 (2008) [arXiv:hep-ph/0603197].
- [8] H. Baer, A. Mustafayev, S. Profumo, A. Belyaev and X. Tata, JHEP **0507**, 065 (2005) [arXiv:hep-ph/0504001]; Phys. Rev. D **71**, 095008 (2005) [arXiv:hep-ph/0412059].

- [9] M. Drees, Phys. Lett. B **181**, 279 (1986); J. S. Hagelin and S. Kelley, Nucl. Phys. B **342**, 95 (1990).
- [10] Y. Kawamura, H. Murayama and M. Yamaguchi, Phys. Lett. B **324** 52 (1994) [arXiv:hep-ph/9402254]; Phys. Rev. D **51** 1337 (1995) [arXiv:hep-ph/9406245].
- [11] A. Datta, A. Datta and M. K. Parida, Phys. Lett. B **431**, 347 (1998) [arXiv:hep-ph/9801242]; A. Datta, A. Datta, M. Drees and D. P. Roy, Phys. Rev. D **61**, 055003 (2000) [arXiv:hep-ph/9907444].
- [12] S. Bhattacharya, A. Datta and B. Mukhopadhyaya, Phys. Rev. D **78**, 035011 (2008) [arXiv:0804.4051 [hep-ph]].
- [13] A. Corsetti and P. Nath, Phys. Rev. D **64**, 125010 (2001) [arXiv:hep-ph/0003186]; U. Chattopadhyay, A. Corsetti and P. Nath, Phys. Rev. D **66**, 035003 (2002) [arXiv:hep-ph/0201001]; U. Chattopadhyay and P. Nath, Phys. Rev. D **65**, 075009 (2002) [arXiv:hep-ph/0110341] ; U. Chattopadhyay and D. P. Roy, Phys. Rev. D **68**, 033010 (2003) [arXiv:hep-ph/0304108]; G. Belanger, F. Boudjema, A. Cottrant, A. Pukhov and A. Semenov, Nucl. Phys. B **706**, 411 (2005) [arXiv:hep-ph/0407218]; K. Huitu, J. Laamanen, P. N. Pandita and S. Roy, Phys. Rev. D **72**, 055013 (2005) [arXiv:hep-ph/0502100]; U. Chattopadhyay, D. Choudhury and D. Das, Phys. Rev. D **72**, 095015 (2005) [arXiv:hep-ph/0509228]; S. F. King, J. P. Roberts and D. P. Roy, JHEP **0710**, 106 (2007) [arXiv:0705.4219 [hep-ph]]; K. Huitu, R. Kinnunen, J. Laamanen, S. Lehti, S. Roy and T. Salminen, Eur. Phys. J. C **58**, 591 (2008) [arXiv:0808.3094 [hep-ph]]; U. Chattopadhyay, D. Das and D. P. Roy, Phys. Rev. D **79**, 095013 (2009) [arXiv:0902.4568 [hep-ph]]; S. P. Martin, Phys. Rev. D **79**, 095019 (2009) [arXiv:0903.3568 [hep-ph]]; D. Feldman, Z. Liu and P. Nath, Phys. Rev. D **80**, 015007 (2009) [arXiv:0905.1148 [hep-ph]].
- [14] S. Bhattacharya, A. Datta and B. Mukhopadhyaya, JHEP **0710**, 080 (2007) [arXiv:0708.2427 [hep-ph]]; Phys. Rev. D **78**, 115018 (2008) [arXiv:0809.2012 [hep-ph]]; S. Bhattacharya and J. Chakraborty, Phys. Rev. D **81**, 015007 (2010) [arXiv:0903.4196 [hep-ph]].
- [15] S. K. Soni and H. A. Weldon, Phys. Lett. **B126**, 215(1983); V. S. Kaplunovsky and J. Louis, Phys. Lett. B **306**, 269 (1993) [arXiv:hep-th/9303040].
- [16] M. Dine, R. G. Leigh and A. Kagan, Phys. Rev. D **48**, 4269 (1993) [arXiv:hep-

- ph/9304299]; P. Pouliot and N. Seiberg, Phys. Lett. B **318**, 169 (1993) [arXiv:hep-ph/9308363]; S. Dimopoulos and G. F. Giudice, Phys. Lett. B **357**, 573 (1995) [arXiv:hep-ph/9507282]; A. G. Cohen, D. B. Kaplan and A. E. Nelson, Phys. Lett. B **388**, 588 (1996) [arXiv:hep-ph/9607394]; A. Pomarol and D. Tommasini, Nucl. Phys. B **466**, 3 (1996) [arXiv:hep-ph/9507462]; M. Misiak, S. Pokorski and J. Rosiek, Adv. Ser. Direct. High Energy Phys. **15**, 795 (1998) [arXiv:hep-ph/9703442]; P. H. Chankowski, K. Kowalska, S. Lavignac and S. Pokorski, arXiv:hep-ph/0507133.
- [17] F. Gabbiani, E. Gabrielli, A. Masiero and L. Silvestrini, Nucl. Phys. B **477**, 321 (1996) [arXiv:hep-ph/9604387]; N. Arkani-Hamed and H. Murayama, Phys. Rev. D **56**, 6733 (1997) [arXiv:hep-ph/9703259].
- [18] R. Barbieri and G.F. Giudice, Nucl. Phys. **B306**,63(1988); P. Ciafaloni and A. Strumia, Nucl. Phys. B **494**, 41 (1997) [arXiv:hep-ph/9611204].
- [19] V. D. Barger, C. Kao and R. J. Zhang, Phys. Lett. B **483**, 184 (2000) [arXiv:hep-ph/9911510].
- [20] J. Bagger, J. L. Feng and N. Polonsky, Nucl. Phys. B **563**, 3 (1999) [arXiv:hep-ph/9905292] . K. Agashe and M. Graesser, Phys. Rev. D **59**, 015007 (1999) [arXiv:hep-ph/9801446]; J. A. Bagger, J. L. Feng, N. Polonsky and R. J. Zhang, Phys. Lett. B **473**, 264 (2000) [arXiv:hep-ph/9911255]; H. Baer, P. Mercadante and X. Tata, Phys. Lett. B **475**, 289 (2000) [arXiv:hep-ph/9912494]; H. Baer, C. Balazs, P. Mercadante, X. Tata and Y. Wang, Phys. Rev. D **63**, 015011 (2001) [arXiv:hep-ph/0008061].
- [21] S. Bhattacharya, U. Chattopadhyay, D. Choudhury, D. Das and B. Mukhopadhyaya, Phys. Rev. D **81**, 075009 (2010) [arXiv:0907.3428 [hep-ph]].
- [22] J. L. Evans, D. E. Morrissey and J. D. Wells, Phys. Rev. D **75**, 055017 (2007) [arXiv:hep-ph/0611185].
- [23] W. Buchmuller, J. Kersten and K. Schmidt-Hoberg, JHEP **0602**, 069 (2006) [arXiv:hep-ph/0512152]; W. Buchmuller, L. Covi, J. Kersten and K. Schmidt-Hoberg, JCAP **0611**, 007 (2006) [arXiv:hep-ph/0609142].
- [24] E. Komatsu *et al.* [WMAP Collaboration], Astrophys. J. Suppl. **180**, 330 (2009) [arXiv:0803.0547 [astro-ph]].
- [25] H. Baer, C. h. Chen, F. Paige and X. Tata, Phys. Rev. D **53**, 6241 (1996)

- [arXiv:hep-ph/9512383]; H. Baer, V. Barger, A. Lessa and X. Tata, JHEP **0909**, 063 (2009) [arXiv:0907.1922 [hep-ph]].
- [26] U. Chattopadhyay, D. Das, A. Datta and S. Poddar, Phys. Rev. D **76**, 055008 (2007) [arXiv:0705.0921 [hep-ph]]; N. Bhattacharyya, A. Datta and S. Poddar, Phys. Rev. D **78**, 075030 (2008) [arXiv:0807.0278 [hep-ph]].
- [27] K. L. Chan, U. Chattopadhyay and P. Nath, Phys. Rev. D **58**, 096004 (1998) [arXiv:hep-ph/9710473]; U. Chattopadhyay, A. Corsetti and P. Nath, Phys. Rev. D **68**, 035005 (2003) [arXiv:hep-ph/0303201]; D. Feldman, Z. Liu and P. Nath, Phys. Rev. D **78**, 083523 (2008) [arXiv:0808.1595 [hep-ph]].
See also: 1st article of Ref. [32].
- [28] J. L. Feng, K. T. Matchev and T. Moroi, Phys. Rev. D **61**, 075005 (2000) [arXiv:hep-ph/9909334]; J. L. Feng, K. T. Matchev and T. Moroi, Phys. Rev. Lett. **84**, 2322 (2000) [arXiv:hep-ph/9908309]; J. L. Feng, K. T. Matchev and F. Wilczek, Phys. Lett. B **482**, 388 (2000) [arXiv:hep-ph/0004043]; U. Chattopadhyay, A. Datta, A. Datta, A. Datta and D. P. Roy, Phys. Lett. B **493**, 127 (2000) [arXiv:hep-ph/0008228];
U. Chattopadhyay, T. Ibrahim and D. P. Roy, Phys. Rev. D **64**, 013004 (2001) [arXiv:hep-ph/0012337]; U. Chattopadhyay, T. Ibrahim and D. P. Roy, Phys. Rev. D **64**, 013004 (2001) [arXiv:hep-ph/0012337]; J. L. Feng and F. Wilczek, Phys. Lett. B **631**, 170 (2005) [arXiv:hep-ph/0507032]; S. P. Das, A. Datta, M. Guchait, M. Maity and S. Mukherjee, Eur. Phys. J. C **54**, 645 (2008) [arXiv:0708.2048 [hep-ph]].
- [29] M. Drees and M. Nojiri, Phys. Rev. D **47**, 376 (1993) [arXiv:hep-ph/9207234].
- [30] P. Nath and R. L. Arnowitt, Phys. Rev. Lett. **70**, 3696 (1993) [arXiv:hep-ph/9302318]; H. Baer and M. Brhlik, Phys. Rev. D **53**, 597 (1996) [arXiv:hep-ph/9508321]; H. Baer, M. Brhlik, M. A. Diaz, J. Ferrandis, P. Mercadante, P. Quintana and X. Tata, Phys. Rev. D **63**, 015007 (2001) [arXiv:hep-ph/0005027]; J. R. Ellis, T. Falk, G. Ganis, K. A. Olive and M. Srednicki, Phys. Lett. B **510**, 236 (2001) [arXiv:hep-ph/0102098]; A. B. Lahanas and V. C. Spanos, Eur. Phys. J. C **23**, 185 (2002) [arXiv:hep-ph/0106345]; A. Djouadi, M. Drees and J. L. Kneur, Phys. Lett. B **624**, 60 (2005) [arXiv:hep-ph/0504090].
- [31] G. Jungman, M. Kamionkowski and K. Greist, Phys. Rep. **267**, 195 (1995).

- [32] A. B. Lahanas, N. E. Mavromatos and D. V. Nanopoulos, *Int. J. Mod. Phys. D* **12**, 1529 (2003) [arXiv:hep-ph/0308251]; C. Munoz, *Int. J. Mod. Phys. A* **19**, 3093 (2004) [arXiv:hep-ph/0309346]; M. Drees, Plenary talk at 11th International Symposium on Particles, Strings and Cosmology (PASCOS 2005), Gyeongju, Korea, 30 May - 4 Jun 2005 (published in *AIP Conf.Proc.*, **805**, 48-54, (2006).
- [33] A. Djouadi, J. L. Kneur and G. Moultaka, *Comput. Phys. Commun.* **176**, 426 (2007) [arXiv:hep-ph/0211331].
- [34] G. Belanger, F. Boudjema, A. Pukhov and A. Semenov, *Comput. Phys. Commun.* **176**, 367 (2007) [arXiv:hep-ph/0607059].
- [35] R. Barate *et al.* [LEP Working Group for Higgs boson searches], *Phys. Lett. B* **565**, 61 (2003) [arXiv:hep-ex/0306033].
- [36] F. Margaroli [CDF and D0 Collaborations], *Nuovo Cim.* **123B**, 763 (2008); T. Aaltonen *et al.* [CDF Collaboration], arXiv:0907.0810 [hep-ex]; arXiv:0906.5613 [hep-ex]; arXiv:0905.3155 [hep-ex].
- [37] G. Degrassi, S. Heinemeyer, W. Hollik, P. Slavich and G. Weiglein, *Eur. Phys. J. C* **28**, 133 (2003) [arXiv:hep-ph/0212020]; B. C. Allanach, A. Djouadi, J. L. Kneur, W. Porod and P. Slavich, *JHEP* **0409**, 044 (2004) [arXiv:hep-ph/0406166]; S. Heinemeyer, [arXiv:hep-ph/0408340].
- [38] A. L. Kagan and M. Neubert, *Eur. Phys. J. C* **7**, 5 (1999) [arXiv:hep-ph/9805303]; K. G. Chetyrkin, M. Misiak and M. Munz, *Phys. Lett. B* **400**, 206 (1997) [Erratum-*ibid.* **B 425**, 414 (1998)] [arXiv:hep-ph/9612313]; P. Gambino and M. Misiak, *Nucl. Phys. B* **611**, 338 (2001) [arXiv:hep-ph/0104034].
- [39] M. Ciuchini, G. Degrassi, P. Gambino and G. F. Giudice, *Nucl. Phys. B* **527**, 21 (1998) [arXiv:hep-ph/9710335]; M. Ciuchini, G. Degrassi, P. Gambino and G. F. Giudice, *Nucl. Phys. B* **534**, 3 (1998) [arXiv:hep-ph/9806308]; G. Degrassi, P. Gambino and G. F. Giudice, *JHEP* **0012**, 009 (2000) [arXiv:hep-ph/0009337].
- [40] S. Chen *et al.* [CLEO Collaboration], *Phys. Rev. Lett.* **87**, 251807 (2001) [arXiv:hep-ex/0108032]; B. Aubert *et al.* [BaBar Collaboration], [arXiv:hep-ex/0207076]; P. Koppenburg *et al.* [Belle Collaboration], *Phys. Rev. Lett.* **93**, 061803 (2004) [arXiv:hep-ex/0403004].

- [41] A. Djouadi, M. Drees and J. L. Kneur, JHEP **0603**, 033 (2006) [arXiv:hep-ph/0602001].
- [42] J. Foster, K. i. Okumura and L. Roszkowski, JHEP **0603**, 044 (2006) [arXiv:hep-ph/0510422].
- [43] A. Dedes, H. K. Dreiner, U. Nierste, and P. Richardson, Phys. Rev. Lett. **87**, 251804 (2001) [arXiv:hep-ph/0108037]; R. Arnowitt, B. Dutta, T. Kamon and M. Tanaka, Phys. Lett. B **538** (2002) 121 [arXiv:hep-ph/0203069]; J. K. Mizukoshi, X. Tata and Y. Wang, Phys. Rev. D **66**, 115003 (2002) [arXiv:hep-ph/0208078]; S. Baek, P. Ko, and W. Y. Song, JHEP **0303**, 054 (2003) [arXiv:hep-ph/0208112]; T. Ibrahim and P. Nath, Phys. Rev. D **67**, 016005 (2003) [arXiv:hep-ph/0208142].
- [44] T. Aaltonen *et al.* [CDF Collaboration], Phys. Rev. Lett. **100**, 101802 (2008) [arXiv:0712.1708 [hep-ex]].
- [45] C. Bobeth, T. Ewerth, F. Kruger and J. Urban, Phys. Rev. D **64**, 074014 (2001) [arXiv:hep-ph/0104284].
- [46] H. E. Haber and Y. Nir, Phys. Lett. B **306**, 327 (1993) [arXiv:hep-ph/9302228]; H. E. Haber and Y. Nir, Phys. Lett. B **306**, 327 (1993) [arXiv:hep-ph/9302228]; J. F. Gunion and H. E. Haber, Phys. Rev. D **67**, 075019 (2003) [arXiv:hep-ph/0207010].
- [47] E. Boos, A. Djouadi, M. Muhlleitner and A. Vologdin, Phys. Rev. D **66**, 055004 (2002) [arXiv:hep-ph/0205160]; E. Boos, A. Djouadi and A. Nikitenko, Phys. Lett. B **578**, 384 (2004) [arXiv:hep-ph/0307079]; A. Djouadi and Y. Mambrini, JHEP **0612**, 001 (2006) [arXiv:hep-ph/0609234].
- [48] D. Pierce and A. Papadopoulos, Nucl. Phys. B **430**, 278 (1994) [arXiv:hep-ph/9403240].
- [49] L. E. Ibanez and C. Lopez, Nucl. Phys. B **233**, 511 (1984).
- [50] T. Sjostrand, S. Mrenna and P. Skands, JHEP **0605**, 026 (2006) [arXiv:hep-ph/0603175].
- [51] P. Skands *et al.*, JHEP **0407**, 036 (2004) [arXiv:hep-ph/0311123].
- [52] H. L. Lai *et al.* [CTEQ Collaboration], Eur. Phys. J. C **12**, 375 (2000) [arXiv:hep-ph/9903282].

- [53] Private communication with Bruce Melado; S. Biswas and B. Mukhopadhyaya, *Phys. Rev. D* **79**, 115009 (2009) [arXiv:0902.4349 [hep-ph]].
- [54] M. Cacciari, S. Frixione, M. L. Mangano, P. Nason and G. Ridolfi, *JHEP* **0809**, 127 (2008) [arXiv:0804.2800 [hep-ph]].
- [55] M. L. Mangano, M. Moretti, F. Piccinini, R. Pittau and A. D. Polosa, *JHEP* **0307** 001 (2003) [arXiv:hep-ph/0206293].
- [56] ATLAS detector and physics performance. Technical design report. Vol. 2, CERN-LHCC-99-15, ATLAS-TDR-15.

Chapter 9

Conclusions

We have performed multichannel analyses of SUSY signals, including $jets + \cancel{E}_T$, single leptons, same sign and opposite sign dilepton (SSD and OSD), trileptons, four leptons as well as hadronically quiet trileptons for a number of high-scale non-universal gaugino and scalar mass scenarios within the ambit of gravity mediated SUSY breaking, and compared them with those corresponding to a universal scenario, namely, mSUGRA in the context of the LHC. We have made some important observations in this regard which might be instrumental in unravelling the nature of high-scale SUSY model at the LHC.

We have considered non-universal gaugino mass models that arise from an extended gauge kinetic function in a SUSY-GUT model in context of $SU(5)$ or $SO(10)$ GUT groups. It turns out that the non-universal gaugino mass ratios at a high scale can be specified depending on the GUT breaking non-singlet Higgs representations that arise from the symmetric product of the adjoint representations of the underlying GUT group. The GUT-breaking representations in case of $SU(5)$, which are rather clearly differentiable from mSUGRA over a substantial region of the parameter space, are **75** and **200**. Such differentiability arises through the suppression of leptonic final states. This is because such cases ($M_1, M_2 > M_3$ at the high-scale) yield low-lying charginos and neutralinos with relatively higher masses and more often with larger Higgsino components. While on one hand, it reduces the decay branching fraction of the gluino through the

second neutralino $\tilde{\chi}_2^0$ or first chargino $\tilde{\chi}_1^\pm$, their subsequent decays to leptons also get suppressed additionally due to their larger higgsino component. In general, distinction is relatively easy for high values of μ , since a low μ enhances the Higgsino component of low-lying charginos and neutralinos, thus tending to partially obliterate the clear stamps of various gaugino mass patterns as manifested in the physical states.

We have also studied the non-universal gaugino mass ratios for the representations **54** and **770** for the breaking chain $SU(4)_C \otimes SU(2)_L \otimes SU(2)_R$ (G_{422}) in an $SO(10)$ SUSY-GUT scenario. We have assumed that the breaking of $SO(10)$ to the intermediate gauge group and the latter in turn to the SM gauge group takes place at the GUT scale itself. We point out some errors in the earlier calculation and derive new results on the gaugino mass ratios. It turns out that the non-universal ratio obtained for **54** is the same as that of **24** of $SU(5)$ under such assumptions. Hence, we scan the parameter space for **770** with different low-energy constraints (including dark matter) taken into account and point out the allowed region of the parameter space. We study collider signatures at some selected benchmark points in context of the LHC as well. The comparison between the non-universal inputs with the mSUGRA ones yields a significant distinction in the multilepton channel parameter space in context of the LHC where **770** shows suppression of leptonic final states compared to mSUGRA. This is basically due to the same reason as that stated for **75** and **200**. In general, we also show that the ratio of rates of two different final states are better discriminators, as they reduce the uncertainty in jet-energy scale or parton distribution functions.

Generalising the feature of high-scale non-universality, we have shown next that SUSY scenarios with non-universality in both gaugino and scalar masses, can envision regions in the parameter space where the usual signals from the cascade decays of strongly interacting superparticles involving hard multi-jets drop below the threshold of observability. Such a region of parameter space where gluino and squarks are much higher than the charginos, neutralinos and sleptons can be obtained from a high scale gaugino mass non-universality with a hierarchy $M_3 \gg M_2, M_1$. This can be achieved within an $SU(5)$ SUSY-GUT framework involving a GUT-breaking Higgs representation in a linear combination of **24** with the singlet and **75**. We have demonstrated that hadronically quiet trileptons can be of significant help in these cases. In a numerical study, we have found that other signals such as single-or dileptons, for which additional hard jets are re-

quired for background suppression, are decidedly less advantageous for such a scenario. We propose such a SUSY spectrum as a new benchmark for investigating non-universal SUSY at the LHC.

In a dedicated analysis of scalar non-universality, we have studied three representative scenarios where the scalar mass spectrum in SUSY can deviate from the predictions of a universal SUGRA model. These are situations with (a) high-scale non-universality of squarks and sleptons, (b) a separate high-scale mass parameter for the third family sfermions, and (c) the effect of $SO(10)$ D-terms. In each case, we have made a detailed scan of the parameter space, in terms of the gluino and squark masses which set the scale of the hard scattering leading to superparticle production. A multichannel analysis performed in each case, comparing the different degrees of non-universality with mSUGRA, reveals some interesting aspects important in context of the LHC. The case where the most strikingly distinct effects are seen in terms of the ratios is one where the first two family squarks have masses on the order of 10 TeV keeping the third generation light as an effect of high-scale family non-universality. This is possible, with a significant increase in the leptonic final state compared to mSUGRA. For models with high-scale squark-slepton non-universality, most interesting was the case, where gluino is light ($\simeq 500$ GeV), 1,2 generation squarks are as heavy as 1000 GeV, but sleptons are light ($\simeq 250$ GeV). Such a scenario is definitely unattainable from a universal scalar mass set-up. Lighter sleptons in such a case, yield higher rates for leptonic final states when compared to mSUGRA with similar values of $(m_{\tilde{g}}, m_{\tilde{q}^{1,2}})$. The distinction however is very difficult for different $SO(10)$ D-terms, except for $D = -1.25$. It is also seen that the trilepton events can be most useful in making distinction among different situations. It is also noted at the end that, unlike in the case of gaugino non-universality, the schemes of parametrising scalar non-universality are more non-uniform. Therefore, different schemes often lead to overlapping portions in the spectrum, where signals may turn out to be of similar nature.

We have also studied a case of non universal scalar masses, where the first two families of squarks as well as sleptons of all generations are much heavier than the third family of squarks and the Higgs scalars. Such a parametrisation yields a significant region where LSP annihilation is efficiently mediated by the light pseudoscalar Higgs, with the ‘funnel region’ being significantly extended toward small values of $\tan\beta$ when compared to mSUGRA. In addition, such

a SUSY parameter space is consistent with all constraints from FCNC and CP-violation and we investigate the signals of this scenario at the LHC. Although stop-pair production is the dominant SUSY process in such scenarios, the stringent cuts that we choose, result in stop-cascades being suppressed. Rather, the dominant contribution to the signal rates turns out to be gluino pair-production. The relatively large multiplicity of top quarks produced in the cascades results in enhanced rates for two, three and four-lepton final states, together with missing E_T and hard jets. The usefulness of four-lepton final states is highlighted through this analysis. In particular, we find that, using the criteria chosen by us, it is possible to probe the above scenario with an integrated luminosity of 30fb^{-1} for gluino masses up to about 1.2 TeV. (Indeed, for certain significant parts of the parameter space, even 2fb^{-1} would be enough.) The reach can be potentially extended further once more luminosity accrues. We also demonstrate that it is possible to distinguish this scenario from an mSUGRA-one tuned at the same gluino mass and satisfying the WMAP constraints. Thus, we succeed in illustrating that a multichannel analysis is not only able to probe such non universal SUSY scenarios satisfying the relic density constraints, but can also highlight notable differences with a simple-minded model based on universal SUGRA.

As a whole, the conclusions that we obtain regarding the distinction of different non-universal gaugino and scalar mass scenarios from the mSUGRA are reasonably robust. They may be of use in the LHC inverse analysis which is of utmost importance in identifying the nature of SUSY breaking, if SUSY is indeed discovered at the LHC.